Dissertation

Role of adipose triglyceride lipase (ATGL) in cancer metabolism

submitted by

Tamara TOMIN

for the Academic Degree of

Doctor of Philosophy

(PhD)

at the

Medical University of Graz

under the supervision of

Prof. Dr. Ruth BIRNER-GRÜNBERGER

2018

Declaration

I hereby declare that this thesis is my own original work and that I have fully acknowledged by name all of those individuals and organizations that have contributed to the research of this thesis. Due acknowledgement has been made in the text to all other material used. Throughout this thesis and in all related publications I follow the guidelines of “Good Scientific Practice”

September 10th, 2018

Disclosures

After brief general introduction about cancer related metabolic alteration, first chapter of this thesis will focus on the role of lipolysis in cancer metabolism. The results of this chapter have been published in Tomin T, Fritz K, Gindlhuber J, Waldherr L, Pucher B, Thallinger GG, Nomura DK, Schittmayer M, Birner-Gruenberger R. Deletion of Adipose Triglyceride Lipase Links Triacylglycerol Accumulation to a More-Aggressive Phenotype in A549 Lung Carcinoma Cells. J Proteome Res. 2018; 17:1415-1425 (1).

In the second chapter a novel methodology for measurement of glutathione status will be introduced and its wide spectra of biological applications will be discussed. This resulted in a my second first author manuscript which is currently in the submission process (Schittmayer M, Tomin T, Rainer P, Birner-Gruenberger R. Altered glutathione redox status in failing hearts revealed by two-step alkylation with N-ethylmaleimide isotopologues). The method has also been patented.

All co-authors have agreed to the use of their data in this thesis.

In addition, I contributed to two other publications as co-author helping with proteomics and metabolomics analyses (2, 3).

Acknowledgment

It has been four years of an amazing journey. I fell in love with science on ways I did not know were possible and while writing this thesis I realized how lucky I am to be doing something which I actually enjoy every part of.

For that and many, many other things I owe my gratitude to my mentor and my true friend, Ruth Birner-Gruenberger for giving me this PhD opportunity. Thank you with all my heart for putting your trust in me, for your guidance, support and freedom to express myself yet always helping me to get back on the course when I felt little lost. You really are a true captain.

Next to Ruth I thank the rest of my pirates: Matthias, for his crazy ideas of which those that work are truly amazing ones, Stefan for repairing everything I ever broke, Babsi, Laura and Juergen for all their experimental help and Petra for all the fun we had along the way. I would also like to thank Kati, Bettina and Laura Nebel for their help with experiments and data analysis.

I am truly thankful to Prof Daniel Nomura and the Nomura research group for hosting me for six months at UC Berkeley. Here I would also like to thank Linda Waldherr for being an amazing lab mate and dear friend.

My gratitude also goes to my thesis committee, Prof Hoefler and Prof Zebisch for all the valuable inputs during the years and my thesis evaluators Prof Haemmerle, Prof Pichler and Prof Gerner for reviewing my thesis.

I would also like to thank my dear friends Isi, Sasha and Jomi that shared this PhD journey with me.

Hvala mojoj porodici na godinama podrške, pre svega mojoj Dž sto je doživljavala moje uspehe sa takvim entuzijazmom i ljubavlju.

Above all, I thank my life partner and other half, my dear Sini. Thank you for all your love and devotion, thank you for your compassion and advices, but mainly thank you for being you and being there for me.

Yours sincerely,

Tamara

Funding

This work was supported by Austrian Science Fund (FWF) Projects P26074, J-3983 and KLI425, and the doctoral school “DK Metabolic and Cardiovascular Disease” (W1226) and by the Austrian Ministry of Science, Research and Economy (Omics Center Graz project).

TABLE OF CONTENT

Abbreviations

1,3BPG - 1,3-bisphospho glycerate

2PG - 2-phosphoglycerate

3PG - 3-phosphoglycerate

α-KG - α-ketoglutarate

AA - arachidonic acid

ACL - ATP citrate ligase

ACC - acetyl-CoA carboxylase

ADP - adenosine diphosphate

ALDOA/B/C - aldolase A/B/C

ATGL - adipose triglyceride lipase

ATP - adenosine triphosphate

CoA - coenzyme A

Cit - citrate

CPT1 - carnitine palmitoyltransferase I

D-2HG - D-2-hydroxyglutarate

DCM - dilated cardiomyopathy

DG - diacylglycerol

DHAP - dihydroxyacetone phosphate

EGF(R) - epidermal growth factor (receptor)

ENO1 - enolase 1

EpoR - erythropoietin receptor

F1,6P -fructose 1,6-bisphosphate;

F6P -fructose-6-phosphate

FAK - focal adhesion kinase

FFA - free fatty acid

FAS - fatty acid synthesis

FASN - fatty acid synthase

FASP - filter aided sample preparation

FAO - fatty acid oxidation

FDR - false discovery rate

FH - fumarate hydratase

G3P - glycerol 3- phosphate

G6P - glucose 6 -phosphate

G0S2 - G0/G1 switch protein 2

GAPDH - glyceraldehyde 3-phosphate dehydrogenase

GF - growth factor

Gln - glutamine

Glu - glutamate

GPI - glucose-6-phosphate isomerase

GSH - glutathione (reduced)

GSSG - oxidized glutathione

GTP - guanosine triphosphate

HC - hierarchical clustering

HDR - homology directed repair

HER2 - human epidermal growth factor receptor 2

HK1/2 - hexokinase 1/2

HIF-1 - hypoxia inducible factor 1

HILPDA - hypoxia-inducible lipid droplet-associated protein

HSL - hormone sensitive lipase

ICM - ischemic cardiomyoptathy

IDH - isocitrate dehydrogenase

IL-8 - interleukin-8

Isocit - isocitrate

JAK2 - janus kinase 2

LC - liquid chromatography

LC-MS/MS - liquid chromatography coupled to mass spectrometry

LD - lipid droplets

LDH - lactate dehydrogenase

LFQ - label free quantification

LOA - lose-of-attachment

LPC - lysophoshatidylcholine

LPL - lysophospholipids

Mal - malate

MAPK - mitogen-activated protein kinase

MCT1-4 - monocarboxylate transporters 1-4

MG - monoacylglycerol

MGL - monoacylglycerol lipase

MMP - matrix metallopeptidases

MRM - multiple reactions monitoring

MS - mass spectrometry/mass spectrometer

mTOR - mammalian target of rapamycin

NAD(P)H - nicotinamide adenine dinucleotide (phosphate)

NEFA - non-esterified fatty acid

NEM - N-ethyl-maleinimid

NL - neutral lipids

OAA - oxaloacetate

OXPHOS - oxidative phosphorylation

PA -palmitic acid

PC - phosphatidylcholine

PCA - principal component analysis

PE - phosphatidylethanolamine

PDH - pyruvate dehydrogenase

PDK-1 - pyruvate dehydrogenase kinase 1

PEDF - pigment epithelium-derived factor

PEP - phosphoenolpyruvate

PFK1 - phosphofructokinase 1

PFKFB3 - 6-phosphofructo-2-kinase/fructose-2,6-biphosphatase 3

PFKC3/4 - fructose-2,6-biphosphatase 3/4

PGAM1 - phosphoglycerate mutase 1

PGK1 - phosphoglycerate kinase 1

PI3K - phosphatidylinositol-3-kinase

PKM2 - pyruvate kinase M2

PL - phospholipids

PLA/B/C -phospholipase A/B/C

PNPLA2 - phospholipase domain containing 2

PPP - pentose phosphate pathway

PTEN - phosphatase and tensin homolog

Pyr- pyruvate

ROS - reactive oxygen species

RTK - receptor tyrosine kinase

SDH -succinate dehydrogenase

SL - sphingolipids

SM - sphingomyelin

STAT3 - signal transducer and activator of transcription 3

TCA - tricarboxylic acid cycle

TCEP - tris(2-carboxyethyl)phosphine hydrochloride

TFE - trifluoroethanol

TG - triacylglycerol

TPI - triosephosphate isomerase

VGF(R) - vascular endothelial growth factor (receptor)

Zusammenfassung

Seit der Entdeckung Otto Warburgs in den 1920er Jahren, ist die Erforschung der Veränderungen des Stoffwechsels im Krebs ein Hauptthema in der globalen wissenschaftlichen Gemeinschaft. Während die Schlüsselrolle des Zuckerabbaustoffwechsels (Glykolyse) sehr gut untersucht ist, hat sich in letzter Zeit auch die Erkenntnis, dass Veränderungen des Fettstoffwechsels (Lipidmetabolismus) wichtig für das Wachstum und die Aggressivität von Krebszellen sind, durchgesetzt. Sowohl die *de novo* Fettsäurebiosynthese, als auch die Aufnahme von Fettsäuren und ihre Verbrennung, sind oft aktivierte Prozesse in Krebszellen. Welche Rolle aber die intrazelluläre Bereitstellung von Fettsäuren durch die Spaltung (Hydrolyse) von Speicherfetten (Triglyzeride) durch sogenannte Lipasen spielt, ist noch nicht ausreichend erforscht.

Im ersten Kapitel meiner Dissertation berichte ich, dass die Triglyzeridhydrolase Adipozyten-Triglycerid-Lipase (ATGL) im Lungenkrebs die Eigenschaft eines Tumorsuppressors besitzt und ihr Verlust Lungenkrebszellen aggressiver macht. Die Deletion des Gens, das ATGL kodiert, in A549 Lungenkrebszellen mittels CRISPR/Cas9 Technologie führte zu einer Akkumulierung von Triacylglycerol reichen Lipidtropfen und onkogenen Signallipiden und einer Aktivierung des Onkogens SRC Kinase. SRC kinase verursachte eine höhere Mobilität der Zellen, die durch einen spezifischen Inhibitor für SRC oder Wiedereinführung des Gens für ATGL normalisiert werden konnte. In Übereinstimmung mit diesen Resultaten, war die Pharmakologische Inhibierung der ATGL Aktivität in Mauslungentumorzellen oder Maushepatozyten ausreichend, um SRC kinase zu aktivieren.

Im zweiten Teil meiner Dissertation beschäftige ich mich mit der Messung von oxidativem Stress, der zur Pathogenese vieler Krankheiten, wie Krebs, sowie neurodegenerativen und kardiovaskulären Krankheiten, beiträgt. Ein üblicher Parameter für die Evaluierung von oxidativem Stress ist der Quotient aus reduziertem zu oxidiertem Glutathion. Ich berichte hier von einem neuen akkuraten und robusten massenspektrometrischen Analyseverfahren zu seiner Bestimmung, das eine zweistufige Alkylierung mit Isotopenmarkierung beinhaltet. Diese neue Methode wurde für Zellen, Gewebe und Blutproben optimiert und zur

Messung des oxidativen Stresses in Lungenkrebszellen und versagenden Herzen angewandt.

Abstract

Since the discovery of Otto Warburg in 1920s, alterations of metabolism in cancer became one of the main research topics in scientific community worldwide. By this end much is understood regarding the pivotal role of glycolysis in cancer, as well as the importance of lipid synthesis, uptake and oxidation. However, despite all advances we are still lacking a clear understanding of the function of lipid catabolism in cancer, especially the contribution of lipolysis to cancer metabolism.

In the first part of this thesis I report that adipose triglyceride lipase (ATGL), a major triglyceride hydrolase, acts as tumor suppressor in lung cancer as its loss or inhibition renders lung cancer cells more aggressive. Deletion of ATGL with CRISPR/Cas9 induced accumulation of triacylglycerol (TG) rich lipid droplets (LD) with concomitant increase in pro-oncogenic signaling lipids and activation of proto-oncogene kinase SRC. SRC stimulated migration in A549 lung cancer cells lacking ATGL which could be reduced by treatment with a selective SRC inhibitor. Both activation of SRC and increase in migratory potential were abolished with lentiviral reintroduction of ATGL in the ATGL knock-out (ATGL-KO) cells. In addition, pharmacological inhibition of ATGL by atglistatin in murine lung cancer LLC1/LL2 and murine hepatocytes (AML-12) was sufficient to recapitulate the phenotype of SRC activation.

The second part of this work is dedicated to assessment of oxidative stress. Oxidative stress contributes to progression of different pathologies, especially cancer, neurodegenerative and cardiovascular diseases. One of the common parameters for the evaluation of cellular redox stress is the ratio of reduced (GSH) to oxidized (GSSG) glutathione. I report a new method for accurate and robust measurement of both glutathione forms in one run using a two-step alkylation procedure and LC-MS/MS. The new method was applied and optimized for measurement of GSH/GSSG as a proxy for oxidative stress in cancer cells, blood and tissue samples. Moreover, GSH/GSSG in heart samples of patients suffering from cardiomyopathies was compared to non-failing hearts, which confirmed GSH/GSSG as potential marker for heart failure.

GENERAL INTRODUCTION

The most important feature of all cancer cells is excessive and uncontrolled proliferation. In order to sustain high growth rates cancer cells have to block apoptotic signals, constitutively activate growth signaling pathways and reprogram their metabolism accordingly (4). This is supported by multiple genomic events that result in upregulation of oncogenes and/or deregulation of tumor suppressors (5, 6). Ultimately, all metabolic actions are directed to production of more biomass to support proliferation and survival (7). Consequent higher metabolic rates (e.g. excessive mitochondrial activity, increased cellar receptor signaling, increased activity of oxidases, cyclooxygenases, lipoxygenases and thymidine phosphorylase) lead to production of reactive oxygen species (ROS) (8). ROS further cause perturbations of cellular redox status and can trigger different metabolic adaptations to sustain viability of cancer cells (9). Taken together, diverse tumorigenic drivers contribute to wide spectra of cancer specific metabolic fingerprints and phenotypes and some of the main oncogenic drivers and key metabolic alterations will be further discussed.

Cancer related genomic and metabolic alterations

Loss of tumor suppressors

As aforementioned, cause of malignant transformation is usually loss of tumor suppressor activity with concomitant activation of oncogene(s). Genes recognized as tumor suppressors act as control points of cell cycle and proliferation. They respond to potential errors in the genome, causing cycle arrest, inhibiting proliferation and/or triggering apoptosis (10).

The most prominent tumor suppressor gene deregulated in cancer is p53. Due to its cell cycle arrest and pro-apoptotic role, activity of this nuclear transcription factor is lost in around 50% of all tumors. Mutations of the p53 gene are considered as one of the initial events in tumorogenesis and, in the majority of cases, lead to loss of p53 tumor suppressor function (11, 12). Resulting mutated p53 proteins not only lose their suppressing abilities but often even gain pro-malignant properties, making p53 one of the central targets in cancer treatment. Current strategies involve replacement of mutated p53 with the wild type protein (12, 13).

Another prominent tumor suppressor gene is phosphatase and tensin homolog (PTEN), the main negative regulator of serine-threonine kinase AKT/phosphatidylinositol-3-kinase (PI3K) signaling cascade. PTEN is lost in approximately 40% of all cancers (13) thus releasing its break on the PI3K/AKT cascade which controls cell proliferation, survival, and metabolism. Loss of PTEN can moreover directly activate pro-oncogenic proteins (e.g. SRC) which will be later discussed (10, 14).

Many therapeutic approaches are based on the restoration of the function of tumor suppressors (13).

Oncogenic drivers of cancer

Genes considered pro-oncogenic usually enhance cellular proliferation and/or inhibit apoptosis. They are tightly connected to cancer initiation and progression and are activated by a mutation, gene fusion, translocation or amplification.

Oncogenes can be transcription factors, growth factors or growth factor receptors, regulators of apoptosis or chromatin remodeling, or signal transducers (6).

Oncogenes as transcription factors

Arguably the most important oncogenic transcription factor is MYC. MYC plays an important role in one fifth of all cancers (15) and it is able to co-operate with many other proto-oncogenes thus contributing to almost all cancer hallmarks: from increased proliferation, cell survival, angiogenesis to crucial metabolic changes (16). Its metabolic effects are numerous. MYC increases the expression of glycolytic enzymes, particularly pyruvate kinase M2 (PKM2) which is specific for proliferating cells. In addition to glucose metabolism, MYC regulates glutamine uptake and glutaminolysis, enabling the cells to switch to glutamine metabolism when glucose or oxygen is limiting (17). Furthermore, MYC increases both nucleotide and lipid biosynthesis either by directly influencing enzymes involved in their synthesis or indirectly by coordinating substrate availability. Protein synthesis is also enhanced by MYC (18). Interestingly, MYC in the same time is able to activate apoptosis, however this branch of MYC activity is suppressed as long as there is enough of pro-survival signals (19). Next to MYC another important transcription factor in regulating cancer metabolism is hypoxia inducible factor 1 (HIF1) (20). Since HIF1 predominantly affects glycolysis and glucose import functions of HIF1 will be discussed alongside glucose metabolism.

Oncogenic growth factors and their receptors

Oncogenic growth factors (GFs) and GF receptors greatly contribute to cancer progression and are among the main drivers of cancer metastasis. Some of the most prominent oncogenes from this group are epidermal GF (EGF), fibroblast GF, platelet-derived GF, transforming GF and vascular endothelial GF (VGF) that together support proliferation, invasion, metastasis and therapy resistance (21). From GF receptors probably the most notable ones in cancer are VGF receptor (VGFR), EGF receptor (EGFR) and human epidermal growth factor receptor 2 (HER2). For EGFR and HER2 activating mutations are reported in around 30% of all solid tumors (22, 23). Downstream of EGFR are many other non-receptor kinases (e.g. PI3K/AKT, SRC) and other signal transducing proteins (e.g. RAS) of which almost all can even independently act as pro-oncogenes (23).

Oncogenes as regulators of apoptosis and chromatin remodeling

Most prominent oncogenic inhibitors of cell death belong to the Bcl-2 family. Although protein domains of the family are highly conserved, some of the family members act as pro-apoptotic proteins, while others act as suppressors of apoptosis. Among the latter the most prominent is the Bcl-2 protein. Its gene is often translocated in human B-cell lymphoma and Bcl-2 is able to work in synergy with MYC (19). Co-expression of both Bcl-2 and MYC in transgenic mice results in rapid tumor development (24).

Oncogenic chromatin remodeling proteins can either add or remove histone modifications, or use adenosine triphosphate (ATP) to remodel nucleosomes. Mutations of these factors are sometimes directly correlated with cancer while in other cases their effects are consequence of their influence on the expression of other genes (25).

Oncogenes as signal transducers

Among oncogenic signal transducers two distinct groups emerged: kinases and guanosine-triphosphate (GTP) binding proteins (6). As aforementioned, some of these kinases are oncogenic as a consequence of an active GF receptor but in many cases they can support the malignant phenotype regardless of GF receptor mutation status. One of such kinase axes is PI3K/AKT that can enhance glucose uptake and expression of glycolytic enzymes. Furthermore, PI3K/AKT can activate mammalian target of rapamycin (mTOR) that acts as nutrient sensor and regulates lipid and glucose metabolism next to protein synthesis (13, 26).

Another important proto-oncogene kinase is SRC. SRC is the best known member of SRC kinase family. SRC is a non-receptor tyrosine kinase that can be activated via GF receptors, integrin, hypoxia or loss of tumor suppressor PTEN (27). SRC protein is commonly upregulated and activated in different tumors and it is involved in processes of cancer progression, invasion and metastasis (28). Main downstream effectors of SRC are signal transducer and activator of transcription 3 (STAT3; stimulates the expression of VEGF, matrix metallopeptidases (MMPs) and interleukin-8 (IL-8)) and AKT. Furthermore, SRC can interact with p120 catenin and focal adhesion kinase (FAK) orchestrating initial events needed for cellular detachment and initiation of metastasis (27). An overview of SRC

downstream targets and protein-protein interactions is shown in Fig. 1. Intriguingly, we observed a correlation between SRC upregulation and down-regulation of lipolysis in lung cancer cells (1) which will be described in detail in Chapter 1.

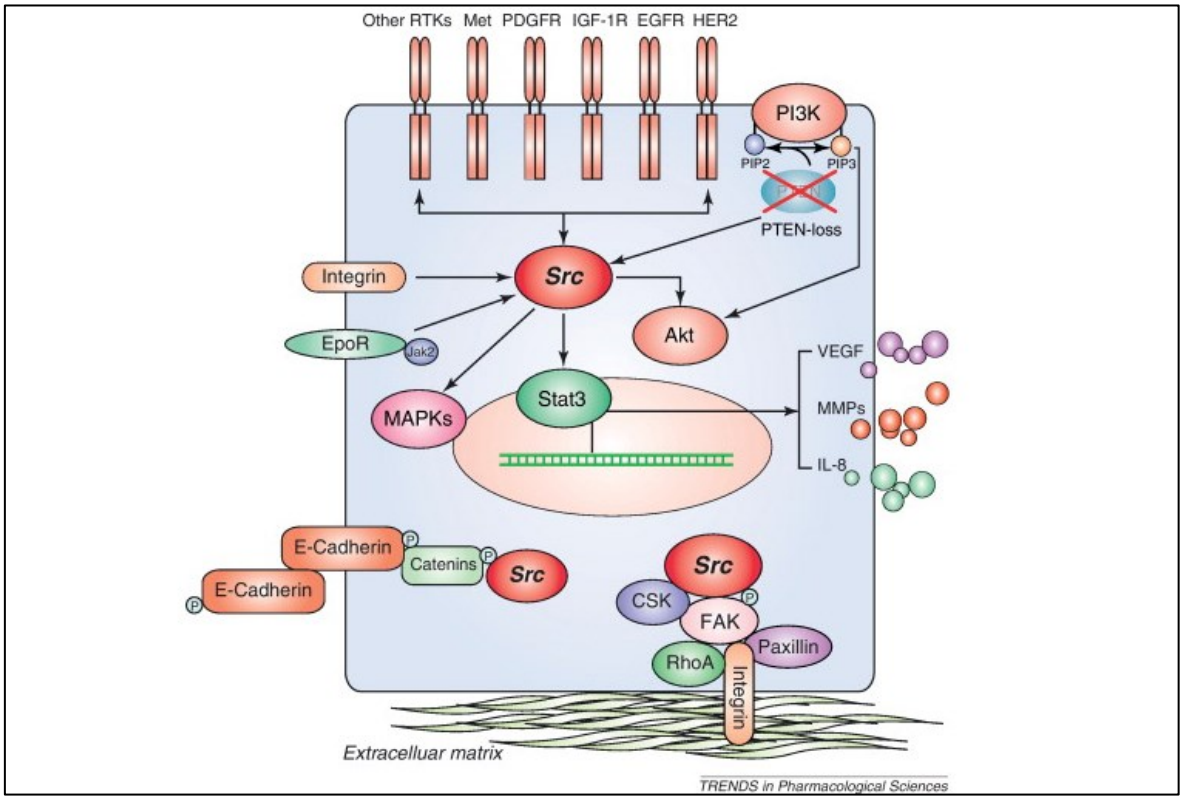

Figure 1. SRC signaling. SRC signaling can be activated via GF receptors, other tyrosine kinase receptors (RTK), other membrane receptors (such as integrins and erythropoietin receptor (EpoR)) and loss of PTEN activity. Human epidermal growth factor receptor 2 (HER2); insulin-like growth factor-1 receptor (IGF-1R); Janus kinase 2 (Jak2); mitogen-activated protein kinase (MAPK); matrix metallopeptidases (MMP); focal adhesion kinase (FAK); signal transducer and activator of transcription 3 (STAT3); vascular endothelial growth factor (VEGF); phosphatase and tensin homolog (PTEN); interleukin-8 (IL-8); reproduced from (27) with permission of publisher (Elsevier).

Of mutated GTP binding proteins the most notable ones are the Ras proteins HRAS, KRAS and NRAS. Ras proteins are mutated in 20% of all cancers (of which mutations of KRAS are most common). Usually mutations are located in the GTP binding pocket rendering proteins constitutively active. Mutated Ras proteins support cancer cell survival and proliferation (13, 29)

Metabolic alterations in cancer

Metabolic switch is one of the emerging cancer hallmarks (4). All cancers consume more glucose, produce more lactic acid even when oxygen is not limiting and generate more biomass (30). Furthermore, cancer cells are able to efficiently fuel their carbon metabolism with glutamine, especially when glucose and oxygen are limiting (17). Next to the changes to central carbon metabolism, alterations in lipid metabolism have been declared as another emerging cancer hallmark (4, 31). Most of cancer related metabolic changes are under strong influence of oncogenes and some of the most prominent cancer metabolic features will be further discussed.

Glucose metabolism

Since the discovery of Otto Warburg in 1920s it became evident that cancer cells metabolize glucose in ways uncommon for the majority of other cells. He observed that all tested tumors behaved uniformly - they used glucose derived pyruvate for the process of fermentation creating lactic acid (32). It was initially believed that this occurs instead of tricarboxylic acid (TCA) cycle and oxidative phosphorylation (OXPHOS) as a consequence of hypoxic induced mitochondrial damage (33), but shortly later became evident that despite increased fermentation mitochondria remain functional in cancer cells (34). However, the contribution of OXPHOS and mitochondria to the pool of ATP production depends on oxygen availability (35). As tumors grow, in their cores oxygen becomes limiting and tumors face hypoxic conditions. This drop in oxygen concentration is sensed by the cells activating HIF1 in response. HIF1 (especially the HIF1α subunit) facilitates glucose import into tumor cells by upregulating the expression of the key glucose transporters, Glut1 and Glut3 (36, 37). In addition to HIF1, other oncogenes such as KRAS, AKT, MYC and mutated p53 can also upregulate glucose import (36). Once glucose is inside of the cell, it is phosphorylated by hexokinases (HK) to yield glucose-6-phosphate (G6P) which in cancer is mainly directed to glycolysis, and partially to glycogenesis or pentose phosphate pathway (PPP). In the majority of normal cells this step is carried out by HK1, while in cancer cells mainly HK2 is active, characterized even as necessary for oncogenic transformation (38, 39). Both of the HK isoforms are HIF1 targets, as well as targets of KRAS, AKT, mTORC1 and MYC (36, 37). Other enzymes involved in glycolysis are as well

under strong oncogenic influence. For example, HIF1 activates aldolases A and C (ALDOA/C), which catalyze the reversible conversion of fructose-1,6-bisphosphate (F1,6BP) to glyceraldehyde 3-phosphate (G3P) and dihydroxyacetone phosphate (DHAP). HIF1, AKT and mutated RAS support the production of fructose 2,6-bisphosphate (F2,6BP) via 6-phosphofructo-2-kinase/fructose-2,6-biphosphatase 3/4 (PFK-2/FBPase 2, PFKFB3/4). F2,6BP is an essential activator of glycolytic flux through allosteric modulation of the rate-limiting enzyme of glycolysis, phosphofructokinase-1 (PFK1) (40). In addition, MYC, mTORC and HIF1 have been shown to activate pyruvate kinase isoform M2 (PKM2). PKM2 catalyzes the conversion of phosphoenolpyruvate (PEP) to pyruvate which is coupled to ATP production. PKM2 is overexpressed in a variety of cancers, and because it is slower than other PK isoforms, it redirects glucose derived carbons to biosynthetic pathways and supports the Warburg effect (41).

However, probably the two main enzymes favoring excessive pyruvate to lactate conversion are pyruvate dehydrogenase kinase 1 (PDK1) and lactate dehydrogenase (LDH) (42). Both of the enzymes are HIF1 targets and are often overexpressed in cancer. PDK1 phosphorylates and inhibits pyruvate dehydrogenase (PDH), preventing pyruvate entry to the TCA cycle (42). In this way, instead of being decarboxylated by PDH and shuffled into the TCA cycle, accumulated pyruvate is used as a substrate for LDH (predominantly isoform A, LDHA) which reduces it to lactate in an NADH dependent manner. For its role PDH is even referred as the “gatekeeper” enzyme, since excessive TCA cycle activity in cells undergoing malignant transformation leads to oxidative stress, manifested through reduced to oxidized glutathione (GSH/GSSG) ratio and induction of ROS dependent genes (43). The main alterations of glycolysis in cancer are shown in Fig. 2 with upregulated enzymes marked in red.

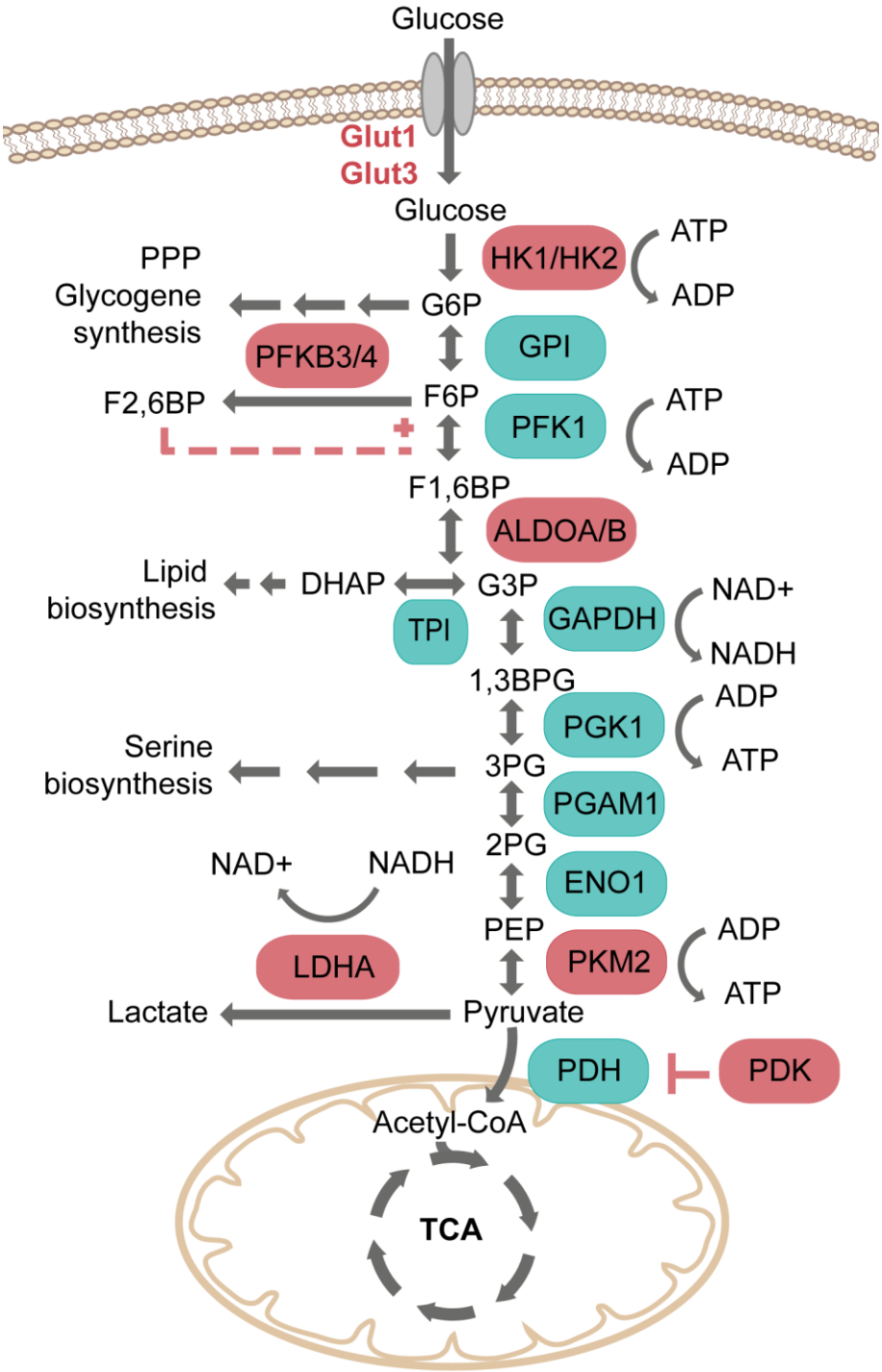

Figure 2. Glycolysis in cancer. Glut transporters and enzymes marked in red are regulated by oncogenes. HK1/2 -hexokinase 1/2; GPI - glucose-6-phosphate isomerase, G6P - glucose-6-phosphate; F6P - fructose-6-phosphate; PPP - pentose phosphate pathway; PFK1 - phosphofructokinase 1; PFKC3/4 - fructose-2,6-biphosphatase 3/4; F1,6P - fructose 1,6-bisphosphate; ALDOA/B - aldolase A/B; TPI - triosephosphate isomerase, G3P - glycerol 3- phosphate; DHAP - dihydroxyacetone phosphate; GAPDH - glyceraldehyde 3-phosphate

dehydrogenase; 1,3BPG - 1,3-bisphospho glycerate; 3PG - 3-phosphoglycerate; PGK1 - phosphoglycerate kinase 1; 2PG -2-phosphoglycerate; PGAM1 - phosphoglycerate mutase 1; PEP - phosphoenolpyruvate; ENO1 - enolase 1; PKM1/2 - pyruvate kinase M1/2; PDH - pyruvate dehydrogenase; PDK - pyruvate dehydrogenase kinase; LDHA/B - lactate dehydrogenase A/B; TCA - tri tricarboxylic acid cycle, ATP - adenosine triphosphate; ADP - adenosine diphosphate; NAD(P)H - nicotinamide adenine dinucleotide (phosphate).

Interestingly, and in line with Otto Warburg's observations, most cancer cells still produce lactate and upregulate glycolytic enzymes and glycolytic rates even when oxygen is not limiting, leading to the overall phenomenon termed aerobic glycolysis or the Warburg effect (30). Nevertheless, the TCA cycle remains functional and TCA metabolites are used to aid cancer growth. Few key enzymes of TCA cycle are mutated in some cancers: isocitrate dehydrogenase (IDH), succinate dehydrogenase (SDH) and fumarate hydratase (FH) (17). IDH mutations result in excessive production of D-2-hydroxyglutarate (D-2HG) from α-KG which does not accumulate under normal conditions and results in decreased α-KG and α-KG-dependent dioxygenase activities leading to an increase in histone and DNA methylation (44, 45).

Taken together, cancer cells modify their glucose metabolism to meet their requirements. While it might seem energetically unreasonable to perform aerobic glycolysis since it yields marely two over 38 ATP molecules produced by the TCA cycle and OXPHOS, cancer cells benefit from the switch in other ways. Firstly, upregulation of glycolysis results in accumulation of glycolytic intermediates that can be used in other anabolic processes needed to fuel cellular growth and proliferation (e.g. G3P to lipid biosynthesis, 3 - phosphoglycerate to serine *de-novo* synthesis, G6P to PPP and nucleotide backbone synthesis) (7, 36). The same is true for some of the TCA intermediates (e.g. citrate is used for fatty acid synthesis (FAS)) (46). Secondly, fermentation is simply a faster processes to restore oxidized nicotinamide-dinucleotide (NAD+) from NADH (42) without compromising oxidative status by performing excessive TCA cycles (43). Thirdly, produced lactate has a role of its own. Excreted lactate via monocarboxylate transporters (MCT1-4) reduces the pH of the tumor microenviroment influencing the immune response, stimulating vascularization and ultimately contributing to

radiotherapy resistance (47). Some cancer cells even re-uptake excreted lactate and use it as a carbon source (4).

Glutamine metabolism

Cancer cells uptake and use much larger amounts of glutamine compared to normal cells, a phenomenon termed “glutamine addiction”. Glutamine supplies cancer cells with carbon and nitrogen, and is involved in protection from oxidative stress (48). An overview of glutamine metabolism is depicted in Fig. 3.

In order for glutamine to be used as a carbon source it first undergoes the process of glutaminolysis, where it is converted to α-ketoglutarate (α-KG). α-KG can enter the TCA cycle and lead to production of downstream TCA metabolites (succinate, fumarate, malate) and reduction of nicotine amide dinucleotide phosphate (NADP+) to NADPH. Alternatively, α-KG can be used as a precursor for citrate by the enzyme IDH2 in a process termed reductive carboxylation (in the opposite direction of the regular TCA cycle). Resulting citrate is transported from mitochondria to the cytoplasm, where it is directed to lipid biosynthesis or used by IDH1 to produce α-KG and D-2HG. While the process of reductive carboxylation via IDH2 regenerates NADP+ from NADPH, the cytoplasmic step carried out by IDH1 uses NADP+ to produce NADPH in the first step (7, 20, 49, 50). Although glutamine cannot fully replace glucose when glucose is limiting cancer cells can run the TCA cycle on glutamine. Both uptake of glutamine and glutaminolysis are driven by MYC and KRAS oncogenes (17, 20). Hypoxia is the main driver for reductive carboxylation and most of reductive carboxylation occurs under hypoxic conditions (51).

Potentially even more important is the contribution of glutamine as a source of nitrogen. Once inside the cell, glutamine is converted to glutamate and released nitrogen can be used for nucleotide synthesis (48). Nitrogen from four glutamine molecules is used for purine biosynthesis, and nitrogen from one glutamine molecule is directed to pyrimidine biosynthesis (52). In the next step, as mentioned above, glutamate is converted to α-KG. This can be either carried out by glutamate dehydrogenase with release of ammonia, or by different aminotransferases that employing the amino group for synthesis of non-essential amino acids (48). Of

note approximately 50% of all non-essential amino acids are derived from glutamine (53).

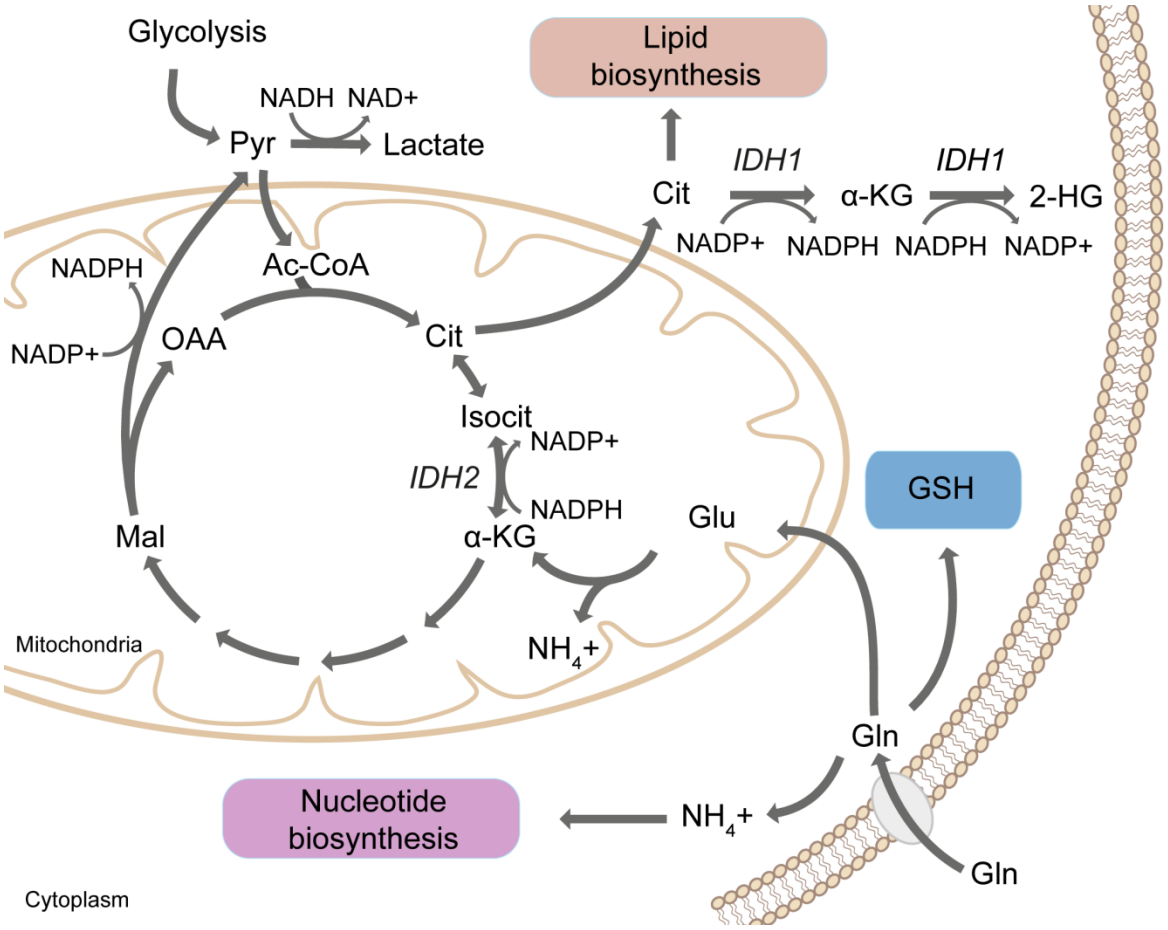

Figure 3 Overview of glutamine (Gln) metabolism in cancer. Glu - glutamic acid; Mal - malate; OAA - oxaloacetate; Ac-CoA - acetyl coenzyme A; GSH - glutathione, Isocit - isocitrate, Pyr - pyruvate, Cit - citrate, Isocit - isocitrate; α-KG - alpha ketoglutarate; IDH1/2 - isocitrate dehydrogenase 1/2; NAD(P)H - nicotinamide adenine dinucleotide (phosphate).

Furthermore, glutamine plays a major role in maintaining the cellular redox state. Firstly, as described above, the direction of glutamine metabolism strongly influences the cellular NADP+/NADPH ratio. Secondly, glutamine is the key precursor in synthesis of glutathione (GSH) (48). GSH (γ-L-glutamyl-L-cysteinyl-glycine) is a potent oxidant that protects the cells from xenobiotics and ROS, supporting cellular survival and proliferation (54). NAPDH enables regeneration of GSH from its inactive, oxidized form (GSSG) (55). GSH metabolism and its role in health and disease will be discussed in detail in Chapter 2.

At the initial step of GSH synthesis, glutamine derived glutamate is ligated with cysteine with the help of glutamate cystein ligase. Here availability of glutamate plays a dual role. In addition to being a central precursor, glutamate dictates cysteine availability. Glutamate is used in an anti-port system that excretes glutamate and imports cystin. Cystin is consequently converted to cysteine and used for GSH synthesis. In this way cellular antioxidant defense and survival rely heavily on glutamine availability (52).

Lipid metabolism in cancer

Cancer cells alter their lipid metabolism to provide more energy, synthesize lipid mediators that can act as signaling molecules and supply the cells with necessary building blocks. This is mainly reflected through an increase in fatty acid (FA) uptake and *de-novo* FA synthesis as well as FA catabolism (β-oxidation) (56, 57). While cancer related changes in FA metabolism are well established, the role of intracellular lipolysis as FA source in cancer remains controversial and will be further discussed in Chapter 1.

Fatty acid synthesis and import

All cells have two FA sources: exogenous (dietary) or endogenous (from *de novo* FA synthesis (FAS) or intracellular lipolysis) (58). Cancer cells perform much more *de novo* FAS compared to normal cells. In addition, they usually express high levels of fatty acid synthase (FASN), a property of highly proliferating tissues (59). The main precursor for FAS is glucose or glutamine derived citrate. Citrate produced in the TCA cycle in mitochondria is exported to the cytoplasm, where it is cleaved into acetyl-coenzyme A (acetyl-CoA) and oxaloacetate. The enzyme responsible for this action is ATP citrate ligase (ACL). ACL inhibition seems like a promising cancer target; however disturbance in acetyl-CoA homeostasis might also impose metabolic dysregulations on normal cells. The significance of ACL in tumorigenesis remains elusive (13, 57). The resulting acetyl-CoA is either carboxylated by acetyl-CoA carboxylase (ACC) to yield malonyl-CoA or directed to cholesterol synthesis (60). Malonyl-CoA is an important metabolite as it is a potent inhibitor of carnitine palmitoyltransferase I (CPT1), the key protein responsible for FA import into mitochondria for β-oxidation. Seven malonyl-CoA and one acetyl-CoA with the help of NADPH equivalents are then stepwise condensed by the

FASN to produce palmitic acid (PA, C16:0) (59). PA is further used for synthesis of non-essential mono- and poly- unsaturated fatty acids, β-oxidation or as a building block for synthesis of various complex lipids (phospholipids, storage lipids and sphingolipids) (58). FASN is commonly overexpressed in a variety of different cancers and some benign and neoplastic lesions (61). An overview of *de novo* FAS and the fate of FA is illustrated in Fig. 4.

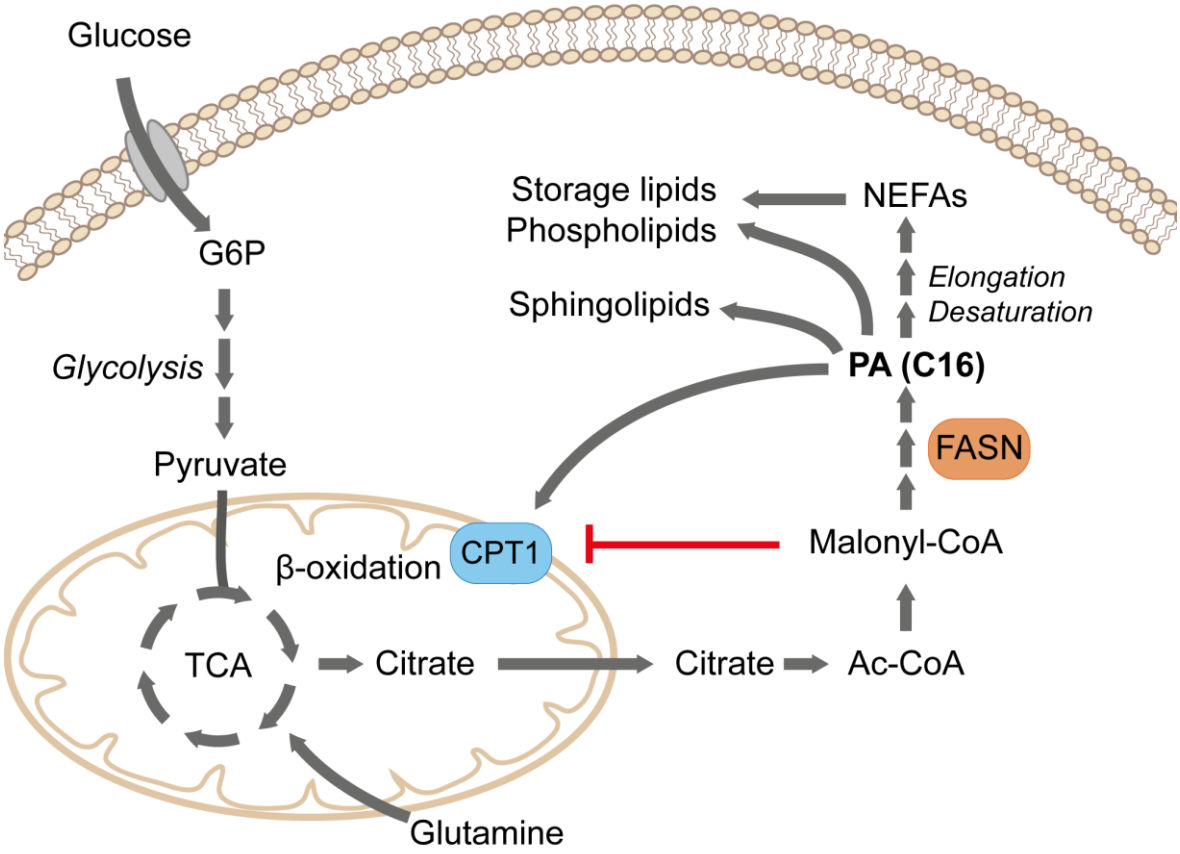

Figure 4. Fatty acid synthesis (FAS) is upregulated in cancer cells. Citrate derived from glucose or glutamine is used as precursor for *de novo* FAS. While ATP citrate ligase (ACL) and acetyl-CoA carboxylase (ACC) are not necessarily overexpressed in cancers with increased FAS, fatty acid synthase (FASN) almost always is. Resulting palmitic acid (PA) can be directed to various different pathways. NEFA - non-esterified fatty acid, TCA - tricarboxylic acid cycle; Ac-CoA - acetyl coenzyme A; G6P - glucose 6-phosphate.

In addition to on *de novo* FAS, already 70 years ago it was noticed that tumors are also likely to depend on their hosts to provide them exogenous lipid sources (62).

In line with these observations, we now know that many cancer cells despite *de novo* FAS also rely on increased FA uptake and tend to upregulate expression of the main FA transporters (especially pre-metastatic and metastatic cancers) (59, 63, 64). Many cancer types are even able to aid that “host dependence” by excreting signaling molecules to endorse FA release from surrounding tissue (59).

Fatty acid oxidation

Fatty acid oxidation (FAO) is a highly efficient process for providing energy. During FAO, FA chains get disassembled in increments of two, producing at each step of the cycle one acetyl-CoA molecule, one NADH and one reduced flavine adenine dinucleotide ($FADH_2$) (65). Electrons from NADH and $FADH_2$ can be then transferred onto oxygen in OXPHOS generating energy for ATP production, while released acetyl-CoA can re-enter the TCA cycle. Although hypoxia reduces FAO rates, FAO remains functional to some extent even under hypoxic conditions (60). The limiting step of FAO is FA import across the outer mitochondrial membrane via previously mentioned CPT1. CPT1 imports FA as carnitine esters and exist in two main isoforms, A and B. Isoform A is most widespread across tissues while isoform B is present mainly in muscles and brown adipose tissue. The third isoform, CPT1C, has also been reported in neurons but is not a mitochondrial enzyme. All three forms are inhibited by malonyl-CoA. In this way, cells can signal when to switch from catabolism to anabolism (FAS instead of FAO) (66). CPT1A is often overexpressed in cancer, especially in those types that show high dependence on exogenous and endogenous FA sources, such as breast and prostate cancer (67, 68). In addition, FAO seems to play a key role in the loss-of-attachment (LOA) to the extracellular matrix process. LOA requires a significant amount of ATP but in the same time results in accumulation of ROS. It seems that if cells are able to perform FAO for ATP production and manage consequent oxidative stress to survive LOA induced death (anoikis), it will likely support more aggressive cancer phenotypes (65).

Lipolysis

Neutral lipases

Exogenous and endogenous derived FAs together with other neutral lipids are eventually stored in the form of lipid droplets (LDs) (56). LDs are dynamic organelles which represent the main storage site of cholesterol and triacylglycerol (TG) in cells. Although the greatest concentration of LDs is found in adipocytes, they are ubiquitously present in all cells, just in much lesser extent (69-71). Intriguingly, higher LD content has been brought into correlation with malignant transformation in colon cancer (72), induction of metastasis in melanoma (73-75) and resistance to chemotherapy (76). LDs can also act as substrate resource for other lipid dependent enzymes that can co-localize to LDs and use the available lipids as precursors for various pro-inflammatory and signaling molecules (77).

In order to degrade TG stored in LDs, the multistep process of lipolysis must occur. The initial step of TG degradation is carried out by adipose triglyceride lipase (ATGL) (Fig. 5) ATGL is a 54 kDa patatin-containing domain (PNPLA2) serine hydrolase that has a high affinity towards TG but can also hydrolize retinyl esters in hepatic stellate cells (78, 79). ATGL hydrolizes TG releasing diacylglycerol (DG) and free FA (FFA) and has a preference towards long chain FA esters and the *sn-2* position of the glycerol backbone (80). Lipolysis is initiated with the activation of ATGL by its co-activator CGI-58. In non-stimulated adrenergic cells such as adipocytes CGI-58 is bound to the surface of LDs and hindered by a LD scaffold protein perilipin-1 (Plin-1). Upon stimulation, Plin-1 releases CGI-58 which can then co-localize with ATGL and activate it. In other cells most likely other members of the Plin family are responsible for this event. In contrast, a small molecule termed G0/G1 Switch Protein 2 (G0S2) acts as ATGL inhibitor. G0S2 also binds directly to ATGL to block its activity, but does not compete with CGI-58 for binding (81). In addition, two other regulators of ATGL have recently emerged: Hypoxia-inducible lipid droplet-associated protein (HILPDA) which inhibits ATGL in hypoxia (82, 83), and pigment epithelium-derived factor (PEDF), that is able to facilitate lipolysis in an ATGL-dependent manner (84, 85). The role of ATGL in cancer is still inconclusive and will be discussed in detail in Chapter 1. The complexity is further expanded by the fact that ATGL regulating

proteins have their own, sometimes as well ambiguous contribution to cancer metabolism, usually even independent of ATGL (86-88). For example, CGI-58 has been reported to exhibit pro- and anticancer properties in the same prostate cancer cell line (89, 90).

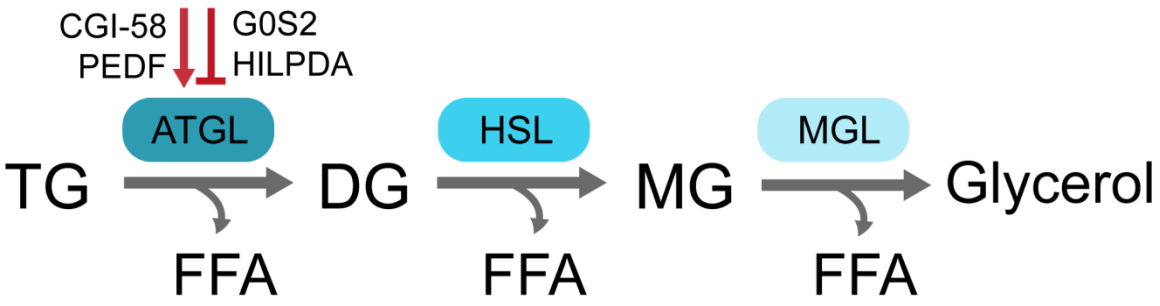

Figure 5. Lipolysis of neutral lipids. The first step is carried out by adipose triglyceride lipase (ATGL) which hydrolizes triacylglycerol (TG) to diacylglycerol (DG) and free fatty acid (FFA). ATGL is positively regulated by CGI-58 and pigment epithelium-derived factor (PEDF), while G0/G1 Switch Protein 2 (G0S2) and hypoxia-inducible lipid droplet-associated protein (HILPDA) act as ATGL inhibitors. In the second step of the cascade DG is converted to monoacylglycerol (MG) and FFA by the activity of hormone sensitive lipase. Lastly, monoacylglycerol lipase (MGL) converts MG to free glycerol and FFA.

The next step of the lipolytic cascade is carried out by hormone sensitive lipase (HSL), which results in conversion of DG to monoacylglycerol (MG) and FFA. HSL has a substrate preference for DG however unlike ATGL, HSL is able to hydrolyze TG, DG, MG, cholesteryl esters as well as retinylesters (91). HSL is mainly regulated via phosphorylation as it is phosphorylated on at least 5 different serine residues (92). In cancer, loss of both HSL and ATGL resulted in development of liposarcoma in mice (93), while the loss of HSL alone aids development of pancreatic ductal carcinoma (94).

Lastly, MG is hydrolyzed to glycerol and FFA by monoacylglycerol lipase (MGL). MGL as well is ubiquitously expressed in all tissues, highest in adipose tissue, testis and kidney (81). Together with fatty acid amide hydrolase, MGL also represents the main enzyme in the endocannabinoid degradation system, thus

exhibiting functions beyond neutral lipid degradation (95). The role of MGL in cancer is as well inconclusive. Fist studies from 2010 reported strong pro-oncogenic function of MGL as a key player in rearrangement of FA network in aggressive cancers, supporting invasion and cancer survival (96). However, recently a tumor suppressive role of MGL has been proposed in lung (97) and colorectal cancer (98). Additional work will be needed to elucidate the contribution of MGL to cancer metabolism.

Phospholipases

Phospholipases hydrolize phospholipids (PL) and as a result produce signaling molecules such as lysophosphatidic acid (LPA) and lysophospholipids (LPL), and precursors of signaling mediators (e.g. released arachidonic acid (AA) can act as a precursor for eicosanoid biosynthesis). Phospholipases A (PLA) can be cytosolic (cPLA) or secretory (sPLA) and cleave the acyl chains from the *sn*-1 (PLA_1) or *sn*-2 (PLA_2) positions of PL producing LPL. Phospholipases C (PLC) and D (PLD) are responsible for phosphodiester bond cleavage, resulting in production of DG, inositol triphosphate (IP_3), and phosphatidic acid (PA). All three phospholipase groups have been brought into connection with cancer. PLC and PLD are commonly activated through aberrant growth factor and/or other oncogene signaling, while PLA has been reported to have both growth promoting and growth inhibiting functions. Metabolites generated by all three phospholipase groups have been implicated in cancer invasion, metastasis, proliferation, inflammation and angiogenesis, mainly contributing to more aggressive cancer phenotypes. For an excellent summary on the phospholipase network in cancer one should refer to Park *et al*. (99).

Taken together, in order to exploit lipolysis as potential cancer therapeutic target we definitely need to understand more. By this end it is obvious that lipases are important nodes in metabolic and signaling cancer networks and hopefully future research will fully elucidate their exact roles.

1. CHAPTER ONE: THE ROLE OF ADIPOSE TRIGLYCERIDE LIPASE IN CANCER METABOLISM

The initial step of lipolysis, the hydrolysis of triacylglycerol, is carried out by ATGL whose implication in cancer is the subject of an ongoing controversy.

In breast cancer, ATGL has been reported to support tumor growth by being the critical element in the interaction between cancer cells and cancer associated adipocytes (100, 101). This is strongly supported through co-culture experiments and as well as clinical studies. However, another study in an aggressive breast cancer cell model suggests a protective role of ATGL from polyunsaturated FA induced lipotoxicity while the loss of ATGL does not significantly influence overall cancer cell death. The same study also reports that lipolytic activity of ATGL can be to some extent compensated with the activity of $sPLA_2$ (102).

For prostate cancer, a study using public cancer datasets showed that CGI-58, the co- activator of ATGL, is lost in metastatic castration-resistant prostate cancer. Their validation experiments performed on LNCaP prostate cancer cells demonstrated that while loss of CGI-58 was beneficial for invasiveness of cancer, loss of ATGL had a negative effect (89). This is in line with previous similar observations in colorectal cancer (87). On the contrary, another study performed on the same LNCaP cell line showed that CGI-58 was markedly increased in prostate cancer cells compared with peripheral blood mononuclear cells and that loss of CGI-58 significantly impaired prostate cancer cell growth inducing apoptosis (90). Another analysis of prostate cancer associated fibroblasts showed that expression of ATGL was significantly reduced compared to non-cancer related fibroblasts (86).

In addition, ATGL is reported to be up-regulated in human hepatocellular carcinoma and higher ATGL expression has been observed in pancreatic ductal adenocarcinoma (87, 103).

A recent study demonstrates inhibition of ATGL in hypoxia and highlights the inhibition as one of the main mechanism enabling cancer survival under oxygen deprived-conditions (83). Furthermore, the ATGL gene deletions are reported to happen in 25% of all cancers, with the highest numbers of loss in ovarian serous cystadenocarcinoma (59%), bladder urothelial carcinomasarcoma (42%), sarcoma

(40%) and lung cancer (38%) (104). This is not surprising as the chromosomal position of the ATGL gene (11p15.5) has been reported to be often mutated or deleted in cancer (105).

Genetic ablation of both ATGL and HSL lead to development of liposarcoma in mice (93) and heart rescue ATGL-KO mice spontaneously developed lung neoplasia as they age (104). While this *in vivo* lung cancer promoting phenotype is not in accordance with a previous study where ATGL was silenced in an *in vitro* lung cell model (106), we show in contrast that deletion of ATGL using CRISPR/Cas9 in lung cancer cells results in more aggressive phenotype (1).

It is noteworthy to mention that in addition to the direct influence on tumor initiation, progression and metabolism, ATGL also contributes to cancer associated cachexia and inhibition of ATGL-driven lipolysis has been recommended as a therapeutic approach in cachexia treatment (107).

Considering that the most prominent phenotype for ATGL has been observed in lung cancer where our knowledge regarding the role of lipolysis is very limited, we knocked-out ATGL in the A549 lung cancer cell model to investigate how that would affect cancer cell aggressiveness.

Lung cancer is the leading cause of cancer related death in both male and females, and in the US in 2017 accounted for the same death incidence as colon, breast, prostate and pancreatic cancer combined (108). Lung cancer is classified in two large groups: small cell lung cancer (around 15% of all cases) and non-small cell lung cancer which is comprised of adenocarcinoma, squamous and large cell carcinoma and accounts for the remaining 85% of all lung cancers (109). Given that approximately every 8^{th} new cancer case in both man and women is due to lung cancer (108), the need for better therapeutic approaches and strategies is high. We observe that inhibition of lipolysis activates pro-oncogenic signaling in lung cancer cells rendering the model more aggressive and provide data in support of a tumor suppressor role of ATGL in this cancer type. Therefore, stimulation of lipolysis might be a promising approach in treatment of lung cancer.

Materials and methods (Chapter 1)

Most of the text from this section has been slightly adapted or entirely taken from my paper Tomin *et al*. 2018 (1).

Reagents

If not stated otherwise chemicals were purchased from Sigma Aldrich.

Cell culture

A549 lung adenocarcinoma cells, human embryonic kidney cells 293 (HEK-293) cells, NCI-23 lung adenocarcinoma cells and AML-12 murine hepatocytes were obtained from CLS (Eppelheim, Germany). A549 cells were cultivated in Ham's F-12K (Kaighn's) (F12K) with 10 % fetal bovine serum (FBS) while AML-12 cells were cultured in 1:1 mixture of Dulbecco's Modified Eagle's Medium (DMEM):F12K supplemented with 10% FBS, 1% ITS Liquid Media Supplement, 40 ng/ml dexamethasone and 1% PenStrep (P/S). HEK293 cells were cultured in DMEM, supplemented with 10% FBS. NCI-H23 cells were kept in RPMI supplemented with 10% FBS. LLC1/LL2 cells were acquired from ATCC and kept in DMEM containing 10% FBS and 1% P/S. All cells were grown at 37 °C, 5% CO_2.

Spheroids preparation (3D culture)

10.000-100.000 ATGL-KO and control A549 cells/well were seeded into Ultra-low attachment multi-well plates (Thermo Fischer Scientific, USA), forced to center by centrifugation and cultivated for 10 days with regular media replenishment. 30 spheroids per each cell line were used for proteomics analysis (a total of 6 samples/cell lines).

ATGL knock-out with CRISPR-Cas9

Procedure was performed as described in the published manuscript (1). CRISPR/Cas9 transfection was performed on 100.000 A549 cells after over-night culture using Lipofectamine3000 (Thermo Scientific, USA) according to the manufacturer's protocol. Human ATGL CRISPR-Cas9 knockout (KO) plasmid (sc-401711; Santa Cruz, USA) was co-transfected with the homology directed repair

(HDR) plasmid (sc-401711-HDR). The HDR plasmid harbored the red fluorescent protein (RFP) which later was used for later monitoring of the transfection and fluorescence activated cell sorting (FACS, one cell per well of 96-wells plate). Single cells clones were expanded and KO was validated by western blot for ATGL and qPCR for ATGL mRNA levels. As control, separate batches of cells was transfected with a control plasmid (Santa Cruz, sc-418922) as aforementioned, then diluted to single cells and expanded. Furthermore, the area in the genomic DNA around Cas9-induced double strand break was sequenced for all clones (ATGL-KO and controls) (LGC Genomics, Berlin, Germany).

Sequencing and sequence alignments of ATGL-KO and control clones

Genomic area of ATGL gene between exon two to exon five was amplified prior to sequencing using LongAmp® Taq PCR Kit (New England Biolabs, USA) according to manufacturer's instructions with primers: 5´ - CCTCTTCCTCTGAACTTTGTCC - 3´(forward) and 3´- CTCCTCTCTCTCTTTCCCTCCT - 5´ (reverse). Obtained PCR products were purified on an agarose gel, then excised from the gel using GenElute gel extraction kit and subjected to sequencing by LGC genomics (Berlin, Germany) with primers: 5´- GGCAGGCAGTTGGGAAATAC -3´ (forward) and 3´- TGGGCACTCAGAAGTCAAAGG -5´ (reverse). Sequence alignments were performed using MUltiple Sequence Comparison by Log- Expectation tool (MUSCLE; http://www.ebi.ac.uk/Tools/msa/muscle/)

LD imaging and volume analysis

LD imaging was carried out as previously described (1). LDs of A549 ATGL-KO and control cells were stained with HCS LipidTOX™ Deep Red Neutral Lipid Stain (Thermo Fisher Scientific, USA) and BODIPY™ 493/503 (Thermo Fisher Scientific, USA), diluted 1:750 and 1:1000 in PBS, respectively. BODIPY™ staining was performed for 10 min at 37 °C followed by 10 min fixation with 3.7 % formaldehyde in PBS, while cells were fixed prior LipidTOX™ Deep Red staining. Cells were then rinsed 3 (if LipidTOX™ Deep Red stained) or 5 times (if BODIPY™ stained) with PBS, after which VECTASHIELD® antifade DAPI containing medium (Szabo-Scandic was mounted. Image acquisition was performed on a Zeiss LSM 100 or a Nikon A1+ confocal laser scanning microscope with a 405 nm diode laser and 450/50 BP filter for DAPI, a 488 nm

argon laser with a 525/50 BP filter for BODIPY™ and a 642 nm NeHe laser and 700/75 BP filter for LipidTOX™ Deep Red. Data interpretation was carried out using FIJI (Version 1.51h). Prior to LD volume quantification, maximum intensity projection and auto-threshold Kapur-Sahoo-Wong (maximum entropy) methods were applied. LD number per cell was derived from 55-86 cells of each of the three individual ATGL-KO (in total 198 cells) and three control cell clones (in total 228 cells), respectively.

Targeted lipidomics

Non-polar metabolite extraction and measurement was carried out as described previously (1, 110, 111). Briefly, pellets from 2 x 10^6 A549 ATGL-KO (three single cell derived clones) and control cells were re-suspended in 1 ml of PBS and combined with a chloroform:methanol mixture (2:1) which contained internal standards (dodecylglycerol for positive and pentadecanoic acid for negative mode). After extraction, the lower lipid containing phase was moved to a new tube and dried down. Dried lipid extracts were re-constituted in 120 µl of chloroform. Injection volume was 10 µl. Samples were analyzed by a published method based on liquid chromatography coupled to mass spectrometry (LC-MS/MS) (111). Chromatography was performed using Luna reverse-phase C5 column (50 mm x 4.6 mm, 5µm, Phenomenex) at the flow rate of 0.5 ml/min. Mobile phase A was 95:5 water:methanol, supplemented with 0.1% formic acid and 5 mM ammonium formate, while B was 60:35:5 isopropanol:methanol:water to which 5 mM ammonium formate and 0.1% ammonium hydroxide were added. The used detector was an Agilent 6430 triple-quadrupole instrument operated in multiple reactions monitoring (MRM) mode with the following parameters: fragmentor voltage 100 V, capillary voltage 3.0 kV, drying gas flow rate 10 l/min, drying gas temperature 350 ^{o}C and nebulizer gas pressure 35 psi. Collision energies were pre-optimized for each analyte.

Normalization of the obtained data was performed based on the internal standard and the area of the total ion chromatogram (sum of all monitored transitions) from each sample. For statistical analysis, Perseus (version 1.5.8.5) (112) was applied. The significance cut-off criteria after upon multiple-testing correction were:

unpaired student's t-test p-value < 0.05, permutation based false discovery rate (FDR) < 0.05 and S0 value of at least 1.5.

Proteomics

Proteomics analysis was done as published (1). In short, cell pallets of four ATGL-KO and four control A549 cell clones were lysed by sonication in lysis buffer (100 mM Tris pH = 8, 1 % sodium dodecyl sulfate (SDS), 10 mM tris(2-carboxyethyl)phosphine hydrochloride (TCEP), 40 mM 2-chloroacetamide). Extracted proteins (200 µg per sample) were further processed according to a modified Filter Aided Sample Preparation (FASP) protocol (113). LC-MS/MS was performed using nano-LC and Acclaim PepMap RSLC C18 nanocolumn (2 µm, 50 x 75 µm) (Thermo Scientific, USA) coupled to a maXis II ETD Q-TOF (Bruker Daltonics, Germany) operated in positive mode.

Proteomics samples from 3D cultured clones were lysed as described but here acetone precipitation for protein isolation was applied. Briefly, upon lysis and protein determination 100 µg of protein of each sample was precipitated with acetone overnight, then re-dissolved in 25% trifluoroethanol (in 100 mM Tris pH=8.5), diluted to 10 % TFE with ammonium bicarbonate and digested with LysC for 2h followed by overnight trypsin treatment. Prior to measurement samples were diluted in running buffer A and analyzed with nano-LC-MS/MS. Chromatographic separation was carried as described for A549 label free quantification (LFQ) data. Orbitrap Velos Pro was used as a detector operated in positive mode.

Data was quantified employing the LFQ algorithm incorporated in MaxQuant (version 1.5.8.3) (114), while for statistical analysis Perseus (version 1.5.8.5)(112) was used. Match-between-run feature was allowed for the retention time window of 1 min with an alignment window of 20 min. For database search the FDR was set to 1%.

Statistical analysis in Perseus was performed on the dataset filtered for at least 4 valid values (i.e. greater than zero) of at least one group. The remaining missing values were imputed from a downshifted normal distribution using standard settings. The statistical test used was an unpaired Student´s t-test with a permutation-based multiple testing correction (S0 value of 2, permutation based

FDR control of 1%). For 3D culture, filtering criteria were at least 3 valid values per group and the S0 value for permutation-based multiple testing correction was 0.5. All other settings were the same as for the 2D culture dataset.

Principle component analysis (PCA) was carried out on the preprocessed dataset with centered variables and hierarchical clustering (HC) employing Euclidean distance measure and Ward's agglomeration method (115). For these purposes the R statistical computing software (v. 3.2.2, https://www.r-project.org/) was used. PCA was performed with the function prcomp; while for HC the functions dist and hclust as well as the function heatmap.2 in R gplots (v. 3.0.1) were employed (https://CRAN.R-project.org/package=gplots). Reprinted from (1). Copyright (2018) American Chemical Society.

For functional analysis of proteomic data, enrichment of gene ontology (GO) terms of biological processes of proteins with a minimum absolute difference of log2 LFQ intensities between groups of 0.5 was performed. Reprinted from (1). Copyright (2018) American Chemical Society.

Published proteomics data was deposited to the ProteomeXchange Consortium (116) (http://proteomecentral.proteomexchange.org) via the PRIDE partner repository with the data set identifier PXD007223. (Reviewer account details: Username: reviewer67902@ebi.ac.uk; Password: r0f0d7se).

MS-based validation of differential SRC protein abundance

Protein samples were prepared as aforementioned. LC-MS/MS was carried out as described with Orbitrap Velos Pro (Thermo Scientific, USA) as detector operated in positive mode with dynamic exclusion enabled. The mass list of expected SRC peptides was imported as an inclusion list (masses: 443.73, 446.76, 494.26, 516.77, 520.30, 608.30, 642.83, 736.05 and 856.92). Data was as well analyzed with MaxQuant (1).

qPCR

Total RNA was isolated from cells using the RNA easy kit (Qiagene, Netherlands) and used for quantitative PCR (qPCR) according to the manufacturer´s instructions using Maxima SYBR Green (Thermo Fisher Scientific, USA). For cDNA synthesis either Maxima RT (Thermo Fisher Scientific, USA) or QuantiTect

Reverse Transcription Kit (Qiagen, Netherlands) were employed. As housekeeping gene cyclophilin A with the primers 5´-CCCACCGTGTTCTTCGACATT-3´ (forward) and 5´-GGACCCGTATGCTTTAGGATGA-3´ (reverse) was used. The primers for SRC were 5´-TGTTCGGAGGCTTCAACTCC-3´ (forward) and 5´-TGTGTTGTTGACAATCTGGAGC-3´ (reverse). For $cPLA_2$ the forward primer was 5´- TACCAGCACATTATAGTGGAGCA-3´ and the reverse one was 3´-GCTGTCAGGGGTTGTAGAGAT-5´. For ATGL two sets of primers were used: 1. forward 5´-GCTTCCTCGGCGTCTACTAC-3´ and reverse 5´-CAATGAACTTGGCACCAGCC-3´and 2. 5´- GGCTTCCTCGGCGTCTACTA-3´ (forward) and 5´-TTTACCAGGTTGAAGGAGGGG-3´ (reverse) (1).

Lentiviral ATGL Knock-in

Third generation lentiviral vectors for human ATGL (pLV[Exp]-Neo-EFS>hPNPLA2[ORF016935]) and control green fluorescent protein (GFP) (pLV[Exp]-Neo-EFS>EGFP) were purchased from VectorBuilder (Cyagen Bioscience, USA). Viral packaging system (Addgene, USA) was consisted of pMD2.G (Addgene plasmid # 12259), pRSV-Rev (Addgene plasmid # 12253) and pMDLg/pRRE (Addgene plasmid # 12251) (1).

Viral transfection of HEK293 was performed in 10 cm dishes in triplicates. On the day of transfection (day 1), HEK293 medium was replaced with 6 ml DMEM containing 10% heat inactivated serum (HIS). Transfection was performed using Lipofectamine LTX (Thermo Scientific, USA) with 2 µg of each packaging plasmid and 2 µg of ATGL or GFP vector per sample. On day 2, the medium from the HEK293 cells was exchanged and the target cells (three different ATGL-KO A549 clones) were prepared for viral transfection. On day 4, target cells' medium was exchanged with 5 mL of DMEM containing 10 µg/mL polybrene. On days 5 and 6, virus containing media from HEK293 cells was transferred onto the target cells after being filtered through a 0.45 µm filter. After a day in culture (day 7), the medium from target cells was replaced with 10 mL of fresh RPMI supplemented with 1000 µg/ml gentamicin. The selection period was two weeks with regular replenishment of fresh medium and antibiotic (1).

Western blotting

Protein extracts were prepared after lysis and sonication in either 100 mM TrisHCl pH 8 or CST buffer (Cell Signaling Technology (CST), Danvers, MA, USA). For treatment with atglistatin cells were incubated with either 80 µM atglistatin (kind gift from Prof Rudolf Zechner, University of Graz) or with the same volume of DMSO used as vehicle (for control cells) for 16 h prior harvesting. For arachidonic acid treatment cell were incubated for 24 h with 30 or 60 µM arachidonic acid prior to lysis. Antibodies against ATGL (#2138S), SRC (#2109) and phospho-SRC (pSRC, #6943) and vinculin (#4650) were obtained from CST, USA. Antibodies for beta-actin and $cPLA_2$ were purchased from Sigma Aldrich (#A5441 and #SAB4200210, respectively). Horse radish peroxidase (HRP)-linked anti-rabbit antibody from CST (#7074) was used as secondary antibody except for the detection of beta-actin where an anti-mouse secondary antibody linked to HRP was used (#7076). Proteins (20-30 µg per lane) were separated on SDS-PAGE gels (Invitrogen, USA) and transferred onto a PVDF membrane (Bio-Rad, USA). Membranes were blocked with either 5 % BSA in tris-buffered saline containing Tween 20 (TBS-T) (pSRC, SRC, $cPLA_2$) or 5% skim milk in TBS-T (ATGL, beta-actin, vinculin). Primary antibodies diluted in their blocking buffers were incubated with membranes overnight at 4 °C. Incubation with secondary antibody was done for 1 h at room temperature. Proteins were visualized using ECL (GE Healthcare, UK) and detected on a ChemiDoc System (Bio-Rad, USA) (1).

Migration

Gap closure ("scratch") assay: Confluent cells in a 12 well plate were washed with PBS, and then scratched in the middle of the well using a p200 pipet. Consequently, cells were washed to remove floating ones and supplied with fresh medium containing: 20 nM SRC inhibitor KX2-391 (Selleckchem, Germany) (for A549 cells), 80 µM atglistatine (for AML-12 cells and LLC1/LL2 cells) or DMSO vehicle. Pictures were acquired from an inverted microscope at 4 x magnification. Gap size was measured at 3 different points using ImageJ software or the change of the gap area was measured (Version 1.46r) (1).

Transwell assay: Prior to the assay, all cells were serum starved for 1h to induce better migration towards the FBS rich media (10% FBS) in the lower chamber.

Then 5-10 x 10^4 serum starved cells were seeded on top of the transwell chambers in serum free medium. For LLC1/LL2 cells the upper part of the transwell chamber was coated with collagen to aid cell spreading. For the migration experiment with SRC inhibitor, seeding medium contained 20 nM of KX2-391, whereas for atglistatin treatment 80 µM atglistatin was added. For both treatments DMSO was used as vehicle control. Cells were allowed to migrate through the membrane during 20-48 h after which they were fixed, stained (Diff Quick Stain kit, Thermo Fisher, USA) and visualized using an inverted microscope. Three fields per well at 20 x magnification were used for counting the cells.

Survival of A549 clones (SRC inhibitor treatment control)

40.000 cells/well (N=3 for ATGL-KO and control, respectively) were seeded in a 96 well plate in serum free media. After 24 h cells were washed once with PBS, then stained with 100 µL Hoechst (0,013 mg/mL) in 10% formaldehyde/PBS and incubated for 15 min in the dark at RT. After incubation, the staining solution was removed, the cells were covered with 100 µL PBS and the absorbance was read out on a SpectraMax i3 (Molecular Devices, USA) with excitation at 350 nm and emission at 461 nm. Reprinted from (1). Copyright Copyright (2018) American Chemical Society.

Statistics

If not stated otherwise a two sided unpaired Student's t-test was performed with $p<0.05$ as significance threshold, and mean and standard error of mean are depicted in bar plots.

Results (Chapter 1)

Low expression of ATGL in cancer is correlated with poor survival outcome

To address how ATGL expression correlates with cancer patient outcome we accessed the public data repository named The Cancer Genome Atlas (TCGA) using Xena Browser (https://xenabrowser.net/heatmap/). For this purpose, the lung adenocarcinoma dataset (LUAD) of 877 patients was used as well as the "all cancers" dataset (PANCAN) comprising data of 12839 patients. In both cases, following the median survival during the period of 16 years, lower ATGL expression was correlated with worse survival outcome (Fig. 6). Similar results were obtained using the Pathology Atlas feature of Protein Atlas (https://www.proteinatlas.org/ENSG00000177666-PNPLA2/pathology/tissue/lung+cancer).

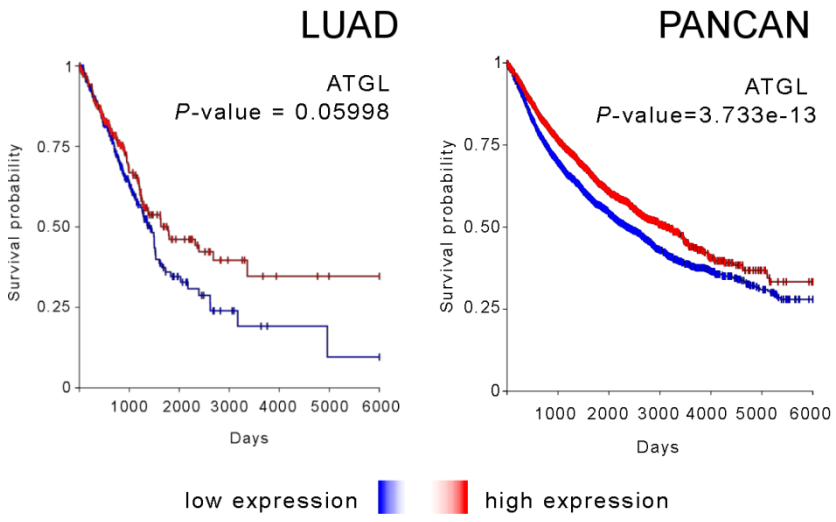

Figure 6. Low ATGL expression correlates to worse survival outcome in cancer patients. LUAD – TCGA lung adenocarcinoma data set, PANCAN – TCGA all cancer data set. Source: https://xenabrowser.net/heatmap/

ATGL knock out in lung cancer cells causes TG and bioactive lipid accumulation

In order to investigate the consequences of ATGL loss in lung cancer, we decided to use CRISPR-Cas9 technology and introduce a double strand break (DSB) in the

ATGL gene in A549 lung carcinoma cells. To reduce mutation probability and facilitate selection of the knock-out (KO) clones we used a homology directed repair (HDR) plasmid which harbored an antibiotic and a fluorescent marker and which was further used as a template for validation of the KO clones by sequencing. Validation experiments revealed that in ATGL-KO cells Cas9 induced the DSB in exon 3 of the ATGL gene which caused deletion of the ATGL ORF between bp 2868 and 3604 due to the integration of the HDR plasmid. Sequence alignments of the clones are shown in Appendix 1AB. Consequently, there was no residual ATGL mRNA (Fig. 7A) or protein (Fig. 7B) in the isolated ATGL-KO single cell clones detectable (1).

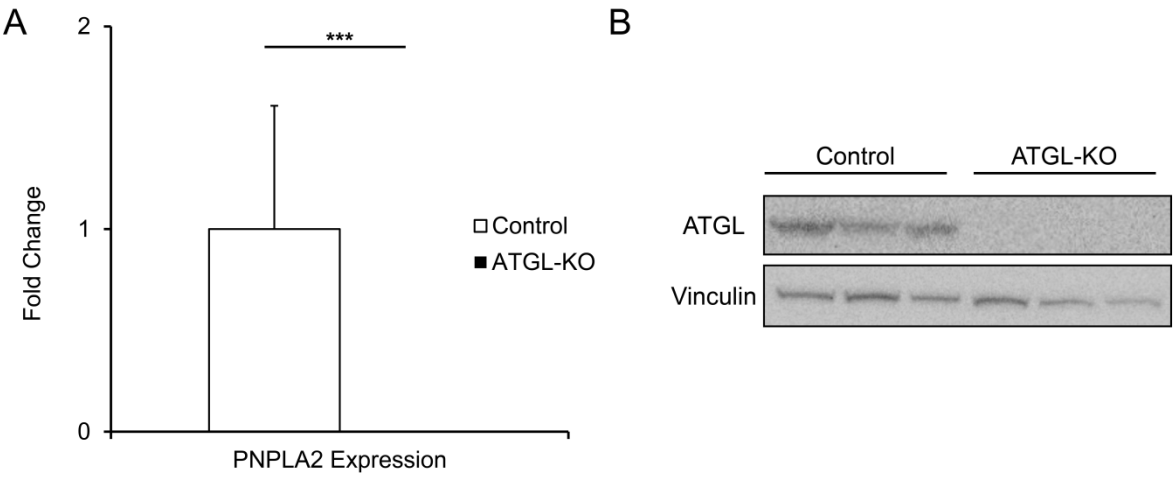

Figure 7. Deletion of ATGL gene by CRISP-R/Cas9 resulted in the loss of ATGL protein and mRNA expression. A: qPCR of PNPLA2 (Patatin Like Phospholipase Domain Containing 2, ATGL gene) with cyclophilin A as housekeeping gene; N=3 single cell derived clones per group, data from two independent experiments; ***p < 0.001; B: Western Blot of ATGL protein. Demonstrated is one of three similar experiments. Reprinted from (1). Copyright (2018) American Chemical Society.

Loss of ATGL caused a fourfold increase in the LD content of the ATGL-KO cells compared to control cells (Fig. 8AB). As expected, the predominantly accumulated lipid class in ATGL-KO was TG. Out of around 180 quantified lipid metabolites, the abundance of TG species was correspondingly three to four times higher in the ATGL-KO as compared to control cells (Fig. 9). List of measured lipid metabolites

in positive mode (which was used for the statistical analysis) is presented in Appendix 2.

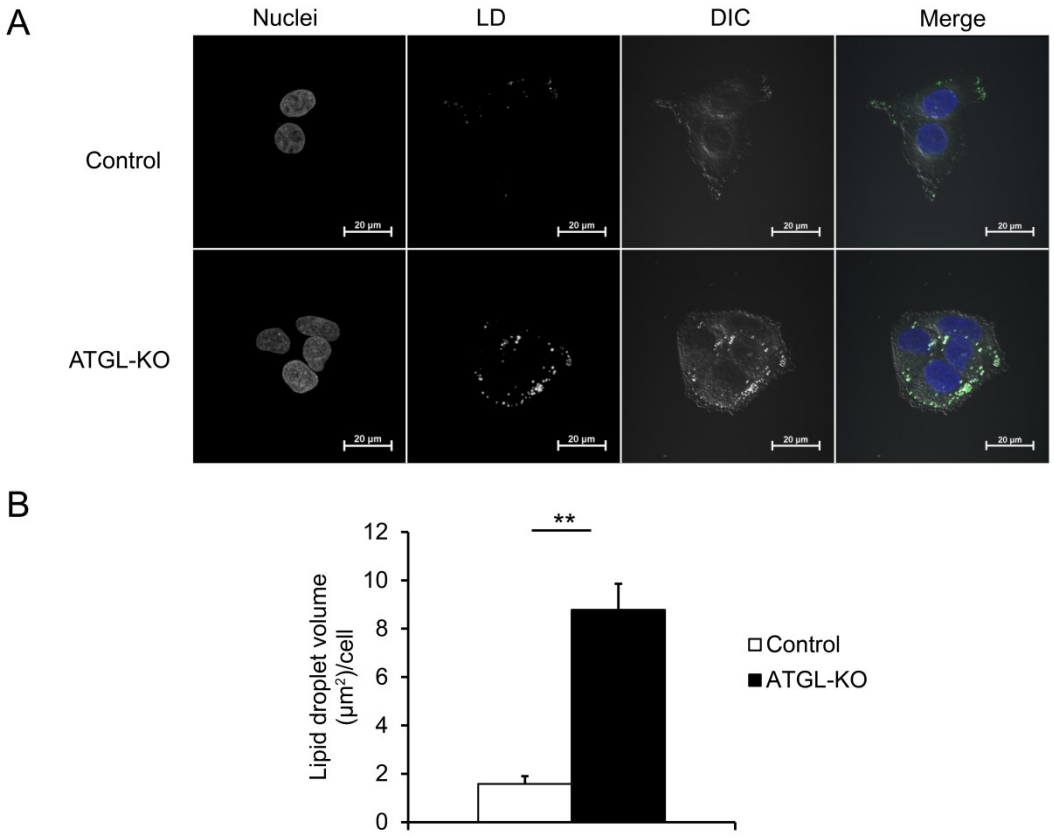

Figure 8. ATGL-KO cells accumulate lipids in form of lipid droplets (LD). A: Cells labelled with DAPI for cell nuclei and BODIPY for LD visualization; B: Results from LD quantitation (N=3 cell lines derived from single cell clones per group, > 50 individual cells per cell line); ** $p < 0.01$. Reprinted from (1). Copyright (2018) American Chemical Society.

In addition to TGs, an increase of around twofold could be observed for different LPL species as well as a slight increase in also bioactive ether lipids (117) in ATGL-KO cells (Fig. 9).

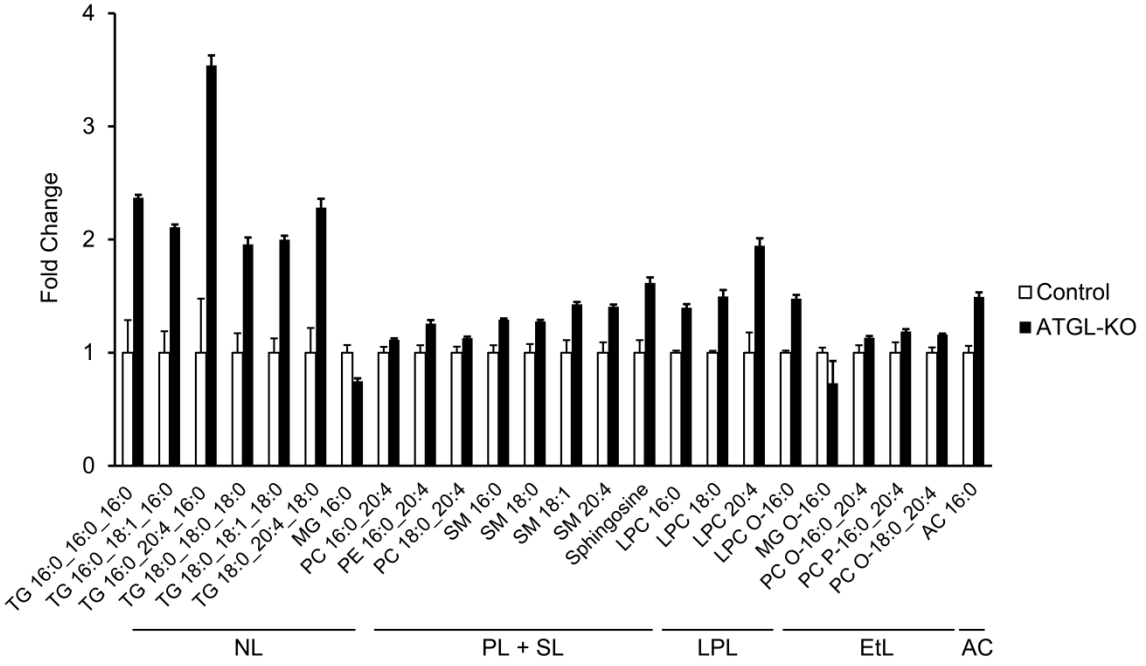

Figure 9. Changes in the lipid profile of A549 ATGL-KO cells. Bars represent fold changes as compared to control ± normalized S.E.M. N=3 individual ATGL-KO single cell derived cell lines, N=5 replicates per cell line, Welch t-test $p < 0.05$, multi-test correction: permutation based FDR < 0.05, S0 = 1.5 (NL - neutral lipids, PL + SL - phospholipids and sphingolipids, LPL - lysophospholipids, EtL - ether lipids, AC - acylcarnitine; TG - triacylglycerol, MG - monoacylglycerol, PC - phosphatidylcholine, PE - phosphatidylethanolamine, SM - sphingomyelin, LPC-lysophosphatidylcholine). Reprinted from (1). Copyright (2018) American Chemical Society.

As previously mentioned, LPLs are products of phospholipase A activity and can have various signaling functions (118-120), leading us to hypothesize that ATGL loss leads to changes in expression of some PLAs. We investigated the enzyme mainly responsible for LPL production, cellular phospholipase A2 (cPLA2) and indeed observed higher levels of both $cPLA_2$ protein and gene in ATGL-KO cells (Fig. 10ABC).

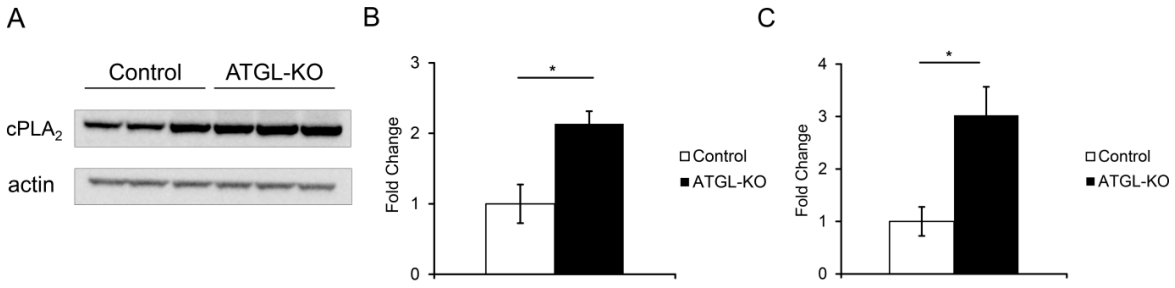

Figure 10. cPLA2 is upregulated in ATGL-KO cells on protein and gene level. A. Western blot for cPLA2 in ATGL-KO and control cells. B. Volume analysis of A. C. qPCR for cPLA2 gene, N=3 individual cell lines derived from single clones, Student t-test, * p-value < 0.05.

ATGL loss results in upregulation of SRC kinase in A549 lung carcinoma cells

Since upregulation of phospholipase activity is usually a secondary event to oncogene activation (99), we decided to measure changes of the proteome of cells lacking ATGL by a label free quantitative proteomics approach (121) (Fig. 11). As pre-requirement was that at least two individual peptides per protein had to be confidently measured otherwise the algorithm returned a value of 0 and these cases were treated as missing values. Prior to statistical testing these values had to be either removed or imputed. Therefore, although our LC-MS/MS measurements from four biological replicates per group (ATGL-KO and control) yielded a list of approximately 2100 proteins, the data matrix was filtered for missing values to keep only those proteins that were quantified in at least all four samples of one group. Remaining missing values were then imputed from a downshifted normal distribution. This resulted in a reduction of the data matrix to 679 proteins (Appendix 3). This data matrix was then subjected to unpaired Student´s t-testing with permutation-based multiple testing correction (FDR of 1% and S0 of 2). With such a stringent significance threshold, two proteins turned out to be significantly upregulated in ATGL-KO cells: proto-oncogene tyrosine kinase SRC and nesprin-1, with the first being the most upregulated one (Fig. 11A). Furthermore, a clear discrimination between ATGL-KO and control cell was

observed by principal component analysis (Fig. 11B) and hierarchical clustering (Fig. 11C).

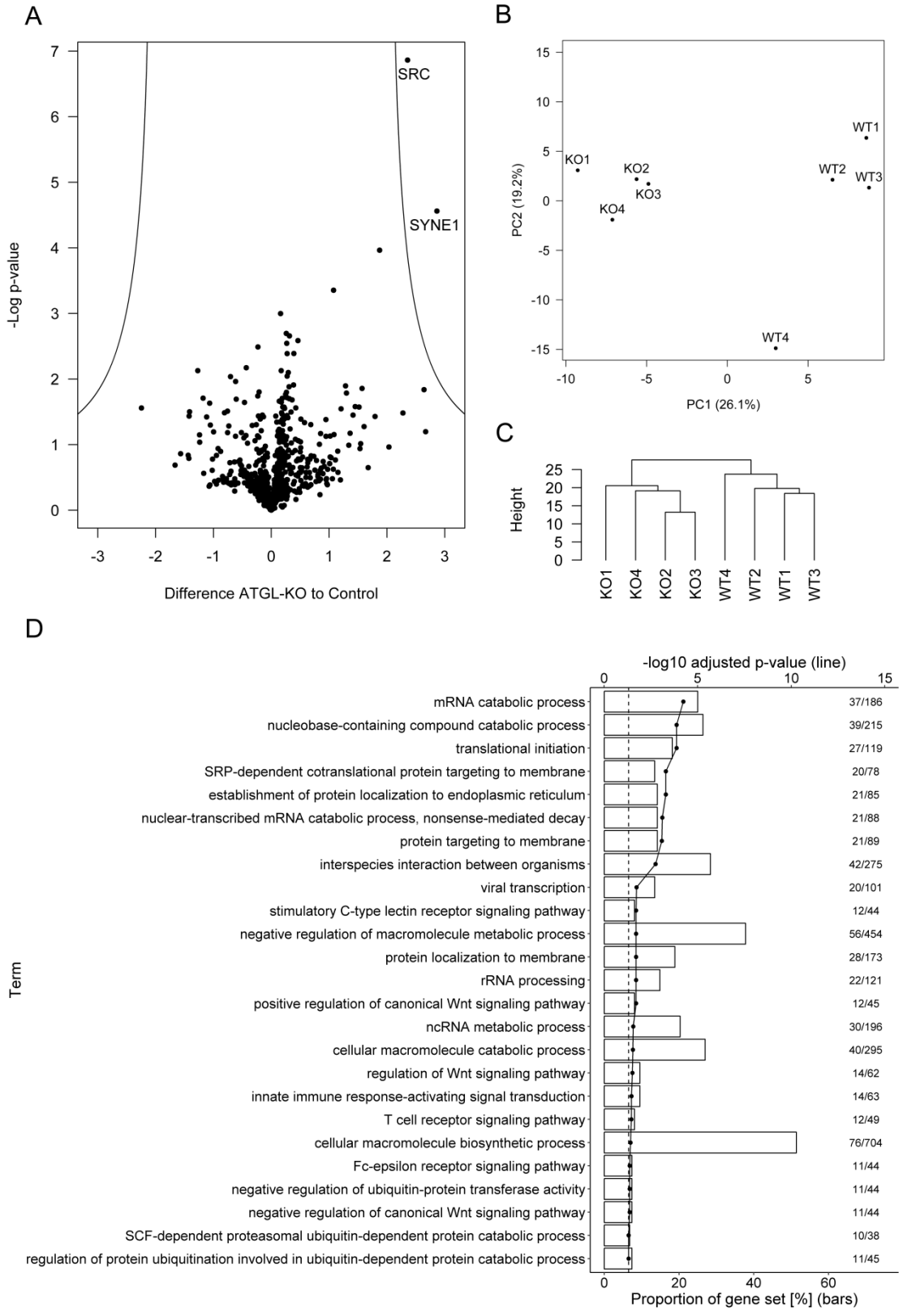

Figure 11. Two proteins appear as significantly upregulated in ATGL-KO cells after label free quantitation (LFQ) of proteomics data (N=4 cell lines derived from single cell clones per group). A: Volcano plot of LFQ data (-log p-values (t-test) plotted against the differences of the means of the log2 LFQ intensities; cut-off: p-value < 0.05, multi-test correction: permutation based FDR < 0.01, S0 = 2), B: PCA of LFQ data sets of ATGL-KO versus control (wildtype (WT)); C: Dendrogram obtained by HC of LFQ datasets; D: Over-represented GO terms of biological processes in the set of proteins with a minimum absolute difference of 0.5 of the log2 LFQ intensities in the KO versus control (WT) group. The dotted line shows the FDR adjusted p-value (-log10(p-value), axis at the top) for over-represented terms, the dashed line indicates the significance threshold of 0.05. The length of the bars represents the proportion of the protein set of interest (= Entrez IDs of the corresponding genes) that is mapped to the respective term (axis at the bottom). Numbers to the right of the bars indicate the number of proteins in the protein set of interest that are mapped to the respective term, the number of proteins shared by the term and the background protein set (term size). Reprinted from (1). Copyright (2018) American Chemical Society. PCA, HC and GO annotation was performed by Bettina Pucher and legend text is quoted from (1). Copyright (2018) American Chemical Society.

As described in the introductory chapter, proto-oncogene kinase SRC is a potent oncogene and signaling transducer, thus it was not surprising it contributed to a large number of biological processes observed in the GO term enrichment analysis in the set of proteins with a minimum absolute difference of 0.5 of the log2 LFQ intensities in the KO versus control group (Fig. 11D, Appendix 4). Of 80 total enriched biological processes, SRC contributed to 23, suggesting the improtancy of this proto-oncogen for cellular metabolism and homeostasis. Some of these processes were immune response-regulating signaling pathways, stimulatory C-type lectin receptor signaling pathway, response to insulin and positive regulation of canonical Wnt signaling pathway. In addition to signaling, processes related to protein translation and degradation were also enriched.

Considering the high importance of SRC in cancer, we decided to further validate our finding. Firstly, SRC protein abundance in A549 ATGL-KO and control cells was additionally measured by a semi-targeted mass spectrometry-based approach, which was in line with the LFQ results (Fig. 12A). Next, western blot for phospho-SRC Y416 (pSRC) and total SRC protein revealed two- to threefold higher levels of activated (phosphorylated) pSRC, in addition to the already observed increase in total SRC protein in ATGL-KO cells (Fig. 12CD). Furthermore, the connection between ATGL and SRC seems to already exist on mRNA level, as SRC mRNA was also increased in the ATGL-KO as measured by qPCR (Fig. 12B). Lastly, we were able to reverse the phenotype of SRC activation by reintroducing ATGL back into ATGL-KO cells. Lentiviral overexpression of ATGL in three single cell derived ATGL-KO clones of A549 cells caused prominent ATGL expression, which was able to reverse activation of SRC (Fig. 12EF) (1).

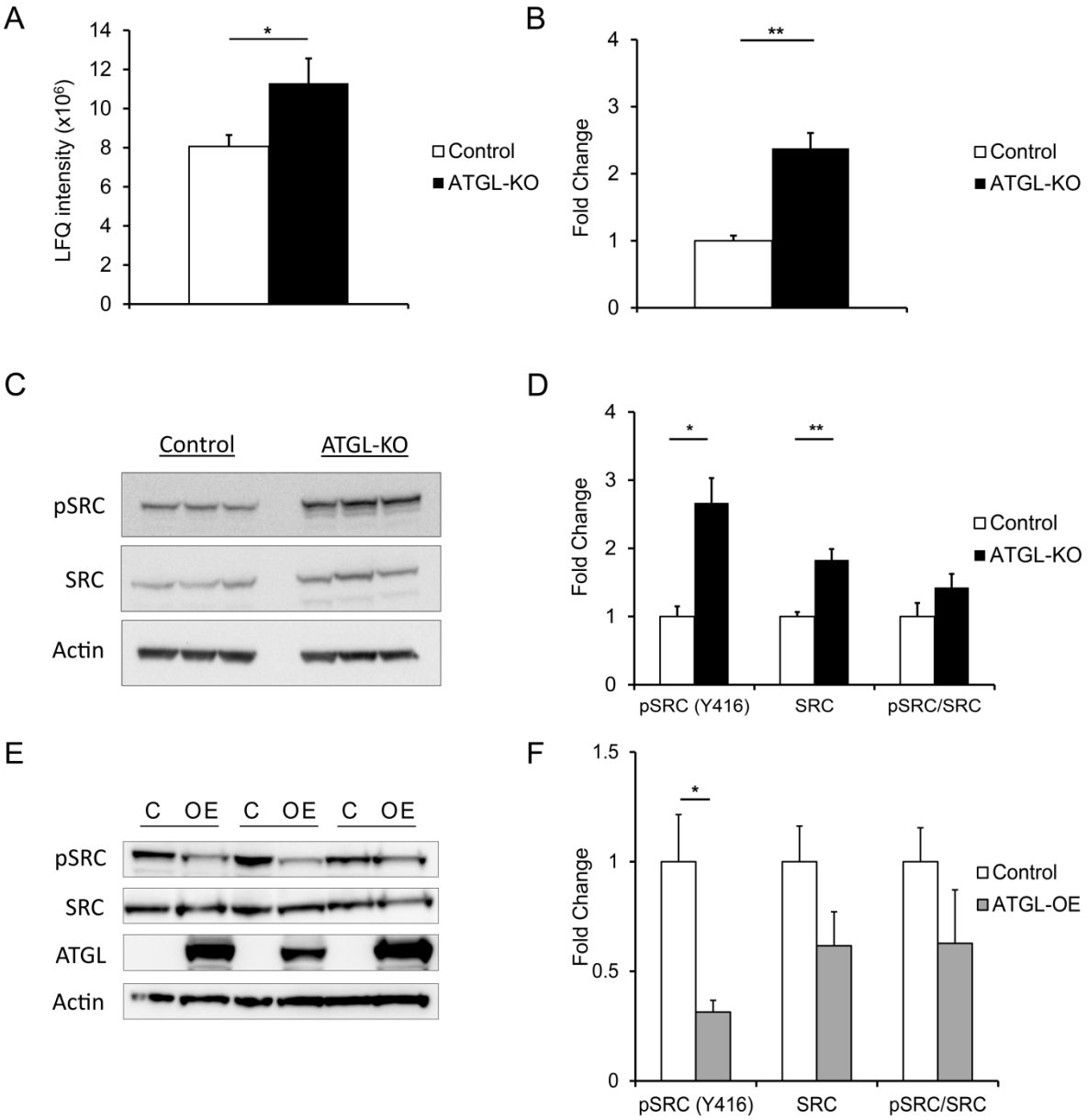

Figure 12. ATGL-KO cells had a higher SRC mRNA content, SRC protein and pSRC expression which can be reversed by re-introduction of ATGL. A: Results from semi-targeted LC-MS/MS measurement of SRC protein (N = 4-5 single cell clone derived cell lines per group), B: qPCR of SRC mRNA (N = 3 single cell clone derived cell lines per group), C: Western blot for SRC and pSRC (Y416); actin as loading control; D: Volume analysis of C, E: Western blot for pSRC, SRC and ATGL after ATGL re-overexpression in three single cell derived ATGL-KO A549 clones (with actin as a loading control), F: Volume analysis of E. ; * p-value < 0.05, ** p-value < 0.01. Reprinted from (1). Copyright (2018) American Chemical Society.

SRC contributes to higher migration of ATGL-KO A549 lung carcinoma cells which is reversible by re-expression of ATGL

As mentioned earlier, SRC is mainly involved in cell metastasis and interestingly, the second upregulated protein from the proteomics screening, nesprin-1, is involved in the same process as well (27, 122, 123). We thus addressed migration and proliferation of ATGL-KO versus control cells. While no difference in proliferation ability was observed between the two groups, migration experiments showed that ATGL-KO cells were able to migrate faster. ATGL-KO migrated faster in both serum free conditions towards collagen as chemo-attractant (transwell assay, Fig. 13A) as well as in serum rich conditions (wound healing assay, Fig. 13B). The effect was mainly supported by the activity of SRC since treatment of the cells with a highly selective SRC inhibitor (124) reduced the migratory potential to the level of the control cells in both experimental setups (Fig. 13). It should be mentioned that the used concentration did not influence survival of ATGL-KO or control cells (Fig. 13C).

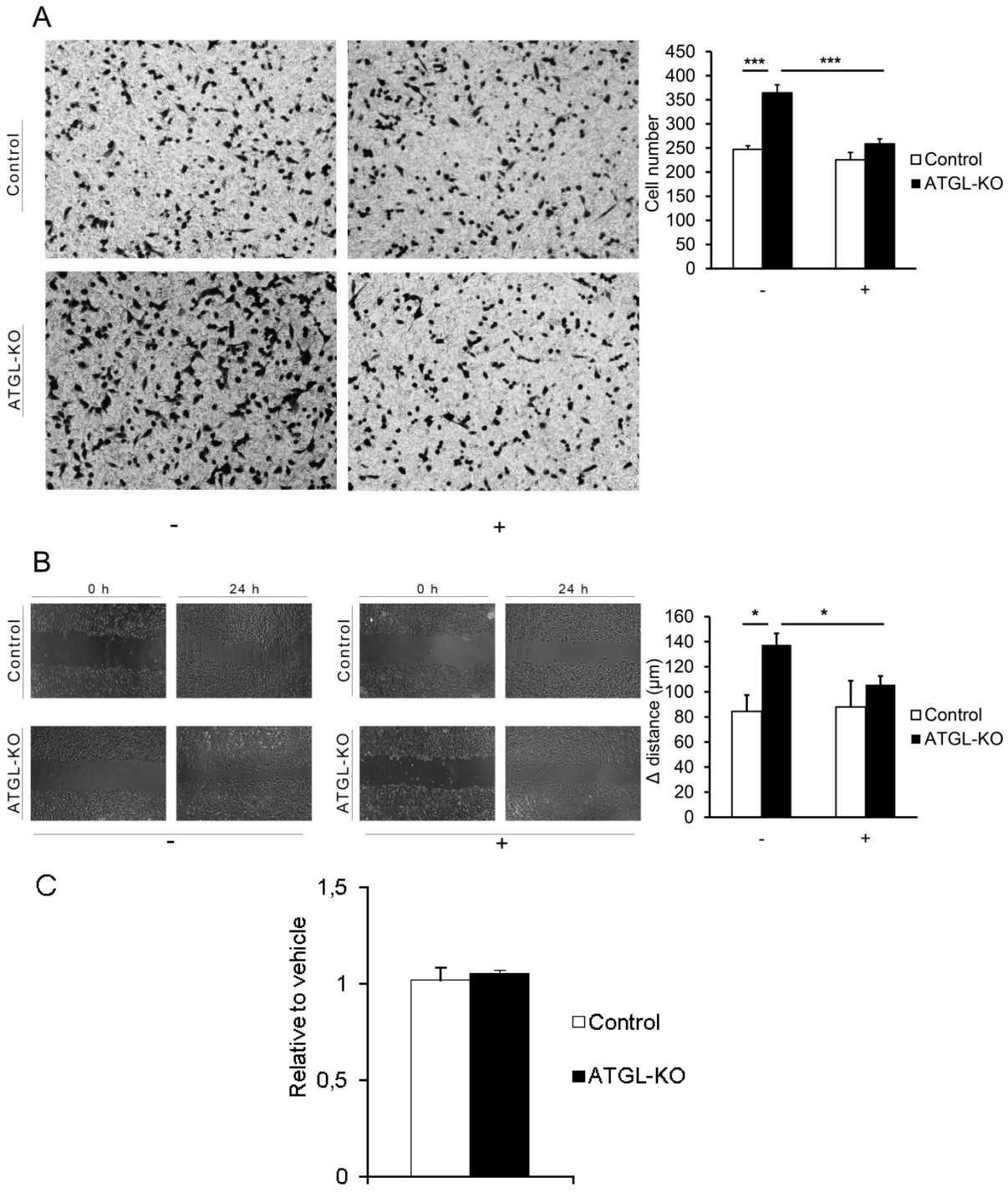

Figure 13. ATGL-KO cells migrated faster in a SRC dependent manner. A549 ATGL-KO and control cells were treated with 20 nM of KX2-391 (+) or vehicle (DMSO) (-). A: Transwell assay with corresponding numbers of migrated cells. B: Scratch assay and corresponding gap closure rate; C. Treatment with SRC inhibitor did not influence the survival of ATGL-KO and control cells. N=3 ATGL-KO cell lines derived from single cell clones, N=3 replicates per cell line; ** p-value

< 0.01, *** p-value < 0.001. Adapted from (1). Copyright (2018) American Chemical Society.

Upon lentiviral re-expression of ATGL back into ATGL-KO cells, cells reduced their LD content and as well their migration potential, as compared to ATGL-KO cells transfected with a lentiviral control (GFP) (Fig. 14).

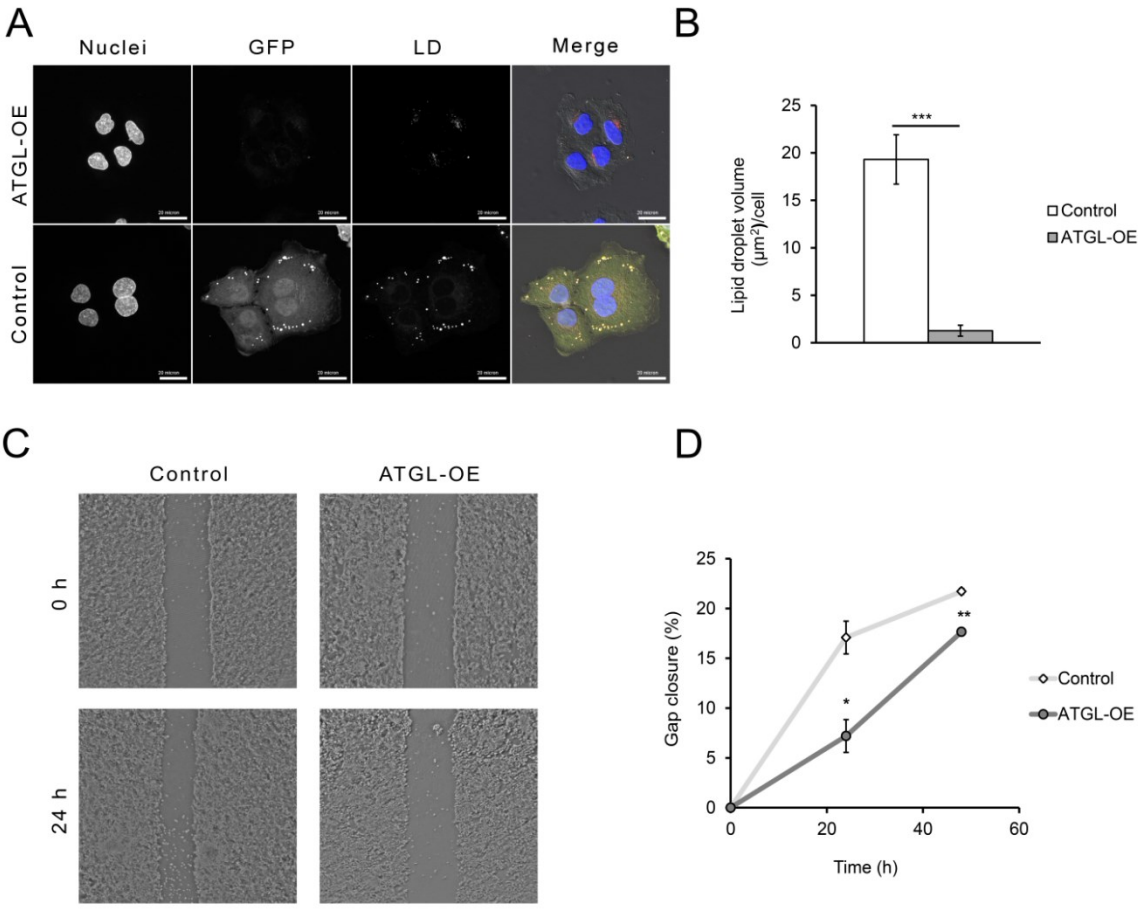

Figure 14. Re-introduction of ATGL in ATGL-KO A549 cells diminished LD accumulation and reduced migratory potential of ATGL-KO cells. A: Fluorescence microscopy of cells labelled with DAPI for cell nuclei and HCS LipidTOX™ for LD visualization. GFP was used as a transfection control. B: Quantitation of LDs (N=69-109 cells per condition). C: Representative scratch assay of ATGL-OE cells compared to the control (ATGL-KO); D: Gap closure after 24 and 48 h determined from scratch assay (N=3 biological replicates per condition, N=3 replicates per cell line); * p < 0.05, ** p < 0.01, *** p < 0.001. Reprinted from (1). Copyright (2018) American Chemical Society.

Pharmacological inhibition of ATGL is sufficient to activate SRC and increases the migratory potential in murine LLC1/LL2 Lewis lung carcinoma cells and AML12 hepatocytes

Next we investigated if pharmacological inhibition of ATGL might be sufficient to trigger more aggressive phenotype. Since development of an human ATGL inhibitor is still ongoing, we had to switch to murine cells to be able to use atglistatin (125), an inhibitor of murine ATGL. We treated LLC1/LL2 mouse Lewis lung cancer cells with 80 µM atglistatin for the treatment period of 16 h. Even such short period of time resulted in an induction of pSRC (Fig. 15AB). Protein levels of SRC protein remained unchanged but nevertheless an increase in migratory potential of the treated cells was observed (Fig. 15CD).

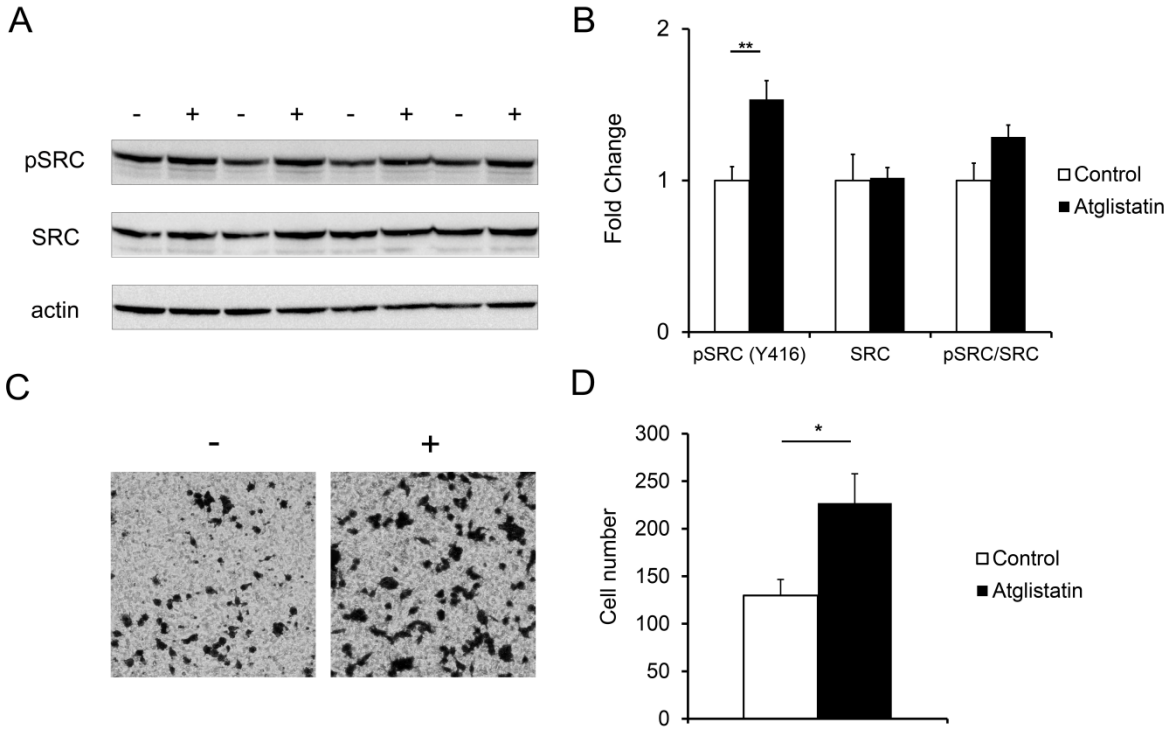

Figure 15. Inhibition of ATGL with atglistatin in murine LLC1/LL2 Lewis lung cancer cells activates SRC and increases their migratory potential. A: Western blot of LLC1/LL2 cells for pSRC (Y416), SRC and beta-actin (loading control) after atglistatin (80 µM) treatment. B: Corresponding volume analysis. C: Transwell migration assay, "-" Control (DMSO vehicle), "+" Atglistatin treatment (80 µM). D: Number of migrated cells in C, N=3 per condition; * p- value < 0.05, ** p-value < 0.01. Reprinted from (1). Copyright (2018) American Chemical Society.

To further validate our hypothesis, we used another mouse cell line, AML12 mouse hepatocytes (Fig. 16) in which the same atglistatin treatment also caused an increase in pSRC as well as in migration ability.

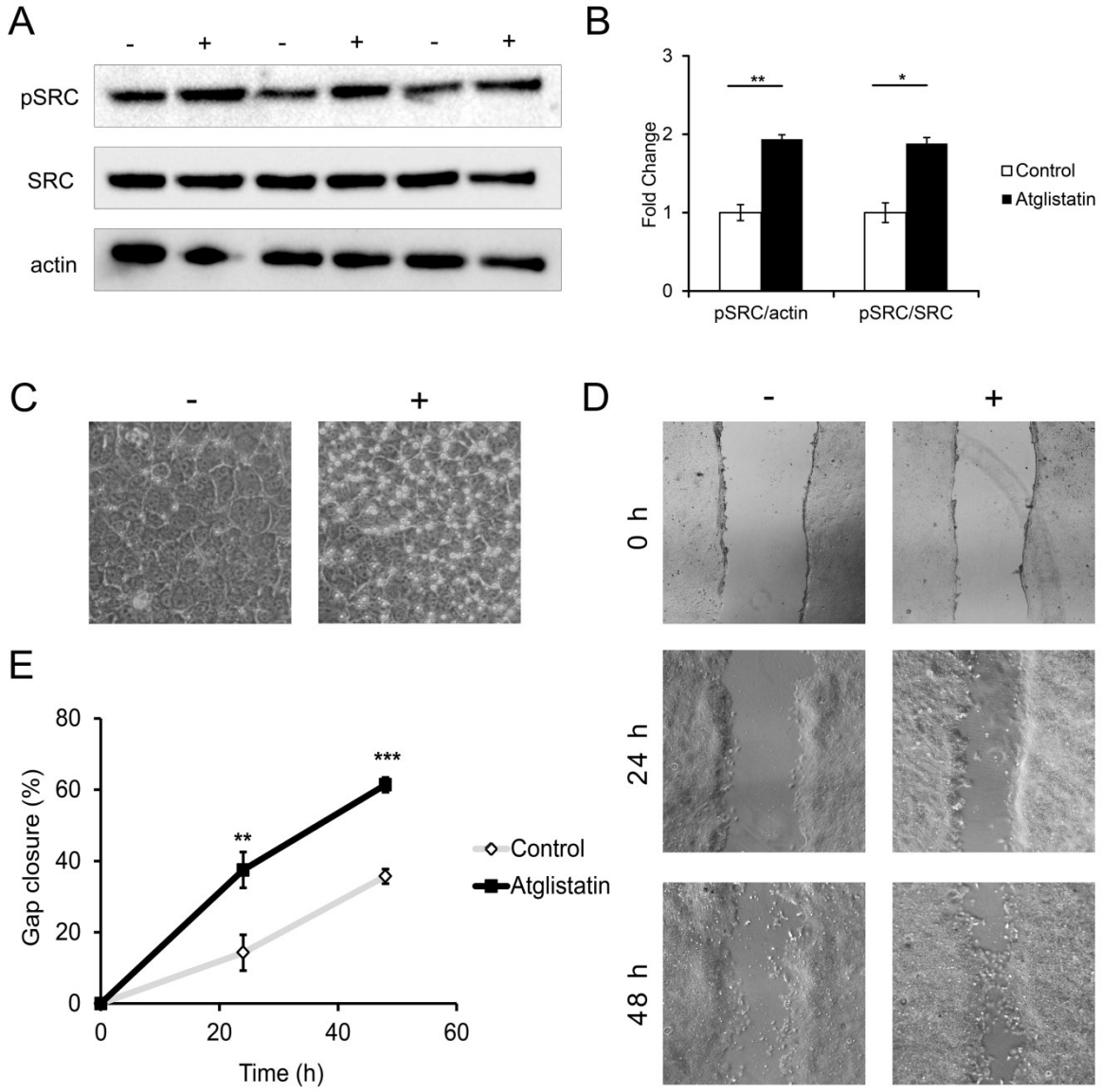

Figure 16. Pharmacological inhibition of ATGL activates SRC and improves migration potential of AML12 cells. A: Western blot of atglistatin treated (+) and control (-) cells. Actin was used as a loading control. B: Volume analysis of A;C: Atglistatin treatment (+) caused lipid accumulation in AML12 cells; D. Representative scratch assay of AML12 cells treated with 80 μM atglistatin (N=5-6 per condition). E: Gap closure rate of scratch assay; * $p<0.05$, ** $p<0.01$, *** $p < 0.001$. Reprinted from (1). Copyright (2018) American Chemical Society.

Potential mechanistic links leading to SRC activation

Since we observed an increase in production of lysophospholipids and they are known to activate SRC (especially LPC) (119) and correspondingly we observe an increase in cPLA2 expression (Fig. 10), we treated the cells with another common product of cPLA2 activity, arachidonic acid. Arachidonic acid caused prominent SRC activation and increased SRC protein levels in A549 cells in a concentration dependent manner. This effect, however, could not be reproduced in another lung cancer cell line, NCI-H23 lung carcinoma cells, suggesting cell specific differences in signaling pathways (Fig. 17).

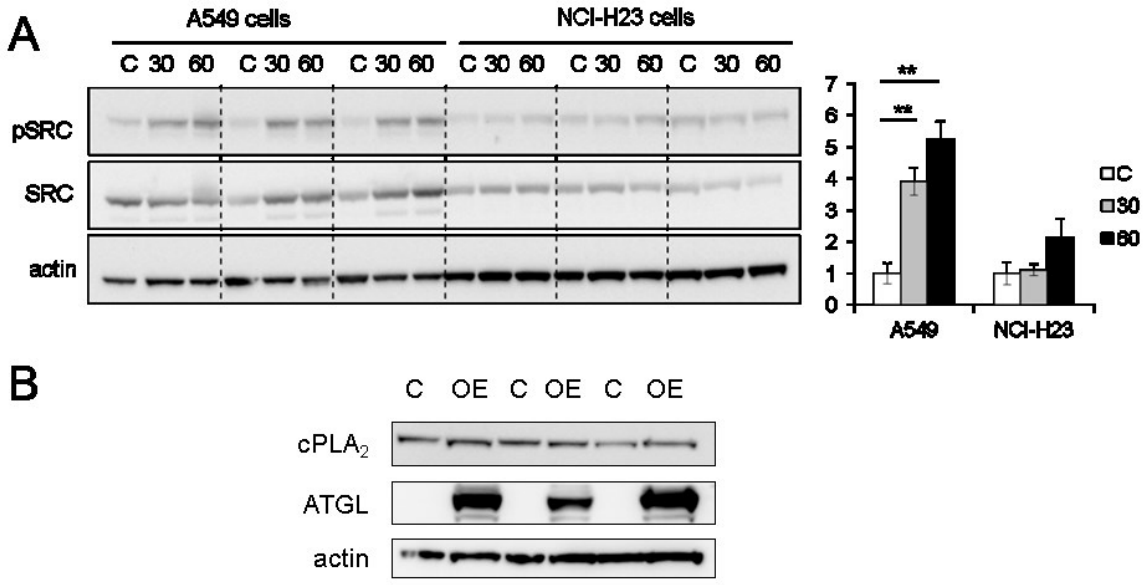

Figure 17. 30 or 60 µM arachidonic acid (AA) treatment causes concentration a dependent activation of SRC in A549, but not in H23 cells and ATGL re-expression does not influence $cPLA_2$ levels in A549 cells. A: Left: Western blot for pSRC and SRC in cells cultured under normal conditions (C) or treated with 30 or 60 µM AA, right: corresponding volume analysis for pSRC (** p-value < 0.01). B: Western blot for $cPLA_2$ after ATGL re-(over)expression in ATGL in ATGL-KO clones. In both cases actin was used as loading control.

Lentiviral re-introduction of ATGL in ATGL-KO cells did not reverse increased cPLA2 protein expression (Fig. 17B) suggesting that the regulatory link between ATGL and cPLA2 expression is neither direct nor SRC-dependent. Alternatively, overexpression of ATGL as well as its deletion might lead to increased cPLA2 levels irrespective of the level of SRC activation. Moreover, cPLA2 might not be

the only responsible enzyme contributing to the pool of LPL. As not only LPL but as well free FA can influence SRC activity (Fig. 17A; (126, 127)), it is possible that loss of ATGL results in de-regulation of other (potentially unknown) lipases which consequently produce lipid mediators responsible for SRC activation.

3D culture resembling tumor formation induces metabolic switch in ATGL-KO cells

To investigate how the cells lacking ATGL would behave in a more tumor like environment, we grew cells in low-attachment cell culture plates forcing them to form three dimensional spheroids. After a few days in culture cells in the core of the sphere become hypoxic (128) and might serve as a better representation of the *in vivo* state. We thus cultured ATGL-KO and control cells for 10 days in such conditions prior to harvesting for LFQ proteomics analysis. The initial data matrix consisted of 2654 proteins which were then filtered for missing values under the criteria that at least all values of one group should be valid prior to imputation. This caused a reduction in matrix size to 1547 proteins which were further used for statistical analysis (Appendix 5). Under the cut off criteria for significance (Student t-test adjusted p-value bellow 0.05, corrected for multi-testing with S0 of 0.5 and FDR of 1%) 20 proteins appear to be significantly deregulated between the two groups. The corresponding volcano plot and the list of significantly changed proteins are shown in Fig. 18.

Firstly, we observed that although each sample consisted of a pool of the same number of spheroids that originated from the same cell number, ATGL-KO samples had much higher protein content than control corresponding to a larger size of ATGL-KO spheroids. Therefore, it came as no surprise that the most upregulated proteins in ATGL-KO cells were mainly involved in translation, suggesting an increase in protein synthesis (Fig. 18, marked with italic in the table). This was an interesting finding as we observed only slight growth advantage when cells were cultured in 2D culture.

Furthermore, growth of ATGL-KO cells in 3D conditions seemed to have led to a pro-Warburg effect. This is mainly manifested through the increase in expression

of the glucose transporter Glut3 (SLC2A3), a common HIF1 target, and ADP-dependent glucose kinase (ADPGK) (Fig. 18, marked in bold). ADPGK is often overexpressed enzyme in cancer capable of phosphorylating glucose in absence of ATP however it is not a HIF-1 target and does not independently drive the Warburg effect (129). Thus the role of ADPGK in cancer still needs to be further elucidated. In addition to these two glycolytic proteins, with slightly less stringent cut-off criteria (S0 value of 0.1 instead of 0.5), ATP-dependent 6-phosphofructokinase (platelet type, PFKP), another HIF1 target, was found to be significantly upregulated in ATGL-KO cells (fold change of 2.44, adjusted p-value 0.025), once again suggesting higher glucose dependence of ATGL-KO cells compared to control in 3D culture. In addition to changes of glucose metabolism, fatty acid metabolism as well appeared to be deregulated in ATGL-KO cells, especially with respect to upregulation of very long chain fatty acid synthesis and fatty acid desaturation and downregulation of beta oxidation. In addition to PFKP, after reducing the S0 value to 0.1, proteins involved in glutathione metabolism and cellular antioxidant defense appear significantly downregulated in ATGL-KO spheroids. Therefore, we applied the method described in detail in Chapter 2 to measure GSH/GSSG ratio of ATGL-KO and control cells cultured in normal (2D) conditions. However, no significant difference could be observed between the groups in 2D culture, suggesting potentially a culture specific effect (Fig. 18B).

Interestingly, SRC protein abundance was not significantly altered under 3D growth conditions (fold change 0.55, adjusted p-value 0.075). This is not too surprising as hypoxia possibly inhibited ATGL in the control cells (83), thus causing increase in SRC expression in the control cells as well. The key role for SRC in cells with downregulated lipolysis might be exclusively in initiation and support of migration and not related to the growth advantage of ATGL-KO cells in 3D culture.

A

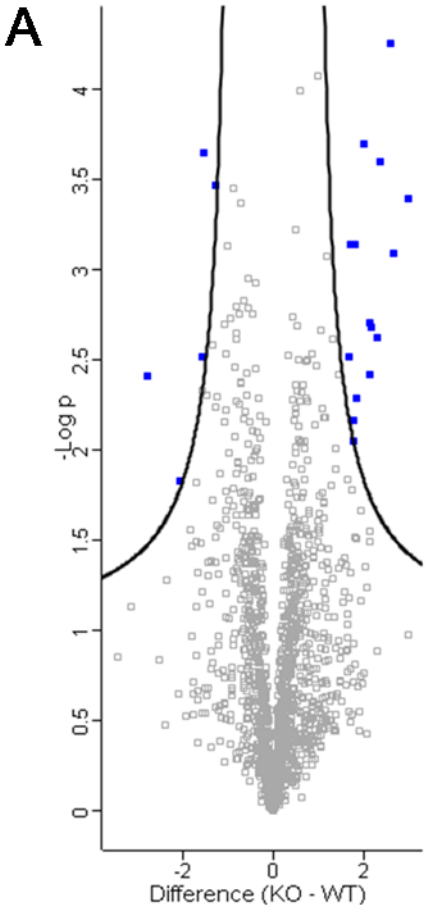

Protein names	Gene names	Fold Change KO/WT
Eukaryotic translation elongation factor 1 epsilon-1	EEF1E1	7.81
Heat shock-related 70 kDa protein 2	HSPA2	6.25
Peptidyl-prolyl cis-trans isomerase FKBP10	FKBP10	5.88
Very-long-chain 3-oxoacyl-CoA reductase	HSD17B12	5.08
Ferritin light chain	FTL	4.83
Solute carrier family 2, facilitated glucose transporter member 3	SLC2A3	4.41
A-kinase anchor protein 12	AKAP12	4.38
ADP-dependent glucokinase	ADPGK	4.33
Fatty acid desaturase 2	FADS2	3.96
Aspartate--tRNA ligase, mitochondrial	DARS2	3.54
Cytochrome b5 type B	CYB5B	3.45
Ribonucleoside-diphosphate reductase large subunit	RRM1	3.41
Mitotic spindle-associated MMXD complex subunit MIP18	FAM96B	3.35
Endothelial protein C receptor	PROCR	3.22
Prolyl 4-hydroxylase subunit alpha-1	P4HA1	3.12
3-ketoacyl-CoA thiolase, mitochondrial	ACAA2	0.41
Transaldolase	TALDO1	0.35
Canalicular multispecific organic anion transporter 2	ABCC3	0.34
Protein FAM98B	FAM98B	0.24
Cleavage and polyadenylation specificity factor subunit 7	CPSF7	0.15

B

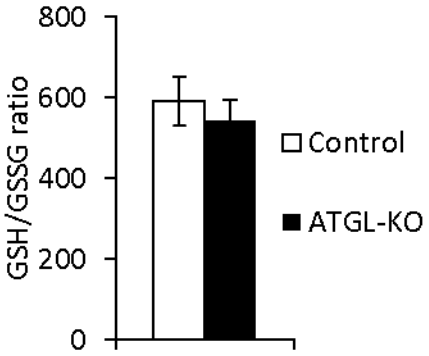

Figure 18. Representation of significant proteomic changes between ATGL-KO and control (WT) cells cultured as 3D spheroids and GSH/GSSG ratio of ATGL-KO and control cells in 2D culture. A. Proteomics of 3D spheroids; B. GSH/GSSG ratio of ATGL-KO and control cells. N=3 individual single cell derived clones, unpaired Student´s t-test adjusted $p < 0.05$, corrected for multi-testing by permutation-based FDR 1%, S0 0.5.

Discussion (Chapter 1)

Cancer lipid metabolism gained much attention in past years as a prominent therapeutic target, especially with regards to FA synthesis, uptake and oxidation (56). Deregulation of lipid metabolism especially may play a role in cancer progression and metastasis. It has been recently reported that high levels of the fatty acid receptor CD36 together with palmitic acid or high fat diet aid initiation of metastasis in human oral cancer (64). It is also known that migration of aggressive breast cancers is highly dependent on exogenous lipid sources (130).

In addition, it has been shown that many cancer types accumulate LDs which is associated with a higher migration potential, rendering LD one of the novel indicators of cancers' aggressiveness (56, 72-75). We are still, however, lacking fundamental knowledge regarding the contribution of lipolysis in cancer, especially with regards to cancer progression. Over the last years neutral lipases such as ATGL and MGL, controversially, have been shown to act both as tumor suppressors and pro-oncogenes, sometimes even in the same cancer types (1, 96, 97, 106). The same is the case for lipolytic regulators such as CGI-58 (89, 90).

Interestingly, in lung cancer the role of lipases seems to be especially important. ATGL was shown to be lost in 38 % of all lung cancer cases (104) and as aforementioned, loss of ATGL correlates with poor survival outcome in lung cancer patients (Fig. 6). In addition, aged ATGL-KO mice over time spontaneously developed lung neoplasia, suggesting a role of ATGL in process of lung tumor initiation (104). Next to ATGL, $MGL^{+/-}$ and $MGL^{-/-}$ mice were shown to spontaneously develop neoplasia in lung, spleen, liver and lymphoid tissues, with lung being the most commonly affected (97). In addition, MGL has been found to be significantly downregulated in lung cancer compared to the surrounding tissue (97).

Accordingly, we demonstrate that loss or of ATGL in A549 lung cancer cells resulted in LD accumulation and an overall more aggressive cancer phenotype with activation of pro-oncogenic SRC kinase signaling, increase in production of pro-oncogenic signaling lipids and enhanced migration. While others have shown that knock-down of ATGL in lung cancer cells results in less aggressive phenotype (106), we observed the opposite with a complete knock out, suggesting that

residual levels of ATGL in the silenced cells may be sufficient for its tumor suppressive function. Strikingly, we expanded the more aggressive cancer phenotype beyond the lung by demonstrating that pharmacological inhibition of AML-12 murine hepatocytes (in addition to LLC1/LL2 murine lung cells) also caused SRC activation and increased the cellular migration potential (Fig. 15 and 16) (1).

Re-introduction of ATGL in ATGL-KO A549 cells by stable overexpression abolished LD accumulation, decreased the activation of SRC and reduced migration potential, confirming that the link between ATGL activity and cancer aggressiveness is reversible and dependent on ATGL. Our combined data suggests that cancer cells do not necessarily rely on intracellular lipolysis and are over time able to reprogram their metabolism accordingly. The strongest metabolic phenotype was found in 3D cultured ATGL-KO cells, which were able to increase levels of proteins responsible for glucose uptake and metabolism. This may enable their survival and proliferation under nutrient deprived conditions (such as in tumor cores) since ATGL-KO cells do not have the ability to mobilize fatty acids from intracellularly stored TG.

Furthermore, LD accumulation that results from the reduction of lipolytic activity may also act as a potent buffer to prevent lipotoxicity of free fatty acids (131-134). Moreover, lipids stored within LDs may be used as substrates for various enzymes that can produce pro-oncogenic signaling lipids (77), such as phospholipases. Consistently, we observe an increase in lysophospolipids and ether lipids, with concomitant increase in the expression of $cPLA_2$ in cells lacking ATGL. LPCs are known to be able to activate SRC and both LPCs and ether lipids are reported to be involved in inflammation, cancer initiation and progression (135-140). We showed here that another product of cPLA2 activity, AA, can also trigger SRC activation. However, our results suggest that cPLA2 is not responsible for SRC activation and also vice versa, ATGL-dependent SRC activation is not responsible for increased cPLA2 expression in A549 cells. More research has to be performed to elucidate which mediator(s) activate SRC and which lipases are deregulated upon ATGL depletion and if they are linked to SRC activation. All together efforts should be made to fully clarify the role of lipases in cancer, especially with regards to lung cancer initiation and progression.

Conclusion (Chapter 1)

Loss of ATGL leads to poor survival outcome in lung cancer patients and it is often downregulated in lung cancer (104). We observe that lung cancer cells lacking ATGL accumulate TG in form of LDs, have elevated levels of ether- and lysophospholipids and activate of pro-oncogenic signaling via SRC kinase. Considering the controversy behind the role of lipases in cancer, we established a mechanistic link between neutral lipid accumulation caused by ATGL loss and elevated cancer cell aggressiveness. In this way we hope to aid discovery of new therapeutic approaches for cancers with possible defects in lipolysis, especially lung cancer where lipases seem to play an essential role in cancer progression.

2. CHAPTER TWO: SENSITIVE TWO-STEP ALKYLATION METHOD FOR GLUTATHIONE STATUS ASSESSMENT

Introduction (Chapter 2)

Glutathione is a potent, thiol- based antioxidant and as previously mentioned exists in reduced (GSH, active) and oxidized (GSSG, inactive) form. Most of the glutathione in our cells is present in the reduced state in a concentration range of 1-10 mM while GSSG accounts for only 1-2 % of the total glutathione pool (141-143). Glutathione is responsible for maintaining the thiol status of proteins and other antioxidants (e.g. ascorbic acid and alpha-tocopherol), for reduction of ribonucleotides for DNA synthesis and for overall protection from oxidative stress (144). In its latter function, GSH is mainly in charge of hydrogen peroxide removal acting as a cofactor for the enzymatic family of glutathione peroxidases (GPx) (143). During this process two GSH molecules donate a pair of electrons reducing hydrogen peroxide to water while in the same time being oxidized to GSSG (145). Glutathione reductase (GR) can restore (recycle) GSH back from GSSG in a NADPH dependent manner (146), however the more oxidative stress, the more GSH is used up and the more GSSG produced, decreasing the GSH/GSSG ratio (147). Therefore, the GSH/GSSG ratio can be used as a readout of tissue redox state (148).

Disturbed glutathione homeostasis has been reported to occur in various different pathological conditions, most prominently in cancer (reviewed in (149, 150)), diabetes (151, 152), neurodegenerative (149, 153, 154) and cardiovascular diseases (149, 155, 156).

In cancer, GSH may play a pivotal role in facilitating cancer metastasis and progression. As previously mentioned, loss of attachment (LOA, the first step of metastasis) is accompanied by high oxidative stress (65). In addition, high proliferation rates observed in cancer also lead to increase in ROS production (9). Therefore it is not surprising that the cellular content of GSH has been correlated to faster growth rates, higher proliferation rates and elevated metastatic potential of cancer cells (150). Some therapeutic approaches even involve depletion of GSH as cancer cells with lower GSH content may be more sensitive to conventional therapy (144, 150).

In heart-related conditions, oxidative stress is correlated to heart failure (HF) and development of coronary diseases ((157), reviewed in (146)). It has been

proposed that GSH/GSSG ratio can act as an independent prognostic marker for atherosclerosis and risk of death in patients with coronary disease (158, 159).

The large difference in abundance between GSH and GSSG as well as the fact that GSH can spontaneously oxidize to GSSG in a non-reducing environment, gave rise to discrepancies in results obtained across different laboratories (145, 160). In order to prevent artificially high GSSG levels, it is now considered mandatory that all biological samples must be first quenched with a thiol-blocking reagent. In this way GSH is efficiently stabilized prior to further sample processing (161, 162). The most commonly used GSH conjugating reagent is N-ethyl-maleimide (NEM) due to its cell permeability and fast kinetics, and it is usually replaced only in glutathione recycling method that employs GR, which is efficiently inhibited by NEM (161). Next to NEM and especially in combination with the GR recycling method, two other alkylating reagents are used: 2-vinylpyridine and iodoacetic acid. However, both have much slower reaction kinetics compared to NEM (161, 163-165).

Since GSSG is usually at least two-orders of magnitude lower in abundance compared to GSH it is the analyte that determines the method´s sensitivity. Therefore it is not surprising that when sample size is limited many researchers (especially in clinics) use combinatory approach by measuring GSH or GSH-NEM on LC or LC-MS/MS while switching to the enzymatic recycling method to be able to measure GSSG. Here we propose that instead of measuring GSSG directly, it is subjected to reduction and a second NEM alkylating step, followed by LC-MS/MS measurement. In our new method, all free GSH is first conjugated to NEM, then residual NEM is removed and GSSG reduced with TCEP. Newly formed GSH is then subjected to a second alkylation step with deuterium labelled NEM (d5-NEM) and measured as GSH-d5-NEM. In this way, a single internal standard can be used (IS, $^{13}C_2$,^{15}N-GSH-d5-NEM) which in a simple way allows absolute quantification of both GSH and GSSG. The novelty of this procedure for GSSG measurement results in an at least 10 fold boost of sensitivity and elimination of any matrix effects by design as all three analytes (GSH-NEM, GSH-d5-NEM and IS) have similar chromatographic behaviour and co-elute from the analytical column.

The method was tested in different sample types and proven to work for cell culture, blood and tissue samples. Lastly, it was applied to propose GSH/GSSG ratio as a biomarker for oxidative stress in heart tissue samples of cardiomyopathy patients.

Materials and methods (Chapter 2)

If not stated otherwise, all chemicals were purchased from Sigma Aldrich.

Standards

Standards for GSH and GSSG were prepared as 10 mM, and for NEM and d5-NEM as 100 mM stock solutions in ultrapure water. Tris(2-carboxyethyl)phosphine (TCEP) was used as 50 mM stock solution prepared in 50 mM ammonium acetate buffer (AA, pH=7.0). For calibration curves, stock solutions were diluted in 50 mM AA, pH = 7.0. Internal standard (IS, $^{13}C_2$,^{15}N-GSH-d5-NEM) was prepared by combining 2 mM glutathione-(glycine-$^{13}C_2$,^{15}N) (Cambridge Isotope laboratories, USA) with 50 mmol/L d5-NEM in 50 mM AA, with subsequent extraction of residual d5-NEM with dichloromethane. The IS working concentration was achieved by 1:80 or 1:100 dilutions.

H_2O_2 treatment

For H_2O_2 treatment, A549 lung cancer cells were seeded in 12-well plates (300.000 cells/well) and after a day in culture treated with 500 µl of control (Ca^{2+}, Mg^{2+}-PBS) or 100 µM H_2O_2 in Ca^{2+}, Mg^{2+}-PBS for 15 min followed by two PBS washing steps and the NEM (2.5 µM in PBS) incubation step. The detailed workflow is depicted in Fig. 19.

Blood samples and collection

Blood samples were collected from five healthy volunteers in VACUETTE® 3.5 ml tubes with Z Serum Separator Clot Activator 13x75 red cap-yellow ring, non-ridged (Greiner bio-one, Vienna) or in VACUETTE® 3.5 ml K2 EDTA tubes, pull-cap, lavender (Greiner bio-one, Austria). For each donor, tubes were pre-customized by adding either 100 µl of 87.5 mM NEM stock solution in PBS (NEM 0 min

sample) or 100 µl of vehicle (PBS). For serum collection, blood samples were coagulated for exactly 20 min at room temperature (RT). After coagulation, samples were centrifuged at 1300 x g at RT for 20 min. Plasma samples were centrifuged for 10 min at 1300 x g, RT. Whole blood samples were stored for 30 min at 4° C. After these described times (50 min at RT for serum, 10 min at RT for plasma and 30 min at 4° C for whole blood) 5 µL of each sample was pipetted into 45 µl of 2.5 mM NEM in PBS (delayed NEM samples) or to 45 µl of PBS (NEM 0 min samples). Further processing was performed according to the workflow in Fig. 19.

Tissue specimens and processing

Left ventricular myocardial tissue samples were obtained from end-stage failing heart explants (n=10) and non-failing human control hearts (n=5) that were not accepted for transplantation. Tissue samples were collected at the time of transplantation, snap frozen in liquid nitrogen, and stored at -80 °C till analysis. Control skeletal muscle was obtained from autopsy of patients with no known skeletal muscle disease. 4-7 mg of the tissue was lysed with 4 x 10 s sonication steps at 70 % amplitude (Bandelin, Germany) and further processed according to the workflow shown in Fig. 19.

Ethical aspects

The use of human biomaterials was approved by the Ethics committee of the Medical University of Graz (20-277 ex 08/09, 26-282 ex 13/14 and 28-508 ex 15/16) and conformed to all pertaining regulations and the principles of the Declaration of Helsinki. Patients provided written informed consent to participate in the study.

LC-MS/MS method and parameters

Chromatography was carried out on a Dionex UltiMate 3000 system equipped with a Zorbax SB-C18 column (50 mm x 4.6 mm, 1.8 µm, Agilent, USA). The flow rate was 0.3 ml/min with solvent A being 0.1 % formic acid in water and solvent B being 0.1 % formic acid in acetonitrile. The following gradient was used: 0 - 10 min 1 - 30 % B, 10 - 15 min 30 - 70 % B, 15 - 20 min 1 % B. Injection volume was 10 µl. For detection ABSciex 4000 QTRAP mass spectrometer was used. The

instrument was operated in positive multiple reaction monitoring (MRM) mode. Transitions with corresponding parameters for each analyte are shown in Table 1. Global instrument parameters included: curtain gas 20 (arbitrary units), collision gas high, ion spray voltage (IS) 4500 V, temperature 450 °C, ion source gas 1 and 2: 25 (arbitrary units) and 40 (arbitrary units), declustering potential 50 V and entrance potential 10 V. Peak integration and analysis was performed using the Analyst software (version 1.6.3). As GSH-NEM is a diastereomer (161, 166), all three GSH-NEM analytes (GSH-NEM, GSH-d5-NEM and $^{13}C_2$, ^{15}N-GSH-d5-NEM) elute as twin peaks and the areas under both peaks were used for integration and quantification.

Statistics and data representation

If not stated otherwise, all bars represent mean values ± standard error of mean (SEM). For significance testing an unpaired Student's t-test was performed with a p-value of 0.05 as significance threshold.

Table 1. MRM transitions and parameters per analyte. Transition 1 (marked in bold) was used for quantification (CE - collision energy, CXP - collision cell exit potential).

Analyte name	Q1 Mass (Da)	Q3 Mass (Da)	Dwell (msec)	CE (V)	CXP (V)
GSSG (***Transition 1)***	613.2	355.3	35	33	14
GSSG (*Transition 2*)	613.2	484.2	235	25	12
GSH (***Transition 1***)	308	179	35	19	15
GSH (*Transition 2*)	308	76.23	35	47	15
GSHNEM (***Transition 1***)	433	201	35	35	15
GSHNEM (*Transition 2*)	433	84.2	35	59	15
GSHd5NEM (***Transition 1***)	438	206	35	35	15

GSHd5NEM (*Transition 2*)	438	84.2	35	59	15
NEM (***Transition 1***)	126	80	35	25	12
NEM (*Transition 2*)	126	98	35	19	16
d5-NEM (***Transition 1***)	131	80	35	25	12
d5-NEM (*Transition 2*)	131	98	35	19	16
^{13}C2,^{15}N GSH-d5-NEM (IS)	441	206	35	35	15

Results (Chapter 2)

Method overview

The method was tested on cells, tissue and blood samples, according to the protocol and amounts shown in Fig. 19. Since the starting material can be as low as 5 µl of blood, 3-5 mg of tissue or 300.000 cells, it can also be used for very limited samples such as fine needle aspiration biopsies (~500.000 cells per FNAB (167)). At the first step (Fig. 19, 1) treatment of the samples for 20 min with 2.5 mM of NEM in PBS proved to be sufficient to fully capture GSH in form of GSH-NEM. In the next step (Fig. 19, 2) proteins are precipitated with cold 80 % methanol (MeOH) with simultaneous introduction of IS. Samples are then centrifuged, the upper phase is transferred to a new reaction tube and dried under a stream of nitrogen. Proteins and cell debris were precipitated with 80 % cold methanol (containing the internal standard, IS, ^{13}C2,^{15}N GSH-d5-NEM) followed by a nitrogen drying step. Dried samples are then re-suspended in 50 mM AA and residual NEM is extracted with dichloromethane (Fig 19, 3). The aqueous NEM free phase is then transferred to a new tube, reduced with TCEP and alkylated with d5-NEM. All three analytes GSH-NEM, GSH-d5-NEM and ^{13}C, ^{15}N-GSH-d5-NEM (IS) are then simultaneously measured by LC-MS/MS using an MRM-based approach (Fig. 19, 4).

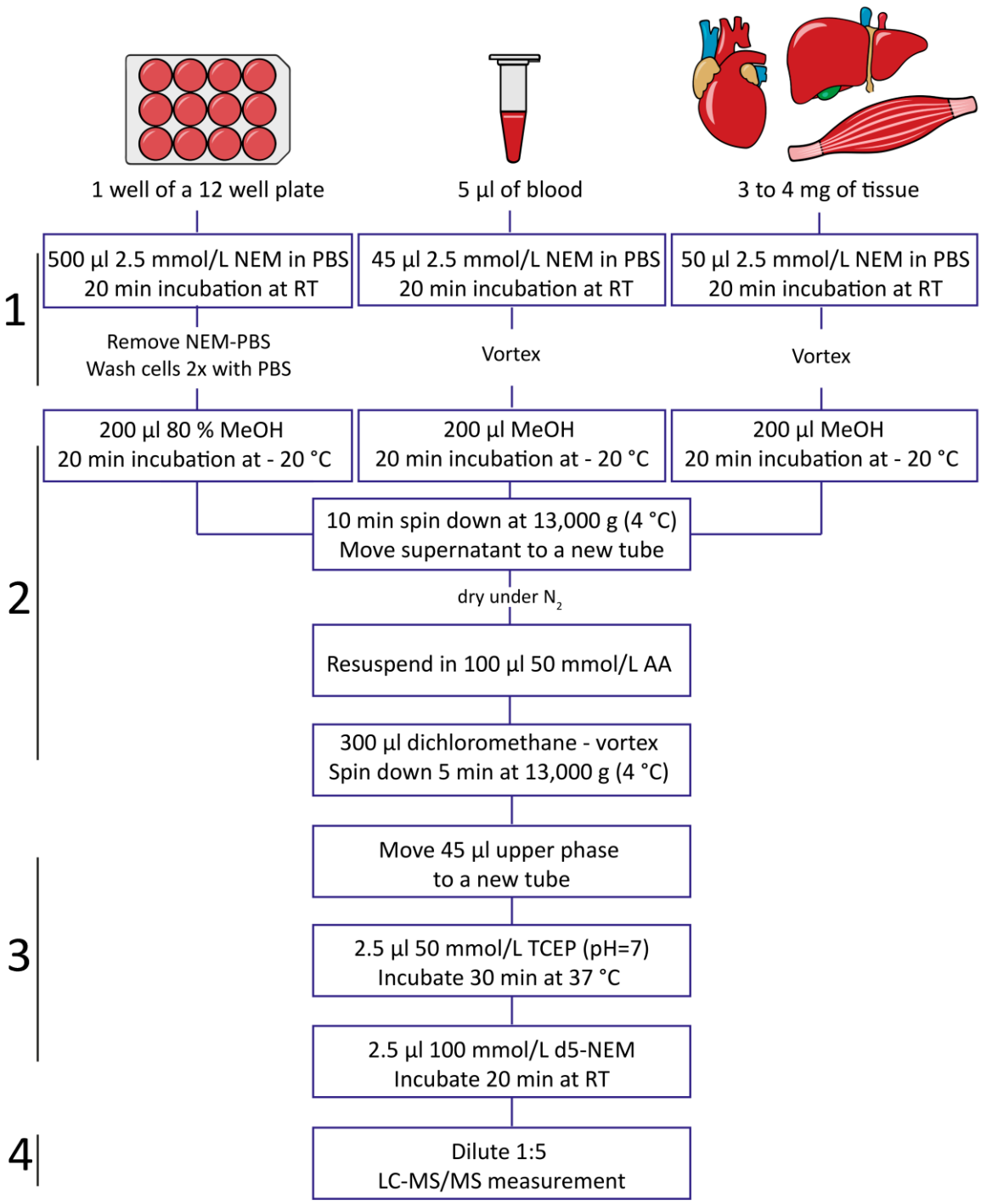

Figure 19. Method workflow. (1) All free GSH is derivatized with NEM in a manner fully optimized to proposed sample types and amounts (2) Proteins are precipitated with methanol and residual NEM is removed with dichloromethane. (3) GSSG is reduced with TCEP to GSH which is then derivatized to GSH-d5-NEM. (4) All analytes are measured in a single run by MRM-based LC-MS/MS.

3.3.1.1 Stepwise method dissection

Immediate alkylation of free GSH is recognized as a mandatory step in GSH/GSSG assessment (161, 163, 168). Otherwise, when exposed to oxygen in the air, GSH will spontaneously oxidize pushing the equilibrium to the GSSG side. For our proposed approach and sample amounts, treatment of the samples for 20 min with 2.5 mM of NEM in PBS proved to be sufficient to fully capture GSH in form of GSH-NEM. To ensure complete derivatization of even more challenging samples such as tissue pieces (Fig. 20A), samples are incubated for 20 min at room temperature in 2.5 mM NEM solution. Additional tissue rupture/sonication steps other than vortexing were proven to be unnecessary as lysis of the tissue with a sonicator did not cause any change in the measured GSH-NEM signal in tested tissues (heart and skeletal muscle) (Fig. 20B) which greatly facilitates sample handling. Completeness of the GSH alkylation was monitored by the extracted ion chromatogram for GSH as shown in Fig. 20A. NEM is an ideal derivatization reagent since it is cell permeable, quickly captures all free GSH (Fig. 20 and Fig. 21A) and also inactivates GR (161).

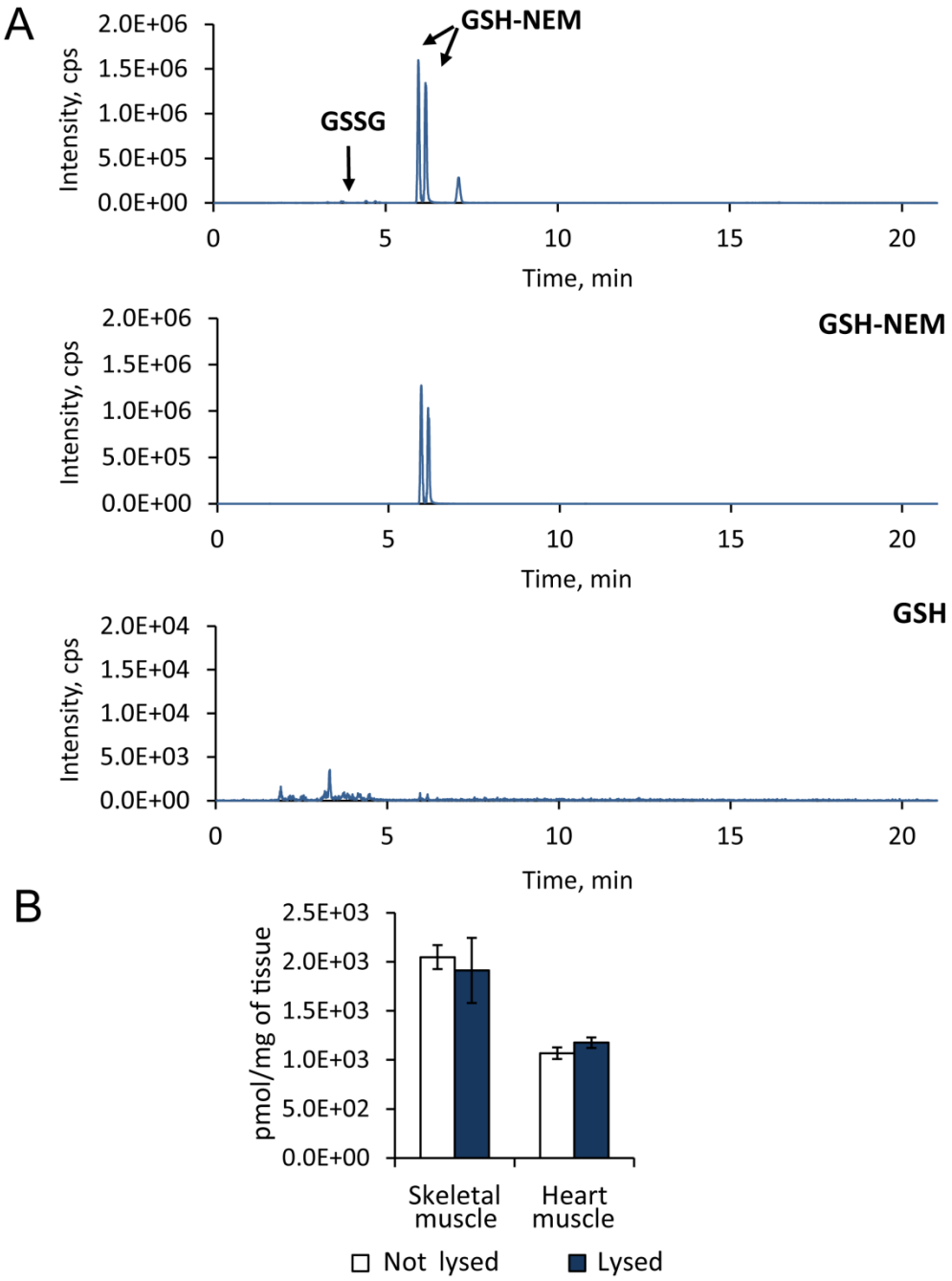

Figure 20. Tissue pieces do not need to be lysed prior initial NEMylation step. A. MRM traces of GSH-NEM and GSH (no residual GSH peak detected, please note the factor 100 difference of the intensity scale) of heart muscle sample after incubation with NEM. B. Additional lysis/tissue rupture steps do not improve GSH alkylation in tissue samples (n=3).

After GSH derivatization in cells or tissues, proteins and cell debris should be removed as only the polar metabolite-rich phase is further used for the analysis. Acid precipitation is the most commonly approach for protein removal upon GSH

alkylation, as a fast solution to prevent GSH oxidation and increase GSH recovery (160, 169, 170). Alternatively, polar organic solvents can be used. As NEM alkylation is best performed at neutral pH for optimal selectivity and reactivity (171) and we intended to introduce another NEM-alkylation step for GSSG derived GSH with isotopically labeled NEM, special care was taken regarding pH. We therefore decided to employ methanol precipitation with 80 % cold methanol (containing the IS) followed by a nitrogen drying step. Dried samples are then re-suspended in 50 mM AA buffered to pH = 7.0 as at the pH > 7.5 NEM has been reported to react with amino groups (160), which could lead to unwanted over-alkylation of GSH.

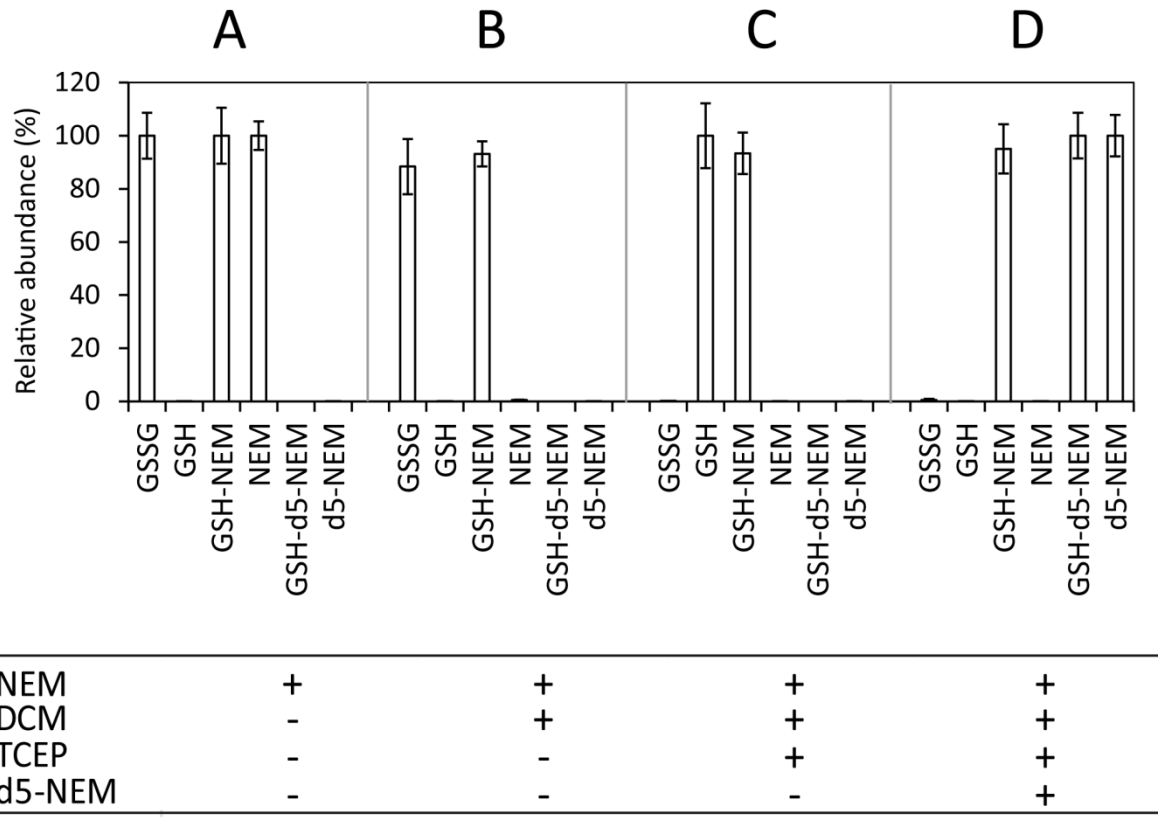

Figure 21. Step by step control experiment. 100 µM of GSH and 10 µM of GSSG standards were mixed (1:10 ratio) and at each step A-D equal aliquot of sample was used for measurement. Non-derivatized samples resulted in a massive standard deviation for both GSH and GSSG due to oxidation, thus they were omitted from this figure. n=4; bars represent means of MRM signal areas normalized on the mean of MRM signal areas of the first appearance in the panel of the corresponding analyte ± normalized S.D.

In order to prevent competition of NEM with d5-NEM at the second derivatization step, dichloromethane extraction of unlabelled NEM is performed. Single extraction with dichloromethane in a volume ratio of 1:3 of sample volume:dichloromethane results in complete NEM removal (Fig. 21B). Any potential residual NEM is quenched in the next step with TCEP. In proteomics TCEP is a frequently used reducing agent due to its wide operating pH range and stability (172) however, it is less well known that TCEP is also able to react with maleimides ((173), Fig. 22).

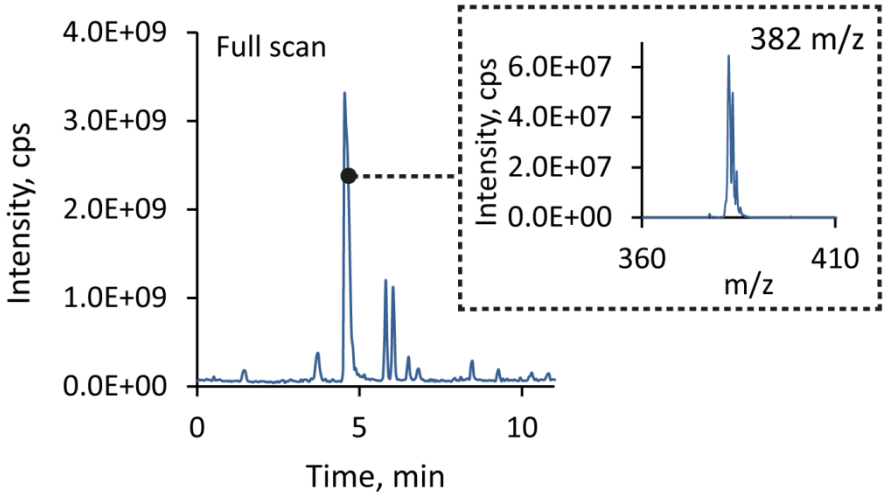

Figure 22. TCEP reacts with d5-NEM (and NEM) yielding a product of the mass to charge ratio (m/z) of 382. 100 µM GSH and 10 µM of GSSG mixture was alkylated with NEM for 20 mins and then incubated for 20 min with different TCEP concentrations after which excess of d5-NEM was added. Represented is a full scan of the sample where 2 mM TCEP and 4.5 mM d5-NEM were used.

TCEP (added to 2.5 mM final concentration) thus quenches any potentially residual NEM while still efficiently performing its intended role of reducing GSSG to GSH (Fig. 21C). However, two precaution measures were proven to be necessary at this step. First, the TCEP stock solution (50 mM) must be prepared in a buffer and adjusted to neutral pH so that addition of TCEP does not perturb the pH and reduce the efficiency of the second alkylation step with d5-NEM. Secondly, d5-NEM must be added in excess over TCEP since TCEP will react with d5-NEM

in the same manner as with unlabelled NEM. Nevertheless, we controlled for any potential off-target labelling of GSSG derived GSH with unlabelled NEM by using a mixture of GSH and GSSG standards in the concentration ratio of 1:10 (100 µM GSH, 10 µML GSSG). Even under these nonnative conditions which support off target labeling, no significant increase of GSH-NEM was observed (Fig. 21BC). Lastly, an excess of d5-NEM (5 mM final concentration) is used to fully quench GSSG derived GSH (Fig. 21D).

Method sensitivity

When sensitivity and responsiveness of the detector for GSSG and GSH-NEM are compared, GSH-NEM proves to be superior to GSSG by around five-fold higher sensitivity, throughout the whole dynamic range (Fig. 23A). Since GSSG reduction yields two molecules of GSH, applying our approach (to measure GSSG as GSH-NEM) results in a 10-fold stronger signal (Table 2).

Table 2. Area under peak ratio of MRM signals of GSH-NEM to GSSG in the low concentration range. Reduction of GSSG with consequent d5-NEM derivatization of released GSH results in approximately 10-fold higher sensitivity compared to direct measurement of GSSG.

c (GSSG) [nM]	MRM signal area ratio GSH-NEM/GSSG
5	**8,48**
10	**9,02**
25	**9,93**
50	**9,26**
100	**9,77**
Mean	**9,29**

Accordingly, the limit of detection (LOD) and the limit of quantitation (LOQ) are in favour of GSH-NEM. For example, 25 fmol of GSSG on column measured as GSSG was beyond the LOD (monitored as MRM trace of GSSG, retention time=

3.71 min) while the same GSSG concentration which was reduced and alkylated with NEM resulted in a reliably quantifiable GSH-NEM peak with a signal to noise ratio (S/N) higher than 10 (MRM for GSH-NEM) (Fig. 23C). The LOD for GSSG was 50 fmol (S/N=7.5) on column, while for GSSG measured as GSH-NEM that value was 5 fmol on column (S/N = 7). For GSSG alone the LOQ was 100 fmol while for GSSG measured as GSH-NEM the LOQ was 10 fmol on column (S/N = 11.5 and 13, respectively). The described 10-fold increase in sensitivity in the low concentration range is also depicted in Fig. 23B)

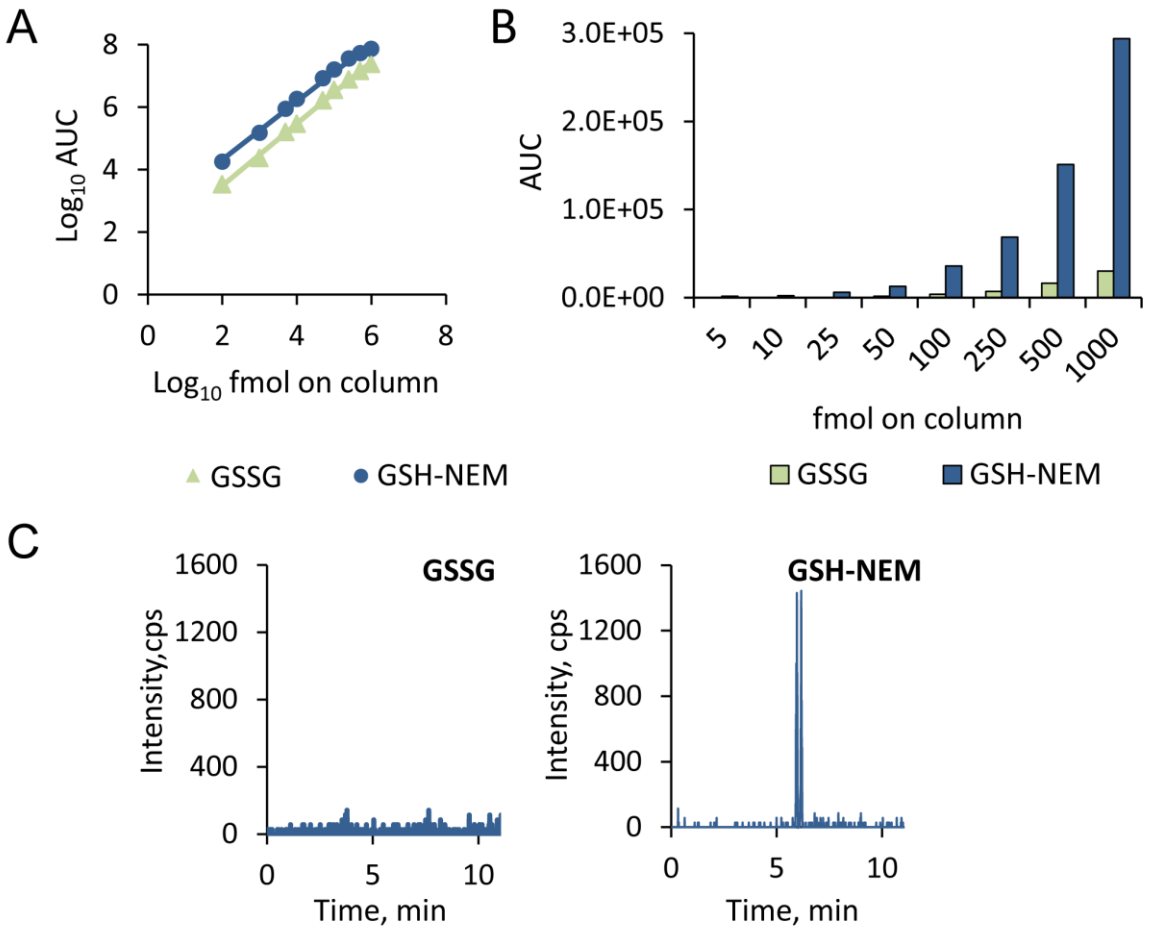

Figure 23. GSH-NEM detection is 10-fold more sensitive than GSSG detection. A. Calibration curves of GSH-NEM (y=0.932x + 3.38, R2=0.994) and GSSG (y=0.994x + 2.49, R2=0.9977). B. Comparison of area responses in low concentration range (5-1000 fmol on column of GSSG) when GSSG is measured as GSSG or processed and measured as GSH-NEM. C. Example – 25 fmol on column of GSSG results in a readily quantifiable GSH-NEM peak.

Biological applications of the method

Analysis of cell culture samples

Our new method was first tested for cell culture samples. For this purpose a single well of a 12-well cell culture plate proved to be sufficient for analysis and the sample could be even further diluted (1:5) prior to measurement. As a proof of concept, we induced oxidative stress in A549 lung cancer cells by treating them with 500 µl of either 100 µM H_2O_2 in Ca^{2+}, Mg^{2+}-PBS or vehicle (Ca^{2+}, Mg^{2+}-PBS). Already 15 min of treatment caused a depletion of GSH with a concomitant accumulation of GSSG, massively altering the GSH/GSSG ratio in treated cells (Fig. 24).

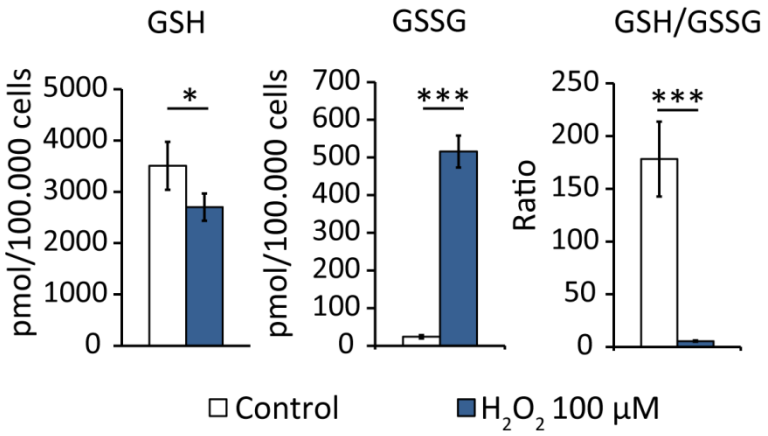

Figure 24. Effect of oxidative stress on the GSH/GSSG ratio. A549 lung cancer cells treated with 100 µM H_2O_2 for 15 min showed a decrease in GSH and a concomitant accumulation of GSSG levels causing a significant reduction of the GSH/GSSG ratio (data from 2 independent experiments, n = 6-8 replicates per condition, Student´s t-test, * p-value < 0.05, *** p-value < 0.001).

Analysis of blood samples

Blood is a particularly tricky analyte for GSH/GSSG assessment due to the following reason: The GSH/GSSG ratio in blood is 3-20 fold larger compared to solid tissues and cultured cells (174). Therefore, in blood, the slightest artificial oxidation of GSH during sample preparation more than anywhere else can result in an overestimation of GSSG (this can be as high as 7-50 folds). The most prominent GSSG artefact effect comes from the delay in NEM addition after blood collection, which leads to rapid depletion of GSH (162). To prevent this, we

pipetted 5 µl of whole blood from three healthy volunteers right after collection into a 2.5 mM NEM containing buffer. After NEM removal with dichloromethane, 10 µl of each sample was taken as a non-reduced control and added to 40 µl of 50 mM AA (1:5 dilution) while another 45 µl of each sample was processed according to the workflow in Fig. 19 and diluted 1:5 prior to measurement. Interestingly, while this approach resulted in full quenching of free GSH, in non-reduced controls the GSSG peak was under LOQ (Fig. 25, left panel). In contrast, reduction of the same samples with TCEP with consequent alkylation with d5-NEM yielded prominent GSH-d5-NEM peaks for all three individuals (Fig. 25, right panel).

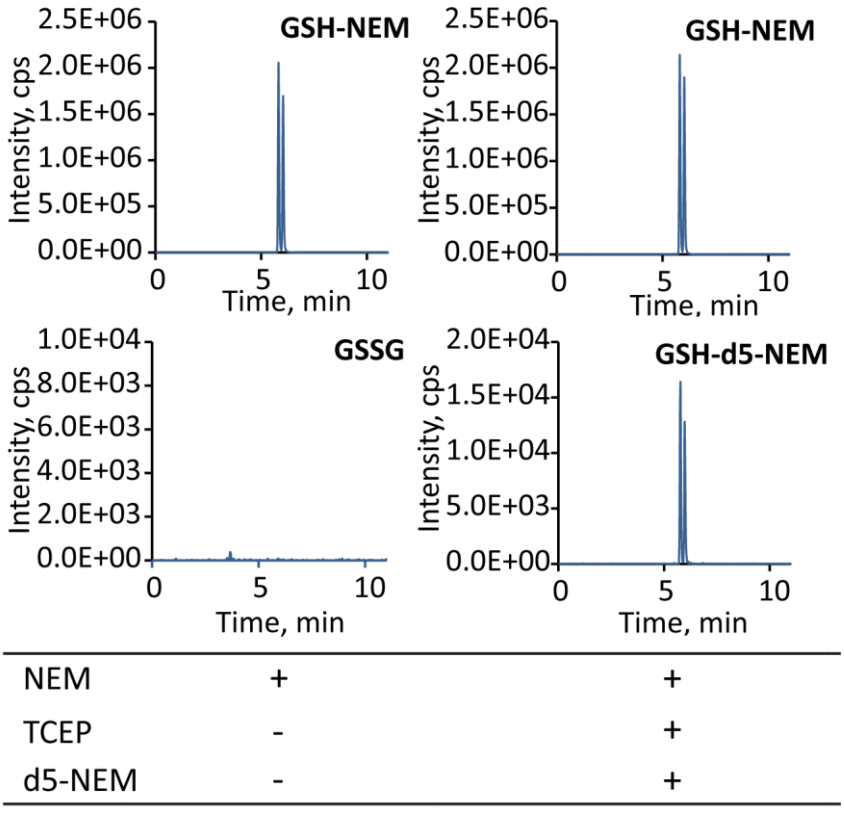

NEM	+	+
TCEP	-	+
d5-NEM	-	+

Figure 25. GSSG is not detectable in 1 µl of whole blood in contrast to GSH-d5-NEM. In 1 µl of whole blood no GSSG peak was detectable before the reduction/d5-NEM alkylation step (left), while the treatment with TCEP and d5-NEM resulted in a quantifiable GSHd5NEM peak originating from GSSG (right).

The addition of NEM without delay is of a particular importance for serum and plasma collection. Both serum and plasma preparations take place at RT for 50 min for serum (30 min. coagulation, 20 min centrifugation) and 10 min for plasma (centrifugation) (175). To access the effect of delayed NEM addition for these

dedicated times, we again collected blood from 5 healthy volunteers but this time pre-customized blood vacuum containers as described in the method section. For all three sample types (serum, plasma and whole blood) from each individual we had one blood container where NEM was introduced prior blood sampling (NEM 0 min samples) and another where samples were pipetted into NEM containing buffer only after previously mentioned preparation times (50 min at RT for serum, 10 min at RT for plasma and 30 min at 4 °C in the case of whole blood; delayed NEM samples). From there on samples were processed as described on Fig. 19. Absolute values for GSH and GSSG are shown in Table 3.

Table 3.. **Absolute GSH and GSSG concentrations in serum, plasma and whole blood of healthy volunteers**. n = 5, mean values ± SEM

	c (GSH) [µmol/L]	c (GSSG) [µmol/L]
Serum		
0 min NEM	38 ± 5	2.7 ± 0.5
50 min NEM	1.4 ± 0.2	4.3 ± 0.5
Plasma		
0 min NEM	5.9 ± 0.8	3.0 ± 0.0
10 min NEM	2.0 ± 0.3	2.6 ± 0.3
Whole blood		
0 min NEM	1249 ± 97	4.1 ± 0.3
30 min NEM	1254 ± 107	4.5 ± 0.3

For both serum and plasma, the delays in NEM addition caused a prominent disturbance of the determined GSH/GSSG ratio. Interestingly, incubation of whole blood at 4 °C for up to 30 min seems to be a safe solution when strictly time controlled processing cannot be guaranteed (Fig. 26).

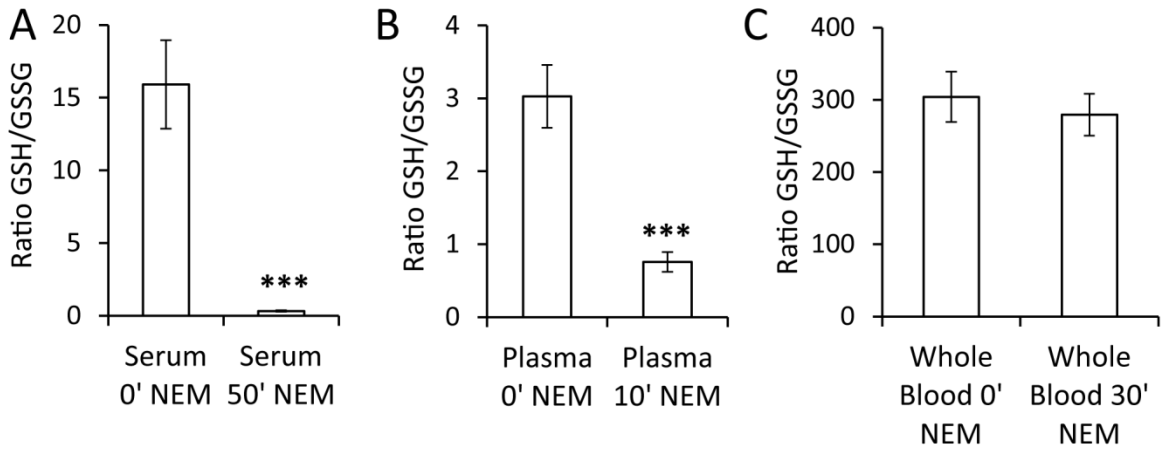

Figure 26. Effect of delayed NEM addition on glutathione redox ratio in blood samples. Serum and plasma preparation (50 and 10 mins at RT, respectively) in the absence of NEM heavily disturb GSH/GSSG ratio while incubation of the whole blood for 30 mins at 4°C does not affect the ratio.

GSH/GSSG ratio is reduced in failing heart tissue

Typically scarce samples where sensitivity plays an essential role are biopsies. Usually, several different tests have to be carried out on a single biopsy and therefore only a small fraction of tissue is available for each of them. To demonstrate that limited tissue amounts as available from biopsies are sufficient for our analytical method we applied it on heart tissue samples. Two patient groups suffering from dilated cardiomyopathy (DCM, n=5, mean age 63 ± 1.5 years) and ischemic cardiomyopathy (ICM; mean age 63 ± 1.6 years) were compared to healthy controls (non-failing heart, NF; n=5, 62 ± 0.8 years). Only 4-7 mg of flash-frozen heart tissue was used as starting material and it was possible to dilute the processed sample 1:5 for measurement while still reliably quantifying both GSH and GSSG. Thus about 1 mg of heart tissue would be sufficient for GSH/GSSG ratio analysis.

Samples from patients suffering from cardiomyopathies showed significantly reduced GSH/GSSG ratios compared to healthy donors' non-failing heart tissues (Fig. 27). In line with a recent publication that ratios of reduced to oxidized thiols (cysteine, cystine, GSH and GSSG) are reduced in coronary artery disease (159), we found that low GSH/GSSG ratios are reduced in failing hearts.

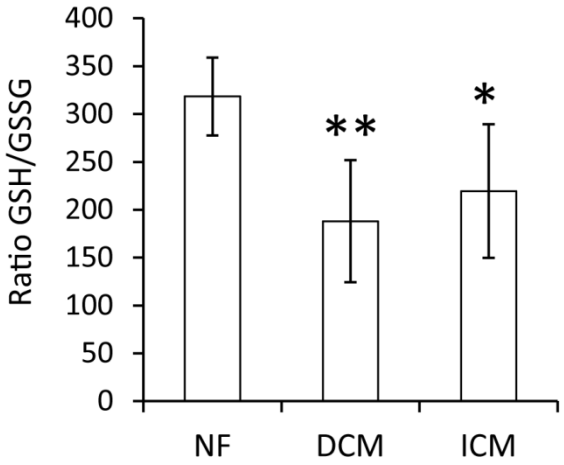

.

Figure 27. Heart tissue from patients suffering from both dilated cardiomyopathy (DCM) and ischemic cardiomyopathy (ICM) exhibit reduced GSH/GSSG ratios compared to non-failing hearts (NF). Bar plot representing GSH/GSSG ratios ± SEM calculated from error propagation of SEMs of GSH and GSSG (n=5 per group, Student t-test, * p-value < 0.05, ** p-value < 0.01).

Discussion (Chapter 2)

Despite a wide variety of published methods for GSH and GSSG analysis (reviewed in (176)), the issue of inconsistency of GSH and GSSG measurements in biological samples is still addressed as an ”elephant in the room” (145), suggesting a continuous need for improvement. Recent considerable efforts provide the main guidelines for sample collection and processing, especially when it comes to blood sample handling and the avoidance of artefacts (162, 174). We here showed how the procedure can be even further simplified.

Firstly, we use fast NEM treatment immediately after sampling to eliminate chemical GSH oxidation artefacts, thus GSSG overestimation is prevented. At this phase there are not many differences to other published methods as GSH is often measured in form of GSH-NEM (161, 163). However, from this step on, for GSSG measurement due to sensitivity issues the most common recommendation is the tedious GSH recycling method, for which NEM extraction is required as even trace amounts of NEM, in addition to many other variables, can influence the

measurement (174). Moreover, measuring GSSG in form of GSH-d5-NEM boosts the sensitivity of the method at least 10-fold (Fig. 23), which proportionally reduces required sample amounts, decreasing the invasiveness of the whole procedure. Furthermore, since both GSH and GSSG are measured as NEM conjugates absolute quantification is greatly facilitated with the usage of only one internal standard (^{13}C2,^{15}N GSH-d5-NEM). Due to the same reason, potential matrix effects are eliminated by design, as they will affect the IS at the same extent as they affect both of the measured analytes. This is particularly important as the matrix can be one main cause of discrepancy in GSSG measurements, like we observed for the whole blood samples where no GSSG could be detected directly in 1 µl (Fig. 25) although its contained amount of about 4000 fmol (Table 3) can be easily determined in a matrix-free standard (Fig. 23B). To put it in a nutshell, we propose a convenient and robust analytical procedure for measuring the glutathione redox ratio which can be easily incorporated and used in various clinical workflows.

Using a sensitive and reliable method for clinical assessment of GSH/GSSG status has a particular relevance since the redox couple can be used as a biomarker for cellular oxidative stress. Oxidative stress plays a significant role in development and progression of various pathologies, in particular cancer and cardiovascular disease. In cancer GSH plays a dual role: it protects cells from carcinogens, however its level also increases as cancer progresses, helping cancer cells to cope with oxidative stress during proliferation and metastasis. Eventually, high GSH content can render cancer cells chemo-resistant (177). In heart disease, oxidative stress has been reported to be closely correlated with the risk of heart failure (HF) (157). This is of special importance considering a growing need for development in the field of HF prognostics. Currently one in eight deaths is due to HF, with a predicted increase in mortality rates by 46% in the course of next 12 years (178). One of the major physiological conditions leading to HF is cardiomyopathy (especially dilated cardiomyopathy (DCM)). DCM has already been brought in correlation with oxidative stress and disturbed GSH homeostasis, with reports suggesting lower GSH/GSSG ratios in patients and animal models with DCM (179, 180). Correspondingly, we report a decreased GSH/GSSG ratio in heart tissue of patients with DCM compared no NF hearts, with no difference

between the two diseased groups. Thus a reduced GSH/GSSG ratio may resemble a potential biomarker for heart related conditions.

Conclusion (Chapter 2)

Our analytical approach is a sensitive, cost-effective and robust alternative for measurement of the GSH/GSSG ratio, one of the main system readouts for redox stress. Using our proposed methodology we suggest that the GSH/GSSG ratio may be a biomarker for heart insufficiency, supporting previous publications which recommend the oxidized thiols status as a marker for arteriosclerosis and cardiovascular related mortality (158, 159). We provide an, in detail optimized, “ready to use” workflow, for which we anticipated potential applications by applying it on blood, tissue and cell samples. In this way, we hope to facilitate and improve glutathione assessment in basic research and in the clinic.

3. REFERENCES

1. Tomin T, Fritz K, Gindlhuber J, Waldherr L, Pucher B, Thallinger GG, et al. Deletion of Adipose Triglyceride Lipase Links Triacylglycerol Accumulation to a More-Aggressive Phenotype in A549 Lung Carcinoma Cells. J Proteome Res. 2018;17(4):1415-25.

2. Radovic B, Vujic N, Leopold C, Schlager S, Goeritzer M, Patankar JV, et al. Lysosomal acid lipase regulates VLDL synthesis and insulin sensitivity in mice. Diabetologia. 2016;59(8):1743-52.

3. Speziali G, Liesinger L, Gindlhuber J, Leopold C, Pucher B, Brandi J, et al. Myristic acid induces proteomic and secretomic changes associated with steatosis, cytoskeleton remodeling, endoplasmic reticulum stress, protein turnover and exosome release in HepG2 cells. J Proteomics. 2018;181:118-30.

4. Hanahan D, Weinberg RA. Hallmarks of cancer: the next generation. Cell. 2011;144(5):646-74.

5. Luo J, Solimini NL, Elledge SJ. Principles of cancer therapy: oncogene and non-oncogene addiction. Cell. 2009;136(5):823-37.

6. Croce CM. Oncogenes and cancer. N Engl J Med. 2008;358(5):502-11.

7. Finley LW, Zhang J, Ye J, Ward PS, Thompson CB. SnapShot: cancer metabolism pathways. Cell Metab. 2013;17(3):466- e2.

8. Liou GY, Storz P. Reactive oxygen species in cancer. Free Radic Res. 2010;44(5):479-96.

9. Kim J, Kim J, Bae JS. ROS homeostasis and metabolism: a critical liaison for cancer therapy. Exp Mol Med. 2016;48(11):e269.

10. Cooper GM. The Cell: A Molecular Approach. Sunderland (MA): Sinauer Associates; 2000.

11. Ozaki T, Nakagawara A. Role of p53 in Cell Death and Human Cancers. Cancers (Basel). 2011;3(1):994-1013.

12. Muller PA, Vousden KH. Mutant p53 in cancer: new functions and therapeutic opportunities. Cancer cell. 2014;25(3):304-17.

13. Counihan JL, Grossman EA, Nomura DK. Cancer Metabolism: Current Understanding and Therapies. Chem Rev. 2018;118(14):6893-923.

14. Milella M, Falcone I, Conciatori F, Cesta Incani U, Del Curatolo A, Inzerilli N, et al. PTEN: Multiple Functions in Human Malignant Tumors. Front Oncol. 2015;5:24.

15. Dang CV, O'Donnell KA, Zeller KI, Nguyen T, Osthus RC, Li F. The c-Myc target gene network. Semin Cancer Biol. 2006;16(4):253-64.

16. Dang CV. MYC, metabolism, cell growth, and tumorigenesis. Cold Spring Harb Perspect Med. 2013;3(8).

17. Raimundo N, Baysal BE, Shadel GS. Revisiting the TCA cycle: signaling to tumor formation. Trends Mol Med. 2011;17(11):641-9.

18. Gabay M, Li Y, Felsher DW. MYC activation is a hallmark of cancer initiation and maintenance. Cold Spring Harb Perspect Med. 2014;4(6).

19. Zornig M, Hueber A, Baum W, Evan G. Apoptosis regulators and their role in tumorigenesis. Biochim Biophys Acta. 2001;1551(2):F1-37.

20. Yin C, Qie S, Sang N. Carbon source metabolism and its regulation in cancer cells. Crit Rev Eukaryot Gene Expr. 2012;22(1):17-35.

21. Witsch E, Sela M, Yarden Y. Roles for growth factors in cancer progression. Physiology (Bethesda). 2010;25(2):85-101.

22. Mitri Z, Constantine T, O'Regan R. The HER2 Receptor in Breast Cancer: Pathophysiology, Clinical Use, and New Advances in Therapy. Chemother Res Pract. 2012;2012:743193.

23. Shostak K, Chariot A. EGFR and NF-kappaB: partners in cancer. Trends Mol Med. 2015;21(6):385-93.

24. Strasser A, Harris AW, Bath ML, Cory S. Novel primitive lymphoid tumours induced in transgenic mice by cooperation between myc and bcl-2. Nature. 1990;348(6299):331-3.

25. Morgan MA, Shilatifard A. Chromatin signatures of cancer. Genes & development. 2015;29(3):238-49.

26. Guertin DA, Sabatini DM. Defining the role of mTOR in cancer. Cancer cell. 2007;12(1):9-22.

27. Zhang S, Yu D. Targeting Src family kinases in anti-cancer therapies: turning promise into triumph. Trends Pharmacol Sci. 2012;33(3):122-8.

28. Irby RB, Yeatman TJ. Role of Src expression and activation in human cancer. Oncogene. 2000;19(49):5636-42.

29. Prior IA, Lewis PD, Mattos C. A comprehensive survey of Ras mutations in cancer. Cancer Res. 2012;72(10):2457-67.

30. Chen X, Qian Y, Wu S. The Warburg effect: evolving interpretations of an established concept. Free Radic Biol Med. 2015;79:253-63.

31. Liu Q, Luo Q, Halim A, Song G. Targeting lipid metabolism of cancer cells: A promising therapeutic strategy for cancer. Cancer Lett. 2017;401:39-45.

32. Warburg O, Wind F, Negelein E. The Metabolism of Tumors in the Body. J Gen Physiol. 1927;8(6):519-30.

33. Warburg O. On the origin of cancer cells. Science. 1956;123(3191):309-14.

34. Weinhouse S. On respiratory impairment in cancer cells. Science. 1956;124(3215):267-9.

35. Rodriguez-Enriquez S, Carreno-Fuentes L, Gallardo-Perez JC, Saavedra E, Quezada H, Vega A, et al. Oxidative phosphorylation is impaired by prolonged hypoxia in breast and possibly in cervix carcinoma. Int J Biochem Cell Biol. 2010;42(10):1744-51.

36. Hay N. Reprogramming glucose metabolism in cancer: can it be exploited for cancer therapy? Nat Rev Cancer. 2016;16(10):635-49.

37. Marin-Hernandez A, Gallardo-Perez JC, Ralph SJ, Rodriguez-Enriquez S, Moreno-Sanchez R. HIF-1alpha modulates energy metabolism in cancer cells by

inducing over-expression of specific glycolytic isoforms. Mini Rev Med Chem. 2009;9(9):1084-101.

38. Patra KC, Hay N. Hexokinase 2 as oncotarget. Oncotarget. 2013;4(11):1862-3.

39. Patra KC, Wang Q, Bhaskar PT, Miller L, Wang Z, Wheaton W, et al. Hexokinase 2 is required for tumor initiation and maintenance and its systemic deletion is therapeutic in mouse models of cancer. Cancer cell. 2013;24(2):213-28.

40. Depre C, Veitch K, Hue L. Role of fructose 2,6-bisphosphate in the control of glycolysis. Stimulation of glycogen synthesis by lactate in the isolated working rat heart. Acta Cardiol. 1993;48(1):147-64.

41. Wong N, Ojo D, Yan J, Tang D. PKM2 contributes to cancer metabolism. Cancer Lett. 2015;356(2 Pt A):184-91.

42. Eales KL, Hollinshead KE, Tennant DA. Hypoxia and metabolic adaptation of cancer cells. Oncogenesis. 2016;5:e190.

43. Kaplon J, Zheng L, Meissl K, Chaneton B, Selivanov VA, Mackay G, et al. A key role for mitochondrial gatekeeper pyruvate dehydrogenase in oncogene-induced senescence. Nature. 2013;498(7452):109-12.

44. Parker SJ, Metallo CM. Metabolic consequences of oncogenic IDH mutations. Pharmacology & therapeutics. 2015;152:54-62.

45. Colvin H, Nishida N, Konno M, Haraguchi N, Takahashi H, Nishimura J, et al. Oncometabolite D-2-Hydroxyglurate Directly Induces Epithelial-Mesenchymal Transition and is Associated with Distant Metastasis in Colorectal Cancer. Sci Rep. 2016;6:36289.

46. Mashima T, Seimiya H, Tsuruo T. De novo fatty-acid synthesis and related pathways as molecular targets for cancer therapy. Br J Cancer. 2009;100(9):1369-72.

47. Hirschhaeuser F, Sattler UG, Mueller-Klieser W. Lactate: a metabolic key player in cancer. Cancer Res. 2011;71(22):6921-5.

48. Choi YK, Park KG. Targeting Glutamine Metabolism for Cancer Treatment. Biomol Ther (Seoul). 2018;26(1):19-28.

49. Smolkova K, Jezek P. The Role of Mitochondrial NADPH-Dependent Isocitrate Dehydrogenase in Cancer Cells. Int J Cell Biol. 2012;2012:273947.

50. Ye D, Guan KL, Xiong Y. Metabolism, Activity, and Targeting of D- and L-2-Hydroxyglutarates. Trends Cancer. 2018;4(2):151-65.

51. Wise DR, Ward PS, Shay JE, Cross JR, Gruber JJ, Sachdeva UM, et al. Hypoxia promotes isocitrate dehydrogenase-dependent carboxylation of alpha-ketoglutarate to citrate to support cell growth and viability. Proc Natl Acad Sci USA. 2011;108(49):19611-6.

52. DeBerardinis RJ, Cheng T. Q's next: the diverse functions of glutamine in metabolism, cell biology and cancer. Oncogene. 2010;29(3):313-24.

53. Alberghina L, Gaglio D. Redox control of glutamine utilization in cancer. Cell Death Dis. 2014;5:e1561.

54. Lu SC. Regulation of glutathione synthesis. Mol Aspects Med. 2009;30(1-2):42-59.

55. Harjes U, Kalucka J, Carmeliet P. Targeting fatty acid metabolism in cancer and endothelial cells. Crit Rev Oncol Hematol. 2016;97:15-21.

56. Beloribi-Djefaflia S, Vasseur S, Guillaumond F. Lipid metabolic reprogramming in cancer cells. Oncogenesis. 2016;5:e189.

57. Currie E, Schulze A, Zechner R, Walther TC, Farese RV, Jr. Cellular fatty acid metabolism and cancer. Cell Metab. 2013;18(2):153-61.

58. Menendez JA, Lupu R. Fatty acid synthase and the lipogenic phenotype in cancer pathogenesis. Nat Rev Cancer. 2007;7(10):763-77.

59. Rohrig F, Schulze A. The multifaceted roles of fatty acid synthesis in cancer. Nat Rev Cancer. 2016;16(11):732-49.

60. Baenke F, Peck B, Miess H, Schulze A. Hooked on fat: the role of lipid synthesis in cancer metabolism and tumour development. Dis Model Mech. 2013;6(6):1353-63.

61. Flavin R, Peluso S, Nguyen PL, Loda M. Fatty acid synthase as a potential therapeutic target in cancer. Future Oncol. 2010;6(4):551-62.

62. Medes G, Thomas A, Weinhouse S. Metabolism of neoplastic tissue. IV. A study of lipid synthesis in neoplastic tissue slices in vitro. Cancer Res. 1953;13(1):27-9.

63. Nath A, Chan C. Genetic alterations in fatty acid transport and metabolism genes are associated with metastatic progression and poor prognosis of human cancers. Sci Rep. 2016;6:18669.

64. Pascual G, Avgustinova A, Mejetta S, Martin M, Castellanos A, Attolini CS, et al. Targeting metastasis-initiating cells through the fatty acid receptor CD36. Nature. 2017;541(7635):41-5.

65. Carracedo A, Cantley LC, Pandolfi PP. Cancer metabolism: fatty acid oxidation in the limelight. Nat Rev Cancer. 2013;13(4):227-32.

66. Casals N, Zammit V, Herrero L, Fado R, Rodriguez-Rodriguez R, Serra D. Carnitine palmitoyltransferase 1C: From cognition to cancer. Prog Lipid Res. 2016;61:134-48.

67. Pucci S, Zonetti MJ, Fisco T, Polidoro C, Bocchinfuso G, Palleschi A, et al. Carnitine palmitoyl transferase-1A (CPT1A): a new tumor specific target in human breast cancer. Oncotarget. 2016;7(15):19982-96.

68. Sadeghi RN, Karami-Tehrani F, Salami S. Targeting prostate cancer cell metabolism: impact of hexokinase and CPT-1 enzymes. Tumour Biol. 2015;36(4):2893-905.

69. Santos CR, Schulze A. Lipid metabolism in cancer. FEBS J. 2012;279(15):2610-23.

70. Thiam AR, Farese RV, Jr., Walther TC. The biophysics and cell biology of lipid droplets. Nat Rev Mol Cell Biol. 2013;14(12):775-86.

71. Boren J, Taskinen MR, Olofsson SO, Levin M. Ectopic lipid storage and insulin resistance: a harmful relationship. J Intern Med. 2013;274(1):25-40.

72. Tirinato L, Liberale C, Di Franco S, Candeloro P, Benfante A, La Rocca R, et al. Lipid droplets: a new player in colorectal cancer stem cells unveiled by spectroscopic imaging. Stem Cells. 2015;33(1):35-44.

73. Giampietri C, Petrungaro S, Cordella M, Tabolacci C, Tomaipitinca L, Facchiano A, et al. Lipid Storage and Autophagy in Melanoma Cancer Cells. Int J Mol Sci. 2017;18(6).

74. Rappa G, Fargeas CA, Le TT, Corbeil D, Lorico A. Letter to the editor: An intriguing relationship between lipid droplets, cholesterol-binding protein CD133 and Wnt/beta-catenin signaling pathway in carcinogenesis. Stem Cells. 2015;33(4):1366-70.

75. Rappa G, Mercapide J, Anzanello F, Le TT, G M, Johlfs RRF, et al. Wnt Interaction and extracellular release of prominin-1/CD133 in human malignant melanoma cells. Exp Cell Res. 2013;319(6):810-9.

76. Qiu B, Ackerman D, Sanchez DJ, Li B, Ochocki JD, Grazioli A, et al. HIF-2α dependent lipid storage promotes endoplasmic reticulum homeostasis in clear cell renal cell carcinoma. Cancer Discov. 2015;5(6):652-67.

77. Accioly MT, Pacheco P, Maya-Monteiro CM, Carrossini N, Robbs BK, Oliveira SS, et al. Lipid bodies are reservoirs of cyclooxygenase-2 and sites of prostaglandin-E2 synthesis in colon cancer cells. Cancer Res. 2008;68(6):1732-40.

78. Zimmermann R, Strauss JG, Haemmerle G, Schoiswohl G, Birner-Gruenberger R, Riederer M, et al. Fat mobilization in adipose tissue is promoted by adipose triglyceride lipase. Science. 2004;306(5700):1383-6.

79. Taschler U, Schreiber R, Chitraju C, Grabner GF, Romauch M, Wolinski H, et al. Adipose triglyceride lipase is involved in the mobilization of triglyceride and retinoid stores of hepatic stellate cells. Biochim Biophys Acta. 2015;1851(7):937-45.

80. Eichmann TO, Kumari M, Haas JT, Farese RV, Jr., Zimmermann R, Lass A, et al. Studies on the substrate and stereo/regioselectivity of adipose triglyceride lipase, hormone-sensitive lipase, and diacylglycerol-O-acyltransferases. J Biol Chem. 2012;287(49):41446-57.

81. Lass A, Zimmermann R, Oberer M, Zechner R. Lipolysis - a highly regulated multi-enzyme complex mediates the catabolism of cellular fat stores. Prog Lipid Res. 2011;50(1):14-27.

82. Padmanabha Das KM, Wechselberger L, Liziczai M, De la Rosa Rodriguez M, Grabner GF, Heier C, et al. Hypoxia-inducible lipid droplet-associated protein inhibits adipose triglyceride lipase. J Lipid Res. 2018;59(3):531-41.

83. Zhang X, Saarinen AM, Hitosugi T, Wang Z, Wang L, Ho TH, et al. Inhibition of intracellular lipolysis promotes human cancer cell adaptation to hypoxia. eLife. 2017;6:e31132.

84. Borg ML, Andrews ZB, Duh EJ, Zechner R, Meikle PJ, Watt MJ. Pigment epithelium-derived factor regulates lipid metabolism via adipose triglyceride lipase. Diabetes. 2011;60(5):1458-66.

85. Zhang H, Sun T, Jiang X, Yu H, Wang M, Wei T, et al. PEDF and PEDF-derived peptide 44mer stimulate cardiac triglyceride degradation via ATGL. J Transl Med. 2015;13:68.

86. Nardi F, Fitchev P, Franco OE, Ivanisevic J, Scheibler A, Hayward SW, et al. PEDF regulates plasticity of a novel lipid-MTOC axis in prostate cancer associated fibroblasts. J Cell Sci. 2018.

87. Ou J, Miao H, Ma Y, Guo F, Deng J, Wei X, et al. Loss of abhd5 promotes colorectal tumor development and progression by inducing aerobic glycolysis and epithelial-mesenchymal transition. Cell reports. 2014;9(5):1798-811.

88. Yim CY, Sekula DJ, Hever-Jardine MP, Liu X, Warzecha JM, Tam J, et al. G0S2 Suppresses Oncogenic Transformation by Repressing a MYC-Regulated Transcriptional Program. Cancer Res. 2016;76(5):1204-13.

89. Chen G, Zhou G, Aras S, He Z, Lucas S, Podgorski I, et al. Loss of ABHD5 promotes the aggressiveness of prostate cancer cells. Sci Rep. 2017;7(1):13021.

90. Mitra R, Le TT, Gorjala P, Goodman OB, Jr. Positive regulation of prostate cancer cell growth by lipid droplet forming and processing enzymes DGAT1 and ABHD5. BMC Cancer. 2017;17(1):631.

91. Kraemer FB, Shen WJ. Hormone-sensitive lipase: control of intracellular tri-(di-)acylglycerol and cholesteryl ester hydrolysis. J Lipid Res. 2002;43(10):1585-94.

92. Zimmermann R, Lass A, Haemmerle G, Zechner R. Fate of fat: the role of adipose triglyceride lipase in lipolysis. Biochim Biophys Acta. 2009;1791(6):494-500.

93. Wu JW, Preuss C, Wang SP, Yang H, Ji B, Carter GW, et al. Epistatic interaction between the lipase-encoding genes Pnpla2 and Lipe causes liposarcoma in mice. PLoS Genet. 2017;13(5):e1006716.

94. Xu M, Chang HH, Jung X, Moro A, Chou CEN, King J, et al. Deficiency in hormone-sensitive lipase accelerates the development of pancreatic cancer in conditional KrasG12D mice. BMC Cancer. 2018;18(1):797.

95. Bedse G, Bluett RJ, Patrick TA, Romness NK, Gaulden AD, Kingsley PJ, et al. Therapeutic endocannabinoid augmentation for mood and anxiety disorders: comparative profiling of FAAH, MAGL and dual inhibitors. Transl Psychiatry. 2018;8(1):92.

96. Nomura DK, Long JZ, Niessen S, Hoover HS, Ng SW, Cravatt BF. Monoacylglycerol lipase regulates a fatty acid network that promotes cancer pathogenesis. Cell. 2010;140(1):49-61.

97. Liu R, Wang X, Curtiss C, Landas S, Rong R, Sheikh MS, et al. Monoglyceride lipase gene knockout in mice leads to increased incidence of lung adenocarcinoma. Cell Death Dis. 2018;9(2):36.

98. Sun H, Jiang L, Luo X, Jin W, He Q, An J, et al. Potential tumor-suppressive role of monoglyceride lipase in human colorectal cancer. Oncogene. 2013;32(2):234-41.

99. Park JB, Lee CS, Jang JH, Ghim J, Kim YJ, You S, et al. Phospholipase signalling networks in cancer. Nat Rev Cancer. 2012;12(11):782-92.

100. Wang YY, Attane C, Milhas D, Dirat B, Dauvillier S, Guerard A, et al. Mammary adipocytes stimulate breast cancer invasion through metabolic remodeling of tumor cells. JCI Insight. 2017;2(4):e87489.

101. Yang D, Li Y, Xing L, Tan Y, Sun J, Zeng B, et al. Utilization of adipocyte-derived lipids and enhanced intracellular trafficking of fatty acids contribute to breast cancer progression. Cell Commun Signal. 2018;16(1):32.

102. Jarc E, Kump A, Malavasic P, Eichmann TO, Zimmermann R, Petan T. Lipid droplets induced by secreted phospholipase A2 and unsaturated fatty acids protect breast cancer cells from nutrient and lipotoxic stress. Biochim Biophys Acta. 2018;1863(3):247-65.

103. Grace SA, Meeks MW, Chen Y, Cornwell M, Ding X, Hou P, et al. Adipose Triglyceride Lipase (ATGL) Expression Is Associated with Adiposity and Tumor Stromal Proliferation in Patients with Pancreatic Ductal Adenocarcinoma. Anticancer Res. 2017;37(2):699-703.

104. Al-Zoughbi W, Pichler M, Gorkiewicz G, Guertl-Lackner B, Haybaeck J, Jahn SW, et al. Loss of adipose triglyceride lipase is associated with human cancer and induces mouse pulmonary neoplasia. Oncotarget. 2016;7(23):33832-40.

105. Vegliante R, Di Leo L, Ciccarone F, Ciriolo MR. Hints on ATGL implications in cancer: beyond bioenergetic clues. Cell Death Dis. 2018;9(3):316.

106. Zagani R, El-Assaad W, Gamache I, Teodoro JG. Inhibition of adipose triglyceride lipase (ATGL) by the putative tumor suppressor G0S2 or a small molecule inhibitor attenuates the growth of cancer cells. Oncotarget. 2015;6(29):28282-95.

107. Das SK, Eder S, Schauer S, Diwoky C, Temmel H, Guertl B, et al. Adipose triglyceride lipase contributes to cancer-associated cachexia. Science. 2011;333(6039):233-8.

108. Siegel RL, Miller KD, Jemal A. Cancer Statistics, 2017. CA Cancer J Clin. 2017;67(1):7-30.

109. Dela Cruz CS, Tanoue LT, Matthay RA. Lung cancer: epidemiology, etiology, and prevention. Clin Chest Med. 2011;32(4):605-44.

110. Kopp F, Komatsu T, Nomura DK, Trauger SA, Thomas JR, Siuzdak G, et al. The glycerophospho metabolome and its influence on amino acid homeostasis revealed by brain metabolomics of GDE1(-/-) mice. Chem Biol. 2010;17(8):831-40.

111. Mulvihill MM, Benjamin DI, Ji X, Le Scolan E, Louie SM, Shieh A, et al. Metabolic profiling reveals PAFAH1B3 as a critical driver of breast cancer pathogenicity. Chem Biol. 2014;21(7):831-40.

112. Tyanova S, Temu T, Sinitcyn P, Carlson A, Hein MY, Geiger T, et al. The Perseus computational platform for comprehensive analysis of (prote)omics data. Nat Methods. 2016;13(9):731-40.

113. Wisniewski JR, Zougman A, Nagaraj N, Mann M. Universal sample preparation method for proteome analysis. Nat Methods. 2009;6(5):359-62.

114. Cox J, Mann M. MaxQuant enables high peptide identification rates, individualized p.p.b.-range mass accuracies and proteome-wide protein quantification. Nat Biotechnol. 2008;26(12):1367-72.

115. Ward JH. Hierarchical Grouping to Optimize an Objective Function. J Am Stat Assoc. 1963;58(301):236-44.

116. Vizcaino JA, Deutsch EW, Wang R, Csordas A, Reisinger F, Rios D, et al. ProteomeXchange provides globally coordinated proteomics data submission and dissemination. Nat Biotechnol. 2014;32(3):223-6.

117. Magnusson CD, Haraldsson GG. Ether lipids. Chem Phys Lipids. 2011;164(5):315-40.

118. Bassa BV, Noh JW, Ganji SH, Shin MK, Roh DD, Kamanna VS. Lysophosphatidylcholine stimulates EGF receptor activation and mesangial cell proliferation: regulatory role of Src and PKC. Biochim Biophys Acta. 2007;1771(11):1364-71.

119. Bassa BV, Roh DD, Vaziri ND, Kirschenbaum MA, Kamanna VS. Lysophosphatidylcholine activates mesangial cell PKC and MAP kinase by PLCgamma-1 and tyrosine kinase-Ras pathways. Am J Physiol. 1999;277(3 Pt 2):F328-37.

120. Ishii I, Fukushima N, Ye X, Chun J. Lysophospholipid receptors: signaling and biology. Annu Rev Biochem. 2004;73:321-54.

121. Cox J, Hein MY, Luber CA, Paron I, Nagaraj N, Mann M. Accurate proteome-wide label-free quantification by delayed normalization and maximal peptide ratio extraction, termed MaxLFQ. Mol Cell Proteomics. 2014;13(9):2513-26.

122. Di Florio A, Capurso G, Milione M, Panzuto F, Geremia R, Fave GD, et al. Src family kinase activity regulates adhesion, spreading and migration of pancreatic endocrine tumour cells. Endocr Relat Cancer. 2007;14(1):111-24.

123. King SJ, Nowak K, Suryavanshi N, Holt I, Shanahan CM, Ridley AJ. Nesprin-1 and nesprin-2 regulate endothelial cell shape and migration. Cytoskeleton (Hoboken). 2014;71(7):423-34.

124. Fallah-Tafti A, Foroumadi A, Tiwari R, Shirazi AN, Hangauer DG, Bu Y, et al. Thiazolyl N-benzyl-substituted acetamide derivatives: synthesis, Src kinase inhibitory and anticancer activities. Eur J Med Chem. 2011;46(10):4853-8.

125. Schweiger M, Romauch M, Schreiber R, Grabner GF, Hutter S, Kotzbeck P, et al. Pharmacological inhibition of adipose triglyceride lipase corrects high-fat diet-induced insulin resistance and hepatosteatosis in mice. Nat Commun. 2017;8:14859.

126. Navarro-Tito N, Robledo T, Salazar EP. Arachidonic acid promotes FAK activation and migration in MDA-MB-231 breast cancer cells. Exp Cell Res. 2008;314(18):3340-55.

127. Park JH, Vithayathil S, Kumar S, Sung PL, Dobrolecki LE, Putluri V, et al. Fatty Acid Oxidation-Driven Src Links Mitochondrial Energy Reprogramming and Oncogenic Properties in Triple-Negative Breast Cancer. Cell reports. 2016;14(9):2154-65.

128. Volkmer E, Drosse I, Otto S, Stangelmayer A, Stengele M, Kallukalam BC, et al. Hypoxia in static and dynamic 3D culture systems for tissue engineering of bone. Tissue Eng Part A. 2008;14(8):1331-40.

129. Richter S, Richter JP, Mehta SY, Gribble AM, Sutherland-Smith AJ, Stowell KM, et al. Expression and role in glycolysis of human ADP-dependent glucokinase. Mol Cell Biochem. 2012;364(1-2):131-45.

130. Antalis CJ, Uchida A, Buhman KK, Siddiqui RA. Migration of MDA-MB-231 breast cancer cells depends on the availability of exogenous lipids and cholesterol esterification. Clin Exp Metastasis. 2011;28(8):733-41.

131. Bailey Andrew P, Koster G, Guillermier C, Hirst Elizabeth M, MacRae James I, Lechene Claude P, et al. Antioxidant Role for Lipid Droplets in a Stem Cell Niche of Drosophila. Cell. 2015;163(2):340-53.

132. Herms A, Bosch M, Ariotti N, Reddy BJ, Fajardo A, Fernandez-Vidal A, et al. Cell-to-cell heterogeneity in lipid droplets suggests a mechanism to reduce lipotoxicity. Curr Biol. 2013;23(15):1489-96.

133. Listenberger LL, Han X, Lewis SE, Cases S, Farese RV, Jr., Ory DS, et al. Triglyceride accumulation protects against fatty acid-induced lipotoxicity. Proc Natl Acad Sci USA. 2003;100(6):3077-82.

134. Nguyen TB, Louie SM, Daniele JR, Tran Q, Dillin A, Zoncu R, et al. DGAT1-Dependent Lipid Droplet Biogenesis Protects Mitochondrial Function during Starvation-Induced Autophagy. Dev Cell. 2017;42(1):9-21 e5.

135. Albert DH, Anderson CE. Ether-linked glycerolipids in human brain tumors. Lipids. 1977;12(2):188-92.

136. Gwak GY, Yoon JH, Lee SH, Lee SM, Lee HS, Gores GJ. Lysophosphatidylcholine suppresses apoptotic cell death by inducing cyclooxygenase-2 expression via a Raf-1 dependent mechanism in human cholangiocytes. J Cancer Res Clin Oncol. 2006;132(12):771-9.

137. Howard BV, Morris HP, Bailey JM. Ether-lipids, -glycerol phosphate dehydrogenase, and growth rate in tumors and cultured cells. Cancer Res. 1972;32(7):1533-8.

138. Meyer zu Heringdorf D, Jakobs KH. Lysophospholipid receptors: signalling, pharmacology and regulation by lysophospholipid metabolism. Biochim Biophys Acta. 2007;1768(4):923-40.

139. Piano V, Benjamin DI, Valente S, Nenci S, Marrocco B, Mai A, et al. Discovery of Inhibitors for the Ether Lipid-Generating Enzyme AGPS as Anti-Cancer Agents. ACS Chem Biol. 2015;10(11):2589-97.

140. Tan M, Hao F, Xu X, Chisolm GM, Cui MZ. Lysophosphatidylcholine activates a novel PKD2-mediated signaling pathway that controls monocyte migration. Arterioscler Thromb Vasc Biol. 2009;29(9):1376-82.

141. Deponte M. Glutathione catalysis and the reaction mechanisms of glutathione-dependent enzymes. Biochim Biophys Acta. 2013;1830(5):3217-66.

142. Forman HJ, Zhang H, Rinna A. Glutathione: overview of its protective roles, measurement, and biosynthesis. Mol Aspects Med. 2009;30(1-2):1-12.

143. Lu SC. Glutathione synthesis. Biochim Biophys Acta. 2013;1830(5):3143-53.

144. Meister A. Glutathione deficiency produced by inhibition of its synthesis, and its reversal; applications in research and therapy. Pharmacology & therapeutics. 1991;51(2):155-94.

145. Giustarini D, Tsikas D, Colombo G, Milzani A, Dalle-Donne I, Fanti P, et al. Pitfalls in the analysis of the physiological antioxidant glutathione (GSH) and its disulfide (GSSG) in biological samples: An elephant in the room. J Chromatogr B Analyt Technol Biomed Life Sci. 2016;1019:21-8.

146. Kanaan GN, Harper ME. Cellular redox dysfunction in the development of cardiovascular diseases. Biochim Biophys Acta. 2017;1861(11 Pt A):2822-9.

147. Townsend DM, Tew KD, Tapiero H. The importance of glutathione in human disease. Biomed Pharmacother. 2003;57(3-4):145-55.

148. Zitka O, Skalickova S, Gumulec J, Masarik M, Adam V, Hubalek J, et al. Redox status expressed as GSH:GSSG ratio as a marker for oxidative stress in paediatric tumour patients. Oncol Lett. 2012;4(6):1247-53.

149. Ballatori N, Krance SM, Notenboom S, Shi S, Tieu K, Hammond CL. Glutathione dysregulation and the etiology and progression of human diseases. Biol Chem. 2009;390(3):191-214.

150. Traverso N, Ricciarelli R, Nitti M, Marengo B, Furfaro AL, Pronzato MA, et al. Role of glutathione in cancer progression and chemoresistance. Oxid Med Cell Longev. 2013;2013:972913.

151. Lenzen S. Chemistry and biology of reactive species with special reference to the antioxidative defence status in pancreatic beta-cells. Biochim Biophys Acta. 2017;1861(8):1929-42.

152. Sekhar RV, McKay SV, Patel SG, Guthikonda AP, Reddy VT, Balasubramanyam A, et al. Glutathione synthesis is diminished in patients with uncontrolled diabetes and restored by dietary supplementation with cysteine and glycine. Diabetes Care. 2011;34(1):162-7.

153. Carvalho AN, Lim JL, Nijland PG, Witte ME, Van Horssen J. Glutathione in multiple sclerosis: more than just an antioxidant? Mult Scler. 2014;20(11):1425-31.

154. Johnson WM, Wilson-Delfosse AL, Mieyal JJ. Dysregulation of glutathione homeostasis in neurodegenerative diseases. Nutrients. 2012;4(10):1399-440.

155. Damy T, Kirsch M, Khouzami L, Caramelle P, Le Corvoisier P, Roudot-Thoraval F, et al. Glutathione deficiency in cardiac patients is related to the functional status and structural cardiac abnormalities. PLoS One. 2009;4(3):e4871.

156. Watanabe Y, Watanabe K, Kobayashi T, Saito Y, Fujioka D, Nakamura T, et al. Chronic depletion of glutathione exacerbates ventricular remodelling and dysfunction in the pressure-overloaded heart. Cardiovasc Res. 2013;97(2):282-92.

157. Keith M, Geranmayegan A, Sole MJ, Kurian R, Robinson A, Omran AS, et al. Increased oxidative stress in patients with congestive heart failure. J Am Coll Cardiol. 1998;31(6):1352-6.

158. Ashfaq S, Abramson JL, Jones DP, Rhodes SD, Weintraub WS, Hooper WC, et al. The relationship between plasma levels of oxidized and reduced thiols and early atherosclerosis in healthy adults. J Am Coll Cardiol. 2006;47(5):1005-11.

159. Patel RS, Ghasemzadeh N, Eapen DJ, Sher S, Arshad S, Ko YA, et al. Novel Biomarker of Oxidative Stress Is Associated With Risk of Death in Patients With Coronary Artery Disease. Circulation. 2016;133(4):361-9.

160. Rossi R, Milzani A, Dalle-Donne I, Giustarini D, Lusini L, Colombo R, et al. Blood glutathione disulfide: in vivo factor or in vitro artifact? Clin Chem. 2002;48(5):742-53.

161. Giustarini D, Dalle-Donne I, Milzani A, Fanti P, Rossi R. Analysis of GSH and GSSG after derivatization with N-ethylmaleimide. Nat Protoc. 2013;8(9):1660-9.

162. Sutton TR, Minnion M, Barbarino F, Koster G, Fernandez BO, Cumpstey AF, et al. A robust and versatile mass spectrometry platform for comprehensive assessment of the thiol redox metabolome. Redox Biol. 2018;16:359-80.

163. Giustarini D, Dalle-Donne I, Milzani A, Rossi R. Detection of glutathione in whole blood after stabilization with N-ethylmaleimide. Anal Biochem. 2011;415(1):81-3.

164. McGill MR, Jaeschke H. A direct comparison of methods used to measure oxidized glutathione in biological samples: 2-vinylpyridine and N-ethylmaleimide. Toxicol Mech Methods. 2015;25(8):589-95.

165. Tipple TE, Rogers LK. Methods for the determination of plasma or tissue glutathione levels. Methods Mol Biol. 2012;889:315-24.

166. Sentellas S, Morales-Ibanez O, Zanuy M, Alberti JJ. GSSG/GSH ratios in cryopreserved rat and human hepatocytes as a biomarker for drug induced oxidative stress. Toxicol In Vitro. 2014;28(5):1006-15.

167. Rajer M, Kmet M. Quantitative analysis of fine needle aspiration biopsy samples. Radiol Oncol. 2005;39(4):269-72.

168. Harwood DT, Kettle AJ, Brennan S, Winterbourn CC. Simultaneous determination of reduced glutathione, glutathione disulphide and glutathione sulphonamide in cells and physiological fluids by isotope dilution liquid chromatography-tandem mass spectrometry. J Chromatogr B Analyt Technol Biomed Life Sci. 2009;877(28):3393-9.

169. Stempak D, Dallas S, Klein J, Bendayan R, Koren G, Baruchel S. Glutathione stability in whole blood: effects of various deproteinizing acids. Ther Drug Monit. 2001;23(5):542-9.

170. Zhang F, Bartels MJ, Geter DR, Jeong YC, Schisler MR, Wood AJ, et al. Quantitation of glutathione by liquid chromatography/positive electrospray ionization tandem mass spectrometry. Rapid Commun Mass Spectrom. 2008;22(22):3608-14.

171. Paulech J, Solis N, Cordwell SJ. Characterization of reaction conditions providing rapid and specific cysteine alkylation for peptide-based mass spectrometry. Biochim Biophys Acta. 2013;1834(1):372-9.

172. Han JC, Han GY. A procedure for quantitative determination of tris(2-carboxyethyl)phosphine, an odorless reducing agent more stable and effective than dithiothreitol. Anal Biochem. 1994;220(1):5-10.

173. Shafer DE, Inman JK, Lees A. Reaction of Tris(2-carboxyethyl)phosphine (TCEP) with maleimide and alpha-haloacyl groups: anomalous elution of TCEP by gel filtration. Anal Biochem. 2000;282(1):161-4.

174. Giustarini D, Colombo G, Garavaglia ML, Astori E, Portinaro NM, Reggiani F, et al. Assessment of glutathione/glutathione disulphide ratio and S-glutathionylated proteins in human blood, solid tissues, and cultured cells. Free Radic Biol Med. 2017;112:360-75.

175. Tuck MK, Chan DW, Chia D, Godwin AK, Grizzle WE, Krueger KE, et al. Standard operating procedures for serum and plasma collection: early detection research network consensus statement standard operating procedure integration working group. J Proteome Res. 2009;8(1):113-7.

176. Iwasaki Y, Saito Y, Nakano Y, Mochizuki K, Sakata O, Ito R, et al. Chromatographic and mass spectrometric analysis of glutathione in biological samples. J Chromatogr B Analyt Technol Biomed Life Sci. 2009;877(28):3309-17.

177. Bansal A, Simon MC. Glutathione metabolism in cancer progression and treatment resistance. J Cell Biol. 2018;217(7):2291-8.

178. Benjamin EJ, Blaha MJ, Chiuve SE, Cushman M, Das SR, Deo R, et al. Heart Disease and Stroke Statistics-2017 Update: A Report From the American Heart Association. Circulation. 2017;135(10):e146-e603.

179. Yucel D, Aydogdu S, Cehreli S, Saydam G, Canatan H, Senes M, et al. Increased oxidative stress in dilated cardiomyopathic heart failure. Clin Chem. 1998;44(1):148-54.

180. Lynch TL, Sivaguru M, Velayutham M, Cardounel AJ, Michels M, Barefield D, et al. Oxidative Stress in Dilated Cardiomyopathy Caused by MYBPC3 Mutation. Oxid Med Cell Longev. 2015;2015:424751.

4. APPENDIX

Appendix 1A: Sequence alignment of the ATGL gene region of A549 cell clones determined with the forward primer

```
A549_clone3_7_ATGL-KO.hATGL_CRIS      -CCTCTGCTGTCTGCCATCCCAGGGGAGGTGGCCAAAGTCCCAACTGTGAGCCAGGCCCC
A549_clone3_3_ATGL-KO.hATGL_CRIS      GCCTCTGCTGTCTGCCATCCCAGGGGAGGTGGCCAAAGTCCCAACTGTGAGCCAGGCCCC
A549_clone3_10_ATGL-KO.hATGL_CRI      GCCTCTGCTGTCTGCCATCCCAGGGGAGGTGGCCAAAGTCCCAACTGTGAGCCAGGCCCC
A549_cloneC7_ATGL-ctrl.hATGL_CRI      GCCTCTGCTGTCTGCCATCCCAGGGGAGGTGGCCAAAGTCCCAACTGTGAGCCAGGCCCC
A549_parental.hATGL_CRISPR_seq_f      GCCTCTGCTGTCTGCCATCCCAGGGGAGGTGGCCAAAGTCCCAACTGTGAGCCAGGCCCC
A549_cloneC8_ATGL-ctrl.hATGL_CRI      GCCTCTGCTGTCTGCCATCCCAGGGGAGGTGGCCAAAGTCCCAACTGTGAGCCAGGCCCC
A549_cloneB8_ATGL-ctrl.hATGL_CRI      GCCTCTGCTGTCTGCCATCCCAGGGGAGGTGGCCAAAGTCCCAACTGTGAGCCAGGCCCC
                                       ************************************************************

A549_clone3_7_ATGL-KO.hATGL_CRIS      ACATTCACTGGGCCTCCTCCAGGGTCTGTATGCCATGGAACCCTGGACATGGGGCTATGA
A549_clone3_3_ATGL-KO.hATGL_CRIS      ACATTCACTGGGCCTCCTCCAGGGTCTGTATGCCATGGAACCCTGGACATGGGGCTATGA
A549_clone3_10_ATGL-KO.hATGL_CRI      ACATTCACTGGGCCTCCTCCAGGGTCTGTATGCCATGGAACCCTGGACATGGGGCTATGA
A549_cloneC7_ATGL-ctrl.hATGL_CRI      ACATTCACTGGGCCTCCTCCAGGGTCTGTATGCCATGGAACCCTGGACATGGGGCTATGA
A549_parental.hATGL_CRISPR_seq_f      ACATTCACTGGGCCTCCTCCAGGGTCTGTATGCCATGGAACCCTGGACATGGGGCTATGA
A549_cloneC8_ATGL-ctrl.hATGL_CRI      ACATTCACTGGGCCTCCTCCAGGGTCTGTATGCCATGGAACCCTGGACATGGGGCTATGA
A549_cloneB8_ATGL-ctrl.hATGL_CRI      ACATTCACTGGGCCTCCTCCAGGGTCTGTATGCCATGGAACCCTGGACATGGGGCTATGA
                                      ************************************************************

A549_clone3_7_ATGL-KO.hATGL_CRIS      AGGAAGGTGGGTGTTGCTAAGCCCAGGAGCATGGGCCCCTAACCTTGGCCCTGTGCCCCA
A549_clone3_3_ATGL-KO.hATGL_CRIS      AGGAAGGTGGGTGTTGCTAAGCCCAGGAGCATGGGCCCCTAACCTTGGCCCTGTGCCCCA
A549_clone3_10_ATGL-KO.hATGL_CRI      AGGAAGGTGGGTGTTGCTAAGCCCAGGAGCATGGGCCCCTAACCTTGGCCCTGTGCCCCA
A549_cloneC7_ATGL-ctrl.hATGL_CRI      AGGAAGGTGGGTGTTGCTAAGCCCAGGAGCATGGGCCCCTAACCTTGGCCCTGTGCCCCA
A549_parental.hATGL_CRISPR_seq_f      AGGAAGGTGGGTGTTGCTAAGCCCAGGAGCATGGGCCCCTAACCTTGGCCCTGTGCCCCA
A549_cloneC8_ATGL-ctrl.hATGL_CRI      AGGAAGGTGGGTGTTGCTAAGCCCAGGAGCATGGGCCCCTAACCTTGGCCCTGTGCCCCA
A549_cloneB8_ATGL-ctrl.hATGL_CRI      AGGAAGGTGGGTGTTGCTAAGCCCAGGAGCATGGGCCCCTAACCTTGGCCCTGTGCCCCA
                                      ************************************************************

A549_clone3_7_ATGL-KO.hATGL_CRIS      GGTGAGGCTGGTGCCAAGTTCATTGAGGTATCTAAAGAGGCCCGGAAGCGGTTCCTGGGC
A549_clone3_3_ATGL-KO.hATGL_CRIS      GGTGAGGCTGGTGCCAAGTTCATTGAGGTATCTAAAGAGGCCCGGAAGCGGTTCCTGGGC
A549_clone3_10_ATGL-KO.hATGL_CRI      GGTGAGGCTGGTGCCAAGTTCATTGAGGTATCTAAAGAGGCCCGGAAGCGGTTCCTGGGC
A549_cloneC7_ATGL-ctrl.hATGL_CRI      GGTGAGGCTGGTGCCAAGTTCATTGAGGTATCTAAAGAGGCCCGGAAGCGGTTCCTGGGC
A549_parental.hATGL_CRISPR_seq_f      GGTGAGGCTGGTGCCAAGTTCATTGAGGTATCTAAAGAGGCCCGGAAGCGGTTCCTGGGC
A549_cloneC8_ATGL-ctrl.hATGL_CRI      GGTGAGGCTGGTGCCAAGTTCATTGAGGTATCTAAAGAGGCCCGGAAGCGGTTCCTGGGC
A549_cloneB8_ATGL-ctrl.hATGL_CRI      GGTGAGGCTGGTGCCAAGTTCATTGAGGTATCTAAAGAGGCCCGGAAGCGGTTCCTGGGC
                                      ************************************************************

A549_clone3_7_ATGL-KO.hATGL_CRIS      CCCCTGCACCCCTCCTTCAACCTGGTAAAGATCATCCGCAGTTTCCTGCTGAAGGTCCTG
A549_clone3_3_ATGL-KO.hATGL_CRIS      CCCCTGCACCCCTCCTTCAACCTGGTAAAGATCATCCGCAGTTTCCTGCTGAAGGTCCTG
A549_clone3_10_ATGL-KO.hATGL_CRI      CCCCTGCACCCCTCCTTCAACCTGGTAAAGATCATCCGCAGTTTCCTGCTGAAGGTCCTG
A549_cloneC7_ATGL-ctrl.hATGL_CRI      CCCCTGCACCCCTCCTTCAACCTGGTAAAGATCATCCGCAGTTTCCTGCTGAAGGTCCTG
A549_parental.hATGL_CRISPR_seq_f      CCCCTGCACCCCTCCTTCAACCTGGTAAAGATCATCCGCAGTTTCCTGCTGAAGGTCCTG
A549_cloneC8_ATGL-ctrl.hATGL_CRI      CCCCTGCACCCCTCCTTCAACCTGGTAAAGATCATCCGCAGTTTCCTGCTGAAGGTCCTG
A549_cloneB8_ATGL-ctrl.hATGL_CRI      CCCCTGCACCCCTCCTTCAACCTGGTAAAGATCATCCGCAGTTTCCTGCTGAAGGTCCTG
                                      ************************************************************

A549_clone3_7_ATGL-KO.hATGL_CRIS      CCTGCTGATAGCCATGAGCATGGGTACCATCGAG-----------CTAGCTGATTGTCGA
A549_clone3_3_ATGL-KO.hATGL_CRIS      CCTGCTGATAGCCATGAGCATGGGTACCATCGAG-----------CTAGCTGATTGTCGA
A549_clone3_10_ATGL-KO.hATGL_CRI      CCTGCTGATAGCCATGAGCATGGGTACCATCGAG-----------CTAGCTGATTGTCGA
A549_cloneC7_ATGL-ctrl.hATGL_CRI      CCTGCTGATAGCCATGAGCATG----CCAGTGGGCGCCTGGGCATCTCCCTGACCCGCGT
A549_parental.hATGL_CRISPR_seq_f      CCTGCTGATAGCCATGAGCATG----CCAGTGGGCGCCTGGGCATCTCCCTGACCCGCGT
A549_cloneC8_ATGL-ctrl.hATGL_CRI      CCTGCTGATAGCCATGAGCATG----CCAGTGGGCGCCTGGGCATCTCCCTGACCCGCGT
A549_cloneB8_ATGL-ctrl.hATGL_CRI      CCTGCTGATAGCCATGAGCATG----CCAGTGGGCGCCTGGGCATCTCCCTGACCCGCGT
                                      **********************    ***  * *           **  ****    **

A549_clone3_7_ATGL-KO.hATGL_CRIS      GTAGGAC----ATAACTTCGTATAATGTATGCTATACGAAGTTATCTGATCAGATCCTGC
A549_clone3_3_ATGL-KO.hATGL_CRIS      GTAGGAC----ATAACTTCGTATAATGTATGCTATACGAAGTTATCTGATCAGATCCTGC
A549_clone3_10_ATGL-KO.hATGL_CRI      GTAGGAC----ATAACTTCGTATAATGTATGCTATACGAAGTTATCTGATCAGATCCTGC
A549_cloneC7_ATGL-ctrl.hATGL_CRI      GTCAGACGGCGAGAATGTCAT----TATATCCCACTTCAACTCCAAGGACGAGCTCATCC
A549_parental.hATGL_CRISPR_seq_f      GTCAGACGGCGAGAATGTCAT----TATATCCCACTTCAACTCCAAGGACGAGCTCATCC
A549_cloneC8_ATGL-ctrl.hATGL_CRI      GTCAGACGGCGAGAATGTCAT----TATATCCCACTTCAACTCCAAGGACGAGCTCATCC
A549_cloneB8_ATGL-ctrl.hATGL_CRI      GTCAGACGGCGAGAATGTCAT----TATATCCCACTTCAACTCCAAGGACGAGCTCATCC
                                      **  ***    * **  ** *    * *** * *    ** *     **  ** ** * *

A549_clone3_7_ATGL-KO.hATGL_CRIS      AGGTA----CTCGAGAAGGCGCGCCGTGGATCTGCGGCCGCGAAGGATCTGCGATCGCTC
A549_clone3_3_ATGL-KO.hATGL_CRIS      AGGTA----CTCGAGAAGGCGCGCCGTGGATCTGCGGCCGCGAAGGATCTGCGATCGCTC
A549_clone3_10_ATGL-KO.hATGL_CRI      AGGTA----CTCGAGAAGGCGCGCCGTGGATCTGCGGCCGCGAAGGATCTGCGATCGCTC
A549_cloneC7_ATGL-ctrl.hATGL_CRI      AGGTGGGGCCTGGTGGAGCCATGCTG------GGTGGCGGTGGGGGG-------------
A549_parental.hATGL_CRISPR_seq_f      AGGTGGGGCCTGGTGGAGCCATGCTG------GGTGGCGGTGGGGGG-------------
A549_cloneC8_ATGL-ctrl.hATGL_CRI      AGGTGGGGCCTGGTGGAGCCATGCTG------GGTGGCGGTGGGGGG-------------
A549_cloneB8_ATGL-ctrl.hATGL_CRI      AGGTGGGGCCTGGTGGAGCCATGCTG------GGTGGCGGTGGGGGG-------------
                                      ****     ** * * ** *  ** *       * *** * *  **

A549_clone3_7_ATGL-KO.hATGL_CRIS      CGGTGCCCGTCAGTGGG-----CAGAGC----GCACA---TCGCCCA--CAGTCCCCGAG
A549_clone3_3_ATGL-KO.hATGL_CRIS      CGGTGCCCGTCAGTGGG-----CAGAGC----GCACA---TCGCCCA--CAGTCCCCGAG
A549_clone3_10_ATGL-KO.hATGL_CRI      CGGTGCCCGTCAGTGGG-----CAGAGC----GCACA---TCGCCCA--CAGTCCCCGAG
A549_cloneC7_ATGL-ctrl.hATGL_CRI      --------GGCAGTGGGAACCTCAAGGCCTCTGCTCATTCTCTCCCACTCTGTCCCTG--
```

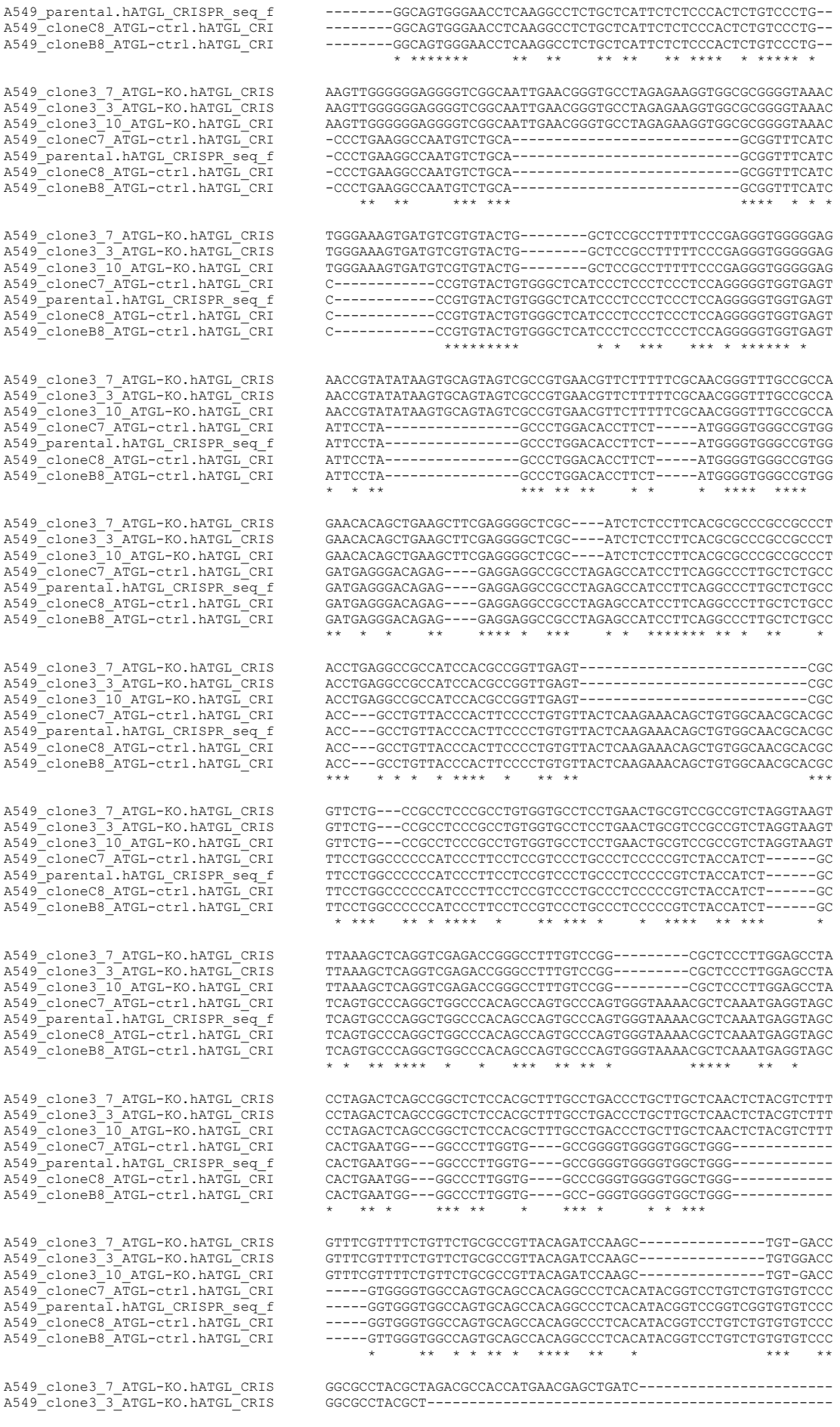
A549_parental.hATGL_CRISPR_seq_f
A549_cloneC8_ATGL-ctrl.hATGL_CRI
A549_cloneB8_ATGL-ctrl.hATGL_CRI
A549_clone3_7_ATGL-KO.hATGL_CRIS
A549_clone3_3_ATGL-KO.hATGL_CRIS
A549_clone3_10_ATGL-KO.hATGL_CRI
A549_cloneC7_ATGL-ctrl.hATGL_CRI

```
A549_clone3_10_ATGL-KO.hATGL_CRI      GGCGCCTACGCTAGACGCCACCATGAGCGAGCTGATCAAGGAGAACATGCCCATGAAGC-
A549_cloneC7_ATGL-ctrl.hATGL_CRI      GTGG-AAACGCTA--------CGTGGATGGTGGCATTTCAGAAAACCTGCCACTCTATGA
A549_parental.hATGL_CRISPR_seq_f      GTGG-AAGCGCTA--------CGTGGATGGT----------------------------
A549_cloneC8_ATGL-ctrl.hATGL_CRI      GGGGAAAGCGCTA--------CGTG------------------------------------
A549_cloneB8_ATGL-ctrl.hATGL_CRI      GTGG-AAGCGCTA--------CGTGGATGGTGGCATTTCAGACAACCGGCCACTCTATGA
                                      *  *    ****

A549_clone3_7_ATGL-KO.hATGL_CRIS      ----------------------------
A549_clone3_3_ATGL-KO.hATGL_CRIS      ----------------------------
A549_clone3_10_ATGL-KO.hATGL_CRI      ----------------------------
A549_cloneC7_ATGL-ctrl.hATGL_CRI      GCTTAAGAACACCATCACAGTGTCC--
A549_parental.hATGL_CRISPR_seq_f      ----------------------------
A549_cloneC8_ATGL-ctrl.hATGL_CRI      ----------------------------
A549_cloneB8_ATGL-ctrl.hATGL_CRI      GCTTAAGAACACCATCACAGTGTCCCC
```

Appendix 1B: Sequence alignment of the ATGL gene region of A549 cell clones determined with the reverse primer

```
A549_parental.hATGL_CRISPR_seq_r      ----TGGCTGGGAGGCCACAGTCCCCGGAGCAGAGCTCACCAGGGGCTCCGGCGGGAAGA
A549_cloneC8_ATGL-ctrl.hATGL_CRI      ----TGGCTGGGAGGCCACAGTCCCCGGAGCAGAGCTCACCAGGGGCTCCGGCGGGAAGA
A549_cloneB8_ATGL-ctrl.hATGL_CRI      ----TGGCTGGGAGGCCACAGTCCCCGGAGCAGAGCTCACCAGGGGCTCCGGCGGGAAGA
A549_cloneC7_ATGL-ctrl.hATGL_CRI      GGAGTGGCTGGGAGGCCACAGTCCCCGGAGCAGAGCTCACCAGGGGCTCCGGCGGGAAGA
A549_clone3_3_ATGL-KO.hATGL_CRIS      ------------------------------------------------------------
A549_clone3_10_ATGL-KO.hATGL_CRI      ----TGGCTGGGAGGCCACAGTCCTCGGAGCAGAGCTCACCAGGGGCTCCGGCGGGAAGA
A549_clone3_7_ATGL-KO.hATGL_CRIS      GGAGTGGCTGGGAGGCCACAGTCCTCGGAGCAGAGCTCACCAGGGGCTCCGGCGGGAAGA


A549_parental.hATGL_CRISPR_seq_r      GGGCCTTGGAGAGGCGGTAGAGGTTGCGCAGGTTGAACTGGATGCTGGTGTTGGTGACCC
A549_cloneC8_ATGL-ctrl.hATGL_CRI      GGGCCTTGGAGAGGCGGTAGAGGTTGCGCAGGTTGAACTGGATGCTGGTGTTGGTGACCC
A549_cloneB8_ATGL-ctrl.hATGL_CRI      GGGCCTTGGAGAGGCGGTAGAGGTTGCGCAGGTTGAACTGGATGCTGGTGTTGGTGACCC
A549_cloneC7_ATGL-ctrl.hATGL_CRI      GGGCCTTGGAGAGGCGGTAGAGGTTGCGCAGGTTGAACTGGATGCTGGTGTTGGTGACCC
A549_clone3_3_ATGL-KO.hATGL_CRIS      ----------GAGGCGGTAGAGGTTGCGCAGGTTGAACTGGATGCTGGTGTTGGTGACCC
A549_clone3_10_ATGL-KO.hATGL_CRI      GGGCCTTGGAGAGGCGGTAGAGGTTGCGCAGGTTGAACTGGATGCTGGTGTTGGTGACCC
A549_clone3_7_ATGL-KO.hATGL_CRIS      GGGCCTTGGAGAGGCGGTAGAGGTTGCGCAGGTTGAACTGGATGCTGGTGTTGGTGACCC
                                      **************************************************


A549_parental.hATGL_CRISPR_seq_r      GCAGCTCGTGGATGTTGGTGGAGCTGTCCTGCGGACAGATGTCACTCTCGCCCGAGAAGG
A549_cloneC8_ATGL-ctrl.hATGL_CRI      GCAGCTCGTGGATGTTGGTGGAGCTGTCCTGCGGACAGATGTCACTCTCGCCCGAGAAGG
A549_cloneB8_ATGL-ctrl.hATGL_CRI      GCAGCTCGTGGATGTTGGTGGAGCTGTCCTGCGGACAGATGTCACTCTCGCCCGAGAAGG
A549_cloneC7_ATGL-ctrl.hATGL_CRI      GCAGCTCGTGGATGTTGGTGGAGCTGTCCTGCGGACAGATGTCACTCTCGCCCGAGAAGG
A549_clone3_3_ATGL-KO.hATGL_CRIS      GCAGCTCGTGGATGTTGGTGGAGTC----------TAGATTATAACTTCGT-----ATAG
A549_clone3_10_ATGL-KO.hATGL_CRI      GCAGCTCGTGGATGTTGGTGGAGTC----------TAGATGATAACTTCGT-----ATAG
A549_clone3_7_ATGL-KO.hATGL_CRIS      GCAGCTCGTGGATGTTGGTGGAGTC----------TAGATGATAACTTCGT-----ATAG
                                      **********************             ****   *   ***      *  *


A549_parental.hATGL_CRISPR_seq_r      GGGACACTGTGATGGTGTTCTTAAGCTCATAGAGTGGCAGGTTGTCTGAAATGCCACCAT
A549_cloneC8_ATGL-ctrl.hATGL_CRI      GGGACACTGTGATGGTGTTCTTAAGCTCATAGAGTGGCAGGTTGTCTGAAATGCCACCAT
A549_cloneB8_ATGL-ctrl.hATGL_CRI      GGGACACTGTGATGGTGTTCTTAAGCTCATAGAGTGGCAGGTTGTCTGAAATGCCACCAT
A549_cloneC7_ATGL-ctrl.hATGL_CRI      GGGACACTGTGATGGTGTTCTTAAGCTCATAGAGTGGCAGGTTGTCTGAAATGCCACCAT
A549_clone3_3_ATGL-KO.hATGL_CRIS      CATACATTAT-ACGAAGTTATCAAAGCTGTA----------------------GCTACGAT
A549_clone3_10_ATGL-KO.hATGL_CRI      CATACATTAT-ACGAAGTTATCAAAGCTGTA----------------------GCTACGAT
A549_clone3_7_ATGL-KO.hATGL_CRIS      CATACATTAT-ACGAAGTTATCAAAGCTGTA----------------------GCTACGAT
                                         *** * * * *  *** * **     **                     ** ** **


A549_parental.hATGL_CRISPR_seq_r      CCACGTAGCGCTTCCACGGGACACACAGACAGGACCGTATGTGAGGG---CCTGTGGCTG
A549_cloneC8_ATGL-ctrl.hATGL_CRI      CCACGTAGCGCTTCCACGGGACACACAGACAGGACCGTATGTGAGGG---CCTGTGGCTG
A549_cloneB8_ATGL-ctrl.hATGL_CRI      CCACGTAGCGCTTCCACGGGACACACAGACAGGACCGTATGTGAGGG---CCTGTGGCTG
A549_cloneC7_ATGL-ctrl.hATGL_CRI      CCACGTAGCGCTTCCACGGGACACACAGACAGGACCGTATGTGAGGG---CCTGTGGCTG
A549_clone3_3_ATGL-KO.hATGL_CRIS      C-----------------------------------------ATGAGGATCCTCTCTGGCTC
A549_clone3_10_ATGL-KO.hATGL_CRI      C-----------------------------------------ATGAGGATCCTCTCTGGCTC
A549_clone3_7_ATGL-KO.hATGL_CRIS      C-----------------------------------------ATGAGGATCCTCTCTGGCTC
                                      *                                          *****     ** *****


A549_parental.hATGL_CRISPR_seq_r      CACTGGCCACCCACCCCAGCCACCCC-ACCCGGCCACCAAGGGCCCCATTCAGTGGCTAC
A549_cloneC8_ATGL-ctrl.hATGL_CRI      CACTGGCCACCCACCCCAGCCACCCC-ACCCGGCCACCAAGGGCCCCATTCAGTGGCTAC
A549_cloneB8_ATGL-ctrl.hATGL_CRI      CACTGGCCACCCACCCCAGCCACCCC-ACCCGGCCACCAAGGGCCCCATTCAGTGGCTAC
A549_cloneC7_ATGL-ctrl.hATGL_CRI      CACTGGCCACCCACCCCAGCCACCCC-ACCCGGCCACCAAGGGCCCCATTCAGTGGCTAC
A549_clone3_3_ATGL-KO.hATGL_CRIS      CATCGTAAGCAAACCTTACAGGTTCTGGCAAGGAGAGAGATGGCTCCAGGAAATGG----
A549_clone3_10_ATGL-KO.hATGL_CRI      CATCGTAAGCAAACCTTAGAGGTTCTGGCAAGGAGAGAGATGGCTCCAGGAAATGG----
A549_clone3_7_ATGL-KO.hATGL_CRIS      CATCGTAAGCAAACCTTAGAGGTTCTGGCAAGGAGAGAGATGGCTCCAGGAAATGG----
                                      **  *    *  ***  *      *   *  **  *   * *** ***   * ***


A549_parental.hATGL_CRISPR_seq_r      CTCATTTGAGCGTTTTACCCACTGGGCACTGGCTGTGGGCCAGCCTGGGCACTGAGCAGA
A549_cloneC8_ATGL-ctrl.hATGL_CRI      CTCATTTGAGCGTTTTACCCACTGGGCACTGGCTGTGGGCCAGCCTGGGCACTGAGCAGA
A549_cloneB8_ATGL-ctrl.hATGL_CRI      CTCATTTGAGCGTTTTACCCACTGGGCACTGGCTGTGGGCCAGCCTGGGCACTGAGCAGA
A549_cloneC7_ATGL-ctrl.hATGL_CRI      CTCATTTGAGCGTTTTACCCACTGGGCACTGGCTGTGGGCCAGCCTGGGCACTGAGCAGA
A549_clone3_3_ATGL-KO.hATGL_CRIS      -------GGGTGTGTCACCAGATAAG----------GAATCTGCCT------------AA
A549_clone3_10_ATGL-KO.hATGL_CRI      -------GGGTGTGTCACCAGATAAG----------GAATCTGCCT------------AA
A549_clone3_7_ATGL-KO.hATGL_CRIS      -------GGGTGTGTCACCAGATAAG----------GAATCTGCCT------------AA
                                             * * ** * ***   *  *          *   * ****            *
```

```
A549_parental.hATGL_CRISPR_seq_r      TGGTAGACGGGGG---------AGGGCAGGGACGGAGGAAGGGATGGGGGGCCAGGAAGC
A549_cloneC8_ATGL-ctrl.hATGL_CRI      TGGTAGACGGGGG---------AGGGCAGGGACGGAGGAAGGGATGGGGGGCCAGGAAGC
A549_cloneB8_ATGL-ctrl.hATGL_CRI      TGGTAGACGGGGG---------AGGGCAGGGACGGAGGAAGGGATGGGGGGCCAGGAAGC
A549_cloneC7_ATGL-ctrl.hATGL_CRI      TGGTAGACGGGGG---------AGGGCAGGGACGGAGGAAGGGATGGGGGGCCAGGAAGC
A549_clone3_3_ATGL-KO.hATGL_CRIS      CAGGAGGTGGGGGTTAGACCCAATATCAGGAGACTAGGAAGGA--GGAGGCCTAAGGATG
A549_clone3_10_ATGL-KO.hATGL_CRI      CAGGAGGTGGGGGTTAGACCCAATATCAGGAGACTAGGAAGGA--GGAGGCCTAAGGATG
A549_clone3_7_ATGL-KO.hATGL_CRIS      CAGGAGGTGGGGGTTAGACCCAATATCAGGAGACTAGGAAGGA--GGAGGCCTAAGGATG
                                        * **  *****         *   ****     *******   ** ** * * * *

A549_parental.hATGL_CRISPR_seq_r      GTGC------GTTGCCACAGCTGTTTCTTGAGTA----ACACAGGGGAAGTGGG---TAA
A549_cloneC8_ATGL-ctrl.hATGL_CRI      GTGC------GTTGCCACAGCTGTTTCTTGAGTA----ACACAGGGGAAGTGGG---TAA
A549_cloneB8_ATGL-ctrl.hATGL_CRI      GTGC------GTTGCCACAGCTGTTTCTTGAGTA----ACACAGGGGAAGTGGG---TAA
A549_cloneC7_ATGL-ctrl.hATGL_CRI      GTGC------GTTGCCACAGCTGTTTCTTGAGTA----ACACAGGGGAAGTGGG---TAA
A549_clone3_3_ATGL-KO.hATGL_CRIS      GAGCTTTTCTGTCACCAATCCTGTCCCT--AGTAGTGTACACCATACCAATGGGCCCTAA
A549_clone3_10_ATGL-KO.hATGL_CRI      GGGCTTTTCTGTCACCAATCCTGTCCCT--AGTAGTGTACACCATACCAATGGGCCCTAA
A549_clone3_7_ATGL-KO.hATGL_CRIS      GGGCTTTTCTGTCACCAATCCTGTCCCT--AGTAGTGTACACCATACCAATGGGCCCTAA
                                      * **      **  ***   ****  **  ****    ****      * ****   ***

A549_parental.hATGL_CRISPR_seq_r      CAGGCGGTGGCAG---AGCAAGGGCCTGAAGGATGGCTCTAGGCGGCCTCCTCCTCT---
A549_cloneC8_ATGL-ctrl.hATGL_CRI      CAGGCGGTGGCAG---AGCAAGGGCCTGAAGGATGGCTCTAGGCGGCCTCCTCCTCT---
A549_cloneB8_ATGL-ctrl.hATGL_CRI      CAGGCGGTGGCAG---AGCAAGGGCCTGAAGGATGGCTCTAGGCGGCCTCCTCCTCT---
A549_cloneC7_ATGL-ctrl.hATGL_CRI      CAGGCGGTGGCAG---AGCAAGGGCCTGAAGGATGGCTCTAGGCGGCCTCCTCCTCT---
A549_clone3_3_ATGL-KO.hATGL_CRIS      AAAAGGAATCCAGTCAATTCCGGGGCTAAA--------CCTGGCTGCCACTGTTTCTTTA
A549_clone3_10_ATGL-KO.hATGL_CRI      AAAAGGAATCCAGTCAATTCCGGGGCTAAA--------CCTGGCTGCCACTGTTTCTTTA
A549_clone3_7_ATGL-KO.hATGL_CRIS      AAAAGGAATCCAGTCAATTCCGGGGCTAAA--------CCTGGCTGCCACTGTTTCTTTA
                                       *   *    ***   *    *** ** **        *  *** *** *    ***

A549_parental.hATGL_CRISPR_seq_r      -GTCCCTCATCCC-------ACGGCCCACCCCATAGA--AGGTGTCCAGGGCTAGG----
A549_cloneC8_ATGL-ctrl.hATGL_CRI      -GTCCCTCATCCC-------ACGGCCCACCCCATAGA--AGGTGTCCAGGGCTAGG----
A549_cloneB8_ATGL-ctrl.hATGL_CRI      -GTCCCTCATCCC-------ACGGCCCACCCCATAGA--AGGTGTCCAGGGCTAGG----
A549_cloneC7_ATGL-ctrl.hATGL_CRI      -GTCCCTCATCCC-------ACGGCCCACCCCATAGA--AGGTGTCCAGGGCTAGG----
A549_clone3_3_ATGL-KO.hATGL_CRIS      GGGACTTCGTTCCTGTGAGGACAGGAAACCCTGCAACCTGGTTGACCAGAGCAAGGGATA
A549_clone3_10_ATGL-KO.hATGL_CRI      GGGACTTCGTTCCTGTGAGGACAGGAAACCCTGCAACCTGGTTGACCAGAGCAAGGGATA
A549_clone3_7_ATGL-KO.hATGL_CRIS      GGGACTTCGTTCCTGTGAGGACAGGAAACCCTGCAACCTGGTTGACCAGAGCAAGGGATA
                                       *  * ** * **       ** *   ****   *     * ** **** ** ***

A549_parental.hATGL_CRISPR_seq_r      --------------------------------AATACTCACCA-----------CCCCCTG
A549_cloneC8_ATGL-ctrl.hATGL_CRI      --------------------------------AATACTCACCA-----------CCCCCTG
A549_cloneB8_ATGL-ctrl.hATGL_CRI      --------------------------------AATACTCACCA-----------CCCCCTG
A549_cloneC7_ATGL-ctrl.hATGL_CRI      --------------------------------AATACTCACCA-----------CCCCCTG
A549_clone3_3_ATGL-KO.hATGL_CRIS      TAAGAACCCAGTTTGGGAACACTGCTGTTTAAATATTAAACAGGGATGTCTTGTCCCCCG
A549_clone3_10_ATGL-KO.hATGL_CRI      TAAGAACCCAGTTTGGGAACACTGCTGTTTAAATATTAAACAGGGATGTCTTGTCCCCCG
A549_clone3_7_ATGL-KO.hATGL_CRIS      TAAGAACCCAGTTTGGGAACACTGCTGTTTAAATATTAAACAGGGATGTCTTGTCCCCCG
                                                                      **** * * **           **** *

A549_parental.hATGL_CRISPR_seq_r      GAGGGAGGGAGGGATGAGCCCACAGTACACGGG--GA-------TGAAACCGCTGCAGAC
A549_cloneC8_ATGL-ctrl.hATGL_CRI      GAGGGAGGGAGGGATGAGCCCACAGTACACGGG--GA-------TGAAACCGCTGCAGAC
A549_cloneB8_ATGL-ctrl.hATGL_CRI      GAGGGAGGGAGGGATGAGCCCACAGTACACGGG--GA-------TGAAACCGCTGCAGAC
A549_cloneC7_ATGL-ctrl.hATGL_CRI      GAGGGAGGGAGGGATGAGCCCACAGTACACGGG--GA-------TGAAACCGCTGCAGAC
A549_clone3_3_ATGL-KO.hATGL_CRIS      GAAGGGAGACCAGATGAGCTTCTGATAGACTAATTGACATCATTTGAGTCAATTCCAGAC
A549_clone3_10_ATGL-KO.hATGL_CRI      GAAGGGAGACCAGATGAGCTTCTGATAGACTAATTGACATCATTTGAGTCAATTCCAGAC
A549_clone3_7_ATGL-KO.hATGL_CRIS      GAAGGGAGACCAGATGAGCTTCTGATAGACTAATTGACATCATTTGAGTCAATTCCAGAC
                                      ** **  *    *******      ** **     **       ***  *   * *****

A549_parental.hATGL_CRISPR_seq_r      ATTG------GCCTTCA-GGGCAGGGACA------GAGTGGGAGAGAATG-AGCAGAGGC
A549_cloneC8_ATGL-ctrl.hATGL_CRI      ATTG------GCCTTCA-GGGCAGGGACA------GAGTGGGAGAGAATG-AGCAGAGGC
A549_cloneB8_ATGL-ctrl.hATGL_CRI      ATTG------GCCTTCA-GGGCAGGGACA------GAGTGGGAGAGAATG-AGCAGAGGC
A549_cloneC7_ATGL-ctrl.hATGL_CRI      ATTG------GCCTTCA-GGGCAGGGACA------GAGTGGGAGAGAATG-AGCAGAGGC
A549_clone3_3_ATGL-KO.hATGL_CRIS      ATGATAAGATACATTGATGAGTTTGGACAAACCACAACTAGAATGCAGTGAAAAAAATGC
A549_clone3_10_ATGL-KO.hATGL_CRI      ATGATAAGATACATTGATGAGTTTGGACAAACCACAACTAGAATGCAGTG-AAAAAATGC
A549_clone3_7_ATGL-KO.hATGL_CRIS      ATGATAAGATACATTGATGAGTTTGGACAAACCACAACTAGAATGCAGTG-AAAAAATGC
                                      **         * ** * * *   *****       * * * *   * ** *  * * **

A549_parental.hATGL_CRISPR_seq_r      CT------TGAGGTTCCCACTGCCCC--CCCCACCGCCACCCAGCATGGCTCCACCAGGC
A549_cloneC8_ATGL-ctrl.hATGL_CRI      CT------TGAGGTTCCCACTGCCCC--CCCCACCGCCACCCAGCATGGCTCCACCAGGC
A549_cloneB8_ATGL-ctrl.hATGL_CRI      CT------TGAGGTTCCCACTGCCCC--CCCCACCGCCACCCAGCATGGCTCCACCAGGC
A549_cloneC7_ATGL-ctrl.hATGL_CRI      CT------TGAGGTTCCCACTGCCCC--CCCCACCGCCACCCAGCATGGCTCCACCAGGC
A549_clone3_3_ATGL-KO.hATGL_CRIS      TTTATTTGTGAAATTTGTGATGCTATTGCTTTATTTGTAACCATTAT----------AAGC
A549_clone3_10_ATGL-KO.hATGL_CRI      TTTATATGTGAAATTTGTGATGCTATTGCTTTATTTGTAACCATTAT----------AAGC
A549_clone3_7_ATGL-KO.hATGL_CRIS      TTTATATGTGAAATTTGTGATGCTATTGCTTTATTTGTAACCATTAT----------AAGC
                                       *      ***  **     ***     *   *     * ***  **         * **

A549_parental.hATGL_CRISPR_seq_r      CCCACCTGGATGAGCTCGTCCTTGGAGTTGAAGTGGGATATAATGACATTCTCGCCGTCT
A549_cloneC8_ATGL-ctrl.hATGL_CRI      CCCACCTGGATGAGCTCGTCCTTGGAGTTGAAGTGGGATATAATGACATTCTCGCCGTCT
A549_cloneB8_ATGL-ctrl.hATGL_CRI      CCCACCTGGATGAGCTCGTCCTTGGAGTTGAAGTGGGATATAATGACATTCTCGCCGTCT
A549_cloneC7_ATGL-ctrl.hATGL_CRI      CCCACCTGGATGAGCTCGTCCTTGGAGTTGAAGTGGGATATAATGACATTCTCGCCGTCT
A549_clone3_3_ATGL-KO.hATGL_CRIS      TGCA-----ATAAACAAGTTT----AGTTAACGCATGATACAAAGGCATTAAAGCAGC--
A549_clone3_10_ATGL-KO.hATGL_CRI      TGCA-----ATAAACAAGTTT----AGTTAACGCATGATACAAAGGCATTAAAGCAGC--
A549_clone3_7_ATGL-KO.hATGL_CRIS      TGCA-----ATAAACAAGTTT----AGTTAACGCATGATACAAAGGCATTA-AGCAGC--
                                        **     ** * *  **      **** * *   **** ** * ****   ** *

A549_parental.hATGL_CRISPR_seq_r      GACACGCGGGTCAGGGAGATGCCCAGGCGCCCACTGGCATGCTCATGGCTATCAGCAGGG
A549_cloneC8_ATGL-ctrl.hATGL_CRI      GACACGCGGGTCAGGGAGATGCCCAGGCGCCCACTGGCATGCTCATGGCTATCAGCAGGC
A549_cloneB8_ATGL-ctrl.hATGL_CRI      GACACGCGGGTCAGGGAGATGCCCAGGCGCCCACTGGCATGCTCATGGCTATCAGCAGGC
A549_cloneC7_ATGL-ctrl.hATGL_CRI      GACACGCGGGTCAGGGAGATGCCCAGGCGCCCACTGGCATGCTCATGGCTATCAGCAGGC
A549_clone3_3_ATGL-KO.hATGL_CRIS      ------------------------------------GTATCCACAT-------AGCGTAA
A549_clone3_10_ATGL-KO.hATGL_CRI      ------------------------------------GTATCCACAT-------AGCGTAA
A549_clone3_7_ATGL-KO.hATGL_CRIS      ------------------------------------GTATCCACAT-------AGCGTAA
```

```
                                                                                                  * ** * ***       ***

A549_parental.hATGL_CRISPR_seq_r      CAGGACCTTCAGCAGGGAAACTGCGGGATGATCTTTTACCAGGTTGAAGGGAGGGGTGCA
A549_cloneC8_ATGL-ctrl.hATGL_CRI      -AGGACCTTCA--GCAGGAAACTGCGGATGATCTTT-ACCAGGTTGAAAG-AGGGGTGCA
A549_cloneB8_ATGL-ctrl.hATGL_CRI      -AGGACCTTCA--GCAGGAAACTGCGGATGATCTTT-ACCAGGTTGAAAGAAGGGTTGCA
A549_cloneC7_ATGL-ctrl.hATGL_CRI      -AGGACCTTCA--GCAGGAAACTGCGGATGATCTTT-ACCAGGTTGAAAGAAGGGGTGCA
A549_clone3_3_ATGL-KO.hATGL_CRIS      GAGGAGCAACATAGTTAAGAATACCAGTCAATCTTTCACAAATTT------TGTAATCCA
A549_clone3_10_ATGL-KO.hATGL_CRI      -AGGAGCAACATAGTTAAGAATACCAGTCAATCTTTCACAAATTT------TGTAATCCA
A549_clone3_7_ATGL-KO.hATGL_CRIS      -AGGAGCAACATAGTTAAGAATACCAGTCAATCTTTCAAAATTTT--------GTATCCA
                                       **** *  **        *      *   ****** *  *  **          * **

A549_parental.hATGL_CRISPR_seq_r      AGGG--GGCCCAGGGAACC--GCTTCCGGGG-----------------------------
A549_cloneC8_ATGL-ctrl.hATGL_CRI      GGGG----GCCCAGGAACC--GCTTCCGGGCC-TCTTTAGATACCTCAATGAAC-TTGGC
A549_cloneB8_ATGL-ctrl.hATGL_CRI      GGGG---GGCCCAGGAACC--GCTTCCGGGGCCTCTTTAGATACCTCAATGAACTTGGGC
A549_cloneC7_ATGL-ctrl.hATGL_CRI      AGGG--GGCCCAAGGAACC--GCTTCCGGGGCCTCTTTAGATACCTCAATGAAC-T----
A549_clone3_3_ATGL-KO.hATGL_CRIS      GAAGTTGATTTCAGGCACCGGGCTTGCGGGTC----------------ATGCAC-CAGGT
A549_clone3_10_ATGL-KO.hATGL_CRI      GAGGTTGATTTCAGGCACCGGGCTTGCGGGTC----------------ATGCAC-CAGGT
A549_clone3_7_ATGL-KO.hATGL_CRIS      GAAGTTGATTTCAGGCACC-GGCTTGCGGGTC----------------ATGCAC-CAGGT
                                         *         ** ***  **** ****

A549_parental.hATGL_CRISPR_seq_r      ------------------------------------------------------------
A549_cloneC8_ATGL-ctrl.hATGL_CRI      ACCAGCCTCACCTGGGGGCACAGGGCCCAAGGGTTAGGGGCCCATGCTCCTGGGGCTTAG
A549_cloneB8_ATGL-ctrl.hATGL_CRI      ACCAGCCTCACCTGGGGGCACAGGGCCCAAGGTTAAGGGGCC------------------
A549_cloneC7_ATGL-ctrl.hATGL_CRI      ------------------------------------------------------------
A549_clone3_3_ATGL-KO.hATGL_CRIS      GCGCGGT-------------------------------------------------------
A549_clone3_10_ATGL-KO.hATGL_CRI      GCGCGGTCCTTCGGGCAACTCGACGTCGGCGGTGACGGTGAAGCCAAACCGCTCGT----
A549_clone3_7_ATGL-KO.hATGL_CRIS      GCGCGGTCCTTCGGGC-ACTCGACGTCGGCGGTGACGGT----------------------

A549_parental.hATGL_CRISPR_seq_r      --
A549_cloneC8_ATGL-ctrl.hATGL_CRI      CA
A549_cloneB8_ATGL-ctrl.hATGL_CRI      --
A549_cloneC7_ATGL-ctrl.hATGL_CRI      --
A549_clone3_3_ATGL-KO.hATGL_CRIS      --
A549_clone3_10_ATGL-KO.hATGL_CRI      --
A549_clone3_7_ATGL-KO.hATGL_CRIS      --
```

Appendix 2: Lipidomics profile of ATGL-KO and control cells (positive mode)

Metabolite name	Fold Change ATGL-KO/Control	Adjusted p-value
C16:0/C16:0/C16:0 TAG	2,37	0,000
C16:0/C18:1/C16:0 TAG	2,10	0,000
C16:0/C20:4/C16:0 TAG	3,53	0,000
C16:0 SM	1,29	0,001
C18:0 SM	1,28	0,001
C18:0/C18:1/C18:0 TAG	1,97	0,001
C18:1 SM	1,43	0,001
C18:0/C18:0/C18:0 TAG	1,93	0,001
C16:0e MAGe	0,73	0,001
C18:0/C20:4/C18:0 TAG	2,27	0,001
C20:4 SM	1,41	0,002
C18:0e/C20:4 PCe	1,16	0,016
C16:0 LPC	1,38	0,020
C20:4 LPC	1,94	0,022
C16:0 AC	1,48	0,022
C18:0/C20:4 PC	1,14	0,030
C16:0/C20:4 PC	1,12	0,031

C16:0/C20:4 PE	1,26	0,032
C16:0e LPCe (lysoPAF)	1,45	0,033
C16:0p/C20:4 PCp	1,21	0,033
C18:0 LPC	1,46	0,034
sphingosine	1,58	0,044
16:0 MAG	0,75	0,045
C16:0e/C20:4 PCe	1,14	0,046
C16:0e/C2:0 MAGe	0,80	0,051
C18:0p/C20:4 PCp	1,12	0,054
C18:0e/C18:1 PSe	0,76	0,056
C18:0e/C20:4 PEe	1,26	0,059
C16:0e/C20:4 PEe	1,26	0,064
C18:0/C20:4 PE	1,12	0,072
C16:0/C18:1 PC	0,92	0,079
C16:0e/C18:1 PCe	0,93	0,079
C18:0e/C18:1 PCe	0,92	0,084
C18:0e/C2:0 MAGe	3,71	0,085
Cholesterol/cholesteryl esters	1,09	0,085
C18:0 MAG	0,78	0,087
C18:0/C20:4 DAG	1,30	0,138
Pregninolone sulfate	0,93	0,140
C18:0 AC	1,59	0,159
C12 MAGE IS	0,96	0,168
C18:0/C18:1 PS	0,92	0,171
C18:1 LPC	1,12	0,190
C18:1 LPE	6,82	0,196
C18:0 LPE	1,41	0,212
sphinganine	0,59	0,227
C20:4 LPE	1,98	0,237
cholesteryl oleate	0,64	0,238
C16:0 Ceramide	0,89	0,263
C18:0e/C18:1 PEe	1,17	0,296
C18:0/C18:1 PC	0,96	0,297
C16:0/C20:4 PG	1,25	0,302
C16:0e LPCe	1,31	0,303
C16:0/C18:1 PE	1,07	0,308
C16:0e/C18:1 PSe	0,94	0,308
C16:0/C18:1 DAG	1,16	0,308
lanosterol	1,89	0,309
C16:0p/C20:4 PEp	1,07	0,331
C18:0/C18:1 DAG	1,21	0,353
C16:0e/C18:1 PEe	1,21	0,356
C20:4 MAG	2,64	0,357
C18:0/C20:4 PG	1,44	0,363
C18:0p/C20:4 PEp	1,06	0,364

farnesyl pyrophosphate	1,12	0,375
C18:0 NAE	2,62	0,421
C18:0e LPCe (lysoPAF)	1,36	0,464
C18:0/C18:1 PE	1,04	0,501
C16:0 LPE	1,40	0,536
C16:0 NAE	2,22	0,565
C18:0e/C18:1 PGe	1,06	0,565
C16:0/C20:4 PS	1,03	0,577
C18:1e LPEe	1,18	0,582
lactosylceramide C18:1/C18:0	0,51	0,679
C18:1e LPCe	1,30	0,680
C18:0e LPCe	1,21	0,689
C12:0 AC	1,70	0,691
C18:0 LPS	0,85	0,694
Estradiol	0,82	0,694
C16:0e/C18:1 PGe	1,43	0,696
C18:0e/C20:4 PSe	0,92	0,755
C18:1e LPCe (lysoPAF)	1,12	0,758
C16:0/C18:1 PG	0,88	0,780
DHT transition #1	1,23	0,787
C16:0/C20:4 DAG	1,32	0,816
C18:1 LPS	0,81	0,816
C16:0/C18:1 PS	1,01	0,827
C18:0e LPSe	0,75	0,829
alpha tocopherol	1,11	0,831
C18:0e LPEe	0,78	0,860
C18:1 MAG	0,99	0,862
DHT transition #2	0,80	0,863
C18:0/C18:1 PG	1,15	0,864
C18:0 Ceramide	0,96	0,864
C18:2 MAG	1,23	0,872
C18:0/C20:4 PS	0,99	0,880
C20:4 Ceramide	1,13	0,885
C20:0 LPC	1,13	0,898
C2:0 Ceramide	0,97	0,901
C18:1 Ceramide	0,82	0,901
Testosterone transition #2	0,84	0,904
C16:0e/C20:4 PGe	0,92	0,905
C16:0e LPEe	1,06	0,915
C18:0e/C20:4 PGe	1,27	0,915
C18:1 NAE	1,04	0,918
Pregninolone transition #2	0,82	0,936
C2:0 AC	0,82	0,938
Testosterone transition #1	1,69	0,957

DHEA-Sulfate	0,96	0,969
C20:4e LPCe	0,84	0,975
C16:0e/C20:4 PSe	1,04	0,976
C18:0e LPGe	N/A	0,976
DHEA tramsition #2	0,84	0,977
C22:6 MAG	1,47	0,978
Estradiol sulfate	0,58	0,979
C6:0 AC	1,03	0,980
C16:0p/C20:4 PSp	0,88	0,981
C18:1e LPGe	0,73	0,982
C4:0 AC	0,90	0,982
C20:4 LPS	1,00	0,982
C20:4e LPGe	0,88	0,983
C18:1 LPG	N/A	0,984
C18:1e LPSe	0,98	0,985
Testosterone sulfate	1,07	0,985
C20:4e LPSe	0,90	0,985
C20:4 NAE	2,00	0,987
C18:0p/C20:4 PSp	1,62	0,987
C20:4 LPG	1,35	0,988
C16:0 LPS	0,84	0,988
C16:0e LPGe	N/A	0,990
C16:0 LPG	3,08	0,991
Pregninolone transition #1	0,84	0,991
gamma tocopherol	1,18	0,994
DHEA tranisition #1	1,01	0,996

Appendix 3. List of proteins in ATGL-KO and control cells upon filtering for four valid values per group

Majority protein IDs	**Fold Change ATGL-KO/control**	**Adjusted Students t-test p-value (q-value)**
sp|P12931|SRC_HUMAN	5,126	0,000
tr|E7ENN3|E7ENN3_HUMAN;tr|Q7RTM4|Q7RTM4_HUMAN;tr|A0A0C4DG40|A0A0C4DG40_HUMAN;sp|Q8NF91|SYNE1_HUMAN	7,287	0,000
tr|B2RE46|B2RE46_HUMAN;sp|P04844|RPN2_HUMAN	3,666	0,080

tr|Q53GE2|Q53GE2_HUMAN;tr|Q53GC7|Q53GC7_HUMAN;tr|A4D0V4|A4D0V4_HUMAN;sp|P47755|CAZA2_HUMAN;tr|C9JUG7|C9JUG7_HUMAN;tr|F8W9N7|F8W9N7_HUMAN;tr|B4DE01|B4DE01_HUMAN	2,111	0,167
tr|Q5SRT3|Q5SRT3_HUMAN;tr|Q53FB0|Q53FB0_HUMAN;sp|O00299|CLIC1_HUMAN	1,118	0,811
tr|Q5U0I6|Q5U0I6_HUMAN;sp|P62820|RAB1A_HUMAN;tr|E7END7|E7END7_HUMAN;tr|B7Z8M7|B7Z8M7_HUMAN;tr|Q96RD8|Q96RD8_HUMAN	1,198	0,810
tr|A0A090N8Y2|A0A090N8Y2_HUMAN;sp|P13667|PDIA4_HUMAN	1,244	0,752
tr|A0A024RAE4|A0A024RAE4_HUMAN;sp|P60953|CDC42_HUMAN;tr|B4E1U9|B4E1U9_HUMAN;tr|B7ZAY4|B7ZAY4_HUMAN;tr|B4DMH5|B4DMH5_HUMAN;tr|A0A024RAE6|A0A024RAE6_HUMAN;tr|A0A024R9T1|A0A024R9T1_HUMAN;tr|Q5JYX0|Q5JYX0_HUMAN;tr|Q9UJM1|Q9UJM1_HUMAN	1,377	0,606
tr|V9HW95|V9HW95_HUMAN;sp|Q15293|RCN1_HUMAN	1,204	0,803
sp|Q15046|SYK_HUMAN;tr|Q6ZTI3|Q6ZTI3_HUMAN	0,852	0,795
tr|E5RIW3|E5RIW3_HUMAN;tr|Q6FGD7|Q6FGD7_HUMAN;sp|O75347|TBCA_HUMAN;tr|E5RJD8|E5RJD8_HUMAN;tr|E5RHG6|E5RHG6_HUMAN	1,312	0,660
tr|Q5JPB8|Q5JPB8_HUMAN;sp|Q9NY33|DPP3_HUMAN;tr|G3V1D3|G3V1D3_HUMAN;tr|G3V180|G3V180_HUMAN;tr|B4E357|B4E357_HUMAN;tr|Q53HL4|Q53HL4_HUMAN;tr|Q53GT4|Q53GT4_HUMAN	1,210	0,801
tr|B4DIT7|B4DIT7_HUMAN;tr|V9HWG3|V9HWG3_HUMAN;sp|P21980|TGM2_HUMAN;tr|B4DTN7|B4DTN7_HUMAN	0,741	0,612
sp|Q96PK6|RBM14_HUMAN;tr|Q59GV2|Q59GV2_HUMAN	1,126	0,810
tr|B2R704|B2R704_HUMAN;sp|Q14244|MAP7_HUMAN;tr|B7Z3Y3|B7Z3Y3_HUMAN;tr|B7Z3E1|B7Z3E1_HUMAN;tr|A0A087WZ40|A0A087WZ40_HUMAN;tr|B7ZB64|B7ZB64_HUMAN	0,414	0,158

tr|E9PIR7|E9PIR7_HUMAN;tr|B2R5P6|B2R5P6_HUMAN;tr|F8W809|F8W809_HUMAN;tr|B7Z2S5|B7Z2S5_HUMAN;tr|A0A087WSW9|A0A087WSW9_HUMAN;tr|E9PNQ6|E9PNQ6_HUMAN;tr|A0A024RBK9|A0A024RBK9_HUMAN;tr|A0A087WSY9|A0A087WSY9_HUMAN;sp|Q16881|TRXR1_HUMAN;tr|Q6ZR44|Q6ZR44_HUMAN;tr|E2QRB9|E2QRB9_HUMAN;tr|E9PKD3|E9PKD3_HUMAN	1,226	0,774
tr|Q53HG7|Q53HG7_HUMAN;sp|Q14247|SRC8_HUMAN;tr|A0A024R5M3|A0A024R5M3_HUMAN;tr|Q76MU0|Q76MU0_HUMAN	1,210	0,802
tr|Q53Z07|Q53Z07_HUMAN;sp|P32969|RL9_HUMAN;tr|E7ESE0|E7ESE0_HUMAN;tr|D6RAN4|D6RAN4_HUMAN;tr|H0Y9V9|H0Y9V9_HUMAN;tr|B4E1M5|B4E1M5_HUMAN;tr|B4DLV8|B4DLV8_HUMAN	0,613	0,368
tr|A0A024R3X4|A0A024R3X4_HUMAN;sp|P10809|CH60_HUMAN;tr|B3GQS7|B3GQS7_HUMAN;tr|B7Z597|B7Z597_HUMAN;tr|B7Z5E7|B7Z5E7_HUMAN;tr|B7Z4F6|B7Z4F6_HUMAN	0,652	0,458
sp|P12270|TPR_HUMAN	1,306	0,661
tr|B4E0N6|B4E0N6_HUMAN;sp|Q969X5|ERGI1_HUMAN	2,435	0,150
sp|Q9UJU6|DBNL_HUMAN;tr|Q59FH4|Q59FH4_HUMAN;tr|H0Y5J4|H0Y5J4_HUMAN;tr|B4DDU5|B4DDU5_HUMAN;tr|B4DKZ4|B4DKZ4_HUMAN	1,238	0,758
sp|P14324|FPPS_HUMAN;tr|A0A087X090|A0A087X090_HUMAN;tr|Q14329|Q14329_HUMAN	2,969	0,150
tr|A0A0D9SFB3|A0A0D9SFB3_HUMAN;tr|A0A0D9SG12|A0A0D9SG12_HUMAN;tr|B5BTY4|B5BTY4_HUMAN;sp|O00571|DDX3X_HUMAN;tr|Q59GX6|Q59GX6_HUMAN;tr|A0A0D9SF53|A0A0D9SF53_HUMAN;tr|Q5S4N1|Q5S4N1_HUMAN;tr|B4E132|B4E132_HUMAN;tr|A0A024R9A4|A0A024R9A4_HUMAN;sp|O15523|DDX3Y_HUMAN;tr|B4DLU5|B4DLU5_HUMAN	6,243	0,019
tr|B2R802|B2R802_HUMAN;sp|P09012|SNRPA_HUMAN;tr|M0R268|M0R268_HUMAN;tr|M0QXK2|M0QXK2_HUMAN;tr|M0R221|M0R221_HUMAN;tr|M0R2B8|M0R2B8_HUMAN;tr|M0QZG7|M0QZG7_HUMAN;tr|B4DDC7|B4DDC7_HUMAN	0,864	0,821

tr|Q59HB8|Q59HB8_HUMAN;tr|A0A024R5M9|A0A024R5M9_HUMAN;sp|Q14980|NUMA1_HUMAN;tr|Q4LE64|Q4LE64_HUMAN;tr|A0A087WY61|A0A087WY61_HUMAN;tr|Q7Z757|Q7Z757_HUMAN;tr|A0A024R5G4|A0A024R5G4_HUMAN	1,200	0,812
tr|A0A024RAM0|A0A024RAM0_HUMAN;sp|Q92973|TNPO1_HUMAN	2,463	0,158
tr|B4DLR8|B4DLR8_HUMAN;sp|P15559|NQO1_HUMAN;tr|Q3B792|Q3B792_HUMAN;tr|Q53G81|Q53G81_HUMAN;tr|H3BNV2|H3BNV2_HUMAN;tr|H3BRK3|H3BRK3_HUMAN	1,187	0,801
tr|Q53T09|Q53T09_HUMAN;sp|P13010|XRCC5_HUMAN	0,851	0,799
tr|Q96HX3|Q96HX3_HUMAN;tr|Q6IBR0|Q6IBR0_HUMAN;tr|Q53EP4|Q53EP4_HUMAN;sp|P04843|RPN1_HUMAN;tr|B7Z4L4|B7Z4L4_HUMAN;tr|B4DL99|B4DL99_HUMAN;tr|B4DNJ5|B4DNJ5_HUMAN	1,204	0,807
sp|P62263|RS14_HUMAN;tr|H0YB22|H0YB22_HUMAN;tr|E5RH77|E5RH77_HUMAN	0,442	0,152
sp|Q03252|LMNB2_HUMAN;tr|J9JID7|J9JID7_HUMAN;tr|A0A0A7M1X5|A0A0A7M1X5_HUMAN	1,140	0,817
sp|P54577|SYYC_HUMAN;tr|A0A0C4DGZ5|A0A0C4DGZ5_HUMAN	1,241	0,763
sp|Q99714|HCD2_HUMAN;tr|Q5H928|Q5H928_HUMAN	0,657	0,481
sp|O60701|UGDH_HUMAN	1,284	0,693
tr|A0A024R652|A0A024R652_HUMAN;sp|P11586|C1TC_HUMAN;tr|F5H2F4|F5H2F4_HUMAN;tr|B7Z809|B7Z809_HUMAN	1,101	0,840
tr|Q4W4Y1|Q4W4Y1_HUMAN;sp|Q8WUM4|PDC6I_HUMAN;tr|B4DHD2|B4DHD2_HUMAN;tr|B7Z5C1|B7Z5C1_HUMAN	1,128	0,812
sp|P11216|PYGB_HUMAN;tr|Q59GM9|Q59GM9_HUMAN;tr|B4DSD8|B4DSD8_HUMAN	0,725	0,590
tr|K7EQZ3|K7EQZ3_HUMAN;sp|Q9GZP8|IMUP_HUMAN;tr|K7EKZ2|K7EKZ2_HUMAN	0,478	0,191

tr|E9PKT8|E9PKT8_HUMAN;tr|C9J6D1|C9J6D1_HUMAN;tr|C9JZI7|C9JZI7_HUMAN;tr|A0A024RCC9|A0A024RCC9_HUMAN;sp|Q99733|NP1L4_HUMAN;tr|B7ZAK9|B7ZAK9_HUMAN;tr|B7ZB83|B7ZB83_HUMAN;tr|B7ZAC7|B7ZAC7_HUMAN;tr|B4DS05|B4DS05_HUMAN;tr|E9PNW0|E9PNW0_HUMAN;tr|E9PJJ2|E9PJJ2_HUMAN;tr|E9PS34|E9PS34_HUMAN;tr|E9PNJ7|E9PNJ7_HUMAN;tr|E9PKI2|E9PKI2_HUMAN;tr|C9J1B1|C9J1B1_HUMAN;tr|E9PP22|E9PP22_HUMAN;tr|A8MXH2|A8MXH2_HUMAN	2,734	0,154
tr|A0A024RA61|A0A024RA61_HUMAN;sp|P22626|ROA2_HUMAN;tr|A0A024RA27|A0A024RA27_HUMAN;tr|A0A024RA28|A0A024RA28_HUMAN;tr|A0A087WUI2|A0A087WUI2_HUMAN;tr|I6L957|I6L957_HUMAN	1,148	0,818
tr|Q05CW6|Q05CW6_HUMAN;tr|B2R6D0|B2R6D0_HUMAN;tr|A0A087WW66|A0A087WW66_HUMAN;sp|Q99460|PSMD1_HUMAN;tr|Q05BX4|Q05BX4_HUMAN	2,864	0,161
tr|Q5CAQ5|Q5CAQ5_HUMAN;tr|V9HWP2|V9HWP2_HUMAN;sp|P14625|ENPL_HUMAN;tr|B4DHT9|B4DHT9_HUMAN;tr|B4DU71|B4DU71_HUMAN;tr|Q59FC6|Q59FC6_HUMAN	1,165	0,811
sp|Q01813|PFKAP_HUMAN;tr|Q8WTZ9|Q8WTZ9_HUMAN;tr|O14943|O14943_HUMAN	1,342	0,629
tr|Q8IWR8|Q8IWR8_HUMAN;tr|J3QR09|J3QR09_HUMAN;tr|J3KTE4|J3KTE4_HUMAN;tr|Q53G49|Q53G49_HUMAN;sp|P84098|RL19_HUMAN;tr|J3QL15|J3QL15_HUMAN	0,211	0,069
tr|Q53G71|Q53G71_HUMAN;tr|V9HW88|V9HW88_HUMAN;sp|P27797|CALR_HUMAN;tr|B4DHR1|B4DHR1_HUMAN;tr|K7EJB9|K7EJB9_HUMAN	1,174	0,795
sp|P28070|PSB4_HUMAN	2,308	0,161
tr|J3QS39|J3QS39_HUMAN;tr|J3QTR3|J3QTR3_HUMAN;tr|F5H6Q2|F5H6Q2_HUMAN;tr|Q3MIH3|Q3MIH3_HUMAN;sp|P62987|RL40_HUMAN;tr|F5GYU3|F5GYU3_HUMAN;tr|F5H2Z3|F5H2Z3_HUMAN;	0,592	0,365

sp|P27348|1433T_HUMAN;tr|Q53S41|Q53S41_HUMAN;tr|B4DMT8|B4DMT8_HUMAN;tr|B4DY04|B4DY04_HUMAN;tr|E9PG15|E9PG15_HUMAN	0,375	0,157
tr|A2VCK8|A2VCK8_HUMAN;sp|P62328|TYB4_HUMAN;tr|Q0P5T0|Q0P5T0_HUMAN;tr|Q0P5U7|Q0P5U7_HUMAN;tr|Q0P5Q0|Q0P5Q0_HUMAN;tr|Q0P5P4|Q0P5P4_HUMAN;tr|Q0P5N8|Q0P5N8_HUMAN	1,268	0,725
tr|M0R0F0|M0R0F0_HUMAN;tr|A0A024R4Q8|A0A024R4Q8_HUMAN;sp|P46782|RS5_HUMAN;tr|Q53G25|Q53G25_HUMAN;tr|M0R0R2|M0R0R2_HUMAN;tr|M0QZN2|M0QZN2_HUMAN	1,132	0,811
sp|P61604|CH10_HUMAN;tr|Q9UNM1|Q9UNM1_HUMAN;tr|B8ZZL8|B8ZZL8_HUMAN;tr|A0A024R3X7|A0A024R3X7_HUMAN;tr|S4R3N1|S4R3N1_HUMAN	0,571	0,308
sp|O14737|PDCD5_HUMAN;tr|K7ESJ4|K7ESJ4_HUMAN;tr|Q3HM38|Q3HM38_HUMAN;tr|X6R2P6|X6R2P6_HUMAN;tr|K7EQA1|K7EQA1_HUMAN	4,848	0,059
sp|P38117|ETFB_HUMAN	1,139	0,817
tr|B4DH02|B4DH02_HUMAN;sp|P34932|HSP74_HUMAN;tr|Q59GF8|Q59GF8_HUMAN;tr|V9HW33|V9HW33_HUMAN;tr|B4E0H6|B4E0H6_HUMAN;tr|B4E354|B4E354_HUMAN;tr|B4DT47|B4DT47_HUMAN;tr|A0A087WYC1|A0A087WYC1_HUMAN;tr|B4DIZ3|B4DIZ3_HUMAN;tr|B4DUS3|B4DUS3_HUMAN;tr|O14992|O14992_HUMAN;tr|A0A087WTS8|A0A087WTS8_HUMAN	0,899	0,826
sp|P18085|ARF4_HUMAN;tr|C9JPM4|C9JPM4_HUMAN;tr|C9JAK5|C9JAK5_HUMAN	2,666	0,146
tr|V9HW92|V9HW92_HUMAN;sp|O00151|PDLI1_HUMAN	1,208	0,803
tr|B2RCM3|B2RCM3_HUMAN;tr|Q59EF6|Q59EF6_HUMAN;tr|B4E1R7|B4E1R7_HUMAN;sp|P17655|CAN2_HUMAN;tr|B4DN77|B4DN77_HUMAN	0,857	0,814
tr|Q5BKY2|Q5BKY2_HUMAN;tr|A0A087WZK9|A0A087WZK9_HUMAN;tr|Q6IB98|Q6IB98_HUMAN;tr|Q53HR0|Q53HR0_HUMAN;tr|Q53HG0|Q53HG0_HUMAN;sp|O15372|EIF3H_HUMAN;tr|B3KS98|B3KS98_HUMAN;tr|E5RGU4|E5RGU4_HUMAN;tr|E5RJT0|E5RJT0_HUMAN	0,373	0,151

tr|F8WJN3|F8WJN3_HUMAN;sp|Q16630|CPSF6_HUMAN	1,056	0,874
tr|Q52NV4|Q52NV4_HUMAN;sp|P12081|SYHC_HUMAN;tr|B3KWE1|B3KWE1_HUMAN;tr|E7ETE2|E7ETE2_HUMAN;tr|B4DEA2|B4DEA2_HUMAN;tr|B4E1C5|B4E1C5_HUMAN;tr|B4DDD8|B4DDD8_HUMAN;tr|B2R7G6|B2R7G6_HUMAN;sp|P49590|SYHM_HUMAN	3,471	0,125
tr|B0ZBD0|B0ZBD0_HUMAN;sp|P39019|RS19_HUMAN;tr|Q8WVX7|Q8WVX7_HUMAN	0,911	0,844
tr|B2RDR4|B2RDR4_HUMAN;tr|A4D0U5|A4D0U5_HUMAN;sp|Q9UGI8|TES_HUMAN;tr|E0X098|E0X098_HUMAN;tr|Q53GU1|Q53GU1_HUMAN	0,461	0,186
tr|V9HWB9|V9HWB9_HUMAN;sp|P00338|LDHA_HUMAN;tr|B4DJI1|B4DJI1_HUMAN;tr|F5GYU2|F5GYU2_HUMAN;tr|F5GXY2|F5GXY2_HUMAN;tr|F5GXH2|F5GXH2_HUMAN	1,162	0,819
tr|Q71UA6|Q71UA6_HUMAN;sp|Q15758|AAAT_HUMAN;tr|Q59ES3|Q59ES3_HUMAN;tr|M0QXM4|M0QXM4_HUMAN;tr|B4DE27|B4DE27_HUMAN	1,221	0,798
tr|E9PK01|E9PK01_HUMAN;sp|P29692|EF1D_HUMAN;tr|A0A087X1X7|A0A087X1X7_HUMAN;tr|Q71RH4|Q71RH4_HUMAN;tr|Q9H7G6|Q9H7G6_HUMAN;tr|D3DWK1|D3DWK1_HUMAN;tr|B2RAR6|B2RAR6_HUMAN;tr|E9PRY8|E9PRY8_HUMAN;tr|E9PPR1|E9PPR1_HUMAN;tr|E9PL12|E9PL12_HUMAN;tr|E9PQ49|E9PQ49_HUMAN;tr|E9PI39|E9PI39_HUMAN;tr|Q9BW34|Q9BW34_HUMAN;tr|E9PMW7|E9PMW7_HUMAN;tr|E9PL71|E9PL71_HUMAN;tr|E9PQZ1|E9PQZ1_HUMAN;tr|E9PIZ1|E9PIZ1_HUMAN;tr|E9PK06|E9PK06_HUMAN;tr|H0YCK7|H0YCK7_HUMAN	1,186	0,804
tr|Q0QF37|Q0QF37_HUMAN;tr|Q75MT9|Q75MT9_HUMAN;tr|Q6FHZ0|Q6FHZ0_HUMAN;tr|A0A024R4K3|A0A024R4K3_HUMAN;sp|P40926|MDHM_HUMAN;tr|G3XAL0|G3XAL0_HUMAN;tr|B3KTM1|B3KTM1_HUMAN	1,184	0,807
tr|A0A024R663|A0A024R663_HUMAN;sp|Q86UP2|KTN1_HUMAN;tr|G3V4Y7|G3V4Y7_HUMAN	0,876	0,819
sp|P23526|SAHH_HUMAN;tr|Q1RMG2|Q1RMG2_HUMAN	1,427	0,589

sp|P52209|6PGD_HUMAN;tr|B4DL86|B4DL86_HUMAN;tr|B4E2U0|B4E2U0_HUMAN;tr|K7EM49|K7EM49_HUMAN;tr|K7EPF6|K7EPF6_HUMAN;tr|K7EMN2|K7EMN2_HUMAN	1,164	0,819
sp|Q27J81|INF2_HUMAN;tr|A0A0A0MQU1|A0A0A0MQU1_HUMAN	1,140	0,819
sp|P38606|VATA_HUMAN;tr|C9JA17|C9JA17_HUMAN;tr|C9JVW8|C9JVW8_HUMAN;tr|B7Z2V6|B7Z2V6_HUMAN	1,925	0,248
tr|B4E299|B4E299_HUMAN;sp|Q7KZF4|SND1_HUMAN;tr|B2R5U1|B2R5U1_HUMAN;tr|Q59FF0|Q59FF0_HUMAN;tr|B3KU67|B3KU67_HUMAN;tr|I6TRR8|I6TRR8_HUMAN	1,111	0,829
tr|B9A041|B9A041_HUMAN;tr|V9HWF2|V9HWF2_HUMAN;sp|P40925|MDHC_HUMAN;tr|B8ZZ51|B8ZZ51_HUMAN;tr|C9JF79|C9JF79_HUMAN	1,069	0,861
sp|O94906|PRP6_HUMAN	1,490	0,525
tr|Q05DH1|Q05DH1_HUMAN;sp|O14818|PSA7_HUMAN;tr|H0Y586|H0Y586_HUMAN	1,155	0,822
sp|P42224|STAT1_HUMAN;tr|J3KPM9|J3KPM9_HUMAN	1,605	0,417
sp|P62269|RS18_HUMAN	0,836	0,801
tr|A0A024R9I0|A0A024R9I0_HUMAN;sp|P21283|VATC1_HUMAN;tr|E7EV59|E7EV59_HUMAN;tr|B7Z593|B7Z593_HUMAN	0,482	0,205
sp|P05141|ADT2_HUMAN;tr|Q6NVC0|Q6NVC0_HUMAN	0,796	0,751
sp|O00116|ADAS_HUMAN;tr|B7Z3Q4|B7Z3Q4_HUMAN;tr|B7ZAC5|B7ZAC5_HUMAN;tr|Q53SG6|Q53SG6_HUMAN	0,601	0,383
tr|Q53F48|Q53F48_HUMAN;tr|A0A024QZK8|A0A024QZK8_HUMAN;sp|P31942|HNRH3_HUMAN;tr|B4DHY1|B4DHY1_HUMAN	3,041	0,147
sp|P27816|MAP4_HUMAN;tr|E7EVA0|E7EVA0_HUMAN;tr|A0A024R2V0|A0A024R2V0_HUMAN;tr|Q86Y04|Q86Y04_HUMAN;tr|H0Y2V1|H0Y2V1_HUMAN;tr|F8W9U4|F8W9U4_HUMAN	1,253	0,747
tr|E7EPN9|E7EPN9_HUMAN;sp|Q9Y520|PRC2C_HUMAN;tr|B4DQN8|B4DQN8_HUMAN;tr|B4DM27|B4DM27_HUMAN	1,100	0,843
sp|O95831|AIFM1_HUMAN;tr|E9PMA0|E9PMA0_HUMAN	1,144	0,827

tr|Q8N6N5|Q8N6N5_HUMAN;tr|Q8IZ29|Q8IZ29_HUMAN;sp|P68371|TBB4B_HUMAN;tr|Q8IWP6|Q8IWP6_HUMAN;tr|B3KML9|B3KML9_HUMAN;tr|Q96HX0|Q96HX0_HUMAN	0,887	0,810
sp|Q9Y490|TLN1_HUMAN	1,085	0,844
tr|V9HWA6|V9HWA6_HUMAN;sp|P60981|DEST_HUMAN;tr|F6RFD5|F6RFD5_HUMAN;tr|B7Z9M9|B7Z9M9_HUMAN	6,361	0,082
tr|Q9BV28|Q9BV28_HUMAN;sp|Q13509|TBB3_HUMAN;tr|A0A0B4J269|A0A0B4J269_HUMAN;tr|Q53G92|Q53G92_HUMAN;tr|B2RBD5|B2RBD5_HUMAN;tr|Q3ZCR3|Q3ZCR3_HUMAN	0,501	0,241
tr|V9HWH9|V9HWH9_HUMAN;sp|P31949|S10AB_HUMAN;tr|B2R5H0|B2R5H0_HUMAN	0,699	0,585
tr|B4DEA3|B4DEA3_HUMAN;tr|Q53F10|Q53F10_HUMAN;sp|P54727|RD23B_HUMAN;tr|Q5W0S5|Q5W0S5_HUMAN;tr|B7ZA74|B7ZA74_HUMAN;tr|B7Z4W4|B7Z4W4_HUMAN	1,102	0,839
tr|Q2NLC8|Q2NLC8_HUMAN;tr|E9PFN5|E9PFN5_HUMAN;tr|Q6FII1|Q6FII1_HUMAN;sp|Q9Y2Q3|GSTK1_HUMAN	0,592	0,368
sp|P25398|RS12_HUMAN	2,572	0,160
tr|A0A024R172|A0A024R172_HUMAN;sp|Q14914|PTGR1_HUMAN;tr|F2Z3J9|F2Z3J9_HUMAN	1,806	0,302
tr|Q6IB71|Q6IB71_HUMAN;sp|P25788|PSA3_HUMAN	1,088	0,849
tr|Q53G72|Q53G72_HUMAN;sp|P51572|BAP31_HUMAN;tr|Q53HT6|Q53HT6_HUMAN;tr|C9JSP1|C9JSP1_HUMAN;tr|C9JQ75|C9JQ75_HUMAN;tr|C9J0M4|C9J0M4_HUMAN	2,122	0,211
tr|Q5RLJ0|Q5RLJ0_HUMAN;tr|Q549M8|Q549M8_HUMAN;sp|Q9Y224|CN166_HUMAN;tr|G3V4C6|G3V4C6_HUMAN	1,088	0,845
tr|A0A024QZ77|A0A024QZ77_HUMAN;sp|Q96C19|EFHD2_HUMAN;tr|H0Y4Y4|H0Y4Y4_HUMAN	0,423	0,155
sp|Q9Y277|VDAC3_HUMAN;tr|E5RHE1|E5RHE1_HUMAN;tr|E5RFP6|E5RFP6_HUMAN;tr|E5RJN6|E5RJN6_HUMAN;tr|E5RHZ6|E5RHZ6_HUMAN	0,738	0,629

tr|A0A024R094|A0A024R094_HUMAN;sp|Q9H074|PAIP1_HUMAN;tr|D6REB4|D6REB4_HUMAN	1,159	0,818
sp|P61981|1433G_HUMAN;tr|B4DE78|B4DE78_HUMAN;tr|B3KNB4|B3KNB4_HUMAN;tr|B4DHC4|B4DHC4_HUMAN	1,137	0,824
sp|Q9Y5B9|SP16H_HUMAN	1,089	0,852
sp|P24666|PPAC_HUMAN;tr|Q59EH3|Q59EH3_HUMAN;tr|G5E9R5|G5E9R5_HUMAN;tr|F2Z2Q9|F2Z2Q9_HUMAN;tr|O75702|O75702_HUMAN	0,848	0,797
sp|P20700|LMNB1_HUMAN;tr|E9PBF6|E9PBF6_HUMAN;tr|Q6DC98|Q6DC98_HUMAN;tr|A0A0D9SFE5|A0A0D9SFE5_HUMAN;tr|B4DZT3|B4DZT3_HUMAN	1,077	0,854
sp|P08579|RU2B_HUMAN;tr|B5BTZ8|B5BTZ8_HUMAN;tr|Q86YK2|Q86YK2_HUMAN	2,027	0,239
sp|Q9BRF8|CPPED_HUMAN	0,651	0,486
sp|Q9Y3I0|RTCB_HUMAN;tr|B4DNA0|B4DNA0_HUMAN	1,927	0,259
tr|K7EK42|K7EK42_HUMAN;sp|Q99426|TBCB_HUMAN;tr|K7EP07|K7EP07_HUMAN	1,203	0,807
tr|Q5U077|Q5U077_HUMAN;sp|P07195|LDHB_HUMAN;tr|A8MW50|A8MW50_HUMAN;tr|C9J7H8|C9J7H8_HUMAN	0,862	0,819
sp|P46087|NOP2_HUMAN;tr|A0A087WV73|A0A087WV73_HUMAN	1,155	0,824
tr|B4DMH3|B4DMH3_HUMAN;tr|Q53G58|Q53G58_HUMAN;tr|B3KN06|B3KN06_HUMAN;tr|A0A024RBI5|A0A024RBI5_HUMAN;sp|Q9ULV4|COR1C_HUMAN;tr|Q59EA2|Q59EA2_HUMAN;tr|B7Z9V0|B7Z9V0_HUMAN;tr|B4E3S0|B4E3S0_HUMAN;tr|H0YHL7|H0YHL7_HUMAN	0,720	0,596
tr|B4DRV5|B4DRV5_HUMAN;tr|Q53FD7|Q53FD7_HUMAN;sp|Q7Z3B4|NUP54_HUMAN;tr|Q53H29|Q53H29_HUMAN	1,336	0,652
sp|Q92896|GSLG1_HUMAN;tr|Q6ZMF1|Q6ZMF1_HUMAN;tr|H3BM42|H3BM42_HUMAN	1,190	0,803
sp|P26599|PTBP1_HUMAN;tr|A6NLN1|A6NLN1_HUMAN;tr|Q59H49|Q59H49_HUMAN	1,105	0,840

tr|V9HW96|V9HW96_HUMAN;sp|P78371|TCPB_HUMAN;tr|F5GWF6|F5GWF6_HUMAN;tr|F8VQ14|F8VQ14_HUMAN;tr|B7Z4R3|B7Z4R3_HUMAN	1,382	0,594
sp|P82979|SARNP_HUMAN;tr|Q567R9|Q567R9_HUMAN;tr|H0YHG0|H0YHG0_HUMAN;tr|F8VZQ9|F8VZQ9_HUMAN;tr|A4D286|A4D286_HUMAN	0,823	0,803
sp|P23246|SFPQ_HUMAN;tr|Q9BSV4|Q9BSV4_HUMAN;tr|Q86VG2|Q86VG2_HUMAN;tr|Q6PIX2|Q6PIX2_HUMAN	1,116	0,827
sp|Q13442|HAP28_HUMAN;tr|F8WBW6|F8WBW6_HUMAN	1,420	0,604
tr|Q6NUR7|Q6NUR7_HUMAN;tr|E7EQR4|E7EQR4_HUMAN;sp|P15311|EZRI_HUMAN;tr|V9HW42|V9HW42_HUMAN;tr|B2R6J2|B2R6J2_HUMAN;tr|B7Z5V2|B7Z5V2_HUMAN;tr|B7Z437|B7Z437_HUMAN;tr|J7M2B1|J7M2B1_HUMAN	1,162	0,826
tr|Q9BR63|Q9BR63_HUMAN;sp|Q9NSD9|SYFB_HUMAN;tr|A8K666|A8K666_HUMAN;tr|B7ZB32|B7ZB32_HUMAN	0,424	0,170
tr|B2RDD7|B2RDD7_HUMAN;sp|O14744|ANM5_HUMAN;tr|H0YJ77|H0YJ77_HUMAN;tr|G3V5L5|G3V5L5_HUMAN;tr|G3V580|G3V580_HUMAN;tr|G3V2L6|G3V2L6_HUMAN;tr|H0YJX6|H0YJX6_HUMAN;tr|B4DV00|B4DV00_HUMAN	1,102	0,842
tr|V9HW43|V9HW43_HUMAN;sp|P04792|HSPB1_HUMAN;tr|B4DL87|B4DL87_HUMAN;tr|F8WE04|F8WE04_HUMAN	1,272	0,730
sp|Q7Z434|MAVS_HUMAN	0,752	0,662
tr|E5RGX5|E5RGX5_HUMAN;tr|B7Z4N6|B7Z4N6_HUMAN;sp|Q93045|STMN2_HUMAN	2,921	0,140
tr|A0A024R542|A0A024R542_HUMAN;sp|Q9C0C2|TB182_HUMAN;tr|B3KXS7|B3KXS7_HUMAN	1,781	0,327
sp|Q09666|AHNK_HUMAN	1,199	0,796
tr|B4E3E6|B4E3E6_HUMAN;tr|B4DDB6|B4DDB6_HUMAN;sp|P51991|ROA3_HUMAN;tr|Q65ZQ3|Q65ZQ3_HUMAN	2,532	0,158
tr|H0Y4R1|H0Y4R1_HUMAN;sp|P12268|IMDH2_HUMAN;tr|B7Z1G4|B7Z1G4_HUMAN;tr|Q6QE17|Q6QE17_HUMAN;tr|E7ETK5|E7ETK5_HUMAN	0,931	0,856

tr|K7EJT5|K7EJT5_HUMAN;tr|K7EP65|K7EP65_HUMAN;tr|K7EKS7|K7EKS7_HUMAN;tr|K7ELC4|K7ELC4_HUMAN;tr|K7EMH1|K7EMH1_HUMAN;tr|K7ERI7|K7ERI7_HUMAN;tr|Q7Z4W8|Q7Z4W8_HUMAN;sp|P35268|RL22_HUMAN	4,101	0,117
tr|F5GYN4|F5GYN4_HUMAN;sp|Q96FW1|OTUB1_HUMAN;tr|Q659F9|Q659F9_HUMAN;tr|J3KR44|J3KR44_HUMAN;tr|F5GYJ8|F5GYJ8_HUMAN;tr|B4DPD5|B4DPD5_HUMAN;tr|F5H6Q1|F5H6Q1_HUMAN	1,424	0,599
tr|Q5VVD0|Q5VVD0_HUMAN;sp|P62913|RL11_HUMAN;tr|Q08ES8|Q08ES8_HUMAN;tr|Q5VVC8|Q5VVC8_HUMAN;tr|Q5VVC9|Q5VVC9_HUMAN	0,529	0,283
tr|E9PJD9|E9PJD9_HUMAN;tr|Q9BQQ5|Q9BQQ5_HUMAN;tr|E9PLL6|E9PLL6_HUMAN;tr|Q6NZ52|Q6NZ52_HUMAN;sp|P46776|RL27A_HUMAN	2,898	0,146
tr|A0A090N8G0|A0A090N8G0_HUMAN;sp|P41250|SYG_HUMAN	1,118	0,830
sp|P11387|TOP1_HUMAN;tr|B9EG90|B9EG90_HUMAN;tr|Q9BVT2|Q9BVT2_HUMAN	0,916	0,848
sp|P52895|AK1C2_HUMAN;tr|B4DK69|B4DK69_HUMAN;tr|A0A0A0MSD5|A0A0A0MSD5_HUMAN;tr|S4R3P0|S4R3P0_HUMAN;tr|Q59GU2|Q59GU2_HUMAN	0,842	0,805
sp|P45974|UBP5_HUMAN	1,114	0,828
tr|V9HWC0|V9HWC0_HUMAN;sp|P26038|MOES_HUMAN	0,917	0,853
tr|E9PF10|E9PF10_HUMAN;tr|B4DLT2|B4DLT2_HUMAN;tr|A0A024R071|A0A024R071_HUMAN;sp|O75694|NU155_HUMAN	1,228	0,796
tr|A8K9U6|A8K9U6_HUMAN;sp|Q7Z2W4|ZCCHV_HUMAN;tr|C9J6P4|C9J6P4_HUMAN;tr|Q05DV5|Q05DV5_HUMAN	1,085	0,838
sp|Q96HE7|ERO1A_HUMAN;tr|G3V3E6|G3V3E6_HUMAN	0,889	0,810

tr|B2R603|B2R603_HUMAN;tr|A8K9A4|A8K9A4_HUMAN;sp|P07910|HNRPC_HUMAN;tr|G3V4W0|G3V4W0_HUMAN;tr|B4DY08|B4DY08_HUMAN;tr|B2R5W2|B2R5W2_HUMAN;tr|G3V2Q1|G3V2Q1_HUMAN;tr|G3V4C1|G3V4C1_HUMAN;tr|G3V576|G3V576_HUMAN;tr|B3KX96|B3KX96_HUMAN;tr|D3DPI2|D3DPI2_HUMAN;tr|G3V555|G3V555_HUMAN;tr|G3V575|G3V575_HUMAN;tr|B4DQQ2|B4DQQ2_HUMAN;tr|G3V5V7|G3V5V7_HUMAN;tr|G3V2D6|G3V2D6_HUMAN	1,332	0,656
tr|Q6PUJ7|Q6PUJ7_HUMAN;tr|Q6FHP5|Q6FHP5_HUMAN;tr|A8K401|A8K401_HUMAN;sp|P35232|PHB_HUMAN;tr|Q53FV0|Q53FV0_HUMAN;tr|C9JW96|C9JW96_HUMAN;tr|C9JZ20|C9JZ20_HUMAN;tr|E7ESE2|E7ESE2_HUMAN;tr|E9PCW0|E9PCW0_HUMAN	1,144	0,825
sp|Q9BUP3|HTAI2_HUMAN;tr|E9PI87|E9PI87_HUMAN	2,218	0,207
sp|P62195|PRS8_HUMAN;tr|Q59GS3|Q59GS3_HUMAN;tr|J3QQM1|J3QQM1_HUMAN;tr|J3QLH6|J3QLH6_HUMAN;tr|J3KRP2|J3KRP2_HUMAN;tr|J3QSA9|J3QSA9_HUMAN	0,545	0,312
tr|B2R4R9|B2R4R9_HUMAN;sp|P62857|RS28_HUMAN	0,889	0,812
tr|A0A024RCN6|A0A024RCN6_HUMAN;sp|P26640|SYVC_HUMAN	1,076	0,853
tr|A0A024R7C7|A0A024R7C7_HUMAN;sp|Q12906|ILF3_HUMAN;tr|F4ZW66|F4ZW66_HUMAN;tr|B4DFG4|B4DFG4_HUMAN;tr|F4ZW64|F4ZW64_HUMAN;tr|A8K590|A8K590_HUMAN;tr|F4ZW65|F4ZW65_HUMAN	1,080	0,851
sp|P56537|IF6_HUMAN;tr|B7ZBH1|B7ZBH1_HUMAN	1,416	0,605
tr|V9HW26|V9HW26_HUMAN;sp|P25705|ATPA_HUMAN;tr|K7EK77|K7EK77_HUMAN	1,152	0,820
tr|K7EPP7|K7EPP7_HUMAN;tr|K7EIH8|K7EIH8_HUMAN;tr|B7Z9W6|B7Z9W6_HUMAN;tr|Q59EH7|Q59EH7_HUMAN;tr|A8K4T2|A8K4T2_HUMAN;sp|Q99615|DNJC7_HUMAN;tr|K7ESP1|K7ESP1_HUMAN;tr|K7EJL5|K7EJL5_HUMAN;tr|K7EN19|K7EN19_HUMAN;tr|K7EJV7|K7EJV7_HUMAN;tr|K7ER44|K7ER44_HUMAN	1,288	0,717

tr|B2RBR9|B2RBR9_HUMAN;sp|Q14974|IMB1_HUMAN;tr|B7Z5M1|B7Z5M1_HUMAN;tr|J3KTM9|J3KTM9_HUMAN;tr|B7Z752|B7Z752_HUMAN	1,137	0,816
tr|A0A024R4A0|A0A024R4A0_HUMAN;sp|P19338|NUCL_HUMAN;tr|B3KTP9|B3KTP9_HUMAN;tr|B3KM80|B3KM80_HUMAN;tr|Q6ZS99|Q6ZS99_HUMAN;tr|Q9BQ02|Q9BQ02_HUMAN;tr|H7BY16|H7BY16_HUMAN	0,865	0,826
tr|C9J0K6|C9J0K6_HUMAN;sp|P30626|SORCN_HUMAN	1,181	0,793
tr|A0A024R9U8|A0A024R9U8_HUMAN;tr|A0A024R9W5|A0A024R9W5_HUMAN;sp|Q7Z6Z7|HUWE1_HUMAN;tr|Q5H924|Q5H924_HUMAN;tr|A0A024R9Y3|A0A024R9Y3_HUMAN	0,954	0,897
tr|B4DSE4|B4DSE4_HUMAN;tr|A0A024R588|A0A024R588_HUMAN;tr|A0A024R566|A0A024R566_HUMAN;tr|B4DJU4|B4DJU4_HUMAN;tr|A0A024R5D9|A0A024R5D9_HUMAN;tr|A0A024R572|A0A024R572_HUMAN;sp|Q15637|SF01_HUMAN;tr|B4DX42|B4DX42_HUMAN	1,084	0,839
tr|K7ER90|K7ER90_HUMAN;tr|K7EL20|K7EL20_HUMAN;tr|K7ENA8|K7ENA8_HUMAN;tr|Q6IAM0|Q6IAM0_HUMAN;tr|A8K5K5|A8K5K5_HUMAN;sp|O75821|EIF3G_HUMAN	0,337	0,143
tr|B3KQT9|B3KQT9_HUMAN;tr|V9HVY3|V9HVY3_HUMAN;sp|P30101|PDIA3_HUMAN;tr|B3KQT2|B3KQT2_HUMAN;tr|B4DDM1|B4DDM1_HUMAN	1,142	0,819
tr|Q68CP7|Q68CP7_HUMAN;tr|A0A0A0MS99|A0A0A0MS99_HUMAN;tr|I3L4X2|I3L4X2_HUMAN;sp|P33527|MRP1_HUMAN;tr|Q9UQ98|Q9UQ98_HUMAN	0,369	0,174
tr|H0YMI6|H0YMI6_HUMAN;tr|H0YMA1|H0YMA1_HUMAN;tr|H0YMZ1|H0YMZ1_HUMAN;tr|H0YL69|H0YL69_HUMAN;sp|P25789|PSA4_HUMAN;tr|H0YKT8|H0YKT8_HUMAN;tr|H0YN18|H0YN18_HUMAN;tr|Q7Z474|Q7Z474_HUMAN;tr|B2RDG0|B2RDG0_HUMAN;tr|H0YKS0|H0YKS0_HUMAN;tr|H0YLS6|H0YLS6_HUMAN;tr|H0YLC2|H0YLC2_HUMAN	0,518	0,285

tr|E7EX90|E7EX90_HUMAN;tr|Q6AWB3|Q6AWB3_HUMAN;tr|Q6AWB1|Q6AWB1_HUMAN;sp|Q14203|DCTN1_HUMAN;tr|Q59F36|Q59F36_HUMAN;tr|Q6MZZ3|Q6MZZ3_HUMAN	1,049	0,898
tr|A8K2Y2|A8K2Y2_HUMAN;tr|A0A024RBY4|A0A024RBY4_HUMAN;sp|P41091|IF2G_HUMAN;tr|Q53HK3|Q53HK3_HUMAN;tr|B2R5N2|B2R5N2_HUMAN;sp|Q2VIR3|IF2GL_HUMAN;tr|F8W810|F8W810_HUMAN	0,932	0,860
tr|A4D177|A4D177_HUMAN;sp|Q13185|CBX3_HUMAN;tr|S4R2Y4|S4R2Y4_HUMAN	1,612	0,458
sp|O75533|SF3B1_HUMAN	1,098	0,845
tr|B3KX11|B3KX11_HUMAN;sp|P49368|TCPG_HUMAN;tr|Q59H77|Q59H77_HUMAN;tr|B4DUR8|B4DUR8_HUMAN;tr|Q2TU64|Q2TU64_HUMAN	1,184	0,805
tr|A0A024R1K8|A0A024R1K8_HUMAN;sp|Q15459|SF3A1_HUMAN;tr|B4E091|B4E091_HUMAN	1,226	0,799
tr|A3KPC7|A3KPC7_HUMAN;sp|Q99878|H2A1J_HUMAN;sp|Q96KK5|H2A1H_HUMAN;tr|B2R5B3|B2R5B3_HUMAN;tr|A4FTV9|A4FTV9_HUMAN;sp|Q6FI13|H2A2A_HUMAN;sp|P0C0S8|H2A1_HUMAN;tr|A0A024RAS2|A0A024RAS2_HUMAN;sp|Q9BTM1|H2AJ_HUMAN;sp|Q16777|H2A2C_HUMAN;sp|P20671|H2A1D_HUMAN;tr|H0YFX9|H0YFX9_HUMAN;tr|B4E0B3|B4E0B3_HUMAN;tr|B2R5B6|B2R5B6_HUMAN;sp|Q96QV6|H2A1A_HUMAN	1,666	0,426
tr|D0PNI1|D0PNI1_HUMAN;sp|P63104|1433Z_HUMAN;tr|E7EX29|E7EX29_HUMAN;tr|B0AZS6|B0AZS6_HUMAN;tr|B7Z2E6|B7Z2E6_HUMAN;tr|H0YB80|H0YB80_HUMAN;tr|E7ESK7|E7ESK7_HUMAN	0,947	0,874
sp|Q5T4S7|UBR4_HUMAN;tr|A0A024RAC9|A0A024RAC9_HUMAN	1,093	0,848
sp|Q7L014|DDX46_HUMAN;tr|A8K6X3|A8K6X3_HUMAN;tr|A0A0C4DG89|A0A0C4DG89_HUMAN;tr|D3DQA6|D3DQA6_HUMAN	1,208	0,808
tr|A0A024RDH8|A0A024RDH8_HUMAN;sp|P49207|RL34_HUMAN	1,162	0,814
sp|P16615|AT2A2_HUMAN;tr|H7C5W9|H7C5W9_HUMAN	1,217	0,805

tr|A0A024RDG1|A0A024RDG1_HUMAN;sp|O60763|USO1_HUMAN	2,027	0,263
sp|P09382|LEG1_HUMAN	1,139	0,819
sp|Q06124|PTN11_HUMAN;tr|B3GUD5|B3GUD5_HUMAN	0,954	0,894
tr|B4DQZ7|B4DQZ7_HUMAN;tr|S4R3H4|S4R3H4_HUMAN;tr|E7EQT4|E7EQT4_HUMAN;sp|Q9UKV3|ACINU_HUMAN;tr|Q69YJ6|Q69YJ6_HUMAN;tr|G3V3B0|G3V3B0_HUMAN	1,456	0,591
tr|Q6NVY0|Q6NVY0_HUMAN;tr|A0A024R904|A0A024R904_HUMAN;sp|Q9HB71|CYBP_HUMAN	1,137	0,812
sp|Q9HDC9|APMAP_HUMAN;tr|H0Y512|H0Y512_HUMAN	1,098	0,845
tr|B4DFL1|B4DFL1_HUMAN;tr|E9PEX6|E9PEX6_HUMAN;tr|B4DMK9|B4DMK9_HUMAN;tr|A0A024R713|A0A024R713_HUMAN;sp|P09622|DLDH_HUMAN	1,202	0,799
tr|H0YLP6|H0YLP6_HUMAN;tr|H0YMF4|H0YMF4_HUMAN;sp|P46779|RL28_HUMAN;tr|H0YKD8|H0YKD8_HUMAN;tr|Q59F34|Q59F34_HUMAN	2,048	0,258
sp|P54136|SYRC_HUMAN;tr|B4DXW6|B4DXW6_HUMAN	1,099	0,842
sp|O75116|ROCK2_HUMAN;tr|E9PF63|E9PF63_HUMAN	0,903	0,838
tr|Q8N1H4|Q8N1H4_HUMAN;tr|Q68DZ9|Q68DZ9_HUMAN;tr|Q59GA1|Q59GA1_HUMAN;tr|B2RDQ3|B2RDQ3_HUMAN;sp|P62995|TRA2B_HUMAN;tr|H7C2L4|H7C2L4_HUMAN	0,373	0,151
tr|Q5JR95|Q5JR95_HUMAN;tr|Q5JR94|Q5JR94_HUMAN;sp|P62241|RS8_HUMAN;tr|Q9BS10|Q9BS10_HUMAN	1,382	0,607
tr|B3KW56|B3KW56_HUMAN;tr|Q6IAX5|Q6IAX5_HUMAN;tr|B2R806|B2R806_HUMAN;sp|P60228|EIF3E_HUMAN;tr|H0YBR5|H0YBR5_HUMAN;tr|E5RGA2|E5RGA2_HUMAN;tr|E5RIT4|E5RIT4_HUMAN	0,494	0,270
tr|F8VS02|F8VS02_HUMAN;sp|P49419|AL7A1_HUMAN	1,590	0,477

tr|E9PLT0|E9PLT0_HUMAN;tr|Q9GZV0|Q9GZV0_HUMAN;tr|A0A024R0K2|A0A024R0K2_HUMAN;tr|A0A024R0E2|A0A024R0E2_HUMAN;sp|O75534|CSDE1_HUMAN;tr|Q9UG93|Q9UG93_HUMAN;tr|Q96L66|Q96L66_HUMAN	1,547	0,515
tr|B2R5W3|B2R5W3_HUMAN;tr|A0A024R3T8|A0A024R3T8_HUMAN;sp|P09874|PARP1_HUMAN;tr|B4E0E1|B4E0E1_HUMAN	1,111	0,829
sp|Q12904|AIMP1_HUMAN;tr|B4DNK3|B4DNK3_HUMAN	1,420	0,610
tr|V9HWE1|V9HWE1_HUMAN;sp|P08670|VIME_HUMAN;tr|B0YJC4|B0YJC4_HUMAN;tr|Q53HU8|Q53HU8_HUMAN;tr|B3KRK8|B3KRK8_HUMAN	1,395	0,597
sp|Q92522|H1X_HUMAN	2,158	0,235
sp|P11177|ODPB_HUMAN	0,687	0,590
tr|V9HW90|V9HW90_HUMAN;sp|P00390|GSHR_HUMAN	0,867	0,822
tr|A0A024QYX7|A0A024QYX7_HUMAN;tr|B3KNZ4|B3KNZ4_HUMAN;tr|B4DRU0|B4DRU0_HUMAN;tr|B4DVU3|B4DVU3_HUMAN;tr|B4E2Z6|B4E2Z6_HUMAN;tr|B4DDN4|B4DDN4_HUMAN;tr|B4DVQ5|B4DVQ5_HUMAN;tr|A1KYQ7|A1KYQ7_HUMAN;tr|A0A024QYU9|A0A024QYU9_HUMAN;sp|Q99613|EIF3C_HUMAN;sp|B5ME19|EIFCL_HUMAN	1,721	0,392
sp|P62424|RL7A_HUMAN;tr|Q5T8U3|Q5T8U3_HUMAN;tr|Q9BY74|Q9BY74_HUMAN;tr|Q5T8U2|Q5T8U2_HUMAN	1,355	0,651
sp|Q5SSJ5|HP1B3_HUMAN;tr|X6RGJ2|X6RGJ2_HUMAN;tr|B0QZK4|B0QZK4_HUMAN;tr|Q5SWC8|Q5SWC8_HUMAN	1,172	0,814
tr|Q53XC0|Q53XC0_HUMAN;sp|P05198|IF2A_HUMAN;tr|H0YJS4|H0YJS4_HUMAN;tr|G3V4T5|G3V4T5_HUMAN	0,918	0,849
tr|A0A0A0MSK5|A0A0A0MSK5_HUMAN;sp|Q5JTV8|TOIP1_HUMAN;tr|J3KN66|J3KN66_HUMAN;tr|H0YD16|H0YD16_HUMAN	1,136	0,814
tr|Q5T123|Q5T123_HUMAN;sp|Q9H299|SH3L3_HUMAN;tr|Q86Z22|Q86Z22_HUMAN;tr|A0A087WV23|A0A087WV23_HUMAN;tr|D3DPK5|D3DPK5_HUMAN	1,863	0,322

tr|D3DVF0|D3DVF0_HUMAN;tr|Q6FIB4|Q6FIB4_HUMAN;sp|Q9Y624|JAM1_HUMAN;tr|B7Z5W1|B7Z5W1_HUMAN	0,676	0,577
tr|Q53SS8|Q53SS8_HUMAN;sp|Q15365|PCBP1_HUMAN	1,099	0,846
tr|B3KXZ4|B3KXZ4_HUMAN;sp|P49736|MCM2_HUMAN;tr|B7Z8Z6|B7Z8Z6_HUMAN;tr|H0Y8E6|H0Y8E6_HUMAN;tr|Q9BWF4|Q9BWF4_HUMAN;tr|B4DSV5|B4DSV5_HUMAN	0,643	0,517
tr|Q8N4P8|Q8N4P8_HUMAN;tr|Q53GS0|Q53GS0_HUMAN;tr|D2CFK9|D2CFK9_HUMAN;sp|Q9BZE4|NOG1_HUMAN;tr|O60747|O60747_HUMAN;tr|B4DHR2|B4DHR2_HUMAN;tr|Q5T3R7|Q5T3R7_HUMAN	0,843	0,805
sp|Q9NZM1|MYOF_HUMAN;tr|H0YD14|H0YD14_HUMAN	1,155	0,823
sp|P42166|LAP2A_HUMAN	1,131	0,808
sp|P61026|RAB10_HUMAN;tr|Q53T70|Q53T70_HUMAN	0,609	0,445
sp|P28074|PSB5_HUMAN	1,551	0,514
sp|P35998|PRS7_HUMAN;tr|Q75L23|Q75L23_HUMAN;tr|C9JLS9|C9JLS9_HUMAN	1,078	0,855
tr|Q6DCA8|Q6DCA8_HUMAN;tr|E9PK09|E9PK09_HUMAN;tr|E9PQN2|E9PQN2_HUMAN;tr|E9PKI6|E9PKI6_HUMAN;tr|E9PK91|E9PK91_HUMAN;sp|Q9NYF8|BCLF1_HUMAN;tr|H0YF00|H0YF00_HUMAN;tr|E9PJA7|E9PJA7_HUMAN	2,010	0,275
sp|P17096|HMGA1_HUMAN;tr|B4DWA0|B4DWA0_HUMAN;tr|A0A024RCT9|A0A024RCT9_HUMAN;tr|Q5T6U8|Q5T6U8_HUMAN	2,015	0,280
tr|Q96DV6|Q96DV6_HUMAN;tr|A2A3R6|A2A3R6_HUMAN;sp|P62753|RS6_HUMAN;tr|A2A3R5|A2A3R5_HUMAN	1,101	0,844
sp|O75367|H2AY_HUMAN;tr|D6RCF2|D6RCF2_HUMAN	1,095	0,844
sp|O75396|SC22B_HUMAN	1,138	0,812
tr|Q6FHU3|Q6FHU3_HUMAN;sp|Q06323|PSME1_HUMAN;tr|H0YLU2|H0YLU2_HUMAN;tr|Q86SZ9|Q86SZ9_HUMAN	0,691	0,600
tr|B4DYY5|B4DYY5_HUMAN;tr|F8W726|F8W726_HUMAN;sp|Q14157|UBP2L_HUMAN;tr|B4DZJ6|B4DZJ6_HUMAN;tr|Q5VU77|Q5VU77_HUMAN	1,239	0,784

sp|P07741|APT_HUMAN;tr|H3BQZ9|H3BQZ9_HUMAN;tr|H3BQB1|H3BQB1_HUMAN;tr|H3BQF1|H3BQF1_HUMAN;tr|H3BSW3|H3BSW3_HUMAN	0,830	0,805
tr|B4DL49|B4DL49_HUMAN;tr|A0A024R374|A0A024R374_HUMAN;sp|P07858|CATB_HUMAN;tr|A8K2H4|A8K2H4_HUMAN;tr|B4DMY4|B4DMY4_HUMAN;tr|B3KUJ8|B3KUJ8_HUMAN;tr|Q6LAF9|Q6LAF9_HUMAN	0,316	0,163
tr|V9HWG9|V9HWG9_HUMAN;tr|B2R983|B2R983_HUMAN;sp|P78417|GSTO1_HUMAN;tr|Q5TA01|Q5TA01_HUMAN;tr|Q5TA02|Q5TA02_HUMAN	1,205	0,803
tr|E9PGT1|E9PGT1_HUMAN;sp|Q15631|TSN_HUMAN;tr|B3KRM8|B3KRM8_HUMAN;tr|B7Z5D9|B7Z5D9_HUMAN;tr|Q53GR3|Q53GR3_HUMAN	0,912	0,845
tr|B4DVZ8|B4DVZ8_HUMAN;sp|P09960|LKHA4_HUMAN	0,701	0,604
tr|B3KTM6|B3KTM6_HUMAN;tr|A2RUM7|A2RUM7_HUMAN;sp|P46777|RL5_HUMAN;tr|Q59GX9|Q59GX9_HUMAN	1,127	0,815
sp|P53004|BIEA_HUMAN	1,889	0,323
tr|Q9BTQ7|Q9BTQ7_HUMAN;tr|A0A024R1Q8|A0A024R1Q8_HUMAN;sp|P62829|RL23_HUMAN;tr|J3KTJ3|J3KTJ3_HUMAN;tr|J3KT29|J3KT29_HUMAN	0,764	0,696
sp|Q15907|RB11B_HUMAN;tr|H3BMH2|H3BMH2_HUMAN;tr|H3BSC1|H3BSC1_HUMAN;tr|A0A024R5Z8|A0A024R5Z8_HUMAN;sp|P62491|RB11A_HUMAN;tr|B4DMN1|B4DMN1_HUMAN	1,090	0,851
sp|P52701|MSH6_HUMAN;tr|A0A087WWJ1|A0A087WWJ1_HUMAN;tr|Q1L838|Q1L838_HUMAN	1,538	0,546
sp|P24752|THIL_HUMAN;tr|H0YEL7|H0YEL7_HUMAN	1,045	0,899
tr|V9HW80|V9HW80_HUMAN;sp|P55072|TERA_HUMAN;tr|Q96IF9|Q96IF9_HUMAN;tr|Q0IIN5|Q0IIN5_HUMAN;tr|Q9NTC4|Q9NTC4_HUMAN	1,058	0,873
tr|J3QT28|J3QT28_HUMAN;sp|O43684|BUB3_HUMAN;tr|J3QSX4|J3QSX4_HUMAN;tr|B4DDM6|B4DDM6_HUMAN	1,295	0,712

sp|P60900|PSA6_HUMAN;tr|G3V5Z7|G3V5Z7_HUMAN;tr|G3V3I1|G3V3I1_HUMAN;tr|G3V295|G3V295_HUMAN;tr|G3V3U4|G3V3U4_HUMAN	1,148	0,826
sp|Q9Y6G9|DC1L1_HUMAN;tr|Q6MZE7|Q6MZE7_HUMAN;tr|B3KM42|B3KM42_HUMAN;tr|E9PHI6|E9PHI6_HUMAN;tr|B4DDM4|B4DDM4_HUMAN	1,417	0,593
tr|B2R4C1|B2R4C1_HUMAN;sp|P62899|RL31_HUMAN;tr|H7C2W9|H7C2W9_HUMAN;tr|C9JU56|C9JU56_HUMAN;tr|B7Z4E3|B7Z4E3_HUMAN;tr|B7Z4C8|B7Z4C8_HUMAN;tr|Q76N53|Q76N53_HUMAN;tr|B8ZZK4|B8ZZK4_HUMAN	3,196	0,159
tr|A8K897|A8K897_HUMAN;sp|Q8N1F7|NUP93_HUMAN;tr|H3BVG0|H3BVG0_HUMAN	1,445	0,606
tr|E5RGS4|E5RGS4_HUMAN;sp|O60925|PFD1_HUMAN	1,083	0,842
tr|B7Z8K4|B7Z8K4_HUMAN;tr|Q6FI03|Q6FI03_HUMAN;tr|Q5U0Q1|Q5U0Q1_HUMAN;tr|Q32P45|Q32P45_HUMAN;sp|Q13283|G3BP1_HUMAN;tr|Q6ZP53|Q6ZP53_HUMAN;tr|Q53HH4|Q53HH4_HUMAN	1,821	0,366
tr|V9HWI5|V9HWI5_HUMAN;sp|P23528|COF1_HUMAN;tr|E9PP50|E9PP50_HUMAN;tr|E9PK25|E9PK25_HUMAN;tr|G3V1A4|G3V1A4_HUMAN;tr|E9PQB7|E9PQB7_HUMAN;tr|B4E112|B4E112_HUMAN	1,112	0,827
tr|A8K8D9|A8K8D9_HUMAN;sp|P11413|G6PD_HUMAN;tr|Q2VF42|Q2VF42_HUMAN;tr|Q2Q9H2|Q2Q9H2_HUMAN;tr|B4DYA7|B4DYA7_HUMAN;tr|Q2Q9B7|Q2Q9B7_HUMAN;tr|E7EUI8|E7EUI8_HUMAN;tr|E9PD92|E9PD92_HUMAN;tr|E7EM57|E7EM57_HUMAN;tr|Q0PHS1|Q0PHS1_HUMAN	1,106	0,845
sp|P25786|PSA1_HUMAN;tr|F5GX11|F5GX11_HUMAN;tr|V9HW55|V9HW55_HUMAN	2,104	0,280
sp|P16152|CBR1_HUMAN;tr|E9PQ63|E9PQ63_HUMAN;tr|A8MTM1|A8MTM1_HUMAN	1,965	0,307
tr|Q6FHF5|Q6FHF5_HUMAN;sp|P12004|PCNA_HUMAN;tr|Q6FI35|Q6FI35_HUMAN	1,249	0,781

tr|H0UID5|H0UID5_HUMAN;tr|H0UID4|H0UID4_HUMAN;sp|P63010|AP2B1_HUMAN;tr|H0UID3|H0UID3_HUMAN;tr|A8K916|A8K916_HUMAN;tr|B4E261|B4E261_HUMAN;tr|A0A087X253|A0A087X253_HUMAN;tr|Q68DI0|Q68DI0_HUMAN;tr|A8K0G3|A8K0G3_HUMAN;tr|Q96EL6|Q96EL6_HUMAN;tr|B4DWG4|B4DWG4_HUMAN;tr|B4DIL5|B4DIL5_HUMAN	1,070	0,864
tr|B4DEP6|B4DEP6_HUMAN;sp|P23588|IF4B_HUMAN;tr|E7EX17|E7EX17_HUMAN;tr|B4DRM3|B4DRM3_HUMAN;tr|Q7Z5Y0|Q7Z5Y0_HUMAN;tr|B4DS01|B4DS01_HUMAN;tr|F8VX11|F8VX11_HUMAN	1,687	0,448
sp|P21912|SDHB_HUMAN;tr|A0A087WXX8|A0A087WXX8_HUMAN;tr|A0A087WWT1|A0A087WWT1_HUMAN	1,435	0,600
sp|Q96HS1|PGAM5_HUMAN;tr|F5GXG4|F5GXG4_HUMAN	1,034	0,927
sp|P67809|YBOX1_HUMAN;tr|A0A087X1S2|A0A087X1S2_HUMAN;tr|H0Y449|H0Y449_HUMAN;tr|Q6PKI6|Q6PKI6_HUMAN;tr|Q05D43|Q05D43_HUMAN;tr|Q7KZ24|Q7KZ24_HUMAN;tr|A0JLU4|A0JLU4_HUMAN;tr|C9J5V9|C9J5V9_HUMAN;tr|Q2VIK8|Q2VIK8_HUMAN	1,067	0,859
sp|O00232|PSD12_HUMAN	0,726	0,629
sp|P35659|DEK_HUMAN;tr|D6RDA2|D6RDA2_HUMAN;tr|B4DFG0|B4DFG0_HUMAN;tr|B4DNW3|B4DNW3_HUMAN;tr|D6R9L5|D6R9L5_HUMAN	1,799	0,378
tr|E9PNW4|E9PNW4_HUMAN;tr|Q6FHM9|Q6FHM9_HUMAN;sp|P13987|CD59_HUMAN;tr|E9PR17|E9PR17_HUMAN;tr|H0YET2|H0YET2_HUMAN	0,493	0,289
tr|A0A024R7F1|A0A024R7F1_HUMAN;sp|P14314|GLU2B_HUMAN;tr|K7ELL7|K7ELL7_HUMAN;tr|B4DJQ5|B4DJQ5_HUMAN;tr|A2VCQ4|A2VCQ4_HUMAN	0,877	0,814
tr|F5GZ78|F5GZ78_HUMAN;tr|B3KVL0|B3KVL0_HUMAN;sp|P49023|PAXI_HUMAN;tr|Q59GS5|Q59GS5_HUMAN;tr|F5H836|F5H836_HUMAN	0,697	0,596
tr|Q59G46|Q59G46_HUMAN;tr|K7ER96|K7ER96_HUMAN;tr|V9HW51|V9HW51_HUMAN;tr|B2R960|B2R960_HUMAN;sp|O43396|TXNL1_HUMAN;tr|B3KT45|B3KT45_HUMAN	1,101	0,844

sp|P52272|HNRPM_HUMAN;tr|A0A087X0X3|A0A087X0X3_HUMAN;tr|Q59ES8|Q59ES8_HUMAN;tr|Q7KYM9|Q7KYM9_HUMAN;tr|M0QZM1|M0QZM1_HUMAN	1,063	0,868
tr|A0A024RC65|A0A024RC65_HUMAN;sp|P46940|IQGA1_HUMAN;tr|A4QPB0|A4QPB0_HUMAN;tr|Q6P1N4|Q6P1N4_HUMAN;tr|H0YLE8|H0YLE8_HUMAN	1,078	0,853
tr|B0YJ88|B0YJ88_HUMAN;sp|P35241|RADI_HUMAN;tr|B7Z2S7|B7Z2S7_HUMAN;tr|Q05CU6|Q05CU6_HUMAN;tr|Q6PKD3|Q6PKD3_HUMAN	1,090	0,843
tr|F1T0B3|F1T0B3_HUMAN;tr|A0A087X2G1|A0A087X2G1_HUMAN;tr|A3RJH1|A3RJH1_HUMAN;sp|Q92499|DDX1_HUMAN;tr|B4DP70|B4DP70_HUMAN	1,048	0,893
sp|P62826|RAN_HUMAN;tr|B5MDF5|B5MDF5_HUMAN;tr|J3KQE5|J3KQE5_HUMAN;tr|F5H018|F5H018_HUMAN	0,617	0,483
sp|Q9BQG0|MBB1A_HUMAN;tr|I3L1L3|I3L1L3_HUMAN;tr|B4DE42|B4DE42_HUMAN	0,617	0,480
tr|V9HVZ4|V9HVZ4_HUMAN;sp|P04406|G3P_HUMAN;tr|E7EUT5|E7EUT5_HUMAN;tr|Q2TSD0|Q2TSD0_HUMAN;tr|Q0QET7|Q0QET7_HUMAN;tr|A4UCT1|A4UCT1_HUMAN;tr|B4DRV9|B4DRV9_HUMAN	0,932	0,860
sp|Q15084|PDIA6_HUMAN	1,183	0,795
tr|Q6IPH7|Q6IPH7_HUMAN;tr|E7EPB3|E7EPB3_HUMAN;tr|A0PJ62|A0PJ62_HUMAN;tr|B7Z6S8|B7Z6S8_HUMAN;sp|P50914|RL14_HUMAN;tr|A8K7N0|A8K7N0_HUMAN	2,225	0,260
tr|B4E0S6|B4E0S6_HUMAN;sp|O43143|DHX15_HUMAN	1,420	0,596
tr|B4DSN3|B4DSN3_HUMAN;tr|G5EA31|G5EA31_HUMAN;tr|A0A024QZM6|A0A024QZM6_HUMAN;sp|P53992|SC24C_HUMAN	1,516	0,570
sp|P27694|RFA1_HUMAN	1,581	0,512
tr|Q549C5|Q549C5_HUMAN;tr|Q53GB0|Q53GB0_HUMAN;sp|Q9NS69|TOM22_HUMAN	1,272	0,750
tr|V9HWH7|V9HWH7_HUMAN;tr|B2R7P8|B2R7P8_HUMAN;sp|P31939|PUR9_HUMAN;tr|B4DP06|B4DP06_HUMAN	0,877	0,814

tr|K7EJE8|K7EJE8_HUMAN;tr|K7EKE6|K7EKE6_HUMAN;tr|B3KU28|B3KU28_HUMAN;tr|Q2VPA0|Q2VPA0_HUMAN;tr|B4DPX0|B4DPX0_HUMAN;tr|B3KXS5|B3KXS5_HUMAN;tr|E5KMI6|E5KMI6_HUMAN;sp|P36776|LONM_HUMAN;tr|K7ER27|K7ER27_HUMAN;tr|A4VCH6|A4VCH6_HUMAN	1,397	0,615
tr|B2R7W4|B2R7W4_HUMAN;sp|O43390|HNRPR_HUMAN;tr|B4DMB1|B4DMB1_HUMAN;tr|Q0VGD6|Q0VGD6_HUMAN;tr|Q6MZS5|Q6MZS5_HUMAN;tr|B4DT28|B4DT28_HUMAN;tr|B4DMD1|B4DMD1_HUMAN	1,072	0,858
tr|J3KTJ8|J3KTJ8_HUMAN;tr|J3QRI7|J3QRI7_HUMAN;tr|J3QQQ9|J3QQQ9_HUMAN;tr|J3QQV1|J3QQV1_HUMAN;tr|E5RIT6|E5RIT6_HUMAN;tr|J3QRC4|J3QRC4_HUMAN;tr|Q6IBH6|Q6IBH6_HUMAN;sp|Q9UNX3|RL26L_HUMAN;sp|P61254|RL26_HUMAN;tr|A0A024RBF6|A0A024RBF6_HUMAN	0,746	0,668
sp|P13639|EF2_HUMAN;tr|B4DPU3|B4DPU3_HUMAN;tr|Q8TA90|Q8TA90_HUMAN;tr|Q6PK56|Q6PK56_HUMAN	0,943	0,872
tr|Q9BRL5|Q9BRL5_HUMAN;tr|B4DJ51|B4DJ51_HUMAN;tr|B2RDW0|B2RDW0_HUMAN;sp|P62158|CALM_HUMAN;tr|H0Y7A7|H0Y7A7_HUMAN;tr|E7ETZ0|E7ETZ0_HUMAN;tr|E7EMB3|E7EMB3_HUMAN;tr|F8WBR5|F8WBR5_HUMAN;tr|M0QZ52|M0QZ52_HUMAN;tr|G3V479|G3V479_HUMAN;tr|A8K1M2|A8K1M2_HUMAN	0,445	0,263
tr|B7Z4W0|B7Z4W0_HUMAN;sp|P23193|TCEA1_HUMAN	0,821	0,813
tr|F5H169|F5H169_HUMAN;tr|F5H5V4|F5H5V4_HUMAN;tr|F5GX23|F5GX23_HUMAN;tr|J3KN29|J3KN29_HUMAN;sp|O00233|PSMD9_HUMAN;tr|F5H7X1|F5H7X1_HUMAN	0,722	0,632
tr|B2RAU8|B2RAU8_HUMAN;sp|Q14978|NOLC1_HUMAN;tr|A0A0A0MRM9|A0A0A0MRM9_HUMAN;tr|Q96J17|Q96J17_HUMAN	1,105	0,844
sp|P15880|RS2_HUMAN;tr|H0YEN5|H0YEN5_HUMAN;tr|E9PQD7|E9PQD7_HUMAN;tr|Q3KQT6|Q3KQT6_HUMAN;tr|Q8N5L9|Q8N5L9_HUMAN;tr|Q6IPX5|Q6IPX5_HUMAN;tr|Q8J014|Q8J014_HUMAN;tr|Q9BSW5|Q9BSW5_HUMAN;tr|Q8NI62|Q8NI62_HUMAN;tr|E9PMM9|E9PMM9_HUMAN	1,859	0,367

tr|H3BU16|H3BU16_HUMAN;tr|A6NGP5|A6NGP5_HUMAN;sp|Q9H910|HN1L_HUMAN;tr|H3BMT0|H3BMT0_HUMAN;tr|H3BTV5|H3BTV5_HUMAN;tr|H3BMV3|H3BMV3_HUMAN;tr|B4DL85|B4DL85_HUMAN	1,264	0,759
tr|A0A024R4F1|A0A024R4F1_HUMAN;sp|P06733|ENOA_HUMAN;tr|E2DRY6|E2DRY6_HUMAN	1,067	0,858
tr|A8K7W3|A8K7W3_HUMAN;tr|A8K5T7|A8K5T7_HUMAN;sp|Q9Y2Z0|SUGT1_HUMAN;tr|B4DYC6|B4DYC6_HUMAN	0,886	0,807
tr|B3KMZ6|B3KMZ6_HUMAN;tr|B2RDF5|B2RDF5_HUMAN;sp|Q9UBT2|SAE2_HUMAN;tr|K7EPL2|K7EPL2_HUMAN	1,762	0,421
sp|P62277|RS13_HUMAN;tr|J3KMX5|J3KMX5_HUMAN;tr|E9PS50|E9PS50_HUMAN	0,929	0,852
sp|Q9UHR4|BI2L1_HUMAN	1,138	0,808
tr|Q96FS1|Q96FS1_HUMAN;tr|Q68DU0|Q68DU0_HUMAN;tr|C9JZR2|C9JZR2_HUMAN;sp|O60716|CTND1_HUMAN;tr|Q7KZJ3|Q7KZJ3_HUMAN;tr|A0A024R4Z0|A0A024R4Z0_HUMAN;tr|A0A024R4Y7|A0A024R4Y7_HUMAN;tr|H0YC95|H0YC95_HUMAN	1,127	0,811
tr|F5H669|F5H669_HUMAN;tr|B4DGF8|B4DGF8_HUMAN;sp|Q8N684|CPSF7_HUMAN;tr|J3QT54|J3QT54_HUMAN;tr|F5H6M0|F5H6M0_HUMAN;tr|F5H047|F5H047_HUMAN	0,788	0,755
tr|V9HW31|V9HW31_HUMAN;sp|P06576|ATPB_HUMAN;tr|Q0QEN7|Q0QEN7_HUMAN;tr|H0YH81|H0YH81_HUMAN	0,936	0,860
sp|Q9NTK5|OLA1_HUMAN;tr|J3KQ32|J3KQ32_HUMAN;tr|Q53SQ6|Q53SQ6_HUMAN	0,916	0,853
tr|E9PID8|E9PID8_HUMAN;tr|B4DUD5|B4DUD5_HUMAN;sp|P33240|CSTF2_HUMAN;tr|E7EWR4|E7EWR4_HUMAN;tr|B3V096|B3V096_HUMAN	0,694	0,594
tr|Q53G61|Q53G61_HUMAN;tr|Q53G21|Q53G21_HUMAN;sp|P09661|RU2A_HUMAN;tr|H0YLR3|H0YLR3_HUMAN;tr|H0YMA0|H0YMA0_HUMAN	1,751	0,421

tr|Q7Z355|Q7Z355_HUMAN;tr|J3KR24|J3KR24_HUMAN;tr|Q7Z3U5|Q7Z3U5_HUMAN;tr|A0A0A0MSX9|A0A0A0MSX9_HUMAN;sp|P41252|SYIC_HUMAN;tr|Q59G75|Q59G75_HUMAN;tr|Q6P0M4|Q6P0M4_HUMAN	0,607	0,474
sp|P49327|FAS_HUMAN	1,138	0,807
tr|B9A067|B9A067_HUMAN;sp|Q16891|MIC60_HUMAN;tr|B4DKR1|B4DKR1_HUMAN;tr|B4DT20|B4DT20_HUMAN;tr|C9J406|C9J406_HUMAN;tr|B4DS66|B4DS66_HUMAN;tr|B4DQY2|B4DQY2_HUMAN;tr|H7C463|H7C463_HUMAN;tr|Q05DN3|Q05DN3_HUMAN	1,117	0,832
tr|Q4KMR3|Q4KMR3_HUMAN;sp|Q12965|MYO1E_HUMAN;sp|O00160|MYO1F_HUMAN;tr|Q6ZNI9|Q6ZNI9_HUMAN	0,752	0,683
sp|Q9UBQ7|GRHPR_HUMAN;tr|Q5M7Z5|Q5M7Z5_HUMAN;tr|U3KQ56|U3KQ56_HUMAN	1,345	0,669
tr|X5D2F4|X5D2F4_HUMAN;sp|Q7L576|CYFP1_HUMAN;tr|H7C229|H7C229_HUMAN;tr|B7Z3H2|B7Z3H2_HUMAN;tr|E7EVJ5|E7EVJ5_HUMAN;tr|B7Z8N7|B7Z8N7_HUMAN;tr|B3KWV6|B3KWV6_HUMAN;sp|Q96F07|CYFP2_HUMAN;tr|A0A087WU52|A0A087WU52_HUMAN;tr|A0A087WWL1|A0A087WWL1_HUMAN;tr|A0A087WVE1|A0A087WVE1_HUMAN;tr|A0A087WTQ3|A0A087WTQ3_HUMAN;tr|A0A087WWZ1|A0A087WWZ1_HUMAN;tr|E7EW33|E7EW33_HUMAN;tr|B7Z217|B7Z217_HUMAN;tr|B7Z4I3|B7Z4I3_HUMAN	1,065	0,859
tr|Q96IR1|Q96IR1_HUMAN;tr|Q53HV1|Q53HV1_HUMAN;tr|B2R491|B2R491_HUMAN;sp|P62701|RS4X_HUMAN	0,827	0,793
tr|V9HWB4|V9HWB4_HUMAN;sp|P11021|GRP78_HUMAN	1,085	0,840
tr|B4DY09|B4DY09_HUMAN;tr|Q53FG3|Q53FG3_HUMAN;tr|F4ZW62|F4ZW62_HUMAN;sp|Q12905|ILF2_HUMAN;tr|F4ZW63|F4ZW63_HUMAN	1,377	0,647
tr|A8K2B4|A8K2B4_HUMAN;tr|A0A097PID1|A0A097PID1_HUMAN;sp|Q8N8S7|ENAH_HUMAN;tr|A0A097PIC4|A0A097PIC4_HUMAN;tr|A0A075B6E5|A0A075B6E5_HUMAN	0,721	0,632
tr|M0QZC5|M0QZC5_HUMAN;sp|P62280|RS11_HUMAN	1,749	0,426

tr|B5BU08|B5BU08_HUMAN;sp|Q01081|U2AF1_HUMAN;tr|Q7Z780|Q7Z780_HUMAN	0,558	0,415
tr|B2ZZ89|B2ZZ89_HUMAN;sp|Q01082|SPTB2_HUMAN;tr|D6W5C0|D6W5C0_HUMAN;tr|A0A087WUZ3|A0A087WUZ3_HUMAN;tr|K9MS24|K9MS24_HUMAN	0,920	0,842
tr|A8K3C3|A8K3C3_HUMAN;sp|P50991|TCPD_HUMAN;tr|B7Z9L0|B7Z9L0_HUMAN;tr|B7Z2Z8|B7Z2Z8_HUMAN;tr|B7Z2F4|B7Z2F4_HUMAN	1,080	0,855
tr|E1NZA1|E1NZA1_HUMAN;sp|Q92616|GCN1L_HUMAN;tr|A0A024RBS1|A0A024RBS1_HUMAN	0,970	0,940
sp|P02545|LMNA_HUMAN;tr|W8QEH3|W8QEH3_HUMAN;tr|Q5I6Y5|Q5I6Y5_HUMAN;tr|Q3BDU5|Q3BDU5_HUMAN;tr|Q8N519|Q8N519_HUMAN;tr|Q5TCI8|Q5TCI8_HUMAN	1,106	0,844
sp|O00567|NOP56_HUMAN;tr|A0PJ92|A0PJ92_HUMAN;tr|A8K9K6|A8K9K6_HUMAN;tr|H0Y653|H0Y653_HUMAN;tr|H0YDU4|H0YDU4_HUMAN	1,515	0,586
tr|E5RFP0|E5RFP0_HUMAN;sp|Q8WVJ2|NUDC2_HUMAN	0,748	0,683
tr|A0A024R0J9|A0A024R0J9_HUMAN;tr|A0A0A0MRA5|A0A0A0MRA5_HUMAN;tr|B7Z4B8|B7Z4B8_HUMAN;tr|A8K6U7|A8K6U7_HUMAN;sp|Q9BUJ2|HNRL1_HUMAN;tr|A8K3W4|A8K3W4_HUMAN;tr|M0R3F1|M0R3F1_HUMAN;tr|A8K5K0|A8K5K0_HUMAN;tr|M0QYZ0|M0QYZ0_HUMAN	1,595	0,529
sp|P15924|DESP_HUMAN;tr|Q4LE79|Q4LE79_HUMAN	0,859	0,825
tr|V9HW74|V9HW74_HUMAN;tr|B2RD14|B2RD14_HUMAN;sp|P09936|UCHL1_HUMAN;tr|D6RE83|D6RE83_HUMAN;tr|D6R974|D6R974_HUMAN;tr|D6R956|D6R956_HUMAN;tr|A6NLJ7|A6NLJ7_HUMAN	1,066	0,861
sp|O76003|GLRX3_HUMAN	0,561	0,425
tr|B4DNN3|B4DNN3_HUMAN;tr|Q53HS0|Q53HS0_HUMAN;tr|A8K3A8|A8K3A8_HUMAN;sp|P47897|SYQ_HUMAN;tr|Q9H3A5|Q9H3A5_HUMAN;tr|Q9BUZ3|Q9BUZ3_HUMAN;tr|B4DDN1|B4DDN1_HUMAN;tr|Q96AW5|Q96AW5_HUMAN	0,892	0,831

sp|Q14126|DSG2_HUMAN	0,753	0,694
tr|B2RNR6|B2RNR6_HUMAN;sp|Q96KR1|ZFR_HUMAN;tr|A8K849|A8K849_HUMAN	0,957	0,897
sp|Q8IVT2|MISP_HUMAN	1,074	0,861
sp|Q13404|UB2V1_HUMAN;tr|I3L0A0|I3L0A0_HUMAN;tr|G3V2F7|G3V2F7_HUMAN;tr|A0A0A0MSL3|A0A0A0MSL3_HUMAN	1,940	0,369
tr|Q5FWY2|Q5FWY2_HUMAN;sp|P63092|GNAS2_HUMAN;sp|Q5JWF2|GNAS1_HUMAN;tr|B0AZR9|B0AZR9_HUMAN;tr|Q14455|Q14455_HUMAN;tr|S4R3E3|S4R3E3_HUMAN	0,584	0,454
sp|P17987|TCPA_HUMAN;tr|E7ERF2|E7ERF2_HUMAN;tr|E7EQR6|E7EQR6_HUMAN	1,098	0,843
sp|P07954|FUMH_HUMAN	2,082	0,305
tr|Q6I9T8|Q6I9T8_HUMAN;tr|B3KUN1|B3KUN1_HUMAN;sp|P67775|PP2AA_HUMAN	0,646	0,566
tr|Q53HW2|Q53HW2_HUMAN;tr|A8K4Z4|A8K4Z4_HUMAN;tr|A0A024RBS2|A0A024RBS2_HUMAN;sp|P05388|RLA0_HUMAN;tr|Q6NSF2|Q6NSF2_HUMAN;tr|F8VWS0|F8VWS0_HUMAN;tr|Q53HK9|Q53HK9_HUMAN;tr|F8VU65|F8VU65_HUMAN;tr|G3V210|G3V210_HUMAN;tr|F8VQY6|F8VQY6_HUMAN;tr|F8VPE8|F8VPE8_HUMAN;tr|F8VRK7|F8VRK7_HUMAN;tr|F8VW21|F8VW21_HUMAN;sp|Q8NHW5|RLA0L_HUMAN;tr|F8VZS0|F8VZS0_HUMAN;tr|B4E3D5|B4E3D5_HUMAN;tr|F8VS58|F8VS58_HUMAN;tr|F8VWV4|F8VWV4_HUMAN	0,892	0,829
tr|I3L397|I3L397_HUMAN;sp|P63241|IF5A1_HUMAN;tr|I3L504|I3L504_HUMAN;tr|F8WCJ1|F8WCJ1_HUMAN;tr|C9J7B5|C9J7B5_HUMAN;tr|C9J4W5|C9J4W5_HUMAN;sp|Q9GZV4|IF5A2_HUMAN;sp|Q6IS14|IF5AL_HUMAN	0,917	0,843
sp|P20290|BTF3_HUMAN;tr|D6RDG3|D6RDG3_HUMAN	0,787	0,759
tr|A0A0C4DFV9|A0A0C4DFV9_HUMAN;tr|B2RCX0|B2RCX0_HUMAN;tr|A0A024R895|A0A024R895_HUMAN;tr|Q5VXV3|Q5VXV3_HUMAN;sp|Q01105|SET_HUMAN;tr|A0A087X027|A0A087X027_HUMAN;sp|P0DME0|SETLP_HUMAN	1,805	0,423

sp|P21796|VDAC1_HUMAN;tr|B3KTS5|B3KTS5_HUMAN;tr|C9JI87|C9JI87_HUMAN;tr|B4DEI3|B4DEI3_HUMAN	0,953	0,896
sp|P27824|CALX_HUMAN	1,137	0,809
tr|V9HWC2|V9HWC2_HUMAN;sp|Q99497|PARK7_HUMAN;tr|K7ELW0|K7ELW0_HUMAN;tr|K7EN27|K7EN27_HUMAN	1,048	0,894
tr|A0A024QZN4|A0A024QZN4_HUMAN;tr|V9HWK2|V9HWK2_HUMAN;sp|P18206|VINC_HUMAN;tr|B3KXA2|B3KXA2_HUMAN;tr|B4E3Q9|B4E3Q9_HUMAN;tr|Q5JQ13|Q5JQ13_HUMAN	1,132	0,813
tr|B2R8R5|B2R8R5_HUMAN;sp|Q13263|TIF1B_HUMAN;tr|M0R0K9|M0R0K9_HUMAN	0,895	0,824
tr|H0YKF0|H0YKF0_HUMAN;tr|H0YLU7|H0YLU7_HUMAN;sp|P13804|ETFA_HUMAN;tr|H0YK49|H0YK49_HUMAN;tr|H0YL12|H0YL12_HUMAN;tr|H0YNX6|H0YNX6_HUMAN	1,931	0,362
tr|A0A087WZH7|A0A087WZH7_HUMAN;sp|P29966|MARCS_HUMAN;tr|Q6NVI1|Q6NVI1_HUMAN	1,208	0,795
sp|Q93009|UBP7_HUMAN;tr|B7ZAX6|B7ZAX6_HUMAN;tr|Q6U8A4|Q6U8A4_HUMAN;tr|H3BMF6|H3BMF6_HUMAN;tr|B7Z7T5|B7Z7T5_HUMAN;tr|H3BND8|H3BND8_HUMAN;tr|B7Z855|B7Z855_HUMAN	1,214	0,807
tr|V9HWD6|V9HWD6_HUMAN;tr|B5BU24|B5BU24_HUMAN;sp|P31946|1433B_HUMAN;tr|Q4VY20|Q4VY20_HUMAN;tr|Q4VY19|Q4VY19_HUMAN;tr|Q59EQ2|Q59EQ2_HUMAN	2,292	0,281
sp|P49411|EFTU_HUMAN	1,038	0,907
tr|V9HWE0|V9HWE0_HUMAN;sp|P08758|ANXA5_HUMAN;tr|D6RBL5|D6RBL5_HUMAN;tr|E9PHT9|E9PHT9_HUMAN	0,531	0,389
tr|B3KPZ2|B3KPZ2_HUMAN;sp|Q9H7Z7|PGES2_HUMAN;tr|A6NHH0|A6NHH0_HUMAN;tr|B4DWP1|B4DWP1_HUMAN;tr|X6RJ95|X6RJ95_HUMAN	0,769	0,731
tr|B4DT77|B4DT77_HUMAN;tr|B4DWU2|B4DWU2_HUMAN;tr|B4DHY4|B4DHY4_HUMAN;tr|Q53HM8|Q53HM8_HUMAN;tr|B2R7L2|B2R7L2_HUMAN;sp|P20073|ANXA7_HUMAN;tr|B2R657|B2R657_HUMAN	1,065	0,860

tr|B5BUB1|B5BUB1_HUMAN;sp|Q9Y265|RUVB1_HUMAN;tr|E7ETR0|E7ETR0_HUMAN;tr|B3KRS7|B3KRS7_HUMAN	1,426	0,609
tr|A0A024RAH8|A0A024RAH8_HUMAN;sp|Q9NVP1|DDX18_HUMAN;tr|Q4ZG72|Q4ZG72_HUMAN	0,832	0,808
tr|H3BRG4|H3BRG4_HUMAN;sp|P22695|QCR2_HUMAN;tr|H3BP04|H3BP04_HUMAN;tr|H3BSJ9|H3BSJ9_HUMAN;tr|A0A087WVZ4|A0A087WVZ4_HUMAN;tr|H3BUE4|H3BUE4_HUMAN;tr|H3BUI9|H3BUI9_HUMAN	1,774	0,444
tr|B4DI38|B4DI38_HUMAN;tr|D3DPU2|D3DPU2_HUMAN;tr|B2RDY9|B2RDY9_HUMAN;sp|Q01518|CAP1_HUMAN;tr|B4DNW7|B4DNW7_HUMAN;tr|B4DNY3|B4DNY3_HUMAN;tr|B4DUZ8|B4DUZ8_HUMAN;tr|B4DNA3|B4DNA3_HUMAN;tr|Q5T0R7|Q5T0R7_HUMAN;tr|Q5T0R6|Q5T0R6_HUMAN;tr|Q5T0R5|Q5T0R5_HUMAN;tr|Q5T0R4|Q5T0R4_HUMAN;tr|Q5T0R3|Q5T0R3_HUMAN;tr|Q5T0R2|Q5T0R2_HUMAN;tr|Q5T0R1|Q5T0R1_HUMAN;tr|Q5T0R9|Q5T0R9_HUMAN	1,080	0,855
sp|P17174|AATC_HUMAN;tr|B7Z1I2|B7Z1I2_HUMAN;tr|Q2TU84|Q2TU84_HUMAN	0,568	0,452
sp|Q08J23|NSUN2_HUMAN	1,048	0,893
sp|Q96CS3|FAF2_HUMAN	1,073	0,858
tr|Q53HU0|Q53HU0_HUMAN;sp|P50990|TCPQ_HUMAN;tr|Q7Z759|Q7Z759_HUMAN	1,070	0,864
sp|P06748|NPM_HUMAN;tr|A4ZU86|A4ZU86_HUMAN;tr|Q9BTI9|Q9BTI9_HUMAN	0,878	0,808
tr|V9HWJ0|V9HWJ0_HUMAN;sp|Q14697|GANAB_HUMAN;tr|B4DJ30|B4DJ30_HUMAN;tr|F5H6X6|F5H6X6_HUMAN;tr|B4DSM6|B4DSM6_HUMAN;tr|A0A024R592|A0A024R592_HUMAN;tr|E9PKU7|E9PKU7_HUMAN;tr|B4DZ53|B4DZ53_HUMAN;tr|B4DIW2|B4DIW2_HUMAN	0,565	0,449
sp|Q96AG4|LRC59_HUMAN	0,507	0,363
tr|V9HW24|V9HW24_HUMAN;sp|P62333|PRS10_HUMAN;tr|A0A087X2I1|A0A087X2I1_HUMAN;tr|H0YJX2|H0YJX2_HUMAN;tr|H0YJC0|H0YJC0_HUMAN	1,319	0,717
tr|A0A024R326|A0A024R326_HUMAN;sp|P47914|RL29_HUMAN;tr|Q6IPI1|Q6IPI1_HUMAN	1,711	0,482

tr|E9KL42|E9KL42_HUMAN;tr|A1L172|A1L172_HUMAN;tr|A0A087X0W7|A0A087X0W7_HUMAN;sp|Q86TX2|ACOT1_HUMAN;tr|G3V4F2|G3V4F2_HUMAN;tr|B7ZMC1|B7ZMC1_HUMAN;tr|B4DV16|B4DV16_HUMAN;tr|A0A087WT95|A0A087WT95_HUMAN;sp|P49753|ACOT2_HUMAN;tr|B3KSA0|B3KSA0_HUMAN	1,104	0,845
tr|A0A024RBR1|A0A024RBR1_HUMAN;sp|P30622|CLIP1_HUMAN;tr|Q59GJ4|Q59GJ4_HUMAN;tr|J3KP58|J3KP58_HUMAN;tr|F5H6A0|F5H6A0_HUMAN;tr|F5H0N7|F5H0N7_HUMAN	1,192	0,790
tr|A8K525|A8K525_HUMAN;sp|Q15233|NONO_HUMAN;tr|H7C367|H7C367_HUMAN	0,880	0,812
tr|E4W6B6|E4W6B6_HUMAN;tr|B2R4D8|B2R4D8_HUMAN;tr|A0A024R1V4|A0A024R1V4_HUMAN;sp|P61353|RL27_HUMAN;tr|K7EQQ9|K7EQQ9_HUMAN;tr|K7ELC7|K7ELC7_HUMAN	0,564	0,449
sp|Q13151|ROA0_HUMAN	1,051	0,896
tr|V9HWC7|V9HWC7_HUMAN;sp|P30041|PRDX6_HUMAN	1,056	0,874
tr|A0A087WXM6|A0A087WXM6_HUMAN;tr|J3QQT2|J3QQT2_HUMAN;tr|J3KRX5|J3KRX5_HUMAN;tr|A0A024R261|A0A024R261_HUMAN;sp|P18621|RL17_HUMAN;tr|A0A0A6YYL6|A0A0A6YYL6_HUMAN;tr|J3KRB3|J3KRB3_HUMAN;tr|A0A087WWH0|A0A087WWH0_HUMAN;tr|J3QS96|J3QS96_HUMAN;tr|J3QLC8|J3QLC8_HUMAN;tr|A0A0A0MRF8|A0A0A0MRF8_HUMAN;tr|A0A087WY81|A0A087WY81_HUMAN	0,803	0,799
tr|J3KRZ2|J3KRZ2_HUMAN;tr|J3KRI4|J3KRI4_HUMAN;tr|A0A024R6Z0|A0A024R6Z0_HUMAN;sp|O43237|DC1L2_HUMAN	1,043	0,898
sp|Q9H9B4|SFXN1_HUMAN	0,593	0,483
sp|Q15056|IF4H_HUMAN	0,624	0,553
tr|C9J9K3|C9J9K3_HUMAN;tr|A0A024R2P0|A0A024R2P0_HUMAN;sp|P08865|RSSA_HUMAN;tr|A0A0C4DG17|A0A0C4DG17_HUMAN;tr|A6NE09|A6NE09_HUMAN;tr|A0A024R7P5|A0A024R7P5_HUMAN;tr|Q96RS2|Q96RS2_HUMAN	0,921	0,842

tr|A0A024QZV0|A0A024QZV0_HUMAN;tr|Q86UY0|Q86UY0_HUMAN;tr|Q6EHZ3|Q6EHZ3_HUMAN;tr|Q658S9|Q658S9_HUMAN;sp|Q8NBS9|TXND5_HUMAN	0,725	0,659
tr|E9PKG1|E9PKG1_HUMAN;tr|Q5U8W9|Q5U8W9_HUMAN;sp|Q99873|ANM1_HUMAN;tr|H7C2I1|H7C2I1_HUMAN;tr|E9PNR9|E9PNR9_HUMAN;tr|E9PQ98|E9PQ98_HUMAN;tr|E9PIX6|E9PIX6_HUMAN;tr|H0YDE4|H0YDE4_HUMAN;tr|A0A087X1W2|A0A087X1W2_HUMAN;tr|B4DJ87|B4DJ87_HUMAN	0,661	0,598
tr|I3L3Q4|I3L3Q4_HUMAN;tr|B3KV49|B3KV49_HUMAN;tr|B4DX01|B4DX01_HUMAN;tr|B7Z403|B7Z403_HUMAN;tr|A8K8F0|A8K8F0_HUMAN;sp|Q9HC38|GLOD4_HUMAN;tr|F6TLX2|F6TLX2_HUMAN;tr|Q9Y3E8|Q9Y3E8_HUMAN	0,755	0,713
tr|Q9BV61|Q9BV61_HUMAN;tr|Q59EK6|Q59EK6_HUMAN;tr|Q53G55|Q53G55_HUMAN;sp|Q12931|TRAP1_HUMAN;tr|K0A7K7|K0A7K7_HUMAN;tr|Q5CAQ4|Q5CAQ4_HUMAN;tr|I3L0K7|I3L0K7_HUMAN;tr|Q8N9Z3|Q8N9Z3_HUMAN;tr|Q53FS6|Q53FS6_HUMAN;tr|I3L239|I3L239_HUMAN	0,620	0,548
tr|Q6NZ55|Q6NZ55_HUMAN;tr|A8K4C8|A8K4C8_HUMAN;sp|P26373|RL13_HUMAN;tr|J3QSB4|J3QSB4_HUMAN	0,934	0,862
sp|P62249|RS16_HUMAN;tr|M0R210|M0R210_HUMAN;tr|M0R3H0|M0R3H0_HUMAN;tr|A0A087WZ27|A0A087WZ27_HUMAN;tr|M0R1M5|M0R1M5_HUMAN;tr|Q6IPX4|Q6IPX4_HUMAN	1,140	0,808
tr|B3KNJ4|B3KNJ4_HUMAN;tr|A0A024R0R4|A0A024R0R4_HUMAN;sp|Q9UBE0|SAE1_HUMAN;tr|M0R054|M0R054_HUMAN;tr|M0QX65|M0QX65_HUMAN;tr|M0QZS6|M0QZS6_HUMAN	0,955	0,894
sp|P46783|RS10_HUMAN;tr|F6U211|F6U211_HUMAN;tr|Q59GE4|Q59GE4_HUMAN;tr|S4R435|S4R435_HUMAN;sp|Q9NQ39|RS10L_HUMAN	0,670	0,610
tr|B3KTJ9|B3KTJ9_HUMAN;sp|Q8N163|CCAR2_HUMAN;tr|E2PSM9|E2PSM9_HUMAN;tr|H0YB24|H0YB24_HUMAN	0,954	0,894
sp|Q00610|CLH1_HUMAN;tr|A0A087WVQ6|A0A087WVQ6_HUMAN	1,040	0,898

tr|A0A024R1S8|A0A024R1S8_HUMAN;sp|Q14847|LASP1_HUMAN;tr|A8K1D2|A8K1D2_HUMAN;tr|B4DIC4|B4DIC4_HUMAN;tr|C9J9W2|C9J9W2_HUMAN;tr|B4DJI4|B4DJI4_HUMAN	1,110	0,841
tr|Q53XL8|Q53XL8_HUMAN;tr|Q53HB3|Q53HB3_HUMAN;sp|P62191|PRS4_HUMAN	0,623	0,553
tr|Q2TAB3|Q2TAB3_HUMAN;tr|Q1ET65|Q1ET65_HUMAN;tr|Q1ET64|Q1ET64_HUMAN;tr|Q1ET63|Q1ET63_HUMAN;tr|Q1ET62|Q1ET62_HUMAN;tr|Q1ET61|Q1ET61_HUMAN;tr|B3KT14|B3KT14_HUMAN;sp|P0DMN0|ST1A4_HUMAN;sp|P0DMM9|ST1A3_HUMAN;tr|A0A0A6YYL2|A0A0A6YYL2_HUMAN;tr|Q59GG0|Q59GG0_HUMAN;tr|E9PKW4|E9PKW4_HUMAN	0,604	0,519
tr|Q8TBK5|Q8TBK5_HUMAN;tr|Q8N5Z7|Q8N5Z7_HUMAN;tr|B2R4K7|B2R4K7_HUMAN;tr|A0A024RBK3|A0A024RBK3_HUMAN;sp|Q02878|RL6_HUMAN;tr|Q9HBB3|Q9HBB3_HUMAN;tr|B4DRX3|B4DRX3_HUMAN	1,945	0,391
tr|Q6FGS1|Q6FGS1_HUMAN;sp|O43399|TPD54_HUMAN;tr|A0A087WYR3|A0A087WYR3_HUMAN;tr|B4DDV4|B4DDV4_HUMAN;tr|Q68E05|Q68E05_HUMAN;tr|Q53GA0|Q53GA0_HUMAN	1,051	0,896
tr|A0A087WYB4|A0A087WYB4_HUMAN;sp|Q9UJZ1|STML2_HUMAN;tr|Q6ZNW0|Q6ZNW0_HUMAN;tr|F2Z2I8|F2Z2I8_HUMAN	1,508	0,596
sp|P62851|RS25_HUMAN	0,834	0,808
tr|A8KAK1|A8KAK1_HUMAN;sp|Q9NYU2|UGGG1_HUMAN	1,173	0,822
tr|Q8TAS0|Q8TAS0_HUMAN;sp|P36542|ATPG_HUMAN;tr|B4DL14|B4DL14_HUMAN	1,304	0,734
tr|V9HW65|V9HW65_HUMAN;tr|A0A024R5Z7|A0A024R5Z7_HUMAN;sp|P07355|ANXA2_HUMAN;tr|H0YN42|H0YN42_HUMAN;tr|H0YMD0|H0YMD0_HUMAN;tr|H0YMU9|H0YMU9_HUMAN;tr|B4DNH8|B4DNH8_HUMAN;tr|H0YKS4|H0YKS4_HUMAN;tr|H0YMM1|H0YMM1_HUMAN;tr|H0YM50|H0YM50_HUMAN	1,054	0,882
sp|P80723|BASP1_HUMAN	0,864	0,824

tr|A0A087X0Q1|A0A087X0Q1_HUMAN;sp|Q7Z739|YTHD3_HUMAN;tr|Q8NA80|Q8NA80_HUMAN;tr|A0A024R7W5|A0A024R7W5_HUMAN;tr|Q96MZ5|Q96MZ5_HUMAN;tr|Q658Z6|Q658Z6_HUMAN;tr|Q8N3V9|Q8N3V9_HUMAN;tr|B3KTL8|B3KTL8_HUMAN;sp|Q9BYJ9|YTHD1_HUMAN	0,791	0,777
tr|Q0QEW2|Q0QEW2_HUMAN;tr|G3V203|G3V203_HUMAN;tr|H0YHA7|H0YHA7_HUMAN;tr|A0A024QZD1|A0A024QZD1_HUMAN;sp|Q07020|RL18_HUMAN;tr|J3QQ67|J3QQ67_HUMAN;tr|F8VUA6|F8VUA6_HUMAN;tr|F8VYV2|F8VYV2_HUMAN;tr|B4DDY5|B4DDY5_HUMAN;tr|A0A075B7A0|A0A075B7A0_HUMAN	0,518	0,392
tr|A0A024RAI1|A0A024RAI1_HUMAN;sp|P61158|ARP3_HUMAN;tr|B4DXW1|B4DXW1_HUMAN;tr|Q59FV6|Q59FV6_HUMAN;tr|B4DTI0|B4DTI0_HUMAN;tr|B4DT29|B4DT29_HUMAN	1,197	0,802
sp|Q8IVF2|AHNK2_HUMAN	0,911	0,845
tr|E9PBS1|E9PBS1_HUMAN;tr|A0A024RD93|A0A024RD93_HUMAN;sp|P22234|PUR6_HUMAN;tr|B4DGX3|B4DGX3_HUMAN;tr|D6RF62|D6RF62_HUMAN	1,068	0,857
sp|P35606|COPB2_HUMAN	1,097	0,847
sp|P31930|QCR1_HUMAN;tr|B4DUL5|B4DUL5_HUMAN	0,925	0,853
tr|A8K9T9|A8K9T9_HUMAN;tr|A8K8N7|A8K8N7_HUMAN;sp|O15067|PUR4_HUMAN	1,081	0,852
tr|Q49AJ9|Q49AJ9_HUMAN;tr|Q9BT63|Q9BT63_HUMAN;tr|Q9NY85|Q9NY85_HUMAN;tr|G5E9G0|G5E9G0_HUMAN;tr|Q8TBW1|Q8TBW1_HUMAN;sp|P39023|RL3_HUMAN;tr|B3KS36|B3KS36_HUMAN;tr|Q96QL0|Q96QL0_HUMAN;tr|B5MCW2|B5MCW2_HUMAN	0,819	0,807
tr|Q59GY3|Q59GY3_HUMAN;tr|V9HVZ0|V9HVZ0_HUMAN;tr|A8K588|A8K588_HUMAN;sp|Q13247|SRSF6_HUMAN	1,609	0,553
tr|Q6FGU2|Q6FGU2_HUMAN;sp|P23919|KTHY_HUMAN;tr|Q53F55|Q53F55_HUMAN;tr|H7BZ20|H7BZ20_HUMAN	0,647	0,588
sp|P62750|RL23A_HUMAN;tr|H7BY10|H7BY10_HUMAN;tr|K7EJV9|K7EJV9_HUMAN;tr|K7ERT8|K7ERT8_HUMAN;tr|A8MUS3|A8MUS3_HUMAN;tr|K7EMA7|K7EMA7_HUM	1,960	0,387

AN		
tr|Q53FS4|Q53FS4_HUMAN;tr|A0A024R2A7|A0A024R2A7_HUMAN;sp|P49257|LMAN1_HUMAN;tr|B2R774|B2R774_HUMAN	1,485	0,597
tr|F5H6E2|F5H6E2_HUMAN;tr|B7Z3E5|B7Z3E5_HUMAN;sp|O00159|MYO1C_HUMAN;tr|D3DTH7|D3DTH7_HUMAN	0,619	0,551
tr|E9KL44|E9KL44_HUMAN;sp|P40939|ECHA_HUMAN;tr|B4DDZ5|B4DDZ5_HUMAN;tr|B4DRH6|B4DRH6_HUMAN	0,942	0,872
sp|P39687|AN32A_HUMAN;tr|H0YN26|H0YN26_HUMAN;tr|Q6PKH8|Q6PKH8_HUMAN;tr|Q08AJ6|Q08AJ6_HUMAN;tr|Q3KPI8|Q3KPI8_HUMAN;tr|Q1AHP8|Q1AHP8_HUMAN	0,480	0,368
tr|E9PSI1|E9PSI1_HUMAN;tr|B7Z6C9|B7Z6C9_HUMAN;tr|E9PQI5|E9PQI5_HUMAN;tr|E9PQ80|E9PQ80_HUMAN;sp|Q9BY43|CHM4A_HUMAN	1,111	0,841
tr|G3V1S6|G3V1S6_HUMAN;tr|B7Z6K2|B7Z6K2_HUMAN;sp|Q10471|GALT2_HUMAN;tr|B7Z462|B7Z462_HUMAN	1,079	0,855
tr|V9HWB8|V9HWB8_HUMAN;sp|P14618|KPYM_HUMAN;tr|A0A024R5Z9|A0A024R5Z9_HUMAN;tr|H3BTN5|H3BTN5_HUMAN;tr|B4DRT3|B4DRT3_HUMAN;tr|B4DNK4|B4DNK4_HUMAN;tr|Q8WUW7|Q8WUW7_HUMAN;tr|A0A024R609|A0A024R609_HUMAN;tr|H3BQ34|H3BQ34_HUMAN;tr|Q504U3|Q504U3_HUMAN;tr|H3BR70|H3BR70_HUMAN	1,042	0,896
sp|Q08211|DHX9_HUMAN;tr|Q58F26|Q58F26_HUMAN;tr|Q6PJK6|Q6PJK6_HUMAN	1,041	0,899
tr|K9JA46|K9JA46_HUMAN;sp|P07900|HS90A_HUMAN;tr|Q2VPJ6|Q2VPJ6_HUMAN;tr|Q8TBA7|Q8TBA7_HUMAN;tr|Q86U12|Q86U12_HUMAN;tr|O75322|O75322_HUMAN;tr|Q96HX7|Q96HX7_HUMAN	0,895	0,828
tr|L7RXH0|L7RXH0_HUMAN;tr|A5YM53|A5YM53_HUMAN;sp|P06756|ITAV_HUMAN;tr|B4DYQ7|B4DYQ7_HUMAN	0,803	0,801
tr|H0YLA2|H0YLA2_HUMAN;sp|P37108|SRP14_HUMAN	1,451	0,608

tr|A6NKB8|A6NKB8_HUMAN;sp|Q9H4A4|AMPB_HUMAN;tr|Q7RU04|Q7RU04_HUMAN	1,109	0,844
tr|Q6PKC2|Q6PKC2_HUMAN;tr|Q86Y74|Q86Y74_HUMAN;tr|B4DJ96|B4DJ96_HUMAN;tr|A8K3C5|A8K3C5_HUMAN;sp|O95232|LC7L3_HUMAN;tr|J3KPP4|J3KPP4_HUMAN	0,754	0,712
tr|A8K6Q8|A8K6Q8_HUMAN;sp|P02786|TFR1_HUMAN;tr|G3V0E5|G3V0E5_HUMAN;tr|B7Z2I6|B7Z2I6_HUMAN	0,867	0,824
tr|B4DVJ0|B4DVJ0_HUMAN	1,046	0,896
tr|B4DG62|B4DG62_HUMAN;tr|A8K7J7|A8K7J7_HUMAN;sp|P19367|HXK1_HUMAN;tr|A0A024QZK7|A0A024QZK7_HUMAN;tr|Q59FD4|Q59FD4_HUMAN;tr|B3KXY9|B3KXY9_HUMAN;tr|B3KRA9|B3KRA9_HUMAN	1,578	0,576
tr|B2R4R0|B2R4R0_HUMAN;sp|P62805|H4_HUMAN;tr|Q0VAS5|Q0VAS5_HUMAN	1,101	0,844
tr|E5KNY5|E5KNY5_HUMAN;sp|P42704|LPPRC_HUMAN;tr|B4DSR0|B4DSR0_HUMAN	0,943	0,873
sp|P49721|PSB2_HUMAN;tr|B7Z478|B7Z478_HUMAN;tr|Q59FJ0|Q59FJ0_HUMAN	1,482	0,595
sp|P60903|S10AA_HUMAN;tr|Q6FGE5|Q6FGE5_HUMAN;tr|D3DV26|D3DV26_HUMAN	0,475	0,368
tr|B5MCF9|B5MCF9_HUMAN;tr|B2RDF2|B2RDF2_HUMAN;sp|O00541|PESC_HUMAN;tr|B3KXD6|B3KXD6_HUMAN;tr|B3KTZ6|B3KTZ6_HUMAN	0,858	0,822
sp|P51114|FXR1_HUMAN;tr|E9PFF5|E9PFF5_HUMAN;tr|B4DM21|B4DM21_HUMAN;tr|B4DXZ6|B4DXZ6_HUMAN	0,933	0,865
sp|Q96IX5|USMG5_HUMAN	0,771	0,752
tr|Q6P452|Q6P452_HUMAN;sp|P09525|ANXA4_HUMAN;tr|V9HW59|V9HW59_HUMAN;tr|Q6LES2|Q6LES2_HUMAN;tr|B4DDZ4|B4DDZ4_HUMAN;tr|B4DE02|B4DE02_HUMAN;tr|Q59FK3|Q59FK3_HUMAN	1,147	0,822
sp|P49588|SYAC_HUMAN;tr|H3BPK7|H3BPK7_HUMAN	1,077	0,860
sp|P37837|TALDO_HUMAN;tr|F2Z393|F2Z393_HUMAN	0,917	0,840
sp|Q08257|QOR_HUMAN;tr|A6NP24|A6NP24_HUMAN;tr|C9JH92|C9JH92_HUMAN	1,070	0,859

tr|Q0VAB1|Q0VAB1_HUMAN;tr|A0A024R0M6|A0A024R0M6_HUMAN;sp|Q3ZCQ8|TIM50_HUMAN;tr|M0R2F8|M0R2F8_HUMAN;tr|M0R0C3|M0R0C3_HUMAN;tr|M0R003|M0R003_HUMAN	0,933	0,863
sp|Q07955|SRSF1_HUMAN;tr|J3KTL2|J3KTL2_HUMAN;tr|Q59FA2|Q59FA2_HUMAN;tr|A8K1L8|A8K1L8_HUMAN;tr|J3KSR8|J3KSR8_HUMAN;tr|B7Z570|B7Z570_HUMAN	0,881	0,812
tr|B3KTA3|B3KTA3_HUMAN;sp|Q16658|FSCN1_HUMAN	1,144	0,813
tr|B4DZC3|B4DZC3_HUMAN;tr|B3KMC9|B3KMC9_HUMAN;sp|Q9H0D6|XRN2_HUMAN;tr|B4E0B9|B4E0B9_HUMAN	1,547	0,602
tr|B2RAH5|B2RAH5_HUMAN;sp|O14974|MYPT1_HUMAN;tr|A0A024RBF1|A0A024RBF1_HUMAN;tr|H0YHI8|H0YHI8_HUMAN	0,913	0,851
tr|Q6NXR8|Q6NXR8_HUMAN;sp|P61247|RS3A_HUMAN;tr|D6RAT0|D6RAT0_HUMAN;tr|H0Y9Y4|H0Y9Y4_HUMAN;tr|D6RG13|D6RG13_HUMAN;tr|A8K4W0|A8K4W0_HUMAN;tr|B7Z3M5|B7Z3M5_HUMAN;tr|E9PFI5|E9PFI5_HUMAN;tr|D6R9B6|D6R9B6_HUMAN;tr|D6RB09|D6RB09_HUMAN;tr|H0Y8L7|H0Y8L7_HUMAN;tr|D6RAS7|D6RAS7_HUMAN	0,959	0,897
sp|Q1KMD3|HNRL2_HUMAN;tr|H3BQZ7|H3BQZ7_HUMAN	1,148	0,818
tr|A0A024RDE8|A0A024RDE8_HUMAN;sp|Q96HC4|PDLI5_HUMAN;tr|Q4W5K9|Q4W5K9_HUMAN;tr|A0A0D9SFR4|A0A0D9SFR4_HUMAN;tr|B7Z8X5|B7Z8X5_HUMAN	1,091	0,842
sp|P78527|PRKDC_HUMAN	1,094	0,854
sp|Q92841|DDX17_HUMAN;tr|H3BLZ8|H3BLZ8_HUMAN;tr|Q59F66|Q59F66_HUMAN;tr|B4DZQ7|B4DZQ7_HUMAN	0,978	0,954

tr|B4DRW3|B4DRW3_HUMAN;tr|A0A0A0N0L3|A0A0A0N0L3_HUMAN;tr|A0A024R4E2|A0A024R4E2_HUMAN;sp|Q13148|TADBP_HUMAN;tr|K7EJM5|K7EJM5_HUMAN;tr|A0A0A0N0N3|A0A0A0N0N3_HUMAN;tr|A0A087WX29|A0A087WX29_HUMAN;tr|A0A0A0N0M3|A0A0A0N0M3_HUMAN;tr|K7EN94|K7EN94_HUMAN;tr|B1AKP7|B1AKP7_HUMAN;tr|G3V162|G3V162_HUMAN;tr|A0A087X260|A0A087X260_HUMAN;tr|A0A087WYY0|A0A087WYY0_HUMAN;tr|A0A087WXQ5|A0A087WXQ5_HUMAN;tr|A0A087WV68|A0A087WV68_HUMAN	0,846	0,818
tr|A8K6V3|A8K6V3_HUMAN;sp|Q15393|SF3B3_HUMAN;tr|B3KQH1|B3KQH1_HUMAN	1,218	0,796
tr|Q63HR1|Q63HR1_HUMAN;tr|Q5VU21|Q5VU21_HUMAN;sp|Q8NC51|PAIRB_HUMAN;tr|D3DQ69|D3DQ69_HUMAN;tr|D3DQ70|D3DQ70_HUMAN	1,064	0,869
tr|Q53HJ4|Q53HJ4_HUMAN;tr|B2R7C5|B2R7C5_HUMAN;sp|P25205|MCM3_HUMAN;tr|Q8NHX6|Q8NHX6_HUMAN;tr|B4DUQ9|B4DUQ9_HUMAN;tr|J3KQ69|J3KQ69_HUMAN;tr|B4DS46|B4DS46_HUMAN	0,932	0,862
tr|A0A0A0MR02|A0A0A0MR02_HUMAN;tr|A0A024QZT0|A0A024QZT0_HUMAN;sp|P45880|VDAC2_HUMAN;tr|A0A024QZN9|A0A024QZN9_HUMAN;tr|B4DKM5|B4DKM5_HUMAN;tr|Q5JSD2|Q5JSD2_HUMAN;tr|Q5JSD1|Q5JSD1_HUMAN	1,113	0,840
sp|Q71DI3|H32_HUMAN;sp|Q16695|H31T_HUMAN;sp|P68431|H31_HUMAN;tr|B4E380|B4E380_HUMAN;tr|K7EK07|K7EK07_HUMAN;tr|B2R4P9|B2R4P9_HUMAN;sp|P84243|H33_HUMAN;tr|K7EMV3|K7EMV3_HUMAN;tr|B4DEB1|B4DEB1_HUMAN;tr|B2R6Y1|B2R6Y1_HUMAN;tr|A8K4Y7|A8K4Y7_HUMAN;tr|K7ES00|K7ES00_HUMAN;tr|Q6TXQ4|Q6TXQ4_HUMAN;sp|Q6NXT2|H3C_HUMAN	1,206	0,808
tr|B4DLK2|B4DLK2_HUMAN;tr|G3V213|G3V213_HUMAN;tr|F8VZG5|F8VZG5_HUMAN;tr|F8W1A4|F8W1A4_HUMAN;sp|P54819|KAD2_HUMAN;tr|F8VY04|F8VY04_HUMAN	1,056	0,876

tr|E9PGZ1|E9PGZ1_HUMAN;tr|E7EX44|E7EX44_HUMAN;tr|B4DPW5|B4DPW5_HUMAN;tr|B7Z6G4|B7Z6G4_HUMAN;sp|Q05682|CALD1_HUMAN;tr|Q9NYG1|Q9NYG1_HUMAN;tr|B4E3I0|B4E3I0_HUMAN;tr|C9J813|C9J813_HUMAN;tr|Q6PJM5|Q6PJM5_HUMAN	1,086	0,839
sp|P16435|NCPR_HUMAN;tr|A8K3B4|A8K3B4_HUMAN;tr|Q59ED7|Q59ED7_HUMAN;tr|H0Y4R2|H0Y4R2_HUMAN;tr|B4DJI8|B4DJI8_HUMAN;tr|Q63HL4|Q63HL4_HUMAN;tr|B2R6E5|B2R6E5_HUMAN;tr|B4DKM8|B4DKM8_HUMAN;tr|E7EMD0|E7EMD0_HUMAN;tr|B4DDH3|B4DDH3_HUMAN;tr|B4E305|B4E305_HUMAN	1,071	0,862
sp|P21333|FLNA_HUMAN;tr|Q5HY54|Q5HY54_HUMAN;tr|Q60FE6|Q60FE6_HUMAN;tr|Q60FE5|Q60FE5_HUMAN;tr|A6NDY9|A6NDY9_HUMAN;tr|A0A087WWY3|A0A087WWY3_HUMAN;tr|Q8TES4|Q8TES4_HUMAN	1,077	0,858
tr|A0A0A0MSS8|A0A0A0MSS8_HUMAN;sp|P42330|AK1C3_HUMAN;tr|S4R3Z2|S4R3Z2_HUMAN	0,827	0,802
tr|C6EMX8|C6EMX8_HUMAN;tr|B2RBA6|B2RBA6_HUMAN;sp|P33993|MCM7_HUMAN;tr|B3KUD7|B3KUD7_HUMAN;tr|B4DDF5|B4DDF5_HUMAN	1,124	0,829
tr|B2RA03|B2RA03_HUMAN;tr|A0A024RAY2|A0A024RAY2_HUMAN;sp|P05783|K1C18_HUMAN;tr|F8VZY9|F8VZY9_HUMAN;tr|I6L965|I6L965_HUMAN	1,063	0,867
tr|B4DMB5|B4DMB5_HUMAN;sp|P17812|PYRG1_HUMAN;tr|B4E1E0|B4E1E0_HUMAN	1,399	0,656
tr|F8W6I7|F8W6I7_HUMAN;tr|A0A024RB53|A0A024RB53_HUMAN;tr|A0A024RAZ7|A0A024RAZ7_HUMAN;sp|P09651|ROA1_HUMAN;tr|Q6IPF2|Q6IPF2_HUMAN;tr|Q9BSM5|Q9BSM5_HUMAN;tr|B4DP35|B4DP35_HUMAN;tr|B4E0B5|B4E0B5_HUMAN;tr|Q0VAC0|Q0VAC0_HUMAN;tr|A0A024RC46|A0A024RC46_HUMAN;tr|F8VZ49|F8VZ49_HUMAN;tr|F8VYN5|F8VYN5_HUMAN;tr|F8W646|F8W646_HUMAN;tr|A0A024QZ98|A0A024QZ98_HUMAN;sp|Q32P51|RA1L2_HUMAN	1,069	0,861
tr|B3KMV8|B3KMV8_HUMAN;sp|O75746|CMC1_HUMAN;tr|B7Z2E2|B7Z2E2_HUMAN	1,230	0,805

sp|P62917|RL8_HUMAN;tr|E9PKZ0|E9PKZ0_HUMAN;tr|E9PP36|E9PP36_HUMAN;tr|G3V1A1|G3V1A1_HUMAN;tr|B4DVG7|B4DVG7_HUMAN;tr|E9PKU4|E9PKU4_HUMAN	0,951	0,895
tr|B4DPW9|B4DPW9_HUMAN;sp|P13797|PLST_HUMAN;tr|A0A0A0MSQ0|A0A0A0MSQ0_HUMAN;tr|Q53GY0|Q53GY0_HUMAN;tr|Q96HI1|Q96HI1_HUMAN	1,132	0,809
tr|Q5QTS3|Q5QTS3_HUMAN;tr|Q53H34|Q53H34_HUMAN;sp|P40429|RL13A_HUMAN;tr|Q8J015|Q8J015_HUMAN;tr|Q9BSQ6|Q9BSQ6_HUMAN;tr|M0QYS1|M0QYS1_HUMAN;tr|Q0VGL3|Q0VGL3_HUMAN	1,095	0,853
tr|C9JFE4|C9JFE4_HUMAN;sp|Q13098|CSN1_HUMAN;tr|A0A096LP07|A0A096LP07_HUMAN;tr|A0A096LPJ3|A0A096LPJ3_HUMAN;tr|A8K070|A8K070_HUMAN;tr|J3QQX0|J3QQX0_HUMAN;tr|B4DND6|B4DND6_HUMAN	0,934	0,861
tr|X5D2J9|X5D2J9_HUMAN;tr|Q499G6|Q499G6_HUMAN;tr|X5D939|X5D939_HUMAN;tr|X5DNP5|X5DNP5_HUMAN;tr|A8K9W7|A8K9W7_HUMAN;tr|B4DH52|B4DH52_HUMAN;tr|X5DR09|X5DR09_HUMAN;sp|P78347|GTF2I_HUMAN;tr|B4DRA9|B4DRA9_HUMAN	1,050	0,897
sp|Q9UKK9|NUDT5_HUMAN;tr|A6NFX8|A6NFX8_HUMAN;tr|C9JYY9|C9JYY9_HUMAN;tr|A6NCQ0|A6NCQ0_HUMAN;tr|A6NJU6|A6NJU6_HUMAN	1,224	0,793
sp|Q92804|RBP56_HUMAN;tr|B4E312|B4E312_HUMAN;tr|A0A075B7F4|A0A075B7F4_HUMAN	0,888	0,831
tr|Q6IBT3|Q6IBT3_HUMAN;tr|Q53HV2|Q53HV2_HUMAN;sp|Q99832|TCPH_HUMAN;tr|B7Z7I4|B7Z7I4_HUMAN;tr|B7Z1C9|B7Z1C9_HUMAN	1,056	0,875
tr|J3K000|J3K000_HUMAN;sp|P12955|PEPD_HUMAN	0,812	0,803

tr|B3KT06|B3KT06_HUMAN;tr|B3KPS3|B3KPS3_HUMAN;sp|P68363|TBA1B_HUMAN;tr|A8JZY9|A8JZY9_HUMAN;sp|Q71U36|TBA1A_HUMAN;tr|Q53GA7|Q53GA7_HUMAN;sp|Q9BQE3|TBA1C_HUMAN;tr|F5H5D3|F5H5D3_HUMAN;tr|Q1ZYQ1|Q1ZYQ1_HUMAN;sp|Q13748|TBA3C_HUMAN;tr|B7Z1K5|B7Z1K5_HUMAN;tr|B4DDU2|B4DDU2_HUMAN;tr|B4DQK4|B4DQK4_HUMAN;sp|Q6PEY2|TBA3E_HUMAN;tr|F8VVB9|F8VVB9_HUMAN;tr|Q8N532|Q8N532_HUMAN;tr|Q9UQM3|Q9UQM3_HUMAN;tr|F8VQQ4|F8VQQ4_HUMAN	1,027	0,944
tr|A0A024R8W0|A0A024R8W0_HUMAN;sp|P38919|IF4A3_HUMAN	1,092	0,837
sp|P07814|SYEP_HUMAN;tr|V9GYZ6|V9GYZ6_HUMAN;tr|Q3KQZ8|Q3KQZ8_HUMAN;tr|B4DKX5|B4DKX5_HUMAN	1,065	0,867
tr|A0A024R1U4|A0A024R1U4_HUMAN;sp|P51148|RAB5C_HUMAN	0,935	0,860
tr|F8W1R7|F8W1R7_HUMAN;sp|P60660|MYL6_HUMAN;tr|G3V1V0|G3V1V0_HUMAN;tr|J3KND3|J3KND3_HUMAN;tr|G8JLA2|G8JLA2_HUMAN;tr|B7Z6Z4|B7Z6Z4_HUMAN;tr|F8VPF3|F8VPF3_HUMAN;tr|G3V1Y7|G3V1Y7_HUMAN;tr|Q6IBG5|Q6IBG5_HUMAN	1,258	0,795
sp|Q9NR30|DDX21_HUMAN	0,964	0,905
tr|V9HWK1|V9HWK1_HUMAN;sp|P60174|TPIS_HUMAN;tr|Q53HE2|Q53HE2_HUMAN;tr|B4DUI5|B4DUI5_HUMAN;tr|Q2QD09|Q2QD09_HUMAN;tr|U3KPZ0|U3KPZ0_HUMAN	1,105	0,845
tr|B4DLR3|B4DLR3_HUMAN;tr|Q7Z4Q5|Q7Z4Q5_HUMAN	1,057	0,874

tr|Q6IPT9|Q6IPT9_HUMAN;tr|Q6IPS9|Q6IPS9_HUMAN;tr|Q6IPN6|Q6IPN6_HUMAN;tr|Q53HQ7|Q53HQ7_HUMAN;tr|Q53HM9|Q53HM9_HUMAN;sp|Q5VTE0|EF1A3_HUMAN;sp|P68104|EF1A1_HUMAN;tr|Q53HR5|Q53HR5_HUMAN;tr|Q53GE9|Q53GE9_HUMAN;tr|Q53GA1|Q53GA1_HUMAN;tr|Q53G85|Q53G85_HUMAN;tr|A8K9C4|A8K9C4_HUMAN;tr|Q96RE1|Q96RE1_HUMAN;tr|Q9NZS6|Q9NZS6_HUMAN;tr|Q53G89|Q53G89_HUMAN;tr|A0A087WVQ9|A0A087WVQ9_HUMAN;tr|Q8IUB0|Q8IUB0_HUMAN;tr|B4DV42|B4DV42_HUMAN;tr|A0A087WV01|A0A087WV01_HUMAN;tr|Q9H2I7|Q9H2I7_HUMAN;tr|Q53HR1|Q53HR1_HUMAN;tr|B4DNE0|B4DNE0_HUMAN;tr|Q504Z0|Q504Z0_HUMAN;tr|B4E2C5|B4E2C5_HUMAN;tr|Q16577|Q16577_HUMAN	0,897	0,842
tr|H0Y3P2|H0Y3P2_HUMAN;tr|D3DQV9|D3DQV9_HUMAN;sp|P78344|IF4G2_HUMAN;tr|Q59G42|Q59G42_HUMAN;tr|B4DZF2|B4DZF2_HUMAN;tr|Q2TU89|Q2TU89_HUMAN;tr|H0YCH5|H0YCH5_HUMAN	1,157	0,821
tr|A8K7A6|A8K7A6_HUMAN;tr|Q6P2R1|Q6P2R1_HUMAN;sp|Q14683|SMC1A_HUMAN;tr|Q68EN4|Q68EN4_HUMAN;tr|Q6MZR8|Q6MZR8_HUMAN;tr|G8JLG1|G8JLG1_HUMAN;tr|Q7Z4C6|Q7Z4C6_HUMAN;tr|H0Y7K8|H0Y7K8_HUMAN;tr|Q5H934|Q5H934_HUMAN;tr|B7Z709|B7Z709_HUMAN	1,236	0,811
sp|P38159|RBMX_HUMAN;tr|B4E352|B4E352_HUMAN;tr|Q2VIN3|Q2VIN3_HUMAN;sp|Q96E39|RMXL1_HUMAN;tr|B3KRG5|B3KRG5_HUMAN;tr|H3BUY5|H3BUY5_HUMAN;tr|H0Y6E7|H0Y6E7_HUMAN;tr|H3BT71|H3BT71_HUMAN	1,044	0,896
sp|Q14444|CAPR1_HUMAN;tr|B4DSF8|B4DSF8_HUMAN;tr|A0A087X082|A0A087X082_HUMAN;tr|E9PLA9|E9PLA9_HUMAN;tr|G3V153|G3V153_HUMAN;tr|B3KXU8|B3KXU8_HUMAN	1,075	0,858
sp|O15371|EIF3D_HUMAN;tr|B0QYA8|B0QYA8_HUMAN;tr|B0QYA6|B0QYA6_HUMAN;tr|B0QYA5|B0QYA5_HUMAN;tr|B4E1K8|B4E1K8_HUMAN	0,781	0,778

tr|A6NJA2|A6NJA2_HUMAN;tr|D3DUG9|D3DUG9_HUMAN;tr|B2RD79|B2RD79_HUMAN;sp|P54578|UBP14_HUMAN;tr|B3KTG4|B3KTG4_HUMAN	1,319	0,748
tr|B1AK87|B1AK87_HUMAN;tr|B2R7T8|B2R7T8_HUMAN;tr|B1AK88|B1AK88_HUMAN;tr|B4DWA6|B4DWA6_HUMAN;sp|P47756|CAPZB_HUMAN;tr|B1AK85|B1AK85_HUMAN	0,645	0,607
sp|P14868|SYDC_HUMAN;tr|D3DP78|D3DP78_HUMAN;tr|Q53T60|Q53T60_HUMAN	1,042	0,898
sp|P05023|AT1A1_HUMAN;tr|B7Z3V1|B7Z3V1_HUMAN;tr|B7Z1Q9|B7Z1Q9_HUMAN;tr|M0R116|M0R116_HUMAN;tr|B7Z3F8|B7Z3F8_HUMAN;tr|Q53ES0|Q53ES0_HUMAN;sp|P13637|AT1A3_HUMAN;tr|B7Z9V4|B7Z9V4_HUMAN;tr|A0A0A0MT26|A0A0A0MT26_HUMAN	0,910	0,848
sp|Q32MZ4|LRRF1_HUMAN;tr|Q05D04|Q05D04_HUMAN	0,957	0,897
tr|A0A024RD80|A0A024RD80_HUMAN;sp|P08238|HS90B_HUMAN;tr|B4DMA2|B4DMA2_HUMAN;tr|B4DGL0|B4DGL0_HUMAN;tr|Q6PK50|Q6PK50_HUMAN	0,890	0,829
tr|A8KAQ5|A8KAQ5_HUMAN;tr|A0A024QZD5|A0A024QZD5_HUMAN;sp|P08621|RU17_HUMAN;tr|M0QYR1|M0QYR1_HUMAN	1,041	0,899
tr|A0A024RAV2|A0A024RAV2_HUMAN;sp|P46063|RECQ1_HUMAN	0,925	0,852
sp|O75369|FLNB_HUMAN;tr|A0A024R321|A0A024R321_HUMAN;tr|Q68CT4|Q68CT4_HUMAN;tr|E7EN95|E7EN95_HUMAN	1,077	0,861
sp|P49189|AL9A1_HUMAN;tr|B9EKV4|B9EKV4_HUMAN;tr|B4DE91|B4DE91_HUMAN;tr|B4DX14|B4DX14_HUMAN	0,945	0,874
tr|A0A024R8S5|A0A024R8S5_HUMAN;sp|P07237|PDIA1_HUMAN;tr|B4DNL5|B4DNL5_HUMAN;tr|B4DLN6|B4DLN6_HUMAN;tr|B4DUA5|B4DUA5_HUMAN;tr|H7BZ94|H7BZ94_HUMAN;tr|I3L398|I3L398_HUMAN;tr|H0Y3Z3|H0Y3Z3_HUMAN	0,937	0,861
tr|Q24JU4|Q24JU4_HUMAN;tr|J9R021|J9R021_HUMAN;sp|Q14152|EIF3A_HUMAN;tr|Q7Z5T5|Q7Z5T5_HUMAN;tr|Q05BS0|Q05BS0_HUMAN;tr|Q6P1R0|Q6P1R0_HUMAN;tr|Q3B770|Q3B770_HUMAN	1,044	0,897

tr|B2R5V9|B2R5V9_HUMAN;tr|A0A024R4E5|A0A024R4E5_HUMAN;sp|Q00341|VIGLN_HUMAN;tr|H0Y394|H0Y394_HUMAN;tr|Q6ZS03|Q6ZS03_HUMAN;tr|B4DKR8|B4DKR8_HUMAN;tr|Q96CF6|Q96CF6_HUMAN	0,855	0,822
tr|B2RDE8|B2RDE8_HUMAN;sp|P51858|HDGF_HUMAN;tr|A8K8G0|A8K8G0_HUMAN;tr|B7Z958|B7Z958_HUMAN	1,356	0,715
sp|O43175|SERA_HUMAN;tr|Q5SZU1|Q5SZU1_HUMAN;tr|B3KSC3|B3KSC3_HUMAN;tr|V9HW79|V9HW79_HUMAN;tr|Q9UMY2|Q9UMY2_HUMAN	1,155	0,818
tr|C9JXB8|C9JXB8_HUMAN;tr|C9JNW5|C9JNW5_HUMAN;tr|V9HW01|V9HW01_HUMAN;sp|P83731|RL24_HUMAN	1,407	0,666
tr|A0A087X2D8|A0A087X2D8_HUMAN;sp|O60271|JIP4_HUMAN;tr|A0A060L980|A0A060L980_HUMAN	0,915	0,840
tr|B9A6K1|B9A6K1_HUMAN;sp|Q92609|TBCD5_HUMAN;tr|A0A024R2J9|A0A024R2J9_HUMAN;tr|A0A024R2H0|A0A024R2H0_HUMAN;tr|C9J3F6|C9J3F6_HUMAN	0,939	0,868
tr|R4GN98|R4GN98_HUMAN;sp|P06703|S10A6_HUMAN;tr|B2R577|B2R577_HUMAN	1,213	0,807
sp|Q9Y2A7|NCKP1_HUMAN	1,137	0,808
tr|V9HWF4|V9HWF4_HUMAN;sp|P00558|PGK1_HUMAN;tr|B4E1H9|B4E1H9_HUMAN	0,974	0,944
tr|Q5QPL9|Q5QPL9_HUMAN;tr|A8K4T9|A8K4T9_HUMAN;sp|Q9UKM9|RALY_HUMAN;tr|Q53GL6|Q53GL6_HUMAN;tr|Q5QPM0|Q5QPM0_HUMAN;tr|Q5QPM1|Q5QPM1_HUMAN	1,022	0,955
sp|P20962|PTMS_HUMAN;tr|O15256|O15256_HUMAN;tr|A2VCM6|A2VCM6_HUMAN	0,852	0,827
sp|Q7Z4H3|HDDC2_HUMAN;tr|H0UI53|H0UI53_HUMAN;tr|H0UI52|H0UI52_HUMAN	0,852	0,824
tr|A0A024R1K7|A0A024R1K7_HUMAN;sp|Q04917|1433F_HUMAN;tr|B2R6N6|B2R6N6_HUMAN;tr|A2IDB2|A2IDB2_HUMAN;tr|Q9H4N8|Q9H4N8_HUMAN	1,081	0,854
tr|B4DDM5|B4DDM5_HUMAN;tr|B2R659|B2R659_HUMAN;sp|P51659|DHB4_HUMAN;tr|E7ER27|E7ER27_HUMAN;tr|E7EWE5|E7EWE5_HUMAN;tr|B4DSD0|B4DSD0_HUMAN	1,076	0,860

tr|A8K6Y1|A8K6Y1_HUMAN;tr|Q6PIN5|Q6PIN5_HUMAN;tr|A0A024RB85|A0A024RB85_HUMAN;sp|Q9UQ80|PA2G4_HUMAN;tr|Q05D08|Q05D08_HUMAN;tr|F8VR77|F8VR77_HUMAN	1,032	0,936
tr|E7EX73|E7EX73_HUMAN;tr|E9PGM1|E9PGM1_HUMAN;tr|E7EUU4|E7EUU4_HUMAN;tr|A0A0A0MR52|A0A0A0MR52_HUMAN	1,028	0,946
tr|F5GZS6|F5GZS6_HUMAN;sp|P08195|4F2_HUMAN;tr|J3KPF3|J3KPF3_HUMAN;tr|B4E2Z3|B4E2Z3_HUMAN;tr|A0A024R599|A0A024R599_HUMAN	0,914	0,843
tr|G3V1C3|G3V1C3_HUMAN;sp|Q9BZZ5|API5_HUMAN;tr|H0YER7|H0YER7_HUMAN;tr|B4DDR3|B4DDR3_HUMAN	0,825	0,800
tr|Q86VX4|Q86VX4_HUMAN;tr|B0AZQ4|B0AZQ4_HUMAN;sp|Q9UQE7|SMC3_HUMAN	1,022	0,952
tr|D9IAI1|D9IAI1_HUMAN;sp|P30086|PEBP1_HUMAN;tr|B4DRT4|B4DRT4_HUMAN	1,059	0,874
tr|A0A0A0MSI0|A0A0A0MSI0_HUMAN;sp|Q06830|PRDX1_HUMAN;tr|B2R4P2|B2R4P2_HUMAN;tr|A0A0A0MRQ5|A0A0A0MRQ5_HUMAN	0,952	0,896
sp|Q9Y3F4|STRAP_HUMAN;tr|B0AZV0|B0AZV0_HUMAN	0,958	0,896
tr|V9HWD9|V9HWD9_HUMAN;tr|Q53EM5|Q53EM5_HUMAN;sp|P29401|TKT_HUMAN;tr|B3KSI4|B3KSI4_HUMAN;tr|B4E022|B4E022_HUMAN;tr|A0A0B4J1R6|A0A0B4J1R6_HUMAN;tr|B3KPZ8|B3KPZ8_HUMAN;tr|B4DVU1|B4DVU1_HUMAN	1,045	0,897
sp|P26447|S10A4_HUMAN;tr|Q5Q9Z3|Q5Q9Z3_HUMAN	1,793	0,561
sp|Q15149|PLEC_HUMAN	1,058	0,875
sp|P53621|COPA_HUMAN	0,953	0,896
tr|E9PPJ0|E9PPJ0_HUMAN;sp|Q13435|SF3B2_HUMAN;tr|Q7Z3K9|Q7Z3K9_HUMAN;tr|A0A087WZZ5|A0A087WZZ5_HUMAN;tr|E9PJT3|E9PJT3_HUMAN;tr|E9PJ04|E9PJ04_HUMAN	0,859	0,816

tr|Q6P6D7|Q6P6D7_HUMAN;tr|Q6FHU2|Q6FHU2_HUMAN;tr|Q53G35|Q53G35_HUMAN;sp|P18669|PGAM1_HUMAN;tr|Q6FHK8|Q6FHK8_HUMAN;tr|Q0D2Q6|Q0D2Q6_HUMAN;tr|B4DKL5|B4DKL5_HUMAN	0,916	0,843
tr|B3KUZ8|B3KUZ8_HUMAN;tr|A0A024R6W0|A0A024R6W0_HUMAN;sp|P00505|AATM_HUMAN;tr|A8K482|A8K482_HUMAN	1,026	0,945
tr|H3BR35|H3BR35_HUMAN;tr|Q7KZX8|Q7KZX8_HUMAN;tr|B2RCT6|B2RCT6_HUMAN;tr|A8K2W7|A8K2W7_HUMAN;sp|P15170|ERF3A_HUMAN;tr|B4DQM6|B4DQM6_HUMAN;sp|Q8IYD1|ERF3B_HUMAN	0,961	0,899
tr|B4DQF6|B4DQF6_HUMAN;sp|Q9Y262|EIF3L_HUMAN;tr|B0QY89|B0QY89_HUMAN;tr|B3KPB9|B3KPB9_HUMAN;tr|C9JHP4|C9JHP4_HUMAN;tr|C9K0Q7|C9K0Q7_HUMAN;tr|B4DEH4|B4DEH4_HUMAN	1,092	0,845
tr|Q4ZG57|Q4ZG57_HUMAN;sp|Q14566|MCM6_HUMAN	1,054	0,890
tr|V9HW56|V9HW56_HUMAN;sp|P67936|TPM4_HUMAN;tr|B4DVY2|B4DVY2_HUMAN;tr|K7ENT6|K7ENT6_HUMAN;tr|B4DTB1|B4DTB1_HUMAN;tr|K7ERG3|K7ERG3_HUMAN	0,959	0,894
tr|A0A024R694|A0A024R694_HUMAN;sp|P12814|ACTN1_HUMAN;tr|H9KV75|H9KV75_HUMAN;tr|B7Z565|B7Z565_HUMAN;tr|Q86TX4|Q86TX4_HUMAN;tr|B4DFY0|B4DFY0_HUMAN	1,065	0,867
tr|B7Z476|B7Z476_HUMAN;tr|Q53FH8|Q53FH8_HUMAN;sp|Q9Y5X3|SNX5_HUMAN;tr|Q6P5V6|Q6P5V6_HUMAN;tr|Q5QPE4|Q5QPE4_HUMAN;tr|A0A087WUY5|A0A087WUY5_HUMAN;tr|Q5QPE5|Q5QPE5_HUMAN	1,030	0,946
tr|Q53HL9|Q53HL9_HUMAN;tr|Q53GY8|Q53GY8_HUMAN;sp|Q13596|SNX1_HUMAN;tr|Q59GU6|Q59GU6_HUMAN;tr|H0YK42|H0YK42_HUMAN	1,095	0,841
tr|A0A024R4M0|A0A024R4M0_HUMAN;sp|P46781|RS9_HUMAN;tr|B5MCT8|B5MCT8_HUMAN;tr|C9JM19|C9JM19_HUMAN;tr|B7Z732|B7Z732_HUMAN;tr|A5D904|A5D904_HUMAN	1,027	0,943

tr|V9HW41|V9HW41_HUMAN;sp|P61088|UBE2N_HUMAN;sp|Q5JXB2|UE2NL_HUMAN;tr|F8VQQ8|F8VQQ8_HUMAN;tr|F8VSD4|F8VSD4_HUMAN;tr|F8VV71|F8VV71_HUMAN	1,212	0,795
sp|O60218|AK1BA_HUMAN	0,884	0,828
sp|P31153|METK2_HUMAN;tr|B4DEX8|B4DEX8_HUMAN	0,917	0,844
sp|O00231|PSD11_HUMAN;tr|B4DTS5|B4DTS5_HUMAN;tr|J3QRY4|J3QRY4_HUMAN	0,949	0,895
tr|B5BUB5|B5BUB5_HUMAN;sp|P05455|LA_HUMAN;tr|E7ERC4|E7ERC4_HUMAN	1,172	0,827
tr|Q53FR7|Q53FR7_HUMAN;sp|P56182|RRP1_HUMAN;tr|Q6PJJ2|Q6PJJ2_HUMAN;tr|Q96J73|Q96J73_HUMAN;tr|B4DZM3|B4DZM3_HUMAN	1,031	0,947
sp|P30048|PRDX3_HUMAN;tr|Q53HC2|Q53HC2_HUMAN	0,941	0,874
sp|Q9Y2W1|TR150_HUMAN;tr|Q7Z5U1|Q7Z5U1_HUMAN;tr|Q05D20|Q05D20_HUMAN;tr|Q6P0P7|Q6P0P7_HUMAN;tr|Q6PJV4|Q6PJV4_HUMAN	0,973	0,947
tr|B4E2G8|B4E2G8_HUMAN;sp|P35221|CTNA1_HUMAN;tr|B3KSR8|B3KSR8_HUMAN;tr|B4DKT9|B4DKT9_HUMAN;tr|B4DU00|B4DU00_HUMAN;tr|G3XAM7|G3XAM7_HUMAN	1,038	0,906
tr|X5D7K9|X5D7K9_HUMAN;tr|X5D2M8|X5D2M8_HUMAN;sp|Q14764|MVP_HUMAN;tr|B4DXN0|B4DXN0_HUMAN;tr|B4DDR2|B4DDR2_HUMAN;tr|B4DP93|B4DP93_HUMAN;tr|X5DNU0|X5DNU0_HUMAN;tr|X5D7S8|X5D7S8_HUMAN	0,935	0,859
tr|B4DUT7|B4DUT7_HUMAN;tr|Q53F90|Q53F90_HUMAN;sp|P49915|GUAA_HUMAN	0,853	0,824
sp|Q9Y230|RUVB2_HUMAN;tr|B3KNL2|B3KNL2_HUMAN;tr|M0R0Y3|M0R0Y3_HUMAN;tr|B4DW30|B4DW30_HUMAN	1,060	0,876
tr|H0Y2Y8|H0Y2Y8_HUMAN;sp|Q15942|ZYX_HUMAN;tr|Q96AF9|Q96AF9_HUMAN;tr|B4DQR8|B4DQR8_HUMAN;tr|Q28617|Q28617_HUMAN;tr|B4DY85|B4DY85_HUMAN;tr|Q9BUS0|Q9BUS0_HUMAN	0,962	0,904

tr|B4DQY1|B4DQY1_HUMAN;tr|B4DDF7|B4DDF7_HUMAN;tr|A8K7B7|A8K7B7_HUMAN;tr|A8K3H8|A8K3H8_HUMAN;sp|P30153|2AAA_HUMAN;tr|B4DE69|B4DE69_HUMAN;tr|Q8NB89|Q8NB89_HUMAN;tr|B3KQV6|B3KQV6_HUMAN;tr|B4E1Q0|B4E1Q0_HUMAN;tr|C9J9C1|C9J9C1_HUMAN	1,075	0,862
tr|A0A024R8V0|A0A024R8V0_HUMAN;sp|Q9UHD8|SEPT9_HUMAN;tr|A0A024R8Q0|A0A024R8Q0_HUMAN;tr|K7EL40|K7EL40_HUMAN;tr|K7EK18|K7EK18_HUMAN	0,940	0,872
tr|H9ZYJ2|H9ZYJ2_HUMAN;sp|P10599|THIO_HUMAN	1,106	0,845
tr|B4DV79|B4DV79_HUMAN;tr|A4D210|A4D210_HUMAN;tr|A0A024R821|A0A024R821_HUMAN;sp|P55884|EIF3B_HUMAN;tr|B4DXN6|B4DXN6_HUMAN;tr|Q96G38|Q96G38_HUMAN;tr|Q86UM1|Q86UM1_HUMAN	1,196	0,824
sp|P19105|ML12A_HUMAN;sp|O14950|ML12B_HUMAN;tr|J3QRS3|J3QRS3_HUMAN;tr|Q2F834|Q2F834_HUMAN;tr|Q53HL1|Q53HL1_HUMAN;tr|Q71U02|Q71U02_HUMAN;tr|Q6IBG1|Q6IBG1_HUMAN;sp|P24844|MYL9_HUMAN;tr|J3KTJ1|J3KTJ1_HUMAN	1,190	0,823
sp|O43707|ACTN4_HUMAN;tr|Q96BG6|Q96BG6_HUMAN	1,028	0,946
sp|O43776|SYNC_HUMAN;tr|K7EIU7|K7EIU7_HUMAN;tr|B4DGT6|B4DGT6_HUMAN	1,026	0,943
tr|V9HWH1|V9HWH1_HUMAN;sp|P30740|ILEU_HUMAN;tr|B4E3A8|B4E3A8_HUMAN	1,097	0,839
sp|P18077|RL35A_HUMAN;tr|C9K025|C9K025_HUMAN;tr|F8WBS5|F8WBS5_HUMAN;tr|F8WB72|F8WB72_HUMAN	0,924	0,850
tr|G3V4F7|G3V4F7_HUMAN;tr|B4DDS7|B4DDS7_HUMAN;sp|P61011|SRP54_HUMAN	1,182	0,819
tr|B4DHC5|B4DHC5_HUMAN;tr|A0A024R458|A0A024R458_HUMAN;sp|P52594|AGFG1_HUMAN;tr|C9J2I0|C9J2I0_HUMAN;tr|B8ZZY2|B8ZZY2_HUMAN	1,062	0,877
tr|A0A0A0MRV0|A0A0A0MRV0_HUMAN;sp|Q9P2E9|RRBP1_HUMAN;tr|A7BI36|A7BI36_HUMAN;tr|A1A5C4|A1A5C4_HUMAN;tr|A0A087WVV2|A0A087WVV2_HUMAN;tr|F8W7S5|F8W7S5_HUMAN;tr|A1A5C5|A1A5C5_HUMAN	1,061	0,874

tr|A0A024R0V4|A0A024R0V4_HUMAN;sp|P50552|VASP_HUMAN;tr|K7EM16|K7EM16_HUMAN	0,949	0,894
tr|Q53GK6|Q53GK6_HUMAN;tr|Q53G99|Q53G99_HUMAN;tr|Q53G76|Q53G76_HUMAN;tr|Q1KLZ0|Q1KLZ0_HUMAN;sp|P60709|ACTB_HUMAN;tr|B4E335|B4E335_HUMAN;tr|Q8WVW5|Q8WVW5_HUMAN;tr|B3KWQ3|B3KWQ3_HUMAN;tr|Q6PJ43|Q6PJ43_HUMAN;tr|B7ZAP6|B7ZAP6_HUMAN;tr|V9HVZ7|V9HVZ7_HUMAN;tr|Q96FU6|Q96FU6_HUMAN	1,042	0,900
tr|Q9UFM8|Q9UFM8_HUMAN;sp|Q9Y639|NPTN_HUMAN;tr|Q9Y499|Q9Y499_HUMAN	0,883	0,830
tr|E9PCY7|E9PCY7_HUMAN;sp|P31943|HNRH1_HUMAN;tr|G8JLB6|G8JLB6_HUMAN;tr|D6RIU0|D6RIU0_HUMAN;tr|D6RBM0|D6RBM0_HUMAN;tr|E7EQJ0|E7EQJ0_HUMAN;tr|D6RAM1|D6RAM1_HUMAN;tr|D6R9T0|D6R9T0_HUMAN;tr|D6RFM3|D6RFM3_HUMAN;tr|D6RIT2|D6RIT2_HUMAN;tr|D6RDU3|D6RDU3_HUMAN;tr|D6RJ04|D6RJ04_HUMAN;tr|D6RIH9|D6RIH9_HUMAN;tr|H0YB39|H0YB39_HUMAN	0,953	0,894
tr|A0A024R1A3|A0A024R1A3_HUMAN;sp|P22314|UBA1_HUMAN;tr|B4DDE4|B4DDE4_HUMAN;tr|B4DL67|B4DL67_HUMAN	0,972	0,945
sp|P43246|MSH2_HUMAN;tr|Q53RU4|Q53RU4_HUMAN;tr|B4DL39|B4DL39_HUMAN;tr|B4DSB9|B4DSB9_HUMAN;tr|V9H019|V9H019_HUMAN;tr|B4DN49|B4DN49_HUMAN;tr|Q53GS1|Q53GS1_HUMAN;tr|Q53FK0|Q53FK0_HUMAN;tr|E9PHA6|E9PHA6_HUMAN;tr|A0A087X078|A0A087X078_HUMAN;tr|V9H068|V9H068_HUMAN;tr|V9H0D5|V9H0D5_HUMAN;tr|A0A087X1E7|A0A087X1E7_HUMAN;tr|V9H023|V9H023_HUMAN	1,053	0,897

tr|A0A0C4DGB5|A0A0C4DGB5_HUMAN;tr|F8W7E0|F8W7E0_HUMAN;tr|A0A024RAN2|A0A024RAN2_HUMAN;tr|D6RGF7|D6RGF7_HUMAN;tr|D6RBR1|D6RBR1_HUMAN;tr|H0Y944|H0Y944_HUMAN;tr|H0YA91|H0YA91_HUMAN;tr|E9PSG1|E9PSG1_HUMAN;tr|E9PDE4|E9PDE4_HUMAN;tr|E7ES10|E7ES10_HUMAN;tr|B7Z5T9|B7Z5T9_HUMAN;tr|E9PCH5|E9PCH5_HUMAN;tr|E7EVY3|E7EVY3_HUMAN;tr|B7Z574|B7Z574_HUMAN;sp|P20810|ICAL_HUMAN;tr|E7EN75|E7EN75_HUMAN;tr|Q6AZE3|Q6AZE3_HUMAN;tr|B7Z6N0|B7Z6N0_HUMAN	1,130	0,829
tr|Q53YD7|Q53YD7_HUMAN;sp|P26641|EF1G_HUMAN	1,028	0,947
tr|Q6IAU5|Q6IAU5_HUMAN;tr|B2R665|B2R665_HUMAN;sp|O15355|PPM1G_HUMAN;tr|B4DDC8|B4DDC8_HUMAN;tr|B3KXL8|B3KXL8_HUMAN	1,060	0,875
tr|A0A024RC87|A0A024RC87_HUMAN;sp|P13489|RINI_HUMAN;tr|H0YCR7|H0YCR7_HUMAN	1,201	0,817
sp|P36578|RL4_HUMAN;tr|B4DMJ6|B4DMJ6_HUMAN;tr|Q59GY2|Q59GY2_HUMAN;tr|Q53G74|Q53G74_HUMAN;tr|H3BM89|H3BM89_HUMAN;tr|B4DFI6|B4DFI6_HUMAN;tr|B4DMJ2|B4DMJ2_HUMAN	0,939	0,872
sp|O60664|PLIN3_HUMAN;tr|K7EL96|K7EL96_HUMAN;tr|K7ERZ3|K7ERZ3_HUMAN	1,062	0,875
sp|P30838|AL3A1_HUMAN;tr|Q6PKA6|Q6PKA6_HUMAN;tr|C9JMC5|C9JMC5_HUMAN;tr|I3L3I9|I3L3I9_HUMAN;tr|E9PNN6|E9PNN6_HUMAN;tr|A8MYB8|A8MYB8_HUMAN;tr|B3KSJ6|B3KSJ6_HUMAN;tr|Q8N9T9|Q8N9T9_HUMAN	1,101	0,856
tr|Q5JP53|Q5JP53_HUMAN;tr|Q5SU16|Q5SU16_HUMAN;sp|P07437|TBB5_HUMAN;tr|B7ZAF0|B7ZAF0_HUMAN;tr|Q6LC01|Q6LC01_HUMAN;tr|B4DY90|B4DY90_HUMAN;tr|Q5ST81|Q5ST81_HUMAN;tr|B7ZAK1|B7ZAK1_HUMAN;tr|Q9BUU9|Q9BUU9_HUMAN;tr|B4E052|B4E052_HUMAN;tr|B4DQN9|B4DQN9_HUMAN;tr|Q96B85|Q96B85_HUMAN;tr|B4DXZ5|B4DXZ5_HUMAN;tr|B4DMU8|B4DMU8_HUMAN;tr|Q1KSF8|Q1KSF8_HUMAN;tr|B4DMJ5|B4DMJ5_HUMAN	1,344	0,777

tr|B4E0R6|B4E0R6_HUMAN;tr|A0A024RDY0|A0A024RDY0_HUMAN;sp|O00410|IPO5_HUMAN;tr|H0Y8C6|H0Y8C6_HUMAN;tr|C9JZD8|C9JZD8_HUMAN;tr|C9JQT6|C9JQT6_HUMAN;tr|E7ESA1|E7ESA1_HUMAN;tr|E7ESZ1|E7ESZ1_HUMAN;tr|E7EWK4|E7EWK4_HUMAN;tr|E7EX05|E7EX05_HUMAN;tr|E7EQT5|E7EQT5_HUMAN;tr|E7ETV8|E7ETV8_HUMAN;tr|E7EV12|E7EV12_HUMAN;tr|E7ETV3|E7ETV3_HUMAN	0,959	0,900
tr|Q9H072|Q9H072_HUMAN;tr|A0A024R5X7|A0A024R5X7_HUMAN;sp|O76031|CLPX_HUMAN	0,939	0,874
tr|V9HWF5|V9HWF5_HUMAN;tr|A8K486|A8K486_HUMAN;sp|P62937|PPIA_HUMAN;tr|B4DM82|B4DM82_HUMAN;tr|B2RE56|B2RE56_HUMAN;tr|F8WE65|F8WE65_HUMAN;tr|C9J5S7|C9J5S7_HUMAN;tr|Q71V99|Q71V99_HUMAN	1,074	0,861
sp|Q13813|SPTN1_HUMAN;tr|A0A024R889|A0A024R889_HUMAN;tr|A0A0D9SGF6|A0A0D9SGF6_HUMAN;tr|A0A0D9SF54|A0A0D9SF54_HUMAN;tr|B4DGT1|B4DGT1_HUMAN;tr|B4DTV8|B4DTV8_HUMAN	1,021	0,958
tr|V9HW83|V9HW83_HUMAN;sp|P00352|AL1A1_HUMAN;tr|V9HVX6|V9HVX6_HUMAN;tr|B4DDF8|B4DDF8_HUMAN;tr|B4DXX3|B4DXX3_HUMAN	1,029	0,945
tr|A0A024R9D2|A0A024R9D2_HUMAN;sp|Q86UE4|LYRIC_HUMAN;tr|E5RJU9|E5RJU9_HUMAN;tr|H0YB56|H0YB56_HUMAN	1,018	0,966
sp|P12429|ANXA3_HUMAN;tr|D6RA82|D6RA82_HUMAN;tr|D6RFG5|D6RFG5_HUMAN	0,966	0,928
tr|V9HWE9|V9HWE9_HUMAN;sp|P09211|GSTP1_HUMAN;tr|A8MX94|A8MX94_HUMAN;tr|A0A087X2E9|A0A087X2E9_HUMAN	0,941	0,878
tr|A0A024RAM4|A0A024RAM4_HUMAN;sp|P46821|MAP1B_HUMAN;tr|A2BDK6|A2BDK6_HUMAN;tr|Q5H9P1|Q5H9P1_HUMAN	0,920	0,854

tr|V9HW22|V9HW22_HUMAN;sp|P11142|HSP7C_HUMAN;tr|E9PKE3|E9PKE3_HUMAN;tr|Q96IS6|Q96IS6_HUMAN;tr|Q53GZ6|Q53GZ6_HUMAN;tr|B3KTV0|B3KTV0_HUMAN;tr|Q53HF2|Q53HF2_HUMAN;tr|E9PNE6|E9PNE6_HUMAN;tr|B4E1Q1|B4E1Q1_HUMAN;tr|E9PN89|E9PN89_HUMAN;tr|A8K7Q2|A8K7Q2_HUMAN	1,031	0,945
sp|P62081|RS7_HUMAN;tr|B5MCP9|B5MCP9_HUMAN	1,015	0,973
tr|A8K9U0|A8K9U0_HUMAN;sp|Q9BWF3|RBM4_HUMAN;tr|E9PB51|E9PB51_HUMAN;sp|Q9BQ04|RBM4B_HUMAN;tr|E9PLB0|E9PLB0_HUMAN;tr|E9PM61|E9PM61_HUMAN;tr|D6R9K7|D6R9K7_HUMAN;tr|U3KQD5|U3KQD5_HUMAN;tr|J3QRR5|J3QRR5_HUMAN	1,030	0,946
tr|A0A024QZB7|A0A024QZB7_HUMAN;sp|Q8WWM7|ATX2L_HUMAN;tr|A0A024QZC0|A0A024QZC0_HUMAN;tr|A0A024QZ91|A0A024QZ91_HUMAN;tr|H3BUF6|H3BUF6_HUMAN	1,015	0,970
tr|B7Z4V2|B7Z4V2_HUMAN;tr|V9HW84|V9HW84_HUMAN;sp|P38646|GRP75_HUMAN;tr|Q8N1C8|Q8N1C8_HUMAN;tr|B7Z1V7|B7Z1V7_HUMAN;tr|B7Z4T3|B7Z4T3_HUMAN	0,967	0,932
tr|Q53HR2|Q53HR2_HUMAN;sp|P49748|ACADV_HUMAN;tr|B4DEA8|B4DEA8_HUMAN;tr|B3KPA6|B3KPA6_HUMAN	0,981	0,962
tr|A0A024R1N1|A0A024R1N1_HUMAN;sp|P35579|MYH9_HUMAN;tr|Q86XU5|Q86XU5_HUMAN	1,048	0,896
tr|Q5TZZ9|Q5TZZ9_HUMAN;sp|P04083|ANXA1_HUMAN;tr|B5BU38|B5BU38_HUMAN;tr|B4DL19|B4DL19_HUMAN	1,048	0,894
sp|Q9UQ35|SRRM2_HUMAN;tr|O60382|O60382_HUMAN	0,864	0,812
tr|B4E1G2|B4E1G2_HUMAN;tr|A0A024RB99|A0A024RB99_HUMAN;tr|V9HW06|V9HW06_HUMAN;tr|Q53ET4|Q53ET4_HUMAN;sp|P34897|GLYM_HUMAN;tr|B4DW25|B4DW25_HUMAN;tr|Q5HYG8|Q5HYG8_HUMAN;tr|B4DJQ3|B4DJQ3_HUMAN;tr|B4DJ63|B4DJ63_HUMAN;tr|B4DLV4|B4DLV4_HUMAN;tr|B4DP88|B4DP88_HUMAN;tr|Q5BJF5|Q5BJF5_HUMAN;tr|B4DWA7|B4DWA7_HUMAN;tr|H0YIZ0|H0YIZ0_HUMAN;tr|G3V2Y4|G3V2Y4_HUMAN	1,030	0,945

sp|Q12797|ASPH_HUMAN	1,049	0,894
tr|A0A024R2M7|A0A024R2M7_HUMAN;sp|O95747|OXSR1_HUMAN;tr|C9JIG9|C9JIG9_HUMAN	0,936	0,867
tr|Q32Q12|Q32Q12_HUMAN;tr|Q6FHN3|Q6FHN3_HUMAN;sp|P22392|NDKB_HUMAN;tr|J3KPD9|J3KPD9_HUMAN;tr|E7ERL0|E7ERL0_HUMAN	1,068	0,866
sp|Q14019|COTL1_HUMAN;tr|H3BT58|H3BT58_HUMAN	1,065	0,875
tr|V9HWI1|V9HWI1_HUMAN;sp|P30043|BLVRB_HUMAN;tr|M0QZL1|M0QZL1_HUMAN;tr|M0R192|M0R192_HUMAN	1,046	0,897
tr|R4SBI6|R4SBI6_HUMAN;sp|P07099|HYEP_HUMAN;tr|Q6FGZ3|Q6FGZ3_HUMAN	0,911	0,840
sp|Q9H2G2|SLK_HUMAN;tr|B4DZC9|B4DZC9_HUMAN	0,914	0,841
tr|Q6IAT1|Q6IAT1_HUMAN;sp|P50395|GDIB_HUMAN;tr|B4DLV7|B4DLV7_HUMAN;tr|Q5SX87|Q5SX87_HUMAN	1,050	0,892
tr|B4DDF4|B4DDF4_HUMAN;tr|Q6FHE4|Q6FHE4_HUMAN;tr|Q53GK7|Q53GK7_HUMAN;sp|Q99439|CNN2_HUMAN;tr|B4DUT8|B4DUT8_HUMAN;tr|A0A087X271|A0A087X271_HUMAN;tr|B4DHU5|B4DHU5_HUMAN;tr|Q6FHC3|Q6FHC3_HUMAN;tr|K7ES69|K7ES69_HUMAN;tr|A0A087X1X5|A0A087X1X5_HUMAN;tr|B4DN57|B4DN57_HUMAN	0,955	0,896
sp|Q99880|H2B1L_HUMAN;tr|B2R4S9|B2R4S9_HUMAN;tr|A8K9J7|A8K9J7_HUMAN;tr|A0A024RCL8|A0A024RCL8_HUMAN;tr|A0A024RCJ9|A0A024RCJ9_HUMAN;tr|A0A024QZZ7|A0A024QZZ7_HUMAN;sp|Q99879|H2B1M_HUMAN;sp|Q99877|H2B1N_HUMAN;sp|Q93079|H2B1H_HUMAN;sp|Q5QNW6|H2B2F_HUMAN;sp|P62807|H2B1C_HUMAN;sp|P58876|H2B1D_HUMAN;sp|O60814|H2B1K_HUMAN;tr|I6L9F7|I6L9F7_HUMAN;tr|U3KQK0|U3KQK0_HUMAN;tr|B4DR52|B4DR52_HUMAN;tr|Q0D2M2|Q0D2M2_HUMAN;sp|P57053|H2BFS_HUMAN;sp|Q96A08|H2B1A_HUMAN	0,970	0,943

tr|Q59ET3|Q59ET3_HUMAN;tr|B2R9K8|B2R9K8_HUMAN;tr|A0A024RDL1|A0A024RDL1_HUMAN;sp|P40227|TCPZ_HUMAN;tr|A1JUI8|A1JUI8_HUMAN;tr|B4DPJ8|B4DPJ8_HUMAN;tr|B4DN39|B4DN39_HUMAN	0,980	0,958
tr|V9HWG7|V9HWG7_HUMAN;tr|Q53H17|Q53H17_HUMAN;tr|Q53GN4|Q53GN4_HUMAN;sp|O75083|WDR1_HUMAN;tr|Q59ER5|Q59ER5_HUMAN;tr|D6RD66|D6RD66_HUMAN;tr|B3KXN4|B3KXN4_HUMAN	1,027	0,945
tr|B4DJV2|B4DJV2_HUMAN;tr|A0A024RB75|A0A024RB75_HUMAN;sp|O75390|CISY_HUMAN;tr|A0A0C4DGI3|A0A0C4DGI3_HUMAN;tr|B3KTN4|B3KTN4_HUMAN	0,973	0,944
sp|P55327|TPD52_HUMAN;tr|F5H0B0|F5H0B0_HUMAN;tr|H0YC42|H0YC42_HUMAN;tr|A5Y5A3|A5Y5A3_HUMAN	0,970	0,944
sp|Q9UPN3|MACF1_HUMAN;tr|H3BPE1|H3BPE1_HUMAN;tr|H3BQK9|H3BQK9_HUMAN;tr|H0Y390|H0Y390_HUMAN	0,954	0,897
tr|Q53SY7|Q53SY7_HUMAN;tr|F8VPD4|F8VPD4_HUMAN;sp|P27708|PYR1_HUMAN	0,961	0,907
sp|P18124|RL7_HUMAN;tr|A0A024R814|A0A024R814_HUMAN;tr|A8MUD9|A8MUD9_HUMAN	1,030	0,947
tr|Q3B7A7|Q3B7A7_HUMAN;sp|P22102|PUR2_HUMAN;tr|Q59HH3|Q59HH3_HUMAN;tr|Q15374|Q15374_HUMAN	1,024	0,954
tr|A0A024R9C1|A0A024R9C1_HUMAN;sp|P11940|PABP1_HUMAN;tr|A0A087WTT1|A0A087WTT1_HUMAN;tr|E7EQV3|E7EQV3_HUMAN;tr|B4DZW4|B4DZW4_HUMAN;tr|E7ERJ7|E7ERJ7_HUMAN;tr|B4DQX0|B4DQX0_HUMAN;tr|B3KT93|B3KT93_HUMAN;tr|A0A024R9E2|A0A024R9E2_HUMAN;tr|H0YAR2|H0YAR2_HUMAN	0,979	0,958
tr|Q7Z726|Q7Z726_HUMAN;tr|Q6NVW7|Q6NVW7_HUMAN;tr|A8K7D9|A8K7D9_HUMAN;sp|P52292|IMA1_HUMAN;tr|J3QLL0|J3QLL0_HUMAN;tr|J3KS65|J3KS65_HUMAN	0,919	0,854
sp|Q96IZ0|PAWR_HUMAN	1,053	0,897

tr|E9PL69|E9PL69_HUMAN;tr|B4DXB0|B4DXB0_HUMAN;tr|B4DS95|B4DS95_HUMAN;tr|B4E0I8|B4E0I8_HUMAN;tr|B4DNN4|B4DNN4_HUMAN;tr|Q53GZ5|Q53GZ5_HUMAN;sp|P23921|RIR1_HUMAN;tr|B4DXD1|B4DXD1_HUMAN	1,045	0,894
sp|Q93008|USP9X_HUMAN;tr|D3DWB6|D3DWB6_HUMAN;sp|O00507|USP9Y_HUMAN	1,023	0,955
tr|V9HW72|V9HW72_HUMAN;tr|A8K690|A8K690_HUMAN;sp|P31948|STIP1_HUMAN	1,015	0,969
sp|Q9NZI8|IF2B1_HUMAN;tr|D3DTW3|D3DTW3_HUMAN	1,017	0,966
sp|O75643|U520_HUMAN;tr|A4FU77|A4FU77_HUMAN;tr|Q9H8B9|Q9H8B9_HUMAN	0,974	0,942
tr|B7ZAY2|B7ZAY2_HUMAN;tr|A0A024RB87|A0A024RB87_HUMAN;sp|P61224|RAP1B_HUMAN;tr|F5H823|F5H823_HUMAN;tr|B7ZB78|B7ZB78_HUMAN;tr|F5GZG1|F5GZG1_HUMAN;sp|A6NIZ1|RP1BL_HUMAN;tr|Q5U0C3|Q5U0C3_HUMAN;tr|A8KAH9|A8KAH9_HUMAN;sp|P62834|RAP1A_HUMAN;tr|E7ESV4|E7ESV4_HUMAN;tr|F5H7Y6|F5H7Y6_HUMAN;tr|F5GX62|F5GX62_HUMAN	0,986	0,969
tr|B2R959|B2R959_HUMAN;tr|Q6NTA2|Q6NTA2_HUMAN;sp|P14866|HNRPL_HUMAN;tr|M0QXS5|M0QXS5_HUMAN	1,011	0,978
tr|B4DZ08|B4DZ08_HUMAN;tr|B2RBW5|B2RBW5_HUMAN;sp|Q99798|ACON_HUMAN;tr|A2A274|A2A274_HUMAN;tr|B4DW08|B4DW08_HUMAN;tr|B4DEC3|B4DEC3_HUMAN;tr|B4DLY4|B4DLY4_HUMAN;tr|B4DJW1|B4DJW1_HUMAN;tr|Q71UF1|Q71UF1_HUMAN;tr|O75944|O75944_HUMAN	1,015	0,968
sp|P55084|ECHB_HUMAN;tr|F5GZQ3|F5GZQ3_HUMAN;tr|B4DY96|B4DY96_HUMAN;tr|B5MD38|B5MD38_HUMAN;tr|B4DDC9|B4DDC9_HUMAN;tr|D6W539|D6W539_HUMAN	0,978	0,953
tr|Q6AI18|Q6AI18_HUMAN;tr|E9PP21|E9PP21_HUMAN;tr|Q9BTA4|Q9BTA4_HUMAN;tr|B4DY28|B4DY28_HUMAN;tr|Q6ZMS3|Q6ZMS3_HUMAN;sp|P21291|CSRP1_HUMAN;tr|E9PND2|E9PND2_HUMAN;tr|B4E2T4|B4E2T4_HUMAN;tr|E9PS42|E9PS42_HUMAN;tr|Q59EQ5|Q59EQ5_HUMAN;tr|B3KVC9|B3KVC9_HUMAN	0,960	0,906

tr|B4DUQ1|B4DUQ1_HUMAN;tr|A0A024R228|A0A024R228_HUMAN;sp|P61978|HNRPK_HUMAN;tr|Q6IBN1|Q6IBN1_HUMAN;tr|Q5EC54|Q5EC54_HUMAN;tr|B4DFF1|B4DFF1_HUMAN;tr|Q5T6W2|Q5T6W2_HUMAN	0,994	0,974
sp|P37802|TAGL2_HUMAN;tr|X6RJP6|X6RJP6_HUMAN	1,037	0,924
tr|A8K5I0|A8K5I0_HUMAN;sp|P0DMV9|HS71B_HUMAN;sp|P0DMV8|HS71A_HUMAN;tr|B4DNT8|B4DNT8_HUMAN;tr|B4DI39|B4DI39_HUMAN;tr|B4DWK5|B4DWK5_HUMAN;tr|Q59EJ3|Q59EJ3_HUMAN;tr|B4DFN9|B4DFN9_HUMAN;tr|B4E1S9|B4E1S9_HUMAN;tr|B4DVU9|B4DVU9_HUMAN;tr|B4E388|B4E388_HUMAN;tr|V9GZ37|V9GZ37_HUMAN;tr|B3KTT5|B3KTT5_HUMAN;tr|B4DNX1|B4DNX1_HUMAN;tr|B4E1T6|B4E1T6_HUMAN	1,016	0,969
tr|Q8NCF7|Q8NCF7_HUMAN;tr|B2RE88|B2RE88_HUMAN;tr|A0A024RBE8|A0A024RBE8_HUMAN;tr|A0A024RBH9|A0A024RBH9_HUMAN;sp|Q00325|MPCP_HUMAN;tr|F8VVM2|F8VVM2_HUMAN;tr|Q53HC3|Q53HC3_HUMAN	1,017	0,965
tr|B2RDX5|B2RDX5_HUMAN;tr|Q53GX7|Q53GX7_HUMAN;sp|P26639|SYTC_HUMAN;tr|B4DKZ9|B4DKZ9_HUMAN;tr|Q5M7Z9|Q5M7Z9_HUMAN;tr|B3KTN2|B3KTN2_HUMAN	1,012	0,977
sp|P05556|ITB1_HUMAN	1,033	0,946
sp|Q13011|ECH1_HUMAN;tr|M0R248|M0R248_HUMAN	1,015	0,971
tr|J3KP15|J3KP15_HUMAN;tr|Q53FN0|Q53FN0_HUMAN;tr|A0A024R8U5|A0A024R8U5_HUMAN;sp|Q01130|SRSF2_HUMAN;tr|B3KX15|B3KX15_HUMAN;tr|J3QL05|J3QL05_HUMAN;tr|Q6NXQ0|Q6NXQ0_HUMAN;tr|Q8N220|Q8N220_HUMAN;tr|B3KVY2|B3KVY2_HUMAN;tr|B3KUF7|B3KUF7_HUMAN;tr|Q8NAK9|Q8NAK9_HUMAN;tr|B3KUY1|B3KUY1_HUMAN;tr|A0A024R3A8|A0A024R3A8_HUMAN;sp|Q9BRL6|SRSF8_HUMAN	0,988	0,978
sp|P36871|PGM1_HUMAN;tr|B4DFP1|B4DFP1_HUMAN;tr|B7Z6C2|B7Z6C2_HUMAN;tr|B4DDQ8|B4DDQ8_HUMAN	0,992	0,975

tr|B4DNE4|B4DNE4_HUMAN;tr|G3V1Q4|G3V1Q4_HUMAN;tr|B4DPQ6|B4DPQ6_HUMAN;tr|A0A023T695|A0A023T695_HUMAN;tr|B4DUD6|B4DUD6_HUMAN;tr|Q8TC62|Q8TC62_HUMAN;tr|E7ES33|E7ES33_HUMAN;tr|Q3LIE9|Q3LIE9_HUMAN;tr|A4GYY8|A4GYY8_HUMAN;tr|A8K3D0|A8K3D0_HUMAN;tr|E7EPK1|E7EPK1_HUMAN;sp|Q16181|SEPT7_HUMAN;tr|H0Y3Y4|H0Y3Y4_HUMAN;tr|Q59EY4|Q59EY4_HUMAN	0,917	0,861
tr|B3KN59|B3KN59_HUMAN;tr|B3KM36|B3KM36_HUMAN;sp|O95816|BAG2_HUMAN	0,935	0,874
tr|E9PDF6|E9PDF6_HUMAN;tr|B0I1S9|B0I1S9_HUMAN;sp|O43795|MYO1B_HUMAN;tr|E7EQD9|E7EQD9_HUMAN;tr|Q05CR5|Q05CR5_HUMAN	1,028	0,945
tr|E9KL35|E9KL35_HUMAN;sp|P63244|GBLP_HUMAN;tr|J3KPE3|J3KPE3_HUMAN;tr|D6RHH4|D6RHH4_HUMAN;tr|D6RAC2|D6RAC2_HUMAN;tr|H0YAF8|H0YAF8_HUMAN;tr|D6R9Z1|D6R9Z1_HUMAN;tr|H0Y8W2|H0Y8W2_HUMAN;tr|D6R9L0|D6R9L0_HUMAN;tr|D6REE5|D6REE5_HUMAN;tr|D6RAU2|D6RAU2_HUMAN;tr|E9PD14|E9PD14_HUMAN;tr|D6RFX4|D6RFX4_HUMAN;tr|D6RFZ9|D6RFZ9_HUMAN;tr|B4DVD2|B4DVD2_HUMAN;tr|H0YAM7|H0YAM7_HUMAN;tr|B4E0C3|B4E0C3_HUMAN;tr|D6RBD0|D6RBD0_HUMAN	0,976	0,952
tr|Q8TB01|Q8TB01_HUMAN;tr|Q6NWZ1|Q6NWZ1_HUMAN;tr|A0A024RBH2|A0A024RBH2_HUMAN;sp|Q07065|CKAP4_HUMAN;tr|B3KVX6|B3KVX6_HUMAN	1,017	0,966
tr|E9PLK3|E9PLK3_HUMAN;tr|B7Z899|B7Z899_HUMAN;sp|P55786|PSA_HUMAN;tr|B7Z4B2|B7Z4B2_HUMAN;tr|B3KU93|B3KU93_HUMAN;tr|B3KTP2|B3KTP2_HUMAN;tr|B7Z1V9|B7Z1V9_HUMAN;tr|B7Z1H4|B7Z1H4_HUMAN	1,023	0,953
sp|O76021|RL1D1_HUMAN;tr|J3QSV6|J3QSV6_HUMAN;tr|A0PJ61|A0PJ61_HUMAN;tr|Q32Q62|Q32Q62_HUMAN	0,970	0,947
tr|B4DU58|B4DU58_HUMAN;tr|V9HW69|V9HW69_HUMAN;tr|B2R9S4|B2R9S4_HUMAN;sp|P40121|CAPG_HUMAN;tr|E7ENU9|E7ENU9_HUMAN;tr|B8ZZL6|B8ZZL6_HUMAN	1,168	0,831

tr|A8K7F6|A8K7F6_HUMAN;sp|P60842|IF4A1_HUMAN;tr|A8K088|A8K088_HUMAN;tr|B4DNH2|B4DNH2_HUMAN;tr|J3KTB5|J3KTB5_HUMAN;tr|J3KT12|J3KT12_HUMAN;tr|Q59F68|Q59F68_HUMAN;tr|J3QS69|J3QS69_HUMAN;tr|J3QL43|J3QL43_HUMAN	1,029	0,946
tr|U3KQE2|U3KQE2_HUMAN;tr|K7EIV0|K7EIV0_HUMAN;tr|A0A075B7C0|A0A075B7C0_HUMAN;sp|P04632|CPNS1_HUMAN;tr|A0A0C4DGQ5|A0A0C4DGQ5_HUMAN;tr|U3KPR7|U3KPR7_HUMAN;tr|K7EM73|K7EM73_HUMAN;tr|K7EKD8|K7EKD8_HUMAN;tr|K7ELJ7|K7ELJ7_HUMAN	0,920	0,862
tr|E7EUY5|E7EUY5_HUMAN;tr|Q567R6|Q567R6_HUMAN;tr|A4D1U3|A4D1U3_HUMAN;sp|Q04837|SSBP_HUMAN;tr|B7Z268|B7Z268_HUMAN;tr|C9K0U8|C9K0U8_HUMAN	0,973	0,944
tr|V9HWI3|V9HWI3_HUMAN;sp|P07339|CATD_HUMAN;tr|C9JH19|C9JH19_HUMAN;tr|F8WD96|F8WD96_HUMAN	0,979	0,958
tr|A0A024R6D4|A0A024R6D4_HUMAN;sp|P84090|ERH_HUMAN	1,128	0,847
sp|Q9BYG3|MK67I_HUMAN;tr|B4DSM4|B4DSM4_HUMAN	0,977	0,954
sp|Q14204|DYHC1_HUMAN	0,989	0,978
tr|J3KPX7|J3KPX7_HUMAN;sp|Q99623|PHB2_HUMAN;tr|F5GY37|F5GY37_HUMAN;tr|F5GWA7|F5GWA7_HUMAN;tr|B4DW05|B4DW05_HUMAN	0,991	0,979
tr|Q8WVC2|Q8WVC2_HUMAN;tr|Q6FGH5|Q6FGH5_HUMAN;sp|P63220|RS21_HUMAN;tr|Q9BYK1|Q9BYK1_HUMAN	1,021	0,958
tr|H0YA96|H0YA96_HUMAN;tr|H0Y8G5|H0Y8G5_HUMAN;tr|Q12771|Q12771_HUMAN;tr|B4DTC3|B4DTC3_HUMAN;tr|A0A024RDF4|A0A024RDF4_HUMAN;tr|A0A024RDB4|A0A024RDB4_HUMAN;tr|A0A024RDF3|A0A024RDF3_HUMAN;sp|Q14103|HNRPD_HUMAN;tr|D6RF44|D6RF44_HUMAN;tr|D6RAF8|D6RAF8_HUMAN;tr|D6RBQ9|D6RBQ9_HUMAN	0,950	0,897
sp|P35658|NU214_HUMAN;tr|A0A024R8B6|A0A024R8B6_HUMAN;tr|Q7Z3C4|Q7Z3C4_HUMAN;tr|A0A0A0MSW3|A0A0A0MSW3_HUMAN	1,021	0,959

sp|P43243|MATR3_HUMAN;tr|A8MXP9|A8MXP9_HUMAN;tr|D6REM6|D6REM6_HUMAN;tr|Q68D11|Q68D11_HUMAN;tr|D6R991|D6R991_HUMAN	0,993	0,973
sp|Q9Y266|NUDC_HUMAN;tr|Q9H2R7|Q9H2R7_HUMAN	1,015	0,970
tr|A0A087WWU8|A0A087WWU8_HUMAN;tr|B2RDE1|B2RDE1_HUMAN;tr|Q5HYB6|Q5HYB6_HUMAN;tr|Q5VU61|Q5VU61_HUMAN;tr|Q8NAG3|Q8NAG3_HUMAN;tr|B4DWT5|B4DWT5_HUMAN;tr|B4DQ80|B4DQ80_HUMAN	1,008	0,974
tr|X1WI28|X1WI28_HUMAN;tr|X5D2T3|X5D2T3_HUMAN;sp|Q96L21|RL10L_HUMAN;sp|P27635|RL10_HUMAN;tr|H7C123|H7C123_HUMAN;tr|H7C2C5|H7C2C5_HUMAN;tr|F8W7C6|F8W7C6_HUMAN;tr|A0A087WV22|A0A087WV22_HUMAN;tr|B8A6G2|B8A6G2_HUMAN;tr|X5D2W5|X5D2W5_HUMAN;tr|A6QRI9|A6QRI9_HUMAN	1,011	0,979
sp|P16403|H12_HUMAN	0,988	0,978
sp|Q13428|TCOF_HUMAN;tr|J3KQ96|J3KQ96_HUMAN;tr|E7ETY2|E7ETY2_HUMAN;tr|Q59FZ2|Q59FZ2_HUMAN;tr|B4DRA2|B4DRA2_HUMAN	1,007	0,974
tr|B4E0X8|B4E0X8_HUMAN;tr|B4DWL1|B4DWL1_HUMAN;sp|Q96AE4|FUBP1_HUMAN;tr|E9PEB5|E9PEB5_HUMAN;tr|B4DT31|B4DT31_HUMAN;tr|Q59FU3|Q59FU3_HUMAN	1,004	0,987
tr|B4DJB4|B4DJB4_HUMAN;tr|H0YL72|H0YL72_HUMAN;tr|B4DSY4|B4DSY4_HUMAN;sp|P50213|IDH3A_HUMAN;tr|H0YLI6|H0YLI6_HUMAN;tr|Q53GF8|Q53GF8_HUMAN;tr|H0YKD0|H0YKD0_HUMAN;tr|H0YMU3|H0YMU3_HUMAN;tr|B7Z9J8|B7Z9J8_HUMAN	0,991	0,978
tr|V9HWK0|V9HWK0_HUMAN;sp|O76094|SRP72_HUMAN;tr|Q86X80|Q86X80_HUMAN;tr|A0PJJ5|A0PJJ5_HUMAN;tr|Q0D2M6|Q0D2M6_HUMAN;tr|Q71V07|Q71V07_HUMAN;tr|R4GNC1|R4GNC1_HUMAN	1,007	0,975
tr|V9HWJ2|V9HWJ2_HUMAN;tr|V9HW78|V9HW78_HUMAN;tr|Q6FIA4|Q6FIA4_HUMAN;tr|B2R5M8|B2R5M8_HUMAN;sp|O75874|IDHC_HUMAN;tr|Q0QER2|Q0QER2_HUMAN;tr|Q6FI37|Q6FI37_HUMAN;tr|C9J4N6|C9J4N6_HUMAN	0,972	0,942

sp|Q9BRP8|WIBG_HUMAN	1,009	0,975
tr|A8K5W7|A8K5W7_HUMAN;sp|Q9NSE4|SYIM_HUMAN	1,012	0,978
tr|A0A0A0MSM0|A0A0A0MSM0_HUMAN;tr|A0A024RDQ0|A0A024RDQ0_HUMAN;tr|A0A024RDS1|A0A024RDS1_HUMAN;sp|Q92598|HS105_HUMAN;tr|B4DY72|B4DY72_HUMAN;tr|B4DF68|B4DF68_HUMAN;tr|B4DZB4|B4DZB4_HUMAN	0,991	0,978
tr|B4DPS6|B4DPS6_HUMAN;tr|B4DUC5|B4DUC5_HUMAN;tr|B4DM31|B4DM31_HUMAN;sp|P55060|XPO2_HUMAN;tr|B4DM67|B4DM67_HUMAN	1,144	0,844
tr|V9HW98|V9HW98_HUMAN;sp|P62258|1433E_HUMAN;tr|G9K389|G9K389_HUMAN;tr|G9K388|G9K388_HUMAN	0,993	0,974
tr|H7BYY1|H7BYY1_HUMAN;tr|Q1ZYL5|Q1ZYL5_HUMAN;tr|F5H7S3|F5H7S3_HUMAN;tr|B7Z596|B7Z596_HUMAN;tr|B7Z722|B7Z722_HUMAN;tr|D9YZV7|D9YZV7_HUMAN;tr|H0YK48|H0YK48_HUMAN;tr|A0A024R5W6|A0A024R5W6_HUMAN;tr|Q59GR8|Q59GR8_HUMAN	0,981	0,962
tr|A0A024R1N4|A0A024R1N4_HUMAN;sp|P12956|XRCC6_HUMAN;tr|B1AHC9|B1AHC9_HUMAN;tr|B2RDN9|B2RDN9_HUMAN;tr|B4DE32|B4DE32_HUMAN;tr|B4E356|B4E356_HUMAN	0,993	0,974
tr|A0A087WTP3|A0A087WTP3_HUMAN;sp|Q92945|FUBP2_HUMAN;tr|B4DV73|B4DV73_HUMAN;tr|M0R0I5|M0R0I5_HUMAN	0,980	0,961
tr|V9HW29|V9HW29_HUMAN;sp|P33176|KINH_HUMAN;tr|A8K048|A8K048_HUMAN;tr|D3DRX6|D3DRX6_HUMAN;tr|M1VRN1|M1VRN1_HUMAN;tr|M1VKJ2|M1VKJ2_HUMAN;tr|M1VE91|M1VE91_HUMAN;tr|C1PHA2|C1PHA2_HUMAN;tr|M1V490|M1V490_HUMAN;tr|M1VPF9|M1VPF9_HUMAN;tr|B4DS27|B4DS27_HUMAN;tr|M1V481|M1V481_HUMAN	0,992	0,973
tr|B3KU41|B3KU41_HUMAN;tr|D3DN77|D3DN77_HUMAN;tr|C9IZ80|C9IZ80_HUMAN;tr|A0A024R3Z6|A0A024R3Z6_HUMAN;sp|Q7L1Q6|BZW1_HUMAN;tr|Q53FN7|Q53FN7_HUMAN	0,975	0,954

tr|B7ZAR1|B7ZAR1_HUMAN;tr|B4DDU6|B4DDU6_HUMAN;tr|B4DZT5|B4DZT5_HUMAN;tr|B4DXI1|B4DXI1_HUMAN;tr|E9PCA1|E9PCA1_HUMAN;tr|Q9BU08|Q9BU08_HUMAN;tr|V9HW37|V9HW37_HUMAN;sp|P48643|TCPE_HUMAN;tr|E7ENZ3|E7ENZ3_HUMAN;tr|B4DYC8|B4DYC8_HUMAN;tr|B4DX08|B4DX08_HUMAN;tr|B4DE30|B4DE30_HUMAN;tr|Q96GI1|Q96GI1_HUMAN;tr|B4DZY9|B4DZY9_HUMAN	0,990	0,979
sp|P13073|COX41_HUMAN;tr|H3BPG0|H3BPG0_HUMAN;tr|H3BN72|H3BN72_HUMAN;tr|H3BNV9|H3BNV9_HUMAN;tr|Q86WV2|Q86WV2_HUMAN	0,991	0,977
tr|B2R9U2|B2R9U2_HUMAN;sp|Q02790|FKBP4_HUMAN	1,016	0,969
tr|B4E0N9|B4E0N9_HUMAN;tr|B4DMG8|B4DMG8_HUMAN;tr|B4DMF5|B4DMF5_HUMAN;tr|B3KT18|B3KT18_HUMAN;tr|Q53GW3|Q53GW3_HUMAN;tr|E9KL48|E9KL48_HUMAN;sp|P49448|DHE4_HUMAN;sp|P00367|DHE3_HUMAN;tr|Q9BSD0|Q9BSD0_HUMAN	1,043	0,930
tr|Q7Z518|Q7Z518_HUMAN;tr|A8K413|A8K413_HUMAN;tr|A0A087WXC5|A0A087WXC5_HUMAN;tr|A0A024R4B3|A0A024R4B3_HUMAN;sp|O95299|NDUAA_HUMAN;tr|E7ESZ7|E7ESZ7_HUMAN;tr|Q8N1B9|Q8N1B9_HUMAN;tr|Q59FM0|Q59FM0_HUMAN;tr|C9J6X0|C9J6X0_HUMAN;tr|Q53SW4|Q53SW4_HUMAN	1,014	0,973
sp|P31947|1433S_HUMAN	0,981	0,966
tr|V9HWN7|V9HWN7_HUMAN;sp|P04075|ALDOA_HUMAN;tr|J3KPS3|J3KPS3_HUMAN;tr|H3BQN4|H3BQN4_HUMAN;tr|H3BPS8|H3BPS8_HUMAN;tr|H3BUH7|H3BUH7_HUMAN;tr|H3BR04|H3BR04_HUMAN	1,010	0,977
tr|A8K168|A8K168_HUMAN;sp|P48163|MAOX_HUMAN;tr|Q8WVX2|Q8WVX2_HUMAN;tr|B4DX99|B4DX99_HUMAN	0,994	0,979
tr|A0A024R222|A0A024R222_HUMAN;sp|Q9Y617|SERC_HUMAN;tr|B4DHQ3|B4DHQ3_HUMAN;tr|A0A024R280|A0A024R280_HUMAN;tr|B4DHX7|B4DHX7_HUMAN	1,008	0,973
sp|P07305|H10_HUMAN	1,013	0,977

tr|E9PL09|E9PL09_HUMAN;tr|Q53G83|Q53G83_HUMAN;sp|P23396|RS3_HUMAN;tr|E9PPU1|E9PPU1_HUMAN;tr|H0YEU2|H0YEU2_HUMAN;tr|E9PQ96|E9PQ96_HUMAN;tr|E9PJH4|E9PJH4_HUMAN;tr|F2Z2S8|F2Z2S8_HUMAN;tr|E9PK82|E9PK82_HUMAN;tr|H0YCJ7|H0YCJ7_HUMAN;tr|Q9NQS8|Q9NQS8_HUMAN	0,996	0,990
tr|Q59GB4|Q59GB4_HUMAN;sp|Q16555|DPYL2_HUMAN;tr|Q53ET2|Q53ET2_HUMAN;tr|Q8NAN9|Q8NAN9_HUMAN	0,990	0,980
tr|B4E0H8|B4E0H8_HUMAN;sp|P26006|ITA3_HUMAN;tr|Q59F03|Q59F03_HUMAN	1,010	0,980
tr|Q53FB6|Q53FB6_HUMAN;sp|P05091|ALDH2_HUMAN;tr|B4YAH7|B4YAH7_HUMAN	1,021	0,964
tr|B8ZZQ6|B8ZZQ6_HUMAN;tr|V9HVW6|V9HVW6_HUMAN;tr|Q15202|Q15202_HUMAN;tr|Q8TBK9|Q8TBK9_HUMAN;tr|Q86YS2|Q86YS2_HUMAN;tr|Q53S24|Q53S24_HUMAN;tr|Q15204|Q15204_HUMAN;sp|P06454|PTMA_HUMAN;tr|Q15200|Q15200_HUMAN;tr|B8ZZA1|B8ZZA1_HUMAN;tr|B8ZZW7|B8ZZW7_HUMAN;tr|H7C2N1|H7C2N1_HUMAN;tr|Q15203|Q15203_HUMAN;tr|Q7KZ52|Q7KZ52_HUMAN;tr|A0A087WUT1|A0A087WUT1_HUMAN;tr|Q7Z4R6|Q7Z4R6_HUMAN	1,014	0,976
sp|P07737|PROF1_HUMAN;tr|K7EJ44|K7EJ44_HUMAN	0,997	0,991
tr|A0A024R7A8|A0A024R7A8_HUMAN;sp|P15121|ALDR_HUMAN;tr|E9PEF9|E9PEF9_HUMAN;tr|Q59EL5|Q59EL5_HUMAN;tr|E9PCX2|E9PCX2_HUMAN	1,010	0,976
sp|Q9UHB9|SRP68_HUMAN;tr|B3KMI9|B3KMI9_HUMAN;tr|B4DVI7|B4DVI7_HUMAN	0,998	0,997
tr|I3L1P8|I3L1P8_HUMAN;tr|Q6IBH0|Q6IBH0_HUMAN;sp|Q02978|M2OM_HUMAN	0,987	0,978
sp|P09496|CLCA_HUMAN;tr|F8WF69|F8WF69_HUMAN	1,002	0,997
sp|Q6P2Q9|PRP8_HUMAN;tr|B4DK16|B4DK16_HUMAN	0,996	0,992
tr|A0A087X0K9|A0A087X0K9_HUMAN;tr|Q6MZU1|Q6MZU1_HUMAN;tr|G5E9E7|G5E9E7_HUMAN;sp|Q07157|ZO1_HUMAN;tr|A9CQZ8|A9CQZ8_HUMAN;tr|G3V1L9|G3V1L9_HUMAN;tr|Q68DX9|Q68DX9_HUMAN	1,001	0,996

tr|V9HWC6|V9HWC6_HUMAN;sp|P23284|PPIB_HUMAN	1,001	0,999
tr|I4AY87|I4AY87_HUMAN;sp|P14174|MIF_HUMAN	0,998	0,999
sp|P16104|H2AX_HUMAN	0,997	0,992
tr|A0A024R6B5|A0A024R6B5_HUMAN;sp|P54652|HSP72_HUMAN;tr|B3KUS2|B3KUS2_HUMAN	1,001	0,998
tr|Q53FF5|Q53FF5_HUMAN;tr|Q53FE8|Q53FE8_HUMAN;sp|Q9UNZ2|NSF1C_HUMAN;tr|F2Z2K0|F2Z2K0_HUMAN	1,000	0,998
tr|A0A024R1Y2|A0A024R1Y2_HUMAN;tr|A0A024R1T9|A0A024R1T9_HUMAN;sp|P53396|ACLY_HUMAN;tr|Q4LE36|Q4LE36_HUMAN;tr|Q8N9C4|Q8N9C4_HUMAN	1,000	0,999

Appendix 4. Gene onthology (GO) anaylsis of the protemics data

GOBPID	Exp Count	Count	Term Size	Term	p-value (adj)	Gene Symbols
GO:0006402	15	37	186	mRNA catabolic process	5,91E-05	EIF4B; EIF3E; TNPO1; PPP2CA; PSMA1; PSMA4; PSMB2; PSMB4; PSMB5; PSMC1; PSMC5; PSMD1; PSME1; RPL6; RPL9; RPL11; RPL18; RPL19; RPL22; RPL23A; RPL27; RPL27A; RPL28; RPL29; RPL31; RPS2; RPS10; RPS11; RPS12; RPS14; SET; UBA52; YWHAB; CSDE1; ANP32A; TNKS1BP1; RPL14

GO:0034655	17	39	215	nucleobase-containing compound catabolic process	1,35E-04	AHCY; EIF4B; XRN2; EIF3E; TNPO1; PPP2CA; PSMA1; PSMA4; PSMB2; PSMB4; PSMB5; PSMC1; PSMC5; PSMD1; PSME1; RPL6; RPL9; RPL11; RPL18; RPL19; RPL22; RPL23A; RPL27; RPL27A; RPL28; RPL29; RPL31; RPS2; RPS10; RPS11; RPS12; RPS14; SET; UBA52; YWHAB; CSDE1; ANP32A; TNKS1BP1; RPL14
GO:0006413	9	27	119	translational initiation	1,35E-04	DDX3X; EIF4B; EIF3E; EIF6; RPL6; RPL9; RPL11; RPL18; RPL19; RPL22; RPL23A; RPL27; RPL27A; RPL28; RPL29; RPL31; RPS2; RPS10; RPS11; RPS12; RPS14; EIF3CL; UBA52; EIF4H; EIF3G; EIF3H; RPL14
GO:0006614	6	20	78	SRP-dependent co-translational protein targeting to membrane	5,12E-04	RPL6; RPL9; RPL11; RPL18; RPL19; RPL22; RPL23A; RPL27; RPL27A; RPL28; RPL29; RPL31; RPS2; RPS10; RPS11; RPS12; RPS14; SRP14; UBA52; RPL14
GO:0072599	7	21	85	Establishing of protein localization to endoplasmic reticulum	5,12E-04	RAB10; RPL6; RPL9; RPL11; RPL18; RPL19; RPL22; RPL23A; RPL27; RPL27A; RPL28; RPL29; RPL31; RPS2; RPS10; RPS11; RPS12; RPS14; SRP14; UBA52; RPL14
GO:0000184	7	21	88	nuclear-transcribed mRNA catabolic process, nonsense-mediated decay	7,93E-04	EIF3E; PPP2CA; RPL6; RPL9; RPL11; RPL18; RPL19; RPL22; RPL23A; RPL27; RPL27A; RPL28; RPL29; RPL31; RPS2; RPS10; RPS11; RPS12; RPS14; UBA52; RPL14

GO:0006612	7	21	89	protein targeting to membrane	8,29E-04	MYO1C; RPL6; RPL9; RPL11; RPL18; RPL19; RPL22; RPL23A; RPL27; RPL27A; RPL28; RPL29; RPL31; RPS2; RPS10; RPS11; RPS12; RPS14; SRP14; UBA52; RPL14
GO:0044419	22	42	275	interspecies interaction between organisms	1,80E-03	HTATIP2; CTSB; DDX3X; FDPS; MSH6; HMGA1; HSPD1; TNPO1; F11R; DYNC1LI1; PSMA4; PSMB2; PSMB4; PSMB5; RAN; RPL6; RPL9; RPL11; RPL18; RPL19; RPL22; RPL23A; RPL27; RPL27A; RPL28; RPL29; RPL31; RPS2; RPS10; RPS11; RPS12; RPS14; SET; SRC; STAT1; UBA52; EIF4H; YWHAB; DEK; EIF3G; RPL14; NUP93
GO:0019083	8	20	101	viral transcription	1,87E-02	RPL6; RPL9; RPL11; RPL18; RPL19; RPL22; RPL23A; RPL27; RPL27A; RPL28; RPL29; RPL31; RPS2; RPS10; RPS11; RPS12; RPS14; UBA52; RPL14; NUP93
GO:0002223	3	12	44	stimulatory C-type lectin receptor signaling pathway	2,00E-02	PSMA1; PSMA4; PSMB2; PSMB4; PSMB5; PSMC1; PSMC5; PSMD1; PSME1; SRC; UBA52; UBE2V1

GO:0010605	36	56	454	negative regulation of macro-molecule metabolic process	2,00E-02	MYBBP1A; YWHAQ; CBX3; DDX3X; EIF4B; MSH6; HMGA1; EIF3E; EIF6; TNPO1; PPP2CA; OTUB1; PSMA1; PSMA4; PSMB2; PSMB4; PSMB5; PSMC1; PSMC5; PSMD1; PSME1; RAN; RPL6; RPL9; RPL11; RPL18; RPL19; RPL22; RPL23A; RPL27; RPL27A; RPL28; RPL29; RPL31; RPS2; RPS10; RPS11; RPS12; RPS14; S100A11; SET; SRSF6; TRA2B; SRC; STAT1; UBA52; YWHAB; CSDE1; CALM3; ANP32A; HIST1H2AH; TNKS1BP1; RPL14; CD59; NUP93; BCLAF1
GO:0072657	14	28	173	protein localization to membrane	2,00E-02	RAB10; YWHAQ; MYO1C; F11R; RPL6; RPL9; RPL11; RPL18; RPL19; RPL22; RPL23A; RPL27; RPL27A; RPL28; RPL29; RPL31; RPS2; RPS10; RPS11; RPS12; RPS14; S100A10; SRP14; UBA52; YWHAB; RPL14; MAP7; PDCD5
GO:0006364	10	22	121	rRNA processing	2,00E-02	NOP56; XRN2; EIF6; RPL6; RPL9; RPL11; RPL18; RPL19; RPL22; RPL23A; RPL27; RPL27A; RPL28; RPL29; RPL31; RPS2; RPS10; RPS11; RPS12; RPS14; UBA52; RPL14
GO:0090263	4	12	45	positive regulation of canonical Wnt signaling pathway	2,00E-02	DDX3X; PSMA1; PSMA4; PSMB2; PSMB4; PSMB5; PSMC1; PSMC5; PSMD1; PSME1; SRC; UBA52

GO:0034660	16	30	196	ncRNA metabolic process	2,82E-02	FARSB; NOP56; CSTF2; XRN2; HSD17B10; HARS; IARS; EIF6; RTCB; RAN; RPL6; RPL9; RPL11; RPL18; RPL19; RPL22; RPL23A; RPL27; RPL27A; RPL28; RPL29; RPL31; RPS2; RPS10; RPS11; RPS12; RPS14; UBA52; RPL14; AIMP1
GO:0044265	23	40	295	cellular macro-molecule catabolic process	2,97E-02	BCAP31; CTSB; EIF4B; XRN2; EIF3E; TNPO1; PPP2CA; PSMA1; PSMA4; PSMB2; PSMB4; PSMB5; PSMC1; PSMC5; PSMD1; PSME1; RPL6; RPL9; RPL11; RPL18; RPL19; RPL22; RPL23A; RPL27; RPL27A; RPL28; RPL29; RPL31; RPS2; RPS10; RPS11; RPS12; RPS14; SET; UBA52; YWHAB; CSDE1; ANP32A; TNKS1BP1; RPL14
GO:0030111	5	14	62	regulation of Wnt signaling pathway	3,11E-02	G3BP1; DDX3X; PPP2CA; PSMA1; PSMA4; PSMB2; PSMB4; PSMB5; PSMC1; PSMC5; PSMD1; PSME1; SRC; UBA52
GO:0002758	5	14	63	innate immune response-activating signal transduction	3,52E-02	CTSB; HSPD1; PSMA1; PSMA4; PSMB2; PSMB4; PSMB5; PSMC1; PSMC5; PSMD1; PSME1; SRC; UBA52; UBE2V1
GO:0050852	4	12	49	T cell receptor signaling pathway	3,57E-02	STOML2; PSMA1; PSMA4; PSMB2; PSMB4; PSMB5; PSMC1; PSMC5; PSMD1; PSME1; UBA52; UBE2V1

GO:0034645	56	76	704	cellular macro-molecule biosynthetic process	3,96E-02	FARSB; TRAP1; MYBBP1A; HTATIP2; YWHAQ; HNRNPUL1; CBX3; CSTF2; DDX3X; EIF4B; XRN2; PRPF6; HARS; STOML2; HMGA1; PRMT1; HSPD1; IARS; EIF3E; EIF6; ARF4; LMAN1; MCM2; PPP2CA; PSMA1; PSMA4; PSMB2; PSMB4; PSMB5; PSMC1; PSMC5; PSMD1; PSME1; RAN; RPA1; RPL6; RPL9; RPL11; RPL18; RPL19; RPL22; RPL23A; RPL27; RPL27A; RPL28; RPL29; RPL31; RPN2; RPS2; RPS10; RPS11; RPS12; RPS14; S100A11; SET; SRSF6; SRC; STAT1; EIF3CL; U2AF1; UBA52; UBE2V1; EIF4H; YWHAB; CSDE1; DEK; ANP32A; HIST1H2AH; TNKS1BP1; RUVBL1; EIF3G; EIF3H; RPL14; AIMP1; NUP93; BCLAF1
GO:0038095	3	11	44	Fc-epsilon receptor signaling pathway	4,40E-02	PSMA1; PSMA4; PSMB2; PSMB4; PSMB5; PSMC1; PSMC5; PSMD1; PSME1; UBA52; UBE2V1
GO:0051444	3	11	44	negative regulation of ubiquitin-protein transferase activity	4,40E-02	PSMA1; PSMA4; PSMB2; PSMB4; PSMB5; PSMC1; PSMC5; PSMD1; PSME1; RPL11; UBA52
GO:0090090	3	11	44	negative regulation of canonical Wnt signaling pathway	4,40E-02	G3BP1; PSMA1; PSMA4; PSMB2; PSMB4; PSMB5; PSMC1; PSMC5; PSMD1; PSME1; UBA52

GO:0031146	3	10	38	SCF-dependent proteasomal ubiquitin-dependent protein catabolic process	4,98E-02	PSMA1; PSMA4; PSMB2; PSMB4; PSMB5; PSMC1; PSMC5; PSMD1; PSME1; UBA52
GO:2000058	4	11	45	Regulation of protein ubiquiti-nation involved in ubiquitin-dependent protein catabolic process	4,99E-02	PSMA1; PSMA4; PSMB2; PSMB4; PSMB5; PSMC1; PSMC5; PSMD1; PSME1; RPL11; UBA52
GO:0046483	75	94	939	heterocycle metabolic process	5,26E-02	FARSB; G3BP1; MYBBP1A; NOP56; HTATIP2; YWHAQ; HNRNPUL1; CBX3; CSTF2; DDX3X; DHX15; DTYMK; AHCY; EIF4B; HNRNPA3; XRN2; ACIN1; PRPF6; GNAS; MSH6; HSD17B10; HARS; STOML2; HK1; HMGA1; HNRNPH3; PRMT1; HSPD1; IARS; EIF3E; EIF6; ARF4; TNPO1; MCM2; ABCC1; RTCB; PDHB; ATP6V1A; PPP2CA; OTUB1; PSMA1; PSMA4; PSMB2; PSMB4; PSMB5; PSMC1; PSMC5; PSMD1; PSME1; RAN; RPA1; RPL6; RPL9; RPL11; RPL18; RPL19; RPL22; RPL23A; RPL27; RPL27A; RPL28; RPL29; RPL31; RPS2; RPS10; RPS11; RPS12; RPS14; S100A11; SET; SRSF6; TRA2B; BLVRA; SNRPA1; SNRPB2; SRC; STAT1; SULT1A3; U2AF1; UBA52; UBE2V1; UQCRC2; YWHAB; CSDE1; DEK; CALM3; ANP32A; HIST1H2AH; TNKS1BP1; RUVBL1; RPL14; AIMP1; NUP93; BCLAF1

GO:0006725	75	94	940	cellular aromatic compound metabolic process	5,26E-02	FARSB; G3BP1; MYBBP1A; NOP56; HTATIP2; YWHAQ; HNRNPUL1; CBX3; CSTF2; DDX3X; DHX15; DTYMK; AHCY; EIF4B; HNRNPA3; XRN2; ACIN1; PRPF6; GNAS; MSH6; HSD17B10; HARS; STOML2; HK1; HMGA1; HNRNPH3; PRMT1; HSPD1; IARS; EIF3E; EIF6; ARF4; TNPO1; MCM2; ABCC1; RTCB; PDHB; ATP6V1A; PPP2CA; OTUB1; PSMA1; PSMA4; PSMB2; PSMB4; PSMB5; PSMC1; PSMC5; PSMD1; PSME1; RAN; RPA1; RPL6; RPL9; RPL11; RPL18; RPL19; RPL22; RPL23A; RPL27; RPL27A; RPL28; RPL29; RPL31; RPS2; RPS10; RPS11; RPS12; RPS14; S100A11; SET; SRSF6; TRA2B; BLVRA; SNRPA1; SNRPB2; SRC; STAT1; SULT1A3; U2AF1; UBA52; UBE2V1; UQCRC2; YWHAB; CSDE1; DEK; CALM3; ANP32A; HIST1H2AH; TNKS1BP1; RUVBL1; RPL14; AIMP1; NUP93; BCLAF1
GO:0051436	3	10	39	negative regulation of ubiquitin-protein ligase activity involved in mitotic cell cycle	5,26E-02	PSMA1; PSMA4; PSMB2; PSMB4; PSMB5; PSMC1; PSMC5; PSMD1; PSME1; UBA52
GO:1904666	4	11	46	regulation of ubiquitin protein ligase activity	5,26E-02	PSMA1; PSMA4; PSMB2; PSMB4; PSMB5; PSMC1; PSMC5; PSMD1; PSME1; RPL11; UBA52

GO:0022613	16	29	201	Ribonucleo-protein complex biogenesis	5,26E-02	NOP56; DDX3X; EIF4B; XRN2; PRPF6; EIF6; RAN; RPL6; RPL9; RPL11; RPL18; RPL19; RPL22; RPL23A; RPL27; RPL27A; RPL28; RPL29; RPL31; RPS2; RPS10; RPS11; RPS12; RPS14; SRSF6; UBA52; EIF4H; RUVBL1; RPL14
GO:0033209	4	11	47	tumor necrosis factor-mediated signaling pathway	5,65E-02	PSMA1; PSMA4; PSMB2; PSMB4; PSMB5; PSMC1; PSMC5; PSMD1; PSME1; STAT1; UBA52
GO:0031145	3	10	40	anaphase-promoting complex-dependent catabolic process	5,65E-02	PSMA1; PSMA4; PSMB2; PSMB4; PSMB5; PSMC1; PSMC5; PSMD1; PSME1; UBA52
GO:0051437	3	10	40	positive regulation of ubiquitin-protein ligase activity involved in regulation of mitotic cell cycle transition	5,65E-02	PSMA1; PSMA4; PSMB2; PSMB4; PSMB5; PSMC1; PSMC5; PSMD1; PSME1; UBA52
GO:0000209	4	12	55	protein polyubiquitination	6,04E-02	OTUB1; PSMA1; PSMA4; PSMB2; PSMB4; PSMB5; PSMC1; PSMC5; PSMD1; PSME1; UBA52; UBE2V1
GO:2000027	4	12	55	regulation of organ morpho-genesis	6,04E-02	PSMA1; PSMA4; PSMB2; PSMB4; PSMB5; PSMC1; PSMC5; PSMD1; PSME1; SRSF6; STAT1; UBA52

GO:0002429	6	14	71	immune response-activating cell surface receptor signaling pathway	6,45E-02	STOML2; MYO1C; PSMA1; PSMA4; PSMB2; PSMB4; PSMB5; PSMC1; PSMC5; PSMD1; PSME1; SRC; UBA52; UBE2V1
GO:1903706	3	10	42	regulation of hemopoiesis	6,52E-02	PSMA1; PSMA4; PSMB2; PSMB4; PSMB5; PSMC1; PSMC5; PSMD1; PSME1; UBA52
GO:1901988	5	13	64	negative regulation of cell cycle phase transition	6,97E-02	PRMT1; DYNC1LI1; PSMA1; PSMA4; PSMB2; PSMB4; PSMB5; PSMC1; PSMC5; PSMD1; PSME1; UBA52; TNKS1BP1
GO:0061418	3	10	42	regulation of transcription from RNA polymerase II promoter in response to hypoxia	7,03E-02	PSMA1; PSMA4; PSMB2; PSMB4; PSMB5; PSMC1; PSMC5; PSMD1; PSME1; UBA52
GO:1902036	3	10	42	regulation of hematopoietic stem cell differentiation	7,03E-02	PSMA1; PSMA4; PSMB2; PSMB4; PSMB5; PSMC1; PSMC5; PSMD1; PSME1; UBA52
GO:0002474	4	11	50	antigen processing and presentation of peptide antigen via MHC class I	7,71E-02	BCAP31; PSMA1; PSMA4; PSMB2; PSMB4; PSMB5; PSMC1; PSMC5; PSMD1; PSME1; SEC24C
GO:0043620	4	11	50	regulation of DNA-templated transcription in response to stress	7,71E-02	PSMA1; PSMA4; PSMB2; PSMB4; PSMB5; PSMC1; PSMC5; PSMD1; PSME1; UBA52; BCLAF1

GO:0051443	3	10	43	positive regulation of ubiquitin-protein transferase activity	7,74E-02	PSMA1; PSMA4; PSMB2; PSMB4; PSMB5; PSMC1; PSMC5; PSMD1; PSME1; UBA52
GO:0019882	7	15	82	antigen processing and presentation	7,74E-02	BCAP31; RAB10; DYNC1LI1; PSMA1; PSMA4; PSMB2; PSMB4; PSMB5; PSMC1; PSMC5; PSMD1; PSME1; CAPZA2; CAPZB; SEC24C
GO:1903321	5	12	58	negative regulation of protein modification by small protein conjugation or removal	7,74E-02	OTUB1; PSMA1; PSMA4; PSMB2; PSMB4; PSMB5; PSMC1; PSMC5; PSMD1; PSME1; RPL11; UBA52
GO:0002764	7	16	91	immune response-regulating signaling pathway	8,12E-02	CTSB; STOML2; HSPD1; MYO1C; PSMA1; PSMA4; PSMB2; PSMB4; PSMB5; PSMC1; PSMC5; PSMD1; PSME1; SRC; UBA52; UBE2V1
GO:1905330	4	11	51	regulation of morpho-genesis of an epithelium	8,19E-02	PSMA1; PSMA4; PSMB2; PSMB4; PSMB5; PSMC1; PSMC5; PSMD1; PSME1; STAT1; UBA52

GO:190 1360	78	95	975	organic cyclic compound metabolic process	8,25E -02	FARSB; G3BP1; MYBBP1A; NOP56; HTATIP2; YWHAQ; HNRNPUL1; CBX3; CSTF2; DDX3X; DHX15; DTYMK; AHCY; EIF4B; HNRNPA3; FDPS; XRN2; ACIN1; PRPF6; GNAS; MSH6; HSD17B10; HARS; STOML2; HK1; HMGA1; HNRNPH3; PRMT1; HSPD1; IARS; EIF3E; EIF6; ARF4; TNPO1; MCM2; ABCC1; RTCB; PDHB; ATP6V1A; PPP2CA; OTUB1; PSMA1; PSMA4; PSMB2; PSMB4; PSMB5; PSMC1; PSMC5; PSMD1; PSME1; RAN; RPA1; RPL6; RPL9; RPL11; RPL18; RPL19; RPL22; RPL23A; RPL27; RPL27A; RPL28; RPL29; RPL31; RPS2; RPS10; RPS11; RPS12; RPS14; S100A11; SET; SRSF6; TRA2B; BLVRA; SNRPA1; SNRPB2; SRC; STAT1; SULT1A3; U2AF1; UBA52; UBE2V1; UQCRC2; YWHAB; CSDE1; DEK; CALM3; ANP32A; HIST1H2AH; TNKS1BP1; RUVBL1; RPL14; AIMP1; NUP93; BCLAF1

GO:0048519	56	73	701	negative regulation of biological process	8,25E-02	TRAP1; G3BP1; MYBBP1A; GLRX3; HTATIP2; YWHAQ; STMN2; CBX3; DDX3X; EIF4B; TES; MSH6; ANXA5; HMGA1; PRMT1; HSPD1; EIF3E; EIF6; ARF4; TNPO1; F11R; DYNC1LI1; PPP2CA; OTUB1; PSMA1; PSMA4; PSMB2; PSMB4; PSMB5; PSMC1; PSMC5; PSMD1; PSME1; RAN; RPL6; RPL9; RPL11; RPL18; RPL19; RPL22; RPL23A; RPL27; RPL27A; RPL28; RPL29; RPL31; RPS2; RPS10; RPS11; RPS12; RPS14; S100A11; SET; SRSF6; TRA2B; SRC; STAT1; SULT1A3; UBA52; YWHAB; CSDE1; CALM3; ANP32A; CAPZA2; CAPZB; HIST1H2AH; TNKS1BP1; RPL14; PDCD5; AIMP1; CD59; NUP93; BCLAF1
GO:0033365	16	28	211	protein localization to organelle	8,72E-02	BCAP31; RAB10; DDX3X; SYNE1; TNPO1; RAN; RPA1; RPL6; RPL9; RPL11; RPL18; RPL19; RPL22; RPL23A; RPL27; RPL27A; RPL29; RPL31; RPS2; RPS10; RPS11; RPS12; RPS14; SRC; SRP14; UBA52; RPL14; NUP93
GO:0010972	4	10	45	negative regulation of G2/M transition of mitotic cell cycle	9,52E-02	PSMA1; PSMA4; PSMB2; PSMB4; PSMB5; PSMC1; PSMC5; PSMD1; PSME1; UBA52

GO:0044106	4	10	45	cellular amine metabolic process	9,52E-02	ALDH7A1; PSMA1; PSMA4; PSMB2; PSMB4; PSMB5; PSMC1; PSMC5; PSMD1; PSME1
GO:0016032	12	22	162	viral process	9,59E-02	HTATIP2; CTSB; DDX3X; FDPS; MSH6; HMGA1; HSPD1; TNPO1; F11R; DYNC1LI1; PSMA4; PSMB2; PSMB4; PSMB5; RAN; SET; SRC; STAT1; EIF4H; YWHAB; DEK; EIF3G
GO:0006521	3	9	38	regulation of cellular amino acid metabolic process	9,59E-02	PSMA1; PSMA4; PSMB2; PSMB4; PSMB5; PSMC1; PSMC5; PSMD1; PSME1
GO:1901575	36	51	451	organic substance catabolic process	9,78E-02	BCAP31; CTSB; AHCY; EIF4B; ETFA; XRN2; GOT1; HSD17B10; HK1; EIF3E; EIF6; TNPO1; LTA4H; ALDH7A1; PPP2CA; PSMA1; PSMA4; PSMB2; PSMB4; PSMB5; PSMC1; PSMC5; PSMD1; PSME1; RPL6; RPL9; RPL11; RPL18; RPL19; RPL22; RPL23A; RPL27; RPL27A; RPL28; RPL29; RPL31; RPS2; RPS10; RPS11; RPS12; RPS14; SET; BLVRA; SULT1A3; UBA52; YWHAB; CSDE1; ANP32A; TNKS1BP1; PL14; NUP93

GO:0002253	8	17	103	activation of immune response	9,80E-02	CTSB; STOML2; HSPD1; MYO1C; PSMA1; PSMA4; PSMB2; PSMB4; PSMB5; PSMC1; PSMC5; PSMD1; PSME1; SRC; UBA52; UBE2V1; CD59
GO:0060071	4	10	46	Wnt signaling pathway, planar cell polarity pathway	1,04E-01	PSMA1; PSMA4; PSMB2; PSMB4; PSMB5; PSMC1; PSMC5; PSMD1; PSME1; UBA52
GO:0048534	9	18	113	hematopoietic or lymphoid organ development	1,06E-01	ACIN1; GNAS; PRMT1; EIF6; PSMA1; PSMA4; PSMB2; PSMB4; PSMB5; PSMC1; PSMC5; PSMD1; PSME1; RPS14; SRC; STAT1; UBA52; SFXN1
GO:1903052	4	11	55	positive regulation of proteolysis involved in cellular protein catabolic process	1,24E-01	BCAP31; PSMA1; PSMA4; PSMB2; PSMB4; PSMB5; PSMC1; PSMC5; PSMD1; PSME1; UBA52

GO:0051649	37	52	469	establishment of localization in cell	1,26E-01	BCAP31; MYBBP1A; HTATIP2; RAB10; YWHAQ; STOML2; HMGA1; HSPD1; EIF6; ARF4; TNPO1; LMAN1; MYO1C; DYNC1LI1; ERGIC1; RAN; RPL6; RPL9; RPL11; RPL18; RPL19; RPL22; RPL23A; RPL27; RPL27A; RPL28; RPL29; RPL31; RPS2; RPS10; RPS11; RPS12; RPS14; SET; SRSF6; SRC; SRP14; U2AF1; UBA52; UQCRC2; YWHAB; CALM3; ANP32A; CAPZA2; CAPZB; RUVBL1; USO1; RPL14; PDCD5; SEC24C; CD59; NUP93
GO:0045089	6	14	80	positive regulation of innate immune response	1,26E-01	CTSB; HSPD1; PSMA1; PSMA4; PSMB2; PSMB4; PSMB5; PSMC1; PSMC5; PSMD1; PSME1; SRC; UBA52; UBE2V1

GO:0044271	59	75	740	cellular nitrogen compound biosynthetic process	1,26E-01	FARSB; TRAP1; MYBBP1A; HTATIP2; YWHAQ; HNRNPUL1; CBX3; CSTF2; DDX3X; DTYMK; EIF4B; XRN2; PRPF6; HARS; STOML2; HMGA1; PRMT1; HSPD1; IARS; EIF3E; EIF6; ARF4; ALDH7A1; PPP2CA; PSMA1; PSMA4; PSMB2; PSMB4; PSMB5; PSMC1; PSMC5; PSMD1; PSME1; RAN; RPA1; RPL6; RPL9; RPL11; RPL18; RPL19; RPL22; RPL23A; RPL27; RPL27A; RPL28; RPL29; RPL31; RPS2; RPS10; RPS11; RPS12; RPS14; SET; SRSF6; SRC; STAT1; EIF3CL; U2AF1; UBA52; UBE2V1; EIF4H; YWHAB; CSDE1; DEK; CALM3; ANP32A; HIST1H2AH; TNKS1BP1; RUVBL1; EIF3G; EIF3H; RPL14; AIMP1; NUP93; BCLAF1
GO:0002478	6	13	73	antigen processing and presentation of exogenous peptide antigen	1,47E-01	DYNC1LI1; PSMA1; PSMA4; PSMB2; PSMB4; PSMB5; PSMC1; PSMC5; PSMD1; PSME1; CAPZA2; CAPZB; SEC24C
GO:0001736	4	10	49	establishment of planar polarity	1,50E-01	PSMA1; PSMA4; PSMB2; PSMB4; PSMB5; PSMC1; PSMC5; PSMD1; PSME1; UBA52

GO:0043488	7	14	82	regulation of mRNA stability	1,50E-01	TNPO1; PSMA1; PSMA4; PSMB2; PSMB4; PSMB5; PSMC1; PSMC5; PSMD1; PSME1; SET; UBA52; YWHAB; ANP32A
GO:0043043	22	34	277	peptide biosynthetic process	1,50E-01	FARSB; TRAP1; DDX3X; EIF4B; HARS; IARS; EIF3E; EIF6; RAN; RPL6; RPL9; RPL11; RPL18; RPL19; RPL22; RPL23A; RPL27; RPL27A; RPL28; RPL29; RPL31; RPS2; RPS10; RPS11; RPS12; RPS14; EIF3CL; UBA52; EIF4H; EIF3G; EIF3H; RPL14; AIMP1; NUP93
GO:0006691	0	3	5	leukotriene metabolic process	1,54E-01	PTGR1; LTA4H; ABCC1
GO:0065004	3	9	42	protein-DNA complex assembly	1,58E-01	MCM2; NAP1L4; PSMC1; PSMC5; RPA1; SET; UBA52; RUVBL1; H1FX
GO:0002244	4	10	50	hematopoietic progenitor cell differentiation	1,59E-01	PSMA1; PSMA4; PSMB2; PSMB4; PSMB5; PSMC1; PSMC5; PSMD1; PSME1; UBA52
GO:0038061	4	10	50	NIK/NF-kappaB signaling	1,59E-01	PSMA1; PSMA4; PSMB2; PSMB4; PSMB5; PSMC1; PSMC5; PSMD1; PSME1; UBA52
GO:0034612	5	11	58	response to tumor necrosis factor	1,59E-01	PSMA1; PSMA4; PSMB2; PSMB4; PSMB5; PSMC1; PSMC5; PSMD1; PSME1; STAT1; UBA52

GO:0002684	10	19	132	positive regulation of immune system process	1,69E-01	CTSB; MSH6; STOML2; HK1; HSPD1; MYO1C; PSMA1; PSMA4; PSMB2; PSMB4; PSMB5; PSMC1; PSMC5; PSMD1; PSME1; SRC; UBA52; UBE2V1; CD59
GO:0002479	3	9	43	antigen processing and presentation of exogenous peptide antigen via MHC class I, TAP-dependent	1,74E-01	PSMA1; PSMA4; PSMB2; PSMB4; PSMB5; PSMC1; PSMC5; PSMD1; PSME1
GO:0042180	5	11	59	cellular ketone metabolic process	1,75E-01	EIF6; PDHB; PSMA1; PSMA4; PSMB2; PSMB4; PSMB5; PSMC1; PSMC5; PSMD1; PSME1
GO:0045930	6	13	76	negative regulation of mitotic cell cycle	1,75E-01	PRMT1; DYNC1LI1; PSMA1; PSMA4; PSMB2; PSMB4; PSMB5; PSMC1; PSMC5; PSMD1; PSME1; UBA52; TNKS1BP1

GO:1901576	72	87	902	organic substance biosynthetic process	1,75E-01	FARSB; TRAP1; MYBBP1A; HTATIP2; YWHAQ; HNRNPUL1; CBX3; CSTF2; DDX3X; DTYMK; AHCY; EIF4B; FDPS; XRN2; PRPF6; GOT1; HARS; STOML2; HMGA1; PRMT1; HSPD1; IARS; EIF3E; EIF6; GSTK1; ARF4; LMAN1; LTA4H; MCM2; ALDH7A1; PDHB; PPP2CA; PSMA1; PSMA4; PSMB2; PSMB4; PSMB5; PSMC1; PSMC5; PSMD1; PSME1; RAN; RPA1; RPL6; RPL9; RPL11; RPL18; RPL19; RPL22; RPL23A; RPL27; RPL27A; RPL28; RPL29; RPL31; RPN2; RPS2; RPS10; RPS11; RPS12; RPS14; S100A11; SET; SRSF6; SRC; STAT1; EIF3CL; U2AF1; UBA52; UBE2V1; EIF4H; YWHAB; CSDE1; DEK; CALM3; ANP32A; HIST1H2AH; AGPS; TNKS1BP1; RUVBL1; EIF3G; EIF3H; CBR1; RPL14; AIMP1; NUP93; BCLAF1
GO:0032868	3	8	36	response to insulin	1,80E-01	RAB10; GOT1; EIF6; MYO1C; ATP6V1A; ATP6V1C1; SRSF6; SRC

Appendix 5. Protein list of ATGL-KO and control cells grown as 3D spheroids after filtering for three valid values per group

Protein names	Fold Change ATGL-KO to control	Adjusted p-value (q-value)
Eukaryotic translation elongation factor 1 epsilon-1	7.27	0.00
Putative heat shock protein HSP 90-beta 2	6.83	0.10
Peptidyl-prolyl cis-trans isomerase FKBP10	5.97	0.00
Heat shock-related 70 kDa protein 2	5.65	0.00
Guanine nucleotide-binding protein G(I)/G(S)/G(O) subunit gamma-12	5.03	0.27
ADP-dependent glucokinase	4.84	0.00
Glycogen phosphorylase, liver form	4.66	0.05
Ferritin light chain	4.63	0.00
UPF0587 protein C1orf123	4.44	0.14
DNA replication licensing factor MCM5	4.41	0.00
Ferritin heavy chain;Ferritin heavy chain, N-terminally processed	4.41	0.05
A-kinase anchor protein 12	4.38	0.01
DNA replication licensing factor MCM3	4.28	0.05
Solute carrier family 2, facilitated glucose transporter member 3;Solute carrier family 2, facilitated glucose transporter member 14	4.14	0.01
Stomatin-like protein 2, mitochondrial	4.12	0.23
NADH dehydrogenase [ubiquinone] 1 beta subcomplex subunit 10	4.01	0.10
Tubulin beta-8 chain	3.95	0.45
Retinol dehydrogenase 10	3.89	0.15
Isopentenyl-diphosphate Delta-isomerase 1	3.88	0.01
DNA replication licensing factor MCM7	3.82	0.09
tRNA (cytosine(34)-C(5))-methyltransferase	3.57	0.12
Squamous cell carcinoma antigen recognized by T-cells 3	3.54	0.06
Lamin-B receptor	3.49	0.05
Cytochrome b5 type B	3.45	0.00
Ribonucleoside-diphosphate reductase large subunit	3.41	0.03
Fatty acid desaturase 2	3.41	0.04
ADP-ribosylation factor-like protein 3	3.38	0.34
Peroxisomal acyl-coenzyme A oxidase 1	3.37	0.18
Protein HEXIM1	3.36	0.21
Protein NDRG1	3.31	0.04
Eukaryotic translation initiation factor 1;Eukaryotic translation initiation factor 1b	3.27	0.39
Mitotic spindle-associated MMXD complex subunit MIP18	3.24	0.08
Aspartate--tRNA ligase, mitochondrial	3.17	0.05
Peptidyl-tRNA hydrolase 2, mitochondrial	3.15	0.43

Prolyl 4-hydroxylase subunit alpha-1	3.12	0.01
Syntenin-1	3.10	0.04
Ubiquitin-conjugating enzyme E2 L3	3.08	0.14
IgGFc-binding protein	3.02	0.52
Thioredoxin, mitochondrial	3.00	0.14
NADH dehydrogenase [ubiquinone] 1 alpha subcomplex subunit 13	2.99	0.10
Mitochondrial fission 1 protein	2.97	0.21
Mitochondrial import inner membrane translocase subunit TIM50	2.91	0.19
Dynamin-1-like protein	2.86	0.23
RRP12-like protein	2.85	0.05
Malignant T-cell-amplified sequence 1	2.76	0.08
Protein mago nashi homolog 2;Protein mago nashi homolog	2.71	0.12
Flap endonuclease 1	2.71	0.08
PC4 and SFRS1-interacting protein	2.68	0.14
40S ribosomal protein S26;Putative 40S ribosomal protein S26-like 1	2.67	0.01
Serine--tRNA ligase, mitochondrial	2.66	0.13
Eukaryotic translation initiation factor 3 subunit K	2.65	0.45
U5 small nuclear ribonucleoprotein 40 kDa protein	2.64	0.11
Nuclear pore complex protein Nup155	2.63	0.09
Eukaryotic translation initiation factor 4E	2.61	0.30
Acetyl-CoA carboxylase 1;Biotin carboxylase	2.59	0.28
Histidine triad nucleotide-binding protein 2, mitochondrial	2.59	0.54
Brain acid soluble protein 1	2.59	0.45
Catechol O-methyltransferase	2.58	0.34
High mobility group protein B3	2.58	0.03
DNA polymerase epsilon subunit 3	2.58	0.05
Large neutral amino acids transporter small subunit 1	2.58	0.10
Neutral amino acid transporter B(0)	2.57	0.28
40S ribosomal protein S15	2.57	0.28
Ferrochelatase, mitochondrial	2.56	0.13
Procollagen-lysine,2-oxoglutarate 5-dioxygenase 2	2.56	0.14
Very-long-chain 3-oxoacyl-CoA reductase	2.55	0.05
Cytochrome c oxidase protein 20 homolog	2.53	0.15
Tumor protein D53	2.52	0.29
Egl nine homolog 1	2.50	0.12
60S ribosomal protein L35	2.47	0.37
Short-chain dehydrogenase/reductase 3	2.46	0.05
Membrane-associated progesterone receptor component 1	2.46	0.30
BRCA2 and CDKN1A-interacting protein	2.44	0.14
ATP-dependent 6-phosphofructokinase, platelet type	2.44	0.01
PIH1 domain-containing protein 1	2.43	0.07
Fatty acid-binding protein, epidermal	2.40	0.05
Niban-like protein 1	2.39	0.54

Ribosome biogenesis protein BOP1	2.38	0.18
Polypeptide N-acetylgalactosaminyltransferase 2;Polypeptide N-acetylgalactosaminyltransferase 2 soluble form	2.33	0.07
Protein S100-P	2.32	0.14
Nucleosome assembly protein 1-like 1	2.30	0.08
Eukaryotic peptide chain release factor subunit 1	2.29	0.07
Spermine synthase	2.28	0.45
Histone acetyltransferase type B catalytic subunit	2.27	0.14
Sec1 family domain-containing protein 1	2.27	0.38
Histone-binding protein RBBP7	2.27	0.18
Glycerol-3-phosphate dehydrogenase, mitochondrial	2.26	0.49
ERO1-like protein alpha	2.24	0.00
Sorcin	2.24	0.34
Ribulose-phosphate 3-epimerase	2.23	0.28
N-acetyltransferase 10	2.22	0.10
Small nuclear ribonucleoprotein Sm D3	2.20	0.57
ERBB receptor feedback inhibitor 1	2.20	0.01
Probable ubiquitin carboxyl-terminal hydrolase FAF-X	2.19	0.09
DnaJ homolog subfamily C member 9	2.19	0.05
Cysteine and histidine-rich domain-containing protein 1	2.19	0.49
Tubulin-specific chaperone E	2.19	0.17
Protein transport protein Sec61 subunit alpha isoform 1	2.18	0.09
Serine/arginine-rich splicing factor 9	2.17	0.34
Ribose-phosphate pyrophosphokinase 1;Ribose-phosphate pyrophosphokinase 3;Ribose-phosphate pyrophosphokinase 2	2.16	0.05
Translationally-controlled tumor protein	2.15	0.28
Fibrinogen gamma chain	2.15	0.61
Voltage-dependent anion-selective channel protein 2	2.15	0.03
Glutamate--cysteine ligase catalytic subunit	2.13	0.05
ADP/ATP translocase 3;ADP/ATP translocase 3, N-terminally processed	2.13	0.03
Voltage-dependent calcium channel subunit alpha-2/delta-1;Voltage-dependent calcium channel subunit alpha-2-1;Voltage-dependent calcium channel subunit delta-1	2.12	0.05
ATP synthase F(0) complex subunit B1, mitochondrial	2.11	0.41
Importin subunit alpha-1	2.08	0.08
Hsp90 co-chaperone Cdc37;Hsp90 co-chaperone Cdc37, N-terminally processed	2.08	0.53
Discoidin, CUB and LCCL domain-containing protein 2	2.08	0.34
Cytoskeleton-associated protein 5	2.08	0.10
Deoxyuridine 5-triphosphate nucleotidohydrolase, mitochondrial	2.07	0.16
Glucosamine 6-phosphate N-acetyltransferase	2.06	0.08
Importin-7	2.04	0.01
Activator of 90 kDa heat shock protein ATPase homolog 1	2.04	0.34
DNA replication licensing factor MCM2	2.04	0.10

Basal cell adhesion molecule	2.04	0.07
Protein MAK16 homolog	2.03	0.25
Importin-4	2.03	0.06
Thioredoxin-related transmembrane protein 1	2.03	0.10
Far upstream element-binding protein 3	2.02	0.41
Proteasome subunit beta type-5	2.00	0.05
28S ribosomal protein S17, mitochondrial	1.99	0.39
GrpE protein homolog 1, mitochondrial	1.99	0.14
Calcineurin B homologous protein 1	1.99	0.23
Acidic leucine-rich nuclear phosphoprotein 32 family member E	1.98	0.06
Dynactin subunit 4	1.97	0.18
Proliferating cell nuclear antigen	1.97	0.18
DNA topoisomerase 1	1.96	0.00
Replication protein A 70 kDa DNA-binding subunit;Replication protein A 70 kDa DNA-binding subunit, N-terminally processed	1.96	0.30
3-hydroxyacyl-CoA dehydrogenase type-2	1.95	0.07
39S ribosomal protein L37, mitochondrial	1.95	0.11
Nucleolar RNA helicase 2	1.95	0.08
ATP-dependent RNA helicase DDX39A	1.95	0.05
Mycophenolic acid acyl-glucuronide esterase, mitochondrial	1.93	0.34
SWI/SNF complex subunit SMARCC2;SWI/SNF complex subunit SMARCC1	1.93	0.50
Fructose-bisphosphate aldolase A	1.92	0.03
Dynein assembly factor 5, axonemal	1.92	0.07
Dual specificity mitogen-activated protein kinase kinase 2	1.91	0.28
Nucleobindin-2;Nesfatin-1	1.90	0.12
60S ribosomal protein L38	1.90	0.14
Insulin-degrading enzyme	1.89	0.52
Complement component 1 Q subcomponent-binding protein, mitochondrial	1.89	0.11
Regulation of nuclear pre-mRNA domain-containing protein 1B	1.89	0.55
Calumenin	1.88	0.04
U6 snRNA-associated Sm-like protein LSm8	1.85	0.26
Solute carrier family 12 member 2	1.85	0.21
60S acidic ribosomal protein P1	1.85	0.08
T-complex protein 1 subunit epsilon	1.84	0.08
NADH dehydrogenase [ubiquinone] 1 alpha subcomplex subunit 9, mitochondrial	1.84	0.46
Fatty acid synthase;[Acyl-carrier-protein] S-acetyltransferase;[Acyl-carrier-protein] S-malonyltransferase;3-oxoacyl-[acyl-carrier-protein] synthase;3-oxoacyl-[acyl-carrier-protein] reductase;3-hydroxyacyl-[acyl-carrier-protein] dehydratase;Enoyl-[acyl-carrier-protein] reductase;Oleoyl-[acyl-carrier-protein] hydrolase	1.84	0.08

Proteasome subunit beta type-6	1.83	0.55
LETM1 and EF-hand domain-containing protein 1, mitochondrial	1.83	0.12
Nuclear pore glycoprotein p62	1.83	0.53
60S ribosomal protein L26;60S ribosomal protein L26-like 1	1.83	0.08
Aldehyde dehydrogenase family 16 member A1	1.83	0.37
Cytochrome c1, heme protein, mitochondrial	1.83	0.10
Dihydrolipoyllysine-residue acetyltransferase component of pyruvate dehydrogenase complex, mitochondrial	1.82	0.20
Copine-1	1.82	0.37
Uridine 5-monophosphate synthase;Orotate phosphoribosyltransferase;Orotidine 5-phosphate decarboxylase	1.81	0.39
ER membrane protein complex subunit 1	1.80	0.03
Phosphatidylinositol-binding clathrin assembly protein	1.80	0.41
NFU1 iron-sulfur cluster scaffold homolog, mitochondrial	1.80	0.28
Mucin-5AC	1.79	0.86
NADH dehydrogenase [ubiquinone] 1 alpha subcomplex subunit 5	1.78	0.39
Trifunctional purine biosynthetic protein adenosine-3;Phosphoribosylamine--glycine ligase;Phosphoribosylformylglycinamidine cyclo-ligase;Phosphoribosylglycinamide formyltransferase	1.78	0.03
40S ribosomal protein S23	1.78	0.37
Serrate RNA effector molecule homolog	1.77	0.65
Eukaryotic peptide chain release factor GTP-binding subunit ERF3A	1.77	0.24
Lysosomal protective protein;Lysosomal protective protein 32 kDa chain;Lysosomal protective protein 20 kDa chain	1.77	0.64
Insulin-like growth factor-binding protein 3	1.77	0.23
Solute carrier family 2, facilitated glucose transporter member 1	1.77	0.70
DAZ-associated protein 1	1.77	0.15
Acyl-coenzyme A thioesterase 1;Acyl-coenzyme A thioesterase 2, mitochondrial	1.76	0.17
Prolyl endopeptidase	1.76	0.19
STE20-like serine/threonine-protein kinase	1.74	0.41
Serum paraoxonase/lactonase 3	1.74	0.26
Transcriptional activator protein Pur-alpha	1.73	0.68
Elongation factor 1-beta	1.73	0.30
Ubiquitin carboxyl-terminal hydrolase 10	1.73	0.37
Enhancer of mRNA-decapping protein 4	1.73	0.29
60S ribosomal protein L9	1.73	0.08
Acylglycerol kinase, mitochondrial	1.72	0.15
26S proteasome non-ATPase regulatory subunit 5	1.72	0.10
Single-stranded DNA-binding protein, mitochondrial	1.72	0.08
Nucleoside diphosphate kinase A	1.72	0.07
Cold shock domain-containing protein E1	1.72	0.46

Integrin beta-4	1.71	0.37
AH receptor-interacting protein	1.71	0.18
Rho guanine nucleotide exchange factor 1	1.70	0.19
Protein RCC2	1.70	0.47
Serine hydroxymethyltransferase, mitochondrial	1.70	0.07
Elongation factor 1-alpha 1;Putative elongation factor 1-alpha-like 3	1.69	0.05
Cytochrome c oxidase subunit 5A, mitochondrial	1.69	0.61
CCR4-NOT transcription complex subunit 1	1.69	0.08
Abl interactor 1;Abl interactor 2	1.69	0.53
Fructose-bisphosphate aldolase C	1.68	0.09
T-complex protein 1 subunit zeta	1.68	0.04
High mobility group protein B2	1.68	0.23
40S ribosomal protein S16	1.68	0.13
Anterior gradient protein 2 homolog	1.68	0.39
Aspartyl/asparaginyl beta-hydroxylase	1.67	0.03
Ribosome biogenesis protein BRX1 homolog	1.67	0.19
Transducin beta-like protein 2	1.67	0.62
Mannose-P-dolichol utilization defect 1 protein	1.66	0.61
Sorting nexin-5	1.66	0.43
Perilipin-2	1.66	0.41
Lysosome-associated membrane glycoprotein 2	1.66	0.71
Tripeptidyl-peptidase 2	1.65	0.41
Eukaryotic translation initiation factor 3 subunit H	1.65	0.57
Endothelial protein C receptor	1.65	0.07
60S ribosomal protein L10	1.64	0.10
60S ribosomal protein L18a	1.64	0.14
ATP-dependent Clp protease ATP-binding subunit clpX-like, mitochondrial	1.64	0.08
Thymosin beta-10	1.64	0.37
Small nuclear ribonucleoprotein Sm D2	1.64	0.04
Very-long-chain (3R)-3-hydroxyacyl-CoA dehydratase 3	1.64	0.68
T-complex protein 1 subunit delta	1.64	0.04
Phosphoglycerate mutase 1	1.64	0.08
Galectin-1	1.63	0.10
Proteasome subunit alpha type-5	1.63	0.08
40S ribosomal protein S13	1.62	0.28
Cytoplasmic FMR1-interacting protein 1;Cytoplasmic FMR1-interacting protein 2	1.62	0.15
Serine--tRNA ligase, cytoplasmic	1.62	0.10
Neutral cholesterol ester hydrolase 1	1.62	0.39
Thymidylate kinase	1.62	0.47
Inosine-5-monophosphate dehydrogenase 2	1.61	0.05
Proteasome subunit beta type-7	1.61	0.12
Hsp70-binding protein 1	1.61	0.10
Lon protease homolog, mitochondrial	1.61	0.08

Cysteine--tRNA ligase, cytoplasmic	1.61	0.41
L-lactate dehydrogenase A chain	1.61	0.05
Transmembrane 9 superfamily member 2	1.60	0.41
60S ribosomal protein L31	1.60	0.10
Ornithine aminotransferase, mitochondrial;Ornithine aminotransferase, hepatic form;Ornithine aminotransferase, renal form	1.60	0.51
Splicing factor 3B subunit 6	1.59	0.53
DNA replication licensing factor MCM6	1.59	0.34
Coactosin-like protein	1.59	0.55
40S ribosomal protein S12	1.59	0.07
Aminoacyl tRNA synthase complex-interacting multifunctional protein 2	1.58	0.33
Integrin alpha-6;Integrin alpha-6 heavy chain;Integrin alpha-6 light chain;Processed integrin alpha-6	1.58	0.63
Eukaryotic translation initiation factor 3 subunit F	1.58	0.10
GTP-binding nuclear protein Ran	1.58	0.07
Phosphoglycerate kinase 1	1.57	0.10
Putative ATP-dependent RNA helicase DHX30	1.57	0.20
Calcium-regulated heat stable protein 1	1.57	0.73
Elongation factor 2	1.56	0.05
Splicing factor, arginine/serine-rich 15;Protein SCAF8	1.56	0.29
Proteasome subunit alpha type-6	1.56	0.25
Nuclear cap-binding protein subunit 1	1.56	0.26
ATPase ASNA1	1.55	0.55
Heterogeneous nuclear ribonucleoprotein A0	1.55	0.56
Phosphoserine aminotransferase	1.55	0.28
Calreticulin	1.55	0.05
Deoxyribose-phosphate aldolase	1.55	0.72
Extended synaptotagmin-2	1.55	0.10
Small nuclear ribonucleoprotein F	1.54	0.28
Proteasome subunit beta type-3	1.54	0.07
Dynamin-2	1.53	0.08
Dolichol-phosphate mannosyltransferase subunit 1	1.53	0.45
Mammalian ependymin-related protein 1	1.53	0.76
LDLR chaperone MESD	1.53	0.09
Annexin A6	1.53	0.33
Protein FAM162A	1.52	0.15
Neutral alpha-glucosidase AB	1.52	0.05
Myoferlin	1.52	0.13
CAAX prenyl protease 1 homolog	1.52	0.14
Prohibitin	1.52	0.09
Methionine--tRNA ligase, cytoplasmic	1.51	0.05
Cytochrome c	1.51	0.10
Poly(rC)-binding protein 2	1.51	0.01
Nuclear transport factor 2	1.51	0.16

Phosphoribosylformylglycinamidine synthase	1.51	0.13
Cancer-related nucleoside-triphosphatase	1.51	0.62
Transmembrane and coiled-coil domain-containing protein 1	1.50	0.12
60S ribosomal protein L7a	1.50	0.06
Gamma-glutamyl hydrolase	1.50	0.36
Isocitrate dehydrogenase [NADP], mitochondrial	1.50	0.18
Prostaglandin E synthase 3	1.50	0.25
Hematological and neurological expressed 1 protein;Hematological and neurological expressed 1 protein, N-terminally processed	1.50	0.09
Heat shock protein HSP 90-beta	1.50	0.10
Plasminogen activator inhibitor 1 RNA-binding protein	1.50	0.14
Exportin-2	1.50	0.15
Mitochondrial import receptor subunit TOM22 homolog	1.49	0.28
E3 ubiquitin/ISG15 ligase TRIM25	1.49	0.79
SH3 domain-binding glutamic acid-rich-like protein 3	1.49	0.69
Heterogeneous nuclear ribonucleoprotein A/B	1.49	0.50
Coatomer subunit beta	1.49	0.18
Carbonic anhydrase 9	1.49	0.57
Stathmin;Stathmin-2	1.48	0.13
Mesencephalic astrocyte-derived neurotrophic factor	1.48	0.10
Heat shock protein 75 kDa, mitochondrial	1.48	0.10
Cell division cycle and apoptosis regulator protein 1	1.48	0.71
Nectin-2	1.47	0.46
Prohibitin-2	1.47	0.11
60S acidic ribosomal protein P0;60S acidic ribosomal protein P0-like	1.47	0.06
Delta-1-pyrroline-5-carboxylate synthase;Glutamate 5-kinase;Gamma-glutamyl phosphate reductase	1.47	0.48
Eukaryotic translation initiation factor 2A;Eukaryotic translation initiation factor 2A, N-terminally processed	1.47	0.59
Purine nucleoside phosphorylase	1.46	0.72
Protein arginine N-methyltransferase 1	1.46	0.18
Protein disulfide-isomerase A4	1.46	0.05
Transferrin receptor protein 1;Transferrin receptor protein 1, serum form	1.46	0.15
26S protease regulatory subunit 6B	1.46	0.34
T-complex protein 1 subunit theta	1.46	0.07
Importin-5	1.46	0.09
Long-chain-fatty-acid--CoA ligase 3	1.45	0.12
GMP synthase [glutamine-hydrolyzing]	1.45	0.11
Tubulin--tyrosine ligase-like protein 12	1.45	0.50
Filamin-B	1.45	0.17
40S ribosomal protein S9	1.45	0.10
Phosphomevalonate kinase	1.45	0.34
T-complex protein 1 subunit alpha	1.44	0.05
Acyl carrier protein, mitochondrial	1.44	0.13

Protein transport protein Sec61 subunit beta	1.44	0.41
Ubiquinone biosynthesis protein COQ9, mitochondrial	1.44	0.76
Dual specificity protein phosphatase 23	1.44	0.71
Transformer-2 protein homolog beta	1.44	0.18
Elongation factor Tu, mitochondrial	1.44	0.08
Endoplasmin	1.44	0.10
Thioredoxin domain-containing protein 12	1.44	0.34
Protein C10	1.44	0.55
Glutaredoxin-3	1.43	0.10
Isoleucine--tRNA ligase, cytoplasmic	1.43	0.05
ADP-sugar pyrophosphatase	1.43	0.14
Survival of motor neuron-related-splicing factor 30	1.43	0.53
T-complex protein 1 subunit beta	1.42	0.11
C-terminal-binding protein 2	1.42	0.15
Sarcoplasmic/endoplasmic reticulum calcium ATPase 2	1.42	0.06
Mitochondrial import inner membrane translocase subunit Tim8 A	1.41	0.08
Eukaryotic translation initiation factor 3 subunit B	1.41	0.04
Hexokinase-1	1.41	0.35
Serine/threonine-protein kinase OSR1	1.41	0.21
Stress-induced-phosphoprotein 1	1.41	0.13
Threonine--tRNA ligase, cytoplasmic	1.41	0.08
Lysine--tRNA ligase	1.41	0.15
Transportin-1	1.40	0.19
T-complex protein 1 subunit gamma	1.40	0.07
60S ribosomal protein L36a-like;60S ribosomal protein L36a	1.40	0.25
Golgi apparatus protein 1	1.40	0.57
Neuropathy target esterase	1.40	0.55
Sterol-4-alpha-carboxylate 3-dehydrogenase, decarboxylating	1.40	0.42
Heterogeneous nuclear ribonucleoproteins C1/C2	1.39	0.12
Nuclear pore complex protein Nup93	1.39	0.06
Hypoxia up-regulated protein 1	1.39	0.08
Acidic leucine-rich nuclear phosphoprotein 32 family member A	1.39	0.21
ATP-citrate synthase	1.39	0.09
Proteasome subunit alpha type-3	1.39	0.14
Nucleoside diphosphate kinase B;Putative nucleoside diphosphate kinase	1.39	0.34
Eukaryotic translation initiation factor 3 subunit J	1.39	0.18
Pyruvate kinase PKM	1.39	0.14
Ribosomal RNA-processing protein 8	1.38	0.55
26S protease regulatory subunit 6A	1.38	0.14
Lamina-associated polypeptide 2, isoforms beta/gamma;Thymopoietin;Thymopentin	1.38	0.23
ATP-dependent RNA helicase DDX3X;ATP-dependent RNA helicase DDX3Y	1.38	0.10

BolA-like protein 2	1.38	0.21
Insulin-like growth factor 2 mRNA-binding protein 1	1.38	0.17
Serine/threonine-protein phosphatase 2A 55 kDa regulatory subunit B alpha isoform	1.38	0.54
40S ribosomal protein S7	1.37	0.69
ES1 protein homolog, mitochondrial	1.37	0.63
Heterogeneous nuclear ribonucleoprotein D0	1.37	0.40
Microsomal glutathione S-transferase 3	1.37	0.57
Ras-related C3 botulinum toxin substrate 1;Ras-related C3 botulinum toxin substrate 3;Ras-related C3 botulinum toxin substrate 2	1.37	0.53
Dolichyl-diphosphooligosaccharide--protein glycosyltransferase subunit 2	1.37	0.57
Desmoplakin	1.37	0.13
Eukaryotic translation initiation factor 3 subunit A	1.37	0.09
Mitochondrial import receptor subunit TOM40 homolog	1.37	0.16
Adenylosuccinate synthetase isozyme 2	1.37	0.26
Coiled-coil domain-containing protein 58	1.36	0.18
60 kDa heat shock protein, mitochondrial	1.36	0.14
60S ribosomal protein L23a	1.36	0.17
Calcyclin-binding protein	1.36	0.17
Glycine--tRNA ligase	1.36	0.08
Copine-3	1.35	0.59
2,4-dienoyl-CoA reductase, mitochondrial	1.35	0.18
60S ribosomal protein L23	1.35	0.55
ADP-ribosylation factor 6	1.35	0.76
Basic leucine zipper and W2 domain-containing protein 2	1.35	0.28
40S ribosomal protein S3a	1.35	0.05
Coatomer subunit epsilon	1.35	0.35
Cellular nucleic acid-binding protein	1.35	0.24
Ubiquitin-conjugating enzyme E2 K	1.35	0.14
Peptidyl-prolyl cis-trans isomerase FKBP4;Peptidyl-prolyl cis-trans isomerase FKBP4, N-terminally processed	1.34	0.13
Fumarate hydratase, mitochondrial	1.34	0.61
CAD protein;Glutamine-dependent carbamoyl-phosphate synthase;Aspartate carbamoyltransferase;Dihydroorotase	1.34	0.21
78 kDa glucose-regulated protein	1.34	0.18
Multifunctional protein ADE2;Phosphoribosylaminoimidazole-succinocarboxamide synthase;Phosphoribosylaminoimidazole carboxylase	1.34	0.12
Ras GTPase-activating protein-binding protein 1	1.34	0.21
Heat shock protein 105 kDa	1.34	0.10
U6 snRNA-associated Sm-like protein LSm2	1.34	0.63
Histone H4	1.33	0.40
NADH-ubiquinone oxidoreductase 75 kDa subunit, mitochondrial	1.33	0.25
FAS-associated factor 2	1.33	0.08

Probable rRNA-processing protein EBP2	1.33	0.55
Vasodilator-stimulated phosphoprotein	1.33	0.09
Heterogeneous nuclear ribonucleoprotein A1;Heterogeneous nuclear ribonucleoprotein A1, N-terminally processed;Heterogeneous nuclear ribonucleoprotein A1-like 2	1.33	0.26
60S ribosomal protein L30	1.33	0.44
Stress-70 protein, mitochondrial	1.33	0.36
Glutathione S-transferase omega-1	1.33	0.27
Derlin-1	1.33	0.28
Serine/threonine-protein phosphatase CPPED1	1.33	0.78
Programmed cell death protein 5	1.33	0.14
ADP-ribosylation factor 4	1.32	0.30
Lamina-associated polypeptide 2, isoform alpha;Thymopoietin;Thymopentin	1.32	0.48
Vesicle-associated membrane protein-associated protein A	1.32	0.53
40S ribosomal protein S10;Putative 40S ribosomal protein S10-like	1.32	0.18
Ubiquitin-associated protein 2-like	1.32	0.14
Basic leucine zipper and W2 domain-containing protein 1	1.32	0.28
Cyclin-T1	1.32	0.71
Ubiquitin-conjugating enzyme E2 N	1.32	0.24
FACT complex subunit SSRP1	1.32	0.22
Ran-specific GTPase-activating protein	1.32	0.46
Nuclear migration protein nudC	1.32	0.67
KH domain-containing, RNA-binding, signal transduction-associated protein 1	1.32	0.52
60S ribosomal protein L11	1.32	0.16
Nucleolar protein 3	1.31	0.71
Calcium-binding mitochondrial carrier protein SCaMC-1	1.31	0.45
Protein ERGIC-53	1.31	0.21
40S ribosomal protein S8	1.31	0.12
Nascent polypeptide-associated complex subunit alpha;Nascent polypeptide-associated complex subunit alpha, muscle-specific form	1.31	0.23
RNA-binding motif protein, X chromosome;RNA-binding motif protein, X chromosome, N-terminally processed;RNA binding motif protein, X-linked-like-1	1.31	0.17
Nuclear autoantigenic sperm protein	1.31	0.59
Isoleucine--tRNA ligase, mitochondrial	1.31	0.33
Coatomer subunit zeta-1	1.31	0.15
Heat shock protein HSP 90-alpha	1.30	0.23
Cytochrome c oxidase subunit 2	1.30	0.52
Importin-9	1.30	0.30
E3 UFM1-protein ligase 1	1.30	0.70
Creatine kinase U-type, mitochondrial	1.30	0.65
Heterogeneous nuclear ribonucleoprotein R	1.30	0.17

Transcription factor BTF3	1.30	0.55
60S ribosomal protein L28	1.30	0.16
RNA-binding protein FUS	1.30	0.31
NEDD8-conjugating enzyme Ubc12	1.30	0.30
Proliferation-associated protein 2G4	1.30	0.23
Alpha-galactosidase A	1.30	0.69
Vacuolar protein sorting-associated protein VTA1 homolog	1.30	0.33
T-complex protein 1 subunit eta	1.30	0.15
60S ribosomal protein L22	1.30	0.15
40S ribosomal protein S5;40S ribosomal protein S5, N-terminally processed	1.30	0.50
Glyceraldehyde-3-phosphate dehydrogenase	1.30	0.32
Oxygen-dependent coproporphyrinogen-III oxidase, mitochondrial	1.30	0.29
ADP/ATP translocase 2;ADP/ATP translocase 2, N-terminally processed	1.30	0.40
ATP-binding cassette sub-family F member 1	1.30	0.11
Protein S100-A4	1.29	0.77
40S ribosomal protein S3	1.29	0.19
Voltage-dependent anion-selective channel protein 1	1.29	0.26
40S ribosomal protein S11	1.29	0.25
Proteasome subunit alpha type-2	1.29	0.28
Signal recognition particle subunit SRP68	1.29	0.68
60S ribosomal protein L8	1.29	0.65
Barrier-to-autointegration factor;Barrier-to-autointegration factor, N-terminally processed	1.29	0.61
Eukaryotic translation initiation factor 2 subunit 1	1.29	0.30
Phosphatidylinositol transfer protein beta isoform	1.29	0.46
Ubiquitin-conjugating enzyme E2 variant 2	1.29	0.14
Alpha-centractin	1.29	0.25
Cytochrome b-c1 complex subunit 8	1.29	0.63
40S ribosomal protein S20	1.29	0.41
10 kDa heat shock protein, mitochondrial	1.28	0.29
Integrin alpha-V;Integrin alpha-V heavy chain;Integrin alpha-V light chain	1.28	0.53
Tryptophan--tRNA ligase, cytoplasmic;T1-TrpRS;T2-TrpRS	1.28	0.32
Tumor protein D52	1.28	0.34
Guanine nucleotide-binding protein subunit beta-2-like 1;Guanine nucleotide-binding protein subunit beta-2-like 1, N-terminally processed	1.28	0.32
Nuclear pore complex protein Nup205	1.28	0.29
Gamma-enolase	1.28	0.54
Cytochrome b-c1 complex subunit Rieske, mitochondrial;Cytochrome b-c1 complex subunit 11;Putative cytochrome b-c1 complex subunit Rieske-like protein 1	1.28	0.25
Heterogeneous nuclear ribonucleoprotein Q	1.28	0.14
Small nuclear ribonucleoprotein-associated protein N;Small nuclear ribonucleoprotein-associated proteins B and B	1.28	0.58

Polyadenylate-binding protein 1	1.28	0.17
Eukaryotic translation initiation factor 2 subunit 2	1.28	0.28
RuvB-like 1	1.28	0.14
DNA damage-binding protein 1	1.28	0.14
40S ribosomal protein S2	1.27	0.23
60S ribosomal protein L3	1.27	0.14
U2 small nuclear ribonucleoprotein B	1.27	0.28
Acidic leucine-rich nuclear phosphoprotein 32 family member B	1.27	0.67
40S ribosomal protein S18	1.27	0.47
Ancient ubiquitous protein 1	1.27	0.61
Tropomyosin alpha-3 chain	1.27	0.55
60S ribosomal protein L10a	1.27	0.18
Reticulocalbin-2	1.27	0.23
Signal recognition particle receptor subunit beta	1.27	0.45
60S ribosomal protein L32	1.26	0.15
Eukaryotic translation initiation factor 4H	1.26	0.41
39S ribosomal protein L12, mitochondrial	1.26	0.33
Plasma membrane calcium-transporting ATPase 1	1.26	0.13
MICOS complex subunit MIC19	1.26	0.53
Myristoylated alanine-rich C-kinase substrate	1.26	0.61
Protein phosphatase methylesterase 1	1.26	0.24
Eukaryotic initiation factor 4A-I	1.26	0.48
Sequestosome-1	1.26	0.59
40S ribosomal protein S28	1.26	0.28
Palmitoyl-protein thioesterase 1	1.26	0.81
Actin, alpha skeletal muscle;Actin, alpha cardiac muscle 1;Actin, gamma-enteric smooth muscle;Actin, aortic smooth muscle	1.26	0.79
Poly [ADP-ribose] polymerase 4	1.26	0.81
RNA-binding protein 25	1.26	0.29
Coiled-coil domain-containing protein 124	1.26	0.83
60S ribosomal protein L7	1.25	0.31
Histone H3.2;Histone H3.1t;Histone H3.3;Histone H3.1;Histone H3.3C	1.25	0.56
Eukaryotic translation initiation factor 4 gamma 1	1.25	0.37
Aspartate--tRNA ligase, cytoplasmic	1.25	0.31
Cofilin-1	1.25	0.09
Eukaryotic translation initiation factor 3 subunit E	1.24	0.45
40S ribosomal protein S25	1.24	0.33
Signal transducer and activator of transcription 1-alpha/beta	1.24	0.70
Junctional adhesion molecule A	1.24	0.78
Adenosine kinase	1.24	0.17
Succinate dehydrogenase [ubiquinone] flavoprotein subunit, mitochondrial	1.24	0.37
Very-long-chain enoyl-CoA reductase	1.24	0.75

Sulfiredoxin-1	1.24	0.79
Lactoylglutathione lyase	1.24	0.37
Bifunctional glutamate/proline--tRNA ligase;Glutamate--tRNA ligase;Proline--tRNA ligase	1.24	0.40
Ras GTPase-activating-like protein IQGAP1	1.24	0.45
Serine-threonine kinase receptor-associated protein	1.23	0.28
Protein phosphatase 1 regulatory subunit 12A	1.23	0.70
Proteasome subunit alpha type-7;Proteasome subunit alpha type-7-like	1.23	0.26
40S ribosomal protein SA	1.23	0.14
Profilin-1	1.23	0.38
Proteasome subunit alpha type-4	1.23	0.64
60S ribosomal protein L27a	1.22	0.45
Leucine-rich repeat-containing protein 59	1.22	0.60
Lipopolysaccharide-responsive and beige-like anchor protein	1.22	0.46
Adenylosuccinate lyase	1.22	0.45
14-3-3 protein eta	1.22	0.59
Cullin-associated NEDD8-dissociated protein 1	1.22	0.18
Eukaryotic translation initiation factor 3 subunit D	1.22	0.56
40S ribosomal protein S6	1.22	0.51
Voltage-dependent anion-selective channel protein 3	1.22	0.23
Mitochondrial import inner membrane translocase subunit Tim13	1.22	0.39
ATP-dependent RNA helicase DDX18	1.22	0.52
Ras-related protein Rab-7a	1.21	0.59
Poly(U)-binding-splicing factor PUF60	1.21	0.25
Tubulin alpha-1C chain	1.21	0.79
Mitochondrial import inner membrane translocase subunit TIM44	1.21	0.75
60S ribosomal protein L13a	1.21	0.37
ATP-dependent DNA helicase Q1	1.21	0.40
Luc7-like protein 3	1.21	0.46
Eukaryotic translation initiation factor 3 subunit G	1.21	0.54
Thioredoxin-dependent peroxide reductase, mitochondrial	1.21	0.70
Thioredoxin reductase 1, cytoplasmic	1.21	0.56
Importin subunit beta-1	1.21	0.46
Calponin-2	1.21	0.61
Na(+)/H(+) exchange regulatory cofactor NHE-RF2	1.21	0.60
Tropomyosin alpha-4 chain	1.21	0.50
Alanine--tRNA ligase, cytoplasmic	1.21	0.32
Elongation factor 1-gamma	1.20	0.54
Carboxypeptidase D	1.20	0.42
Probable ATP-dependent RNA helicase DDX23	1.20	0.69
Signal recognition particle receptor subunit alpha	1.20	0.45
Protein disulfide-isomerase A6	1.20	0.30
Tyrosine-protein kinase BAZ1B	1.20	0.53

Double-stranded RNA-binding protein Staufen homolog 1	1.20	0.68
60S ribosomal protein L15	1.20	0.34
Minor histocompatibility antigen H13	1.20	0.71
Alpha-enolase	1.20	0.48
Translational activator GCN1	1.20	0.24
Malate dehydrogenase, mitochondrial	1.20	0.52
Zinc finger CCCH-type antiviral protein 1-like	1.20	0.82
26S proteasome non-ATPase regulatory subunit 4	1.19	0.35
Ubiquitin thioesterase OTUB1	1.19	0.53
Fascin	1.19	0.64
Platelet-activating factor acetylhydrolase IB subunit alpha	1.19	0.68
Phenylalanine--tRNA ligase beta subunit	1.19	0.30
Serine/threonine-protein kinase MRCK beta	1.19	0.63
Alpha-actinin-1	1.19	0.41
Eukaryotic translation initiation factor 5B	1.19	0.35
Integrin beta-5	1.19	0.42
Protein SET;Protein SETSIP	1.19	0.50
Protein-glutamine gamma-glutamyltransferase 2	1.19	0.68
Ras suppressor protein 1	1.19	0.79
Serpin B6	1.18	0.63
Heterogeneous nuclear ribonucleoproteins A2/B1	1.18	0.25
SEC23-interacting protein	1.18	0.79
F-actin-capping protein subunit alpha-1	1.18	0.27
Eukaryotic translation initiation factor 3 subunit C;Eukaryotic translation initiation factor 3 subunit C-like protein	1.18	0.45
Transmembrane 9 superfamily member 3	1.18	0.54
60S ribosomal protein L21	1.18	0.62
60S ribosomal protein L19	1.18	0.68
Nucleolar and coiled-body phosphoprotein 1	1.18	0.45
Casein kinase II subunit alpha 3;Casein kinase II subunit alpha	1.18	0.25
Calpain-2 catalytic subunit	1.17	0.56
Golgi resident protein GCP60	1.17	0.33
X-ray repair cross-complementing protein 5	1.17	0.61
DNA-dependent protein kinase catalytic subunit	1.17	0.29
Protein phosphatase 1 regulatory subunit 14B	1.17	0.65
TAR DNA-binding protein 43	1.17	0.25
Leucine-rich PPR motif-containing protein, mitochondrial	1.17	0.53
Eukaryotic translation initiation factor 3 subunit L	1.17	0.51
Histidine--tRNA ligase, cytoplasmic	1.17	0.54
Transmembrane emp24 domain-containing protein 2	1.17	0.71
Aminoacyl tRNA synthase complex-interacting multifunctional protein 1;Endothelial monocyte-activating polypeptide 2	1.17	0.70
Glucosamine-6-phosphate isomerase 1;Glucosamine-6-phosphate isomerase 2	1.17	0.80

Tubulin beta chain	1.16	0.69
CD109 antigen	1.16	0.79
Proteasome activator complex subunit 3	1.16	0.55
40S ribosomal protein S14	1.16	0.62
Splicing factor 1	1.16	0.76
B-cell receptor-associated protein 31	1.16	0.55
Nucleolin	1.16	0.59
Cleavage stimulation factor subunit 2;Cleavage stimulation factor subunit 2 tau variant	1.16	0.71
60S ribosomal protein L14	1.16	0.68
Tubulin-folding cofactor B	1.16	0.39
Cytoskeleton-associated protein 4	1.16	0.74
ATP-dependent 6-phosphofructokinase, liver type	1.16	0.64
ATP-binding cassette sub-family E member 1	1.16	0.47
Coiled-coil-helix-coiled-coil-helix domain-containing protein 2;Putative coiled-coil-helix-coiled-coil-helix domain-containing protein CHCHD2P9, mitochondrial	1.16	0.72
Histone H1x	1.16	0.70
40S ribosomal protein S19	1.15	0.34
Basigin	1.15	0.79
40S ribosomal protein S15a	1.15	0.67
General transcription factor IIF subunit 1	1.15	0.78
40S ribosomal protein S27-like	1.15	0.75
Protein disulfide-isomerase A3	1.15	0.56
Calcineurin B homologous protein 3	1.15	0.68
H/ACA ribonucleoprotein complex subunit 3	1.15	0.75
Reticulon-4 receptor-like 2	1.15	0.87
Ubiquitin-40S ribosomal protein S27a;Ubiquitin;40S ribosomal protein S27a;Ubiquitin-60S ribosomal protein L40;Ubiquitin;60S ribosomal protein L40;Polyubiquitin-B;Ubiquitin;Polyubiquitin-C;Ubiquitin	1.15	0.53
Histone-binding protein RBBP4	1.15	0.73
Signal peptidase complex catalytic subunit SEC11A	1.15	0.70
Dihydrolipoyl dehydrogenase, mitochondrial	1.15	0.63
BH3-interacting domain death agonist;BH3-interacting domain death agonist p15;BH3-interacting domain death agonist p13;BH3-interacting domain death agonist p11	1.15	0.76
Rho GTPase-activating protein 18	1.15	0.79
Glucose-6-phosphate 1-dehydrogenase	1.14	0.69
Beta-arrestin-1	1.14	0.75
60S ribosomal protein L4	1.14	0.51
Protein DEK	1.14	0.54
Adenylate kinase 2, mitochondrial;Adenylate kinase 2, mitochondrial, N-terminally processed	1.14	0.42
Ran GTPase-activating protein 1	1.14	0.56
Protein RRP5 homolog	1.14	0.73
60S ribosomal protein L36	1.14	0.51

Beta-centractin	1.14	0.65
Perilipin-3	1.14	0.76
Eukaryotic translation initiation factor 4 gamma 2	1.14	0.59
Arginine--tRNA ligase, cytoplasmic	1.14	0.41
Tumor protein D54	1.14	0.78
Histone deacetylase 1	1.14	0.46
Thioredoxin-like protein 1	1.14	0.74
Spermidine synthase	1.14	0.71
NADH dehydrogenase [ubiquinone] iron-sulfur protein 3, mitochondrial	1.14	0.61
RNA-binding protein 39	1.14	0.53
Elongation factor G, mitochondrial	1.14	0.68
Coronin-1C	1.14	0.54
N-acetylgalactosaminyltransferase 7	1.14	0.82
Pre-mRNA-processing-splicing factor 8	1.14	0.60
Torsin-1A-interacting protein 1	1.13	0.60
Nucleosome assembly protein 1-like 4	1.13	0.50
Probable 28S rRNA (cytosine(4447)-C(5))-methyltransferase	1.13	0.67
Plastin-3	1.13	0.64
Protein SON	1.13	0.73
tRNA pseudouridine synthase A, mitochondrial	1.13	0.57
Glutaredoxin-related protein 5, mitochondrial	1.13	0.69
Vimentin	1.13	0.44
4F2 cell-surface antigen heavy chain	1.13	0.82
OCIA domain-containing protein 1	1.13	0.82
Double-stranded RNA-specific adenosine deaminase	1.13	0.80
Dynactin subunit 1	1.13	0.59
26S proteasome non-ATPase regulatory subunit 6	1.13	0.55
Cytochrome b-c1 complex subunit 1, mitochondrial	1.12	0.60
28 kDa heat- and acid-stable phosphoprotein	1.12	0.69
TBC1 domain family member 15	1.12	0.68
Serine/arginine-rich splicing factor 7	1.12	0.64
40S ribosomal protein S4, X isoform	1.12	0.76
Coatomer subunit beta	1.12	0.77
COP9 signalosome complex subunit 8	1.12	0.61
Inositol 1,4,5-trisphosphate receptor type 3	1.12	0.92
Probable ATP-dependent RNA helicase DDX5	1.12	0.74
RNA-binding protein 14	1.12	0.54
Nuclease-sensitive element-binding protein 1	1.12	0.58
Structural maintenance of chromosomes protein 3	1.12	0.66
26S protease regulatory subunit 8	1.12	0.71
60S ribosomal protein L12	1.12	0.72
ATP synthase subunit e, mitochondrial	1.11	0.71
Transcription elongation factor B polypeptide 1	1.11	0.61
Uncharacterized protein C19orf43	1.11	0.80

6-phosphogluconate dehydrogenase, decarboxylating	1.11	0.53
Spliceosome RNA helicase DDX39B	1.11	0.70
ATP synthase subunit delta, mitochondrial	1.11	0.80
pre-rRNA processing protein FTSJ3	1.11	0.75
26S proteasome non-ATPase regulatory subunit 1	1.11	0.79
ATP synthase subunit f, mitochondrial	1.11	0.69
60S ribosomal protein L27	1.11	0.76
Arf-GAP domain and FG repeat-containing protein 1	1.11	0.73
Protein FAM49B	1.11	0.69
UPF0568 protein C14orf166	1.11	0.74
Polypyrimidine tract-binding protein 1	1.11	0.55
Heterogeneous nuclear ribonucleoprotein D-like	1.11	0.60
Trans-Golgi network integral membrane protein 2	1.11	0.79
Splicing factor 3A subunit 1	1.11	0.69
Signal recognition particle 14 kDa protein	1.10	0.86
Transmembrane emp24 domain-containing protein 7	1.10	0.84
Putative peptidyl-tRNA hydrolase PTRHD1	1.10	0.80
Citrate synthase, mitochondrial	1.10	0.79
Caprin-1	1.10	0.73
Clathrin interactor 1	1.10	0.84
COP9 signalosome complex subunit 2	1.10	0.80
Interleukin enhancer-binding factor 2	1.10	0.56
Cell division control protein 42 homolog	1.10	0.77
Histone H2A type 1-J;Histone H2A type 1-H;Histone H2A.J;Histone H2A type 2-C;Histone H2A type 2-A;Histone H2A type 1-D;Histone H2A type 1	1.10	0.87
Tubulin alpha-1B chain	1.10	0.79
Rab GDP dissociation inhibitor beta	1.10	0.79
Proteasome subunit alpha type-1	1.10	0.74
60S ribosomal protein L18	1.10	0.69
Glucose-6-phosphate isomerase	1.10	0.71
Eukaryotic translation initiation factor 5A-1;Eukaryotic translation initiation factor 5A-1-like	1.10	0.80
MICOS complex subunit MIC60	1.10	0.75
Heterochromatin protein 1-binding protein 3	1.10	0.89
Apoptosis-inducing factor 1, mitochondrial	1.10	0.74
Anamorsin	1.10	0.79
Succinate dehydrogenase [ubiquinone] iron-sulfur subunit, mitochondrial	1.10	0.81
AP-1 complex subunit gamma-1	1.10	0.68
Cation-independent mannose-6-phosphate receptor	1.10	0.60
Protein FAM107B	1.09	0.82
5-nucleotidase domain-containing protein 1	1.09	0.78
Protein phosphatase 1G	1.09	0.79
Zinc finger CCCH domain-containing protein 15	1.09	0.75
NADH dehydrogenase [ubiquinone] flavoprotein 1,	1.09	0.70

mitochondrial		
Zinc finger RNA-binding protein	1.09	0.76
V-type proton ATPase catalytic subunit A	1.09	0.79
RNA-binding protein 8A	1.09	0.78
Rho-related GTP-binding protein RhoG	1.09	0.82
Mitochondrial intermembrane space import and assembly protein 40	1.09	0.82
Clathrin heavy chain 1	1.09	0.79
Prothymosin alpha;Prothymosin alpha, N-terminally processed;Thymosin alpha-1	1.09	0.87
26S protease regulatory subunit 4	1.09	0.81
SUMO-activating enzyme subunit 1;SUMO-activating enzyme subunit 1, N-terminally processed	1.09	0.81
Eukaryotic translation initiation factor 6	1.09	0.70
Phosphoenolpyruvate carboxykinase [GTP], mitochondrial	1.09	0.84
Leukotriene A-4 hydrolase	1.09	0.71
26S proteasome non-ATPase regulatory subunit 11	1.09	0.68
Mitogen-activated protein kinase 1	1.09	0.89
Integrin beta-1	1.09	0.82
Putative RNA-binding protein Luc7-like 2	1.09	0.82
Protein arginine N-methyltransferase 5;Protein arginine N-methyltransferase 5, N-terminally processed	1.09	0.68
Protein S100-A13	1.08	0.90
ADP-ribosylation factor 1;ADP-ribosylation factor 3	1.08	0.78
ADP-ribosylation factor-like protein 6-interacting protein 1	1.08	0.91
Desmoglein-2	1.08	0.92
SUMO-activating enzyme subunit 2	1.08	0.71
Small nuclear ribonucleoprotein Sm D1	1.08	0.83
FACT complex subunit SPT16	1.08	0.85
Splicing factor 3B subunit 3	1.08	0.70
Protein deglycase DJ-1	1.08	0.69
Nucleolar transcription factor 1	1.08	0.79
SRA stem-loop-interacting RNA-binding protein, mitochondrial	1.08	0.81
Sulfide:quinone oxidoreductase, mitochondrial	1.08	0.79
Nucleoprotein TPR	1.08	0.76
NADH dehydrogenase [ubiquinone] flavoprotein 2, mitochondrial	1.08	0.71
Tumor suppressor p53-binding protein 1	1.08	0.70
Drebrin	1.08	0.85
Peroxisomal multifunctional enzyme type 2;(3R)-hydroxyacyl-CoA dehydrogenase;Enoyl-CoA hydratase 2	1.08	0.82
Secernin-1	1.08	0.87
Annexin A1	1.08	0.84
Annexin A7	1.08	0.78
Heat shock cognate 71 kDa protein	1.08	0.80
Protein disulfide-isomerase	1.08	0.83

Platelet-activating factor acetylhydrolase IB subunit gamma	1.07	0.71
40S ribosomal protein S17	1.07	0.89
Serine/arginine repetitive matrix protein 2	1.07	0.81
RuvB-like 2	1.07	0.75
Calnexin	1.07	0.71
Secretory carrier-associated membrane protein 3	1.07	0.80
Peroxiredoxin-4	1.07	0.68
Methionine aminopeptidase 2	1.07	0.84
Peptidyl-prolyl cis-trans isomerase A;Peptidyl-prolyl cis-trans isomerase A, N-terminally processed	1.07	0.81
Heterogeneous nuclear ribonucleoprotein U	1.07	0.70
Triosephosphate isomerase	1.07	0.71
Ubiquitin carboxyl-terminal hydrolase 14	1.07	0.86
Tyrosine--tRNA ligase, cytoplasmic;Tyrosine--tRNA ligase, cytoplasmic, N-terminally processed	1.07	0.80
Staphylococcal nuclease domain-containing protein 1	1.07	0.75
NADH dehydrogenase [ubiquinone] 1 alpha subcomplex subunit 10, mitochondrial	1.07	0.79
NSFL1 cofactor p47	1.07	0.81
L-lactate dehydrogenase B chain	1.07	0.77
Cytochrome c oxidase subunit 5B, mitochondrial	1.07	0.82
26S proteasome non-ATPase regulatory subunit 13	1.07	0.79
Eukaryotic initiation factor 4A-III;Eukaryotic initiation factor 4A-III, N-terminally processed	1.07	0.86
Inosine triphosphate pyrophosphatase	1.06	0.83
Coatomer subunit gamma-1	1.06	0.79
14-3-3 protein epsilon	1.06	0.81
Dolichyl-diphosphooligosaccharide--protein glycosyltransferase 48 kDa subunit	1.06	0.75
Protein diaphanous homolog 1	1.06	0.86
Glutamine--tRNA ligase	1.06	0.78
Vesicular integral-membrane protein VIP36	1.06	0.77
LIM and cysteine-rich domains protein 1	1.06	0.90
Dehydrogenase/reductase SDR family member 7	1.06	0.96
26S proteasome non-ATPase regulatory subunit 3	1.06	0.80
Aldo-keto reductase family 1 member C2	1.05	0.89
Chromobox protein homolog 3	1.05	0.88
Poly [ADP-ribose] polymerase 1	1.05	0.83
Mitochondrial import receptor subunit TOM70	1.05	0.87
Dihydrolipoyllysine-residue succinyltransferase component of 2-oxoglutarate dehydrogenase complex, mitochondrial	1.05	0.89
Macrophage-capping protein	1.05	0.94
14-3-3 protein sigma	1.05	0.92
Atlastin-3	1.05	0.89
Dynactin subunit 2	1.05	0.86
Multidrug resistance-associated protein 1	1.05	0.94
Heterogeneous nuclear ribonucleoprotein K	1.05	0.83

F-actin-capping protein subunit beta	1.05	0.90
Hydroxyacylglutathione hydrolase, mitochondrial	1.05	0.94
S-formylglutathione hydrolase	1.05	0.86
Coatomer subunit delta	1.05	0.84
Sideroflexin-1	1.05	0.89
Probable ATP-dependent RNA helicase DDX46	1.05	0.85
DnaJ homolog subfamily A member 1	1.05	0.84
Adenylyl cyclase-associated protein 1	1.05	0.92
Lamin-B1	1.05	0.85
Ezrin	1.05	0.91
Regulator of chromosome condensation	1.04	0.86
Acyl-coenzyme A thioesterase 9, mitochondrial	1.04	0.91
Cytochrome c oxidase subunit 4 isoform 1, mitochondrial	1.04	0.88
Biliverdin reductase A	1.04	0.91
Microtubule-associated protein RP/EB family member 1	1.04	0.88
PEST proteolytic signal-containing nuclear protein	1.04	0.94
60S ribosomal protein L17	1.04	0.92
26S protease regulatory subunit 10B	1.04	0.92
Asparagine--tRNA ligase, cytoplasmic	1.04	0.85
26S proteasome non-ATPase regulatory subunit 8	1.04	0.88
Leucine--tRNA ligase, cytoplasmic	1.04	0.83
X-ray repair cross-complementing protein 6	1.04	0.86
Apolipoprotein B-100;Apolipoprotein B-48	1.04	0.96
Peroxiredoxin-5, mitochondrial	1.04	0.94
Adipocyte plasma membrane-associated protein	1.04	0.92
Dolichyl-diphosphooligosaccharide--protein glycosyltransferase subunit 1	1.04	0.86
U5 small nuclear ribonucleoprotein 200 kDa helicase	1.04	0.82
Aflatoxin B1 aldehyde reductase member 2	1.04	0.94
60S ribosomal protein L13	1.04	0.90
Inositol monophosphatase 1	1.04	0.91
RNA-binding protein with multiple splicing	1.04	0.96
Zinc finger CCCH-type antiviral protein 1	1.03	0.93
Density-regulated protein	1.03	0.91
Signal recognition particle subunit SRP72	1.03	0.93
60S ribosomal protein L5	1.03	0.87
Histone H2B type 1-L;Histone H2B type 1-M;Histone H2B type 1-N;Histone H2B type 1-H;Histone H2B type 2-F;Histone H2B type 1-C/E/F/G/I;Histone H2B type 1-D;Histone H2B type F-S;Histone H2B type 1-K;Histone H2B type 1-A	1.03	0.96
60S ribosomal protein L35a	1.03	0.93
Ras-related protein Rab-2A	1.03	0.92
U2 small nuclear ribonucleoprotein A	1.03	0.94
Elongation factor 1-alpha 2	1.03	0.98
General vesicular transport factor p115	1.03	0.94

60S acidic ribosomal protein P2	1.03	0.92
E3 ubiquitin-protein ligase UBR4	1.03	0.92
Nucleophosmin	1.03	0.96
Glucosidase 2 subunit beta	1.03	0.94
Peroxiredoxin-6	1.03	0.90
Macrophage migration inhibitory factor	1.02	0.95
Platelet-activating factor acetylhydrolase IB subunit beta	1.02	0.92
Peroxiredoxin-1	1.02	0.94
Annexin A11	1.02	0.93
Aspartate aminotransferase, mitochondrial	1.02	0.90
Pyruvate dehydrogenase E1 component subunit beta, mitochondrial	1.02	0.94
40S ribosomal protein S21	1.02	0.94
Dolichyl-diphosphooligosaccharide--protein glycosyltransferase subunit STT3A	1.02	0.92
Eukaryotic translation initiation factor 2 subunit 3;Putative eukaryotic translation initiation factor 2 subunit 3-like protein	1.02	0.94
H/ACA ribonucleoprotein complex subunit 1	1.02	0.97
Protein PRRC2C	1.02	0.96
Pre-mRNA-processing factor 19	1.02	0.94
Protein S100-A16	1.02	0.97
Valine--tRNA ligase	1.02	0.92
Inorganic pyrophosphatase 2, mitochondrial	1.02	0.94
5-3 exoribonuclease 2	1.02	0.97
Integrin alpha-3;Integrin alpha-3 heavy chain;Integrin alpha-3 light chain	1.02	0.94
Phosphate carrier protein, mitochondrial	1.02	0.96
Uncharacterized protein C7orf50	1.02	0.96
Probable ATP-dependent RNA helicase DDX6	1.02	0.96
Importin subunit alpha-3	1.02	0.97
Pre-mRNA-splicing factor ATP-dependent RNA helicase DHX15	1.01	0.96
Nuclear pore membrane glycoprotein 210	1.01	0.96
THUMP domain-containing protein 1	1.01	0.96
Coatomer subunit alpha;Xenin;Proxenin	1.01	0.96
ATP synthase subunit O, mitochondrial	1.01	0.97
Lupus La protein	1.01	0.98
Activated RNA polymerase II transcriptional coactivator p15	1.01	0.97
Tubulin beta-2A chain;Tubulin beta-2B chain	1.01	0.97
Serpin B9	1.01	0.98
UMP-CMP kinase	1.01	0.97
Myb-binding protein 1A	1.01	0.97
Non-specific lipid-transfer protein	1.01	0.96
116 kDa U5 small nuclear ribonucleoprotein component	1.01	0.97
Aldo-keto reductase family 1 member C3	1.01	0.98
Tubulin beta-4B chain	1.01	0.96

Dolichyl-diphosphooligosaccharide--protein glycosyltransferase subunit DAD1	1.01	0.98
Peroxisomal trans-2-enoyl-CoA reductase	1.01	0.99
Transitional endoplasmic reticulum ATPase	1.00	0.99
Endoplasmic reticulum resident protein 44	1.00	0.99
Acyl-CoA-binding protein	1.00	0.99
ATP-dependent RNA helicase A	1.00	0.99
Mitochondrial 2-oxoglutarate/malate carrier protein	1.00	0.99
NAD(P)H dehydrogenase [quinone] 1	1.00	0.99
Low molecular weight phosphotyrosine protein phosphatase	1.00	1.00
Serpin H1	1.00	1.00
DnaJ homolog subfamily A member 2	1.00	1.00
Spermatogenesis-associated serine-rich protein 2	1.00	0.99
CD99 antigen-like protein 2	1.00	1.00
UDP-glucose:glycoprotein glucosyltransferase 1	1.00	0.99
Splicing factor, proline- and glutamine-rich	1.00	0.99
Tetratricopeptide repeat protein 1	1.00	0.99
Hypoxanthine-guanine phosphoribosyltransferase	1.00	0.99
Tubulin-specific chaperone A	1.00	0.99
Clustered mitochondria protein homolog	0.99	0.99
Ras-related protein Rab-6B;Ras-related protein Rab-6A	0.99	0.99
Heterogeneous nuclear ribonucleoprotein L	0.99	0.97
Protein unc-45 homolog A	0.99	0.98
Transmembrane protein 43	0.99	0.98
Host cell factor 1;HCF N-terminal chain 1;HCF N-terminal chain 2;HCF N-terminal chain 3;HCF N-terminal chain 4;HCF N-terminal chain 5;HCF N-terminal chain 6;HCF C-terminal chain 1;HCF C-terminal chain 2;HCF C-terminal chain 3;HCF C-terminal chain 4;HCF C-terminal chain 5;HCF C-terminal chain 6	0.99	0.98
Enhancer of rudimentary homolog	0.99	0.99
Ubiquilin-2	0.99	0.99
Cytoplasmic dynein 1 heavy chain 1	0.99	0.97
YTH domain-containing family protein 3	0.99	0.98
Secretogranin-1;PE-11;GAWK peptide;CCB peptide	0.99	0.99
D-dopachrome decarboxylase;D-dopachrome decarboxylase-like protein	0.99	0.98
Vigilin	0.99	0.97
Exportin-1	0.99	0.97
Apoptotic chromatin condensation inducer in the nucleus	0.99	0.98
cAMP-regulated phosphoprotein 19	0.99	0.98
14-3-3 protein gamma;14-3-3 protein gamma, N-terminally processed	0.99	0.97
ADP-ribosylation factor-like protein 8B;ADP-ribosylation factor-like protein 8A	0.99	0.99
60S ribosomal protein L24	0.99	0.97
V-type proton ATPase subunit G 1;V-type proton ATPase	0.98	0.96

subunit G 2		
Transcription elongation factor B polypeptide 2	0.98	0.96
Peptidyl-prolyl cis-trans isomerase B	0.98	0.96
DNA topoisomerase 2-beta	0.98	0.94
Heterogeneous nuclear ribonucleoprotein M	0.98	0.95
WD repeat-containing protein 1	0.98	0.94
Vacuolar protein sorting-associated protein 4B;Vacuolar protein sorting-associated protein 4A	0.98	0.95
Serine/threonine-protein phosphatase PP1-alpha catalytic subunit	0.98	0.97
Elongation factor 1-delta	0.98	0.96
General transcription factor II-I	0.98	0.94
Guanine nucleotide-binding protein G(I)/G(S)/G(T) subunit beta-2;Guanine nucleotide-binding protein subunit beta-4	0.98	0.96
ATP synthase subunit gamma, mitochondrial	0.98	0.93
Cytoplasmic dynein 1 intermediate chain 2	0.98	0.95
Ras-related protein Rab-1B	0.98	0.93
Adenine phosphoribosyltransferase	0.98	0.94
Ribosomal L1 domain-containing protein 1	0.98	0.93
Serine/arginine-rich splicing factor 1	0.97	0.93
Splicing factor 3A subunit 3	0.97	0.92
Twinfilin-1	0.97	0.92
Splicing factor U2AF 65 kDa subunit	0.97	0.96
Hsc70-interacting protein;Putative protein FAM10A4;Putative protein FAM10A5	0.97	0.93
2,3-cyclic-nucleotide 3-phosphodiesterase	0.97	0.97
Ras-related protein Rab-11B	0.97	0.92
Nucleoporin NUP53	0.97	0.93
NADPH--cytochrome P450 reductase	0.97	0.94
Transcription intermediary factor 1-beta	0.97	0.91
Serine/threonine-protein phosphatase 2A catalytic subunit beta isoform	0.97	0.89
60S ribosomal protein L6	0.97	0.91
Septin-2	0.97	0.92
Membrane-associated progesterone receptor component 2	0.97	0.92
Eukaryotic translation initiation factor 3 subunit I	0.97	0.91
ATP synthase subunit alpha, mitochondrial	0.97	0.89
28S ribosomal protein S23, mitochondrial	0.97	0.93
U1 small nuclear ribonucleoprotein 70 kDa	0.97	0.85
Serine/threonine-protein phosphatase 2A 65 kDa regulatory subunit A alpha isoform	0.97	0.88
Serine/arginine-rich splicing factor 3	0.97	0.90
ATP synthase subunit d, mitochondrial	0.97	0.87
UDP-glucose 6-dehydrogenase	0.97	0.91
Rab GDP dissociation inhibitor alpha	0.97	0.92
Protein LYRIC	0.96	0.89
NADH dehydrogenase [ubiquinone] 1 alpha subcomplex	0.96	0.95

subunit 6		
NADH dehydrogenase [ubiquinone] iron-sulfur protein 2, mitochondrial	0.96	0.89
Melanophilin	0.96	0.98
Nicotinamide phosphoribosyltransferase	0.96	0.96
C-Jun-amino-terminal kinase-interacting protein 4	0.96	0.92
Vacuolar protein sorting-associated protein 35	0.96	0.86
Heterogeneous nuclear ribonucleoprotein H;Heterogeneous nuclear ribonucleoprotein H, N-terminally processed	0.96	0.89
RNA-binding protein 4	0.96	0.89
Vinculin	0.96	0.82
Isocitrate dehydrogenase [NAD] subunit alpha, mitochondrial	0.96	0.88
AP-2 complex subunit beta	0.96	0.90
Heat shock 70 kDa protein 4	0.96	0.89
Eukaryotic translation initiation factor 5	0.96	0.83
Programmed cell death protein 4	0.96	0.88
Tubulin beta-3 chain	0.96	0.89
26S proteasome non-ATPase regulatory subunit 12	0.96	0.87
FLYWCH family member 2	0.96	0.90
Thioredoxin domain-containing protein 5	0.95	0.91
dCTP pyrophosphatase 1	0.95	0.89
Calcium-binding mitochondrial carrier protein Aralar2	0.95	0.81
AP-3 complex subunit beta-1	0.95	0.83
Dolichyl-diphosphooligosaccharide--protein glycosyltransferase subunit STT3B	0.95	0.89
Sorting nexin-1	0.95	0.89
Cytochrome b-c1 complex subunit 2, mitochondrial	0.95	0.84
NADH dehydrogenase [ubiquinone] 1 alpha subcomplex subunit 2	0.95	0.83
Acetyl-CoA acetyltransferase, mitochondrial	0.95	0.89
C-1-tetrahydrofolate synthase, cytoplasmic;Methylenetetrahydrofolate dehydrogenase;Methenyltetrahydrofolate cyclohydrolase;Formyltetrahydrofolate synthetase;C-1-tetrahydrofolate synthase, cytoplasmic, N-terminally processed	0.95	0.86
Paraspeckle component 1	0.95	0.81
3(2),5-bisphosphate nucleotidase 1	0.95	0.86
Programmed cell death 6-interacting protein	0.95	0.76
Actin, cytoplasmic 1;Actin, cytoplasmic 1, N-terminally processed	0.95	0.81
Myeloid-associated differentiation marker	0.95	0.89
Pescadillo homolog	0.95	0.89
Mitotic checkpoint protein BUB3	0.95	0.81
ATP synthase subunit beta, mitochondrial	0.95	0.80
Talin-1	0.95	0.80
Omega-amidase NIT2	0.95	0.82

Extended synaptotagmin-1	0.94	0.83
U2 snRNP-associated SURP motif-containing protein	0.94	0.86
Ubiquitin carboxyl-terminal hydrolase 5	0.94	0.76
Aldose reductase	0.94	0.92
Baculoviral IAP repeat-containing protein 6	0.94	0.90
Ras-related protein Rab-5C	0.94	0.77
Protein TFG	0.94	0.80
Protein CDV3 homolog	0.94	0.87
Glutathione reductase, mitochondrial	0.94	0.82
SAP domain-containing ribonucleoprotein	0.94	0.80
Bleomycin hydrolase	0.94	0.92
Cytochrome b-c1 complex subunit 7	0.94	0.85
Splicing factor 3B subunit 1	0.94	0.81
26S protease regulatory subunit 7	0.94	0.78
Cell division cycle 5-like protein	0.94	0.79
Guanine nucleotide-binding protein G(k) subunit alpha	0.93	0.83
Polyadenylate-binding protein 2	0.93	0.80
Aminoacylase-1	0.93	0.82
Copper transport protein ATOX1	0.93	0.86
Vacuolar protein sorting-associated protein 26A	0.93	0.82
Proteasome inhibitor PI31 subunit	0.93	0.87
Cytoplasmic dynein 1 light intermediate chain 1	0.93	0.74
Lysophosphatidylcholine acyltransferase 1	0.93	0.74
Nuclear pore complex protein Nup98-Nup96;Nuclear pore complex protein Nup98;Nuclear pore complex protein Nup96	0.93	0.81
LIM and calponin homology domains-containing protein 1	0.93	0.93
Protein-L-isoaspartate(D-aspartate) O-methyltransferase	0.93	0.86
Sorting nexin-3	0.93	0.86
Mitochondrial carrier homolog 2	0.93	0.85
Electron transfer flavoprotein subunit alpha, mitochondrial	0.93	0.71
Leucine-rich repeat-containing protein 47	0.93	0.80
Hematological and neurological expressed 1-like protein	0.93	0.83
Delta(3,5)-Delta(2,4)-dienoyl-CoA isomerase, mitochondrial	0.93	0.83
45 kDa calcium-binding protein	0.93	0.82
Nucleolar GTP-binding protein 1	0.93	0.89
CD2-associated protein	0.93	0.79
Glutathione S-transferase P	0.93	0.87
Developmentally-regulated GTP-binding protein 1	0.93	0.76
Shootin-1	0.93	0.71
Diablo homolog, mitochondrial	0.93	0.75
Thiosulfate sulfurtransferase	0.92	0.75
Glycylpeptide N-tetradecanoyltransferase 1	0.92	0.87
Ras-related protein R-Ras	0.92	0.89
SWI/SNF-related matrix-associated actin-dependent regulator of chromatin subfamily A member 5	0.92	0.84

RNA-binding protein Raly	0.92	0.76
Clusterin;Clusterin beta chain;Clusterin alpha chain	0.92	0.87
Ras-related protein Ral-B	0.92	0.92
Proteasome subunit beta type-1	0.92	0.74
Cadherin-17	0.92	0.89
Serine/threonine-protein kinase PAK 2;PAK-2p27;PAK-2p34	0.92	0.79
Actin-related protein 3	0.92	0.68
Protein transport protein Sec24C	0.92	0.71
14-3-3 protein zeta/delta	0.92	0.79
Ubiquitin-like modifier-activating enzyme 1	0.91	0.70
Protein S100-A10	0.91	0.86
Drebrin-like protein	0.91	0.77
Lamin-B2	0.91	0.71
Phospholipase D3	0.91	0.74
Cytochrome c-type heme lyase	0.91	0.65
Chloride intracellular channel protein 1	0.91	0.74
PRA1 family protein 3	0.91	0.86
Importin subunit alpha-7;Importin subunit alpha-6	0.91	0.61
Small acidic protein	0.91	0.73
3-mercaptopyruvate sulfurtransferase	0.91	0.75
Kynureninase	0.90	0.80
Cleavage and polyadenylation specificity factor subunit 6	0.90	0.66
Non-POU domain-containing octamer-binding protein	0.90	0.75
Alpha-actinin-4	0.90	0.74
Adenosylhomocysteinase	0.90	0.71
Serine/arginine-rich splicing factor 10;Serine/arginine-rich splicing factor 12	0.90	0.80
Protein SEC13 homolog	0.90	0.53
Kinectin	0.90	0.55
Serine/threonine-protein phosphatase PP1-beta catalytic subunit	0.90	0.61
Protein NipSnap homolog 1	0.90	0.86
Sorbitol dehydrogenase	0.90	0.84
ATP-binding cassette sub-family F member 2	0.90	0.80
Double-strand break repair protein MRE11A	0.90	0.77
Enoyl-CoA hydratase, mitochondrial	0.90	0.76
Glycogen phosphorylase, brain form	0.90	0.74
Ras-related protein Rab-14	0.90	0.69
Exportin-7	0.90	0.65
tRNA-splicing ligase RtcB homolog	0.90	0.73
Ceruloplasmin	0.90	0.80
RUN and FYVE domain-containing protein 1	0.90	0.65
Far upstream element-binding protein 1	0.90	0.71
Serine/threonine-protein kinase PAK 4	0.90	0.71
Succinyl-CoA ligase [ADP/GDP-forming] subunit alpha, mitochondrial	0.90	0.80

Endoplasmic reticulum metallopeptidase 1	0.89	0.78
Charged multivesicular body protein 2a	0.89	0.81
GTP-binding protein SAR1a	0.89	0.79
Lysophospholipid acyltransferase 7	0.89	0.62
Cleavage and polyadenylation specificity factor subunit 5	0.89	0.77
Alcohol dehydrogenase class-3	0.89	0.63
Reticulocalbin-1	0.89	0.73
Apoptosis inhibitor 5	0.89	0.28
THO complex subunit 4	0.89	0.61
F-actin-capping protein subunit alpha-2	0.89	0.67
Bifunctional purine biosynthesis protein PURH;Phosphoribosylaminoimidazolecarboxamide formyltransferase;IMP cyclohydrolase	0.89	0.57
26S proteasome non-ATPase regulatory subunit 2	0.89	0.73
Probable ATP-dependent RNA helicase DDX17	0.89	0.58
DNA-(apurinic or apyrimidinic site) lyase;DNA-(apurinic or apyrimidinic site) lyase, mitochondrial	0.89	0.71
Radixin	0.89	0.75
Interferon regulatory factor 2-binding protein 2	0.89	0.73
Nuclear protein localization protein 4 homolog	0.89	0.57
Programmed cell death protein 6	0.89	0.79
ATP-dependent RNA helicase DDX1	0.89	0.57
Methionine adenosyltransferase 2 subunit beta	0.88	0.53
Peptidyl-prolyl cis-trans isomerase-like 1	0.88	0.76
Endothelial differentiation-related factor 1	0.88	0.55
Heme-binding protein 2	0.88	0.66
Nucleobindin-1	0.88	0.69
NADH dehydrogenase [ubiquinone] 1 alpha subcomplex subunit 8	0.88	0.62
Carbonic anhydrase 12	0.88	0.78
Heterogeneous nuclear ribonucleoprotein H3	0.88	0.72
Transmembrane emp24 domain-containing protein 10	0.88	0.74
Ras-related protein Rab-1A	0.88	0.91
Nuclear mitotic apparatus protein 1	0.88	0.45
Cytochrome P450 2S1	0.88	0.88
Matrin-3	0.87	0.72
Puromycin-sensitive aminopeptidase	0.87	0.51
ADP-ribosylation factor-like protein 1	0.87	0.70
Partner of Y14 and mago	0.87	0.66
Transcription elongation factor A protein 1	0.87	0.73
Thioredoxin	0.87	0.69
Serine/threonine-protein phosphatase 2A activator	0.87	0.63
Ras-related protein Rab-10	0.87	0.75
Chromobox protein homolog 5	0.87	0.85
Inorganic pyrophosphatase	0.87	0.53
14-3-3 protein beta/alpha;14-3-3 protein beta/alpha, N-	0.87	0.55

terminally processed		
Aminopeptidase B	0.87	0.37
Guanine nucleotide-binding protein G(I)/G(S)/G(T) subunit beta-1	0.87	0.63
Proteolipid protein 2	0.87	0.75
ATP-dependent RNA helicase DDX19A;ATP-dependent RNA helicase DDX19B	0.87	0.61
26S proteasome non-ATPase regulatory subunit 9	0.87	0.55
AP-2 complex subunit alpha-2	0.87	0.70
Charged multivesicular body protein 4b	0.87	0.28
Myosin-9	0.87	0.61
Small ubiquitin-related modifier 1	0.87	0.71
U6 snRNA-associated Sm-like protein LSm3	0.86	0.75
Cytochrome c oxidase subunit 6C	0.86	0.85
Apoptosis regulator BAX	0.86	0.64
Splicing factor 3B subunit 2	0.86	0.55
Sodium/potassium-transporting ATPase subunit beta-1	0.86	0.75
Calcium-binding mitochondrial carrier protein Aralar1	0.86	0.70
Trifunctional enzyme subunit alpha, mitochondrial;Long-chain enoyl-CoA hydratase;Long chain 3-hydroxyacyl-CoA dehydrogenase	0.86	0.32
Probable ATP-dependent RNA helicase DDX27	0.86	0.67
Oxidoreductase HTATIP2	0.86	0.89
Persulfide dioxygenase ETHE1, mitochondrial	0.86	0.70
Kinesin-1 heavy chain	0.86	0.47
60 kDa SS-A/Ro ribonucleoprotein	0.86	0.63
rRNA 2-O-methyltransferase fibrillarin	0.86	0.57
Protein kinase C alpha type	0.86	0.71
Sodium/potassium-transporting ATPase subunit alpha-1;Sodium/potassium-transporting ATPase subunit alpha-3;Sodium/potassium-transporting ATPase subunit alpha-2	0.86	0.64
Electron transfer flavoprotein subunit beta	0.86	0.28
Dynamin-1	0.86	0.71
Adapter molecule crk	0.86	0.55
Tropomodulin-3	0.86	0.52
Transmembrane emp24 domain-containing protein 9	0.86	0.52
High mobility group protein HMG-I/HMG-Y	0.85	0.77
Cyclin-dependent kinase inhibitor 1B	0.85	0.75
SNW domain-containing protein 1	0.85	0.79
SH3 domain-binding glutamic acid-rich-like protein	0.85	0.69
Vesicle-fusing ATPase	0.85	0.30
S-phase kinase-associated protein 1	0.85	0.70
ATP synthase-coupling factor 6, mitochondrial	0.85	0.70
RNA-binding protein EWS	0.85	0.46
Malate dehydrogenase, cytoplasmic	0.85	0.52
Fragile X mental retardation syndrome-related protein 1	0.85	0.79

Carcinoembryonic antigen-related cell adhesion molecule 6	0.85	0.93
Carbonyl reductase [NADPH] 1	0.85	0.61
AP-1 complex subunit mu-1	0.85	0.71
Cytochrome c oxidase assembly factor 6 homolog	0.85	0.50
Prosaposin;Saposin-A;Saposin-B-Val;Saposin-B;Saposin-C;Saposin-D	0.85	0.45
Enoyl-CoA delta isomerase 1, mitochondrial	0.84	0.50
H/ACA ribonucleoprotein complex subunit 4	0.84	0.29
Aconitate hydratase, mitochondrial	0.84	0.49
Cystatin-B	0.84	0.76
Alcohol dehydrogenase 6	0.84	0.88
Septin-7	0.84	0.36
AP-2 complex subunit alpha-1	0.84	0.30
Mucin-5B	0.84	0.89
Coronin-1B	0.84	0.82
ELAV-like protein 1	0.84	0.61
Y-box-binding protein 3	0.84	0.54
Microtubule-associated protein 4	0.84	0.47
Actin-related protein 2/3 complex subunit 4	0.84	0.61
Calpain-1 catalytic subunit	0.84	0.29
Unconventional myosin-Ib	0.84	0.72
Thioredoxin domain-containing protein 17	0.84	0.61
Nucleoside diphosphate kinase 3	0.84	0.55
cAMP-dependent protein kinase type II-alpha regulatory subunit	0.84	0.24
Cytochrome c oxidase subunit 6B1	0.84	0.63
Phosphoglucomutase-1	0.84	0.45
Peptidyl-prolyl cis-trans isomerase FKBP3	0.84	0.25
Cell cycle and apoptosis regulator protein 2	0.84	0.34
Interleukin enhancer-binding factor 3	0.84	0.32
NADH dehydrogenase [ubiquinone] iron-sulfur protein 6, mitochondrial	0.84	0.60
Catalase	0.83	0.64
Protein transport protein Sec23A	0.83	0.47
Clathrin light chain A	0.83	0.55
Heterogeneous nuclear ribonucleoprotein U-like protein 2	0.83	0.41
NADH dehydrogenase [ubiquinone] 1 alpha subcomplex subunit 12	0.83	0.29
Actin-related protein 2/3 complex subunit 1B	0.83	0.26
Putative adenosylhomocysteinase 2;Putative adenosylhomocysteinase 3	0.83	0.29
Neuropilin-1	0.83	0.59
Malectin	0.83	0.26
Proline synthase co-transcribed bacterial homolog protein	0.83	0.79
Heterogeneous nuclear ribonucleoprotein H2	0.83	0.28
Histone H2A.V;Histone H2A.Z	0.83	0.50

S-adenosylmethionine synthase isoform type-2	0.83	0.29
High mobility group protein B1	0.83	0.68
GTP:AMP phosphotransferase AK3, mitochondrial	0.83	0.68
Endoplasmic reticulum resident protein 29	0.83	0.62
Protein flightless-1 homolog	0.82	0.39
Pyruvate dehydrogenase E1 component subunit alpha, somatic form, mitochondrial	0.82	0.83
N(G),N(G)-dimethylarginine dimethylaminohydrolase 2	0.82	0.16
	0.82	0.61
Aspartate aminotransferase, cytoplasmic	0.82	0.36
Vesicle-associated membrane protein-associated protein B/C	0.82	0.32
Spectrin beta chain, non-erythrocytic 1	0.82	0.21
Syndecan-1	0.82	0.74
Charged multivesicular body protein 4a	0.82	0.40
Leucine-rich repeat flightless-interacting protein 1	0.82	0.42
Melanoma-associated antigen D2	0.82	0.54
Alkyldihydroxyacetonephosphate synthase, peroxisomal	0.82	0.13
Medium-chain specific acyl-CoA dehydrogenase, mitochondrial	0.82	0.12
Cleft lip and palate transmembrane protein 1	0.82	0.79
Lysosome membrane protein 2	0.82	0.59
Calpain small subunit 1	0.82	0.53
Protein FAM134C	0.82	0.61
Pterin-4-alpha-carbinolamine dehydratase	0.81	0.53
Aldehyde dehydrogenase, dimeric NADP-preferring	0.81	0.71
Far upstream element-binding protein 2	0.81	0.42
Phylloquinone omega-hydroxylase CYP4F11;Phylloquinone omega-hydroxylase CYP4F2;Docosahexaenoic acid omega-hydroxylase CYP4F3;Cytochrome P450 4F12	0.81	0.80
UPF0160 protein MYG1, mitochondrial	0.81	0.38
Dynein light chain 1, cytoplasmic	0.81	0.54
Gelsolin	0.81	0.41
Echinoderm microtubule-associated protein-like 4	0.81	0.58
Rho-related GTP-binding protein RhoC	0.81	0.57
Flavin reductase (NADPH)	0.81	0.25
Very long-chain specific acyl-CoA dehydrogenase, mitochondrial	0.81	0.13
LanC-like protein 1	0.81	0.66
Core histone macro-H2A.1	0.81	0.20
Histidine triad nucleotide-binding protein 1	0.81	0.65
E3 ubiquitin-protein ligase HUWE1	0.81	0.10
Protein S100-A11;Protein S100-A11, N-terminally processed	0.81	0.76
Small glutamine-rich tetratricopeptide repeat-containing protein alpha	0.80	0.73
Cytosol aminopeptidase	0.80	0.53
Rabankyrin-5	0.80	0.53
Protein transport protein Sec31A	0.80	0.33

1,4-alpha-glucan-branching enzyme	0.80	0.57
MARCKS-related protein	0.80	0.34
Poly(rC)-binding protein 1	0.80	0.23
Ribosome maturation protein SBDS	0.80	0.78
E3 SUMO-protein ligase RanBP2	0.80	0.28
Interferon-inducible double-stranded RNA-dependent protein kinase activator A	0.80	0.36
ATP-dependent RNA helicase DDX42	0.80	0.29
Neuroblast differentiation-associated protein AHNAK	0.80	0.38
Xaa-Pro dipeptidase	0.80	0.16
Neurolysin, mitochondrial	0.80	0.35
Trifunctional enzyme subunit beta, mitochondrial;3-ketoacyl-CoA thiolase	0.80	0.14
Proteasome subunit beta type-4	0.80	0.74
Emerin	0.80	0.46
Septin-11	0.80	0.25
Laminin subunit beta-1	0.80	0.32
Chromatin target of PRMT1 protein	0.79	0.62
Myosin regulatory light chain 12A;Myosin regulatory light chain 12B;Myosin regulatory light polypeptide 9	0.79	0.28
Scaffold attachment factor B1	0.79	0.32
Cytosolic phospholipase A2;Phospholipase A2;Lysophospholipase	0.79	0.76
Microtubule-associated protein 1B;MAP1B heavy chain;MAP1 light chain LC1	0.79	0.38
Ubiquitin carboxyl-terminal hydrolase isozyme L1	0.79	0.36
Histone H1.4	0.79	0.65
Heterogeneous nuclear ribonucleoprotein U-like protein 1	0.79	0.18
14-3-3 protein theta	0.79	0.27
Serum deprivation-response protein	0.79	0.69
BRO1 domain-containing protein BROX	0.79	0.24
NADP-dependent malic enzyme	0.79	0.20
Serum paraoxonase/arylesterase 2	0.79	0.15
Histone H2B type 2-E;Histone H2B type 1-B;Histone H2B type 1-O;Histone H2B type 1-J;Histone H2B type 3-B	0.79	0.69
Bifunctional ATP-dependent dihydroxyacetone kinase/FAD-AMP lyase (cyclizing);ATP-dependent dihydroxyacetone kinase;FAD-AMP lyase (cyclizing)	0.78	0.30
YLP motif-containing protein 1	0.78	0.23
Tricarboxylate transport protein, mitochondrial	0.78	0.15
Epsin-1	0.78	0.44
Inverted formin-2	0.78	0.10
Ataxin-2-like protein	0.78	0.78
NADH-cytochrome b5 reductase 3;NADH-cytochrome b5 reductase 3 membrane-bound form;NADH-cytochrome b5 reductase 3 soluble form	0.78	0.62
Protein canopy homolog 2	0.78	0.50
Annexin A2;Putative annexin A2-like protein	0.78	0.28

LIM and SH3 domain protein 1	0.78	0.54
Heterogeneous nuclear ribonucleoprotein A3	0.77	0.14
Actin-related protein 2	0.77	0.10
DNA fragmentation factor subunit alpha	0.77	0.56
ATP synthase subunit g, mitochondrial	0.77	0.53
Plastin-1	0.77	0.23
Filamin-A	0.77	0.17
Obg-like ATPase 1	0.77	0.12
LIM domain only protein 7	0.77	0.46
AP-2 complex subunit mu	0.77	0.14
Interferon-induced, double-stranded RNA-activated protein kinase	0.77	0.41
Thyroid hormone receptor-associated protein 3	0.77	0.26
Guanine nucleotide-binding protein G(s) subunit alpha isoforms short;Guanine nucleotide-binding protein G(s) subunit alpha isoforms XLas	0.77	0.18
Glucocorticoid receptor	0.77	0.17
Polymerase I and transcript release factor	0.77	0.68
Cytoplasmic dynein 1 light intermediate chain 2	0.77	0.37
N-acetylglucosamine-6-sulfatase	0.76	0.26
Translocon-associated protein subunit delta	0.76	0.36
BUB3-interacting and GLEBS motif-containing protein ZNF207	0.76	0.12
Spectrin alpha chain, non-erythrocytic 1	0.76	0.08
Nucleolar protein 58	0.76	0.10
Protein S100-A6	0.76	0.62
Bifunctional 3-phosphoadenosine 5-phosphosulfate synthase 2;Sulfate adenylyltransferase;Adenylyl-sulfate kinase	0.76	0.11
Cytosolic non-specific dipeptidase	0.76	0.06
Saccharopine dehydrogenase-like oxidoreductase	0.76	0.32
CDGSH iron-sulfur domain-containing protein 1	0.76	0.33
Ribosome-binding protein 1	0.76	0.14
Vesicle-trafficking protein SEC22b	0.76	0.32
UTP--glucose-1-phosphate uridylyltransferase	0.76	0.28
Rho GTPase-activating protein 1	0.76	0.21
Ras-related protein Rap-1b;Ras-related protein Rap-1b-like protein	0.76	0.40
Serine/arginine-rich splicing factor 2	0.75	0.24
Estradiol 17-beta-dehydrogenase 11	0.75	0.41
Sorting and assembly machinery component 50 homolog	0.75	0.17
Synaptophysin-like protein 1	0.75	0.09
Actin-related protein 2/3 complex subunit 5	0.75	0.17
Annexin A5	0.75	0.28
Guanine nucleotide-binding protein G(i) subunit alpha-2	0.75	0.24
Arylsulfatase E	0.75	0.26
Neuron-specific calcium-binding protein hippocalcin;Hippocalcin-like protein 1;Neurocalcin-delta	0.75	0.28

Syntaxin-binding protein 3	0.75	0.14
Transmembrane emp24 domain-containing protein 4	0.75	0.47
EH domain-containing protein 2	0.75	0.14
Zinc finger protein 428	0.74	0.11
Constitutive coactivator of PPAR-gamma-like protein 1	0.74	0.10
Reticulon-3	0.74	0.14
NADH dehydrogenase [ubiquinone] 1 beta subcomplex subunit 4	0.74	0.21
Alpha-parvin	0.74	0.27
Insulin-like growth factor 2 mRNA-binding protein 3	0.74	0.10
Actin-related protein 2/3 complex subunit 2	0.74	0.25
Eukaryotic translation initiation factor 4B	0.74	0.34
Exocyst complex component 4	0.74	0.08
Moesin	0.74	0.29
Heterogeneous nuclear ribonucleoprotein F;Heterogeneous nuclear ribonucleoprotein F, N-terminally processed	0.74	0.19
Nucleolar protein 56	0.73	0.15
La-related protein 4B	0.73	0.75
Myosin light polypeptide 6	0.73	0.14
Plectin	0.73	0.20
CD166 antigen	0.73	0.21
Polyadenylate-binding protein-interacting protein 1	0.73	0.45
Rho GDP-dissociation inhibitor 1	0.73	0.25
Disintegrin and metalloproteinase domain-containing protein 10	0.73	0.10
Flotillin-1	0.73	0.09
Grancalcin	0.73	0.48
Cation-dependent mannose-6-phosphate receptor	0.73	0.12
Caldesmon	0.73	0.05
Beta-glucuronidase	0.73	0.46
Catenin delta-1	0.72	0.10
Destrin	0.72	0.37
Ankyrin repeat and SAM domain-containing protein 4B	0.72	0.50
Sialic acid synthase	0.72	0.12
Protein MEMO1	0.72	0.29
DnaJ homolog subfamily B member 1	0.72	0.52
3-ketoacyl-CoA thiolase, peroxisomal	0.72	0.11
Vesicle-associated membrane protein 3;Vesicle-associated membrane protein 2	0.72	0.20
Alpha/beta hydrolase domain-containing protein 14B	0.72	0.12
Aldehyde dehydrogenase, mitochondrial	0.72	0.10
Mitochondrial ribonuclease P protein 1	0.72	0.76
Hepatoma-derived growth factor	0.72	0.11
Mitotic interactor and substrate of PLK1	0.71	0.08
Histone H1.0;Histone H1.0, N-terminally processed	0.71	0.61
Acylamino-acid-releasing enzyme	0.71	0.10

NHP2-like protein 1;NHP2-like protein 1, N-terminally processed	0.71	0.25
Unconventional myosin-Ic	0.71	0.18
Succinyl-CoA ligase [GDP-forming] subunit beta, mitochondrial	0.70	0.08
Band 4.1-like protein 1	0.70	0.15
Heat shock protein beta-1	0.70	0.19
Cathepsin B;Cathepsin B light chain;Cathepsin B heavy chain	0.70	0.16
Treacle protein	0.70	0.11
UDP-glucose 4-epimerase	0.70	0.09
Tripeptidyl-peptidase 1	0.70	0.17
Actin-related protein 2/3 complex subunit 3	0.70	0.21
Tyrosine-protein phosphatase non-receptor type 11	0.70	0.28
Calcium uniporter protein, mitochondrial	0.70	0.37
Glyoxalase domain-containing protein 4	0.70	0.21
Proteasome activator complex subunit 1	0.70	0.14
Dipeptidyl peptidase 1;Dipeptidyl peptidase 1 exclusion domain chain;Dipeptidyl peptidase 1 heavy chain;Dipeptidyl peptidase 1 light chain	0.69	0.14
6-phosphogluconolactonase	0.69	0.09
Src substrate cortactin	0.69	0.06
Keratin, type I cytoskeletal 18	0.69	0.10
182 kDa tankyrase-1-binding protein	0.69	0.15
Stromal interaction molecule 1	0.69	0.29
Epoxide hydrolase 1	0.69	0.25
Unconventional myosin-Ie	0.69	0.26
DDRGK domain-containing protein 1	0.69	0.15
Aldo-keto reductase family 1 member B10	0.69	0.37
Cytoplasmic aconitate hydratase	0.69	0.04
Rho-associated protein kinase 2	0.69	0.13
NAD(P)H-hydrate epimerase	0.69	0.28
PDZ and LIM domain protein 5	0.69	0.13
Beta-hexosaminidase subunit beta;Beta-hexosaminidase subunit beta chain B;Beta-hexosaminidase subunit beta chain A	0.68	0.15
Calcium/calmodulin-dependent protein kinase type II subunit delta	0.68	0.09
Actin-binding LIM protein 1	0.68	0.17
E3 ubiquitin-protein ligase Midline-1	0.68	0.08
Septin-8	0.68	0.28
Ribosomal protein S6 kinase alpha-3	0.68	0.04
Quinone oxidoreductase PIG3	0.68	0.08
Vacuolar protein sorting-associated protein 29	0.68	0.17
Dipeptidyl peptidase 3	0.68	0.07
Aldose 1-epimerase	0.68	0.35
Glutathione synthetase	0.68	0.16

4-trimethylaminobutyraldehyde dehydrogenase	0.68	0.09
Calpastatin	0.68	0.39
Galectin-3	0.68	0.41
Reticulon-4	0.67	0.10
Serine/arginine-rich splicing factor 6	0.67	0.44
Retinal dehydrogenase 1	0.67	0.20
Microsomal glutathione S-transferase 1	0.67	0.11
Mannose-6-phosphate isomerase	0.67	0.26
Cysteine and glycine-rich protein 1	0.67	0.37
Superoxide dismutase [Cu-Zn]	0.67	0.70
Peptidyl-prolyl cis-trans isomerase FKBP1A	0.67	0.13
Glutaredoxin-1	0.67	0.10
Prostaglandin reductase 1	0.66	0.16
Syntaxin-7	0.66	0.08
Tight junction protein ZO-1	0.66	0.05
Annexin A13	0.66	0.25
Beta-hexosaminidase subunit alpha	0.66	0.10
PRA1 family protein 2	0.66	0.10
PRKC apoptosis WT1 regulator protein	0.66	0.05
Flotillin-2	0.66	0.18
Prelamin-A/C;Lamin-A/C	0.66	0.12
Cathepsin Z	0.66	0.14
Fumarylacetoacetase	0.66	0.09
Carnitine O-palmitoyltransferase 1, liver isoform	0.65	0.11
Growth factor receptor-bound protein 2	0.65	0.43
Transgelin-2	0.65	0.10
Myosin-10	0.65	0.10
Dihydropyrimidinase-related protein 2	0.65	0.05
Carboxymethylenebutenolidase homolog	0.65	0.20
Sulfotransferase 1A4;Sulfotransferase 1A3	0.64	0.10
Zyxin	0.64	0.21
Glutamine--fructose-6-phosphate aminotransferase [isomerizing] 1	0.64	0.08
Complexin-2	0.64	0.20
Septin-9	0.64	0.07
Acyl-protein thioesterase 1	0.64	0.05
Serine dehydratase-like	0.64	0.28
N-acetyl-D-glucosamine kinase	0.64	0.15
Cytochrome b5	0.64	0.16
NADH dehydrogenase [ubiquinone] 1 beta subcomplex subunit 11, mitochondrial	0.64	0.64
Heat shock 70 kDa protein 1B;Heat shock 70 kDa protein 1A	0.64	0.09
Unconventional myosin-XVIIIa	0.64	0.10
Sideroflexin-3	0.64	0.12
Histone H1.2	0.64	0.55

Cold-inducible RNA-binding protein	0.64	0.21
TATA-binding protein-associated factor 2N	0.64	0.28
Leukocyte elastase inhibitor	0.63	0.06
40S ribosomal protein S24	0.63	0.75
Isocitrate dehydrogenase [NADP] cytoplasmic	0.63	0.03
Glutamate dehydrogenase 1, mitochondrial;Glutamate dehydrogenase 2, mitochondrial	0.63	0.16
UV excision repair protein RAD23 homolog B	0.63	0.34
Neudesin	0.63	0.60
Ester hydrolase C11orf54	0.62	0.08
Transketolase	0.62	0.08
Glyoxylate reductase/hydroxypyruvate reductase	0.62	0.09
Selenium-binding protein 1	0.61	0.09
Microtubule-associated tumor suppressor 1	0.61	0.12
Fatty aldehyde dehydrogenase	0.61	0.04
Receptor expression-enhancing protein 5	0.61	0.10
5-nucleotidase	0.61	0.24
Alpha-aminoadipic semialdehyde dehydrogenase	0.61	0.01
Succinyl-CoA ligase [ADP-forming] subunit beta, mitochondrial	0.61	0.25
Ras GTPase-activating-like protein IQGAP2	0.61	0.10
N-acylneuraminate cytidylyltransferase	0.61	0.07
Pyridoxal kinase	0.60	0.04
Junction plakoglobin	0.60	0.03
Epidermal growth factor receptor kinase substrate 8-like protein 2	0.60	0.04
Muscleblind-like protein 1	0.59	0.55
Annexin A4	0.59	0.09
3-hydroxyisobutyrate dehydrogenase, mitochondrial	0.58	0.05
CAP-Gly domain-containing linker protein 2	0.58	0.60
Protein POF1B	0.58	0.10
Plakophilin-3	0.58	0.09
Phosphatidylethanolamine-binding protein 1;Hippocampal cholinergic neurostimulating peptide	0.58	0.08
Acid ceramidase;Acid ceramidase subunit alpha;Acid ceramidase subunit beta	0.58	0.05
Mitochondrial antiviral-signaling protein	0.57	0.04
Catenin beta-1	0.57	0.02
HLA class I histocompatibility antigen, A-30 alpha chain;HLA class I histocompatibility antigen, Cw-16 alpha chain;HLA class I histocompatibility antigen, Cw-12 alpha chain;HLA class I histocompatibility antigen, B-59 alpha chain;HLA class I histocompatibility antigen, B-55 alpha chain;HLA class I histocompatibility antigen, B-54 alpha chain;HLA class I histocompatibility antigen, A-36 alpha chain;HLA class I histocompatibility antigen, A-23 alpha chain;HLA class I histocompatibility antigen, A-1 alpha chain;HLA class I histocompatibility antigen, A-11 alpha chain;HLA class I	0.57	0.09

histocompatibility antigen, A-24 alpha chain;HLA class I histocompatibility antigen, A-3 alpha chain;HLA class I histocompatibility antigen, Cw-14 alpha chain;HLA class I histocompatibility antigen, Cw-4 alpha chain;HLA class I histocompatibility antigen, Cw-5 alpha chain;HLA class I histocompatibility antigen, Cw-6 alpha chain;HLA class I histocompatibility antigen, Cw-15 alpha chain;HLA class I histocompatibility antigen, Cw-8 alpha chain;HLA class I histocompatibility antigen, B-42 alpha chain;HLA class I histocompatibility antigen, B-41 alpha chain;HLA class I histocompatibility antigen, B-18 alpha chain;HLA class I histocompatibility antigen, B-14 alpha chain;HLA class I histocompatibility antigen, B-8 alpha chain;HLA class I histocompatibility antigen, B-37 alpha chain;HLA class I histocompatibility antigen, B-35 alpha chain;HLA class I histocompatibility antigen, B-78 alpha chain;HLA class I histocompatibility antigen, B-56 alpha chain;HLA class I histocompatibility antigen, B-53 alpha chain;HLA class I histocompatibility antigen, B-52 alpha chain;HLA class I histocompatibility antigen, B-46 alpha chain;HLA class I histocompatibility antigen, B-15 alpha chain;HLA class I histocompatibility antigen, B-57 alpha chain;HLA class I histocompatibility antigen, B-51 alpha chain;HLA class I histocompatibility antigen, B-58 alpha chain;Putative HLA class I histocompatibility antigen, alpha chain H;HLA class I histocompatibility antigen, Cw-18 alpha chain;HLA class I histocompatibility antigen, Cw-2 alpha chain		
Galactokinase	0.57	0.05
Synaptic vesicle membrane protein VAT-1 homolog	0.57	0.03
Golgi reassembly-stacking protein 2	0.57	0.07
Glutathione S-transferase kappa 1	0.56	0.07
Major vault protein	0.56	0.03
Ubiquilin-1	0.56	0.55
Lipoma-preferred partner	0.56	0.05
Glutathione peroxidase 1	0.56	0.15
Dynein light chain roadblock-type 1;Dynein light chain roadblock-type 2	0.56	0.57
Carbamoyl-phosphate synthase [ammonia], mitochondrial	0.56	0.61
Proto-oncogene tyrosine-protein kinase Src	0.56	0.03
Apolipoprotein C-III	0.55	0.19
Ribonuclease inhibitor	0.55	0.00
Arylsulfatase A;Arylsulfatase A component B;Arylsulfatase A component C	0.55	0.12
Lysosomal alpha-glucosidase;76 kDa lysosomal alpha-glucosidase;70 kDa lysosomal alpha-glucosidase	0.54	0.16
Protein AHNAK2	0.54	0.15
Homogentisate 1,2-dioxygenase	0.54	0.05
Beta-lactamase-like protein 2	0.54	0.27
Cysteine-rich protein 2	0.54	0.21
E3 ubiquitin-protein ligase RNF213	0.53	0.17
DnaJ homolog subfamily B member 11	0.53	0.33

Adenylate kinase 4, mitochondrial	0.53	0.47
COX assembly mitochondrial protein homolog	0.53	0.03
Dipeptidyl peptidase 2	0.53	0.23
Beta-galactosidase	0.52	0.01
Apolipoprotein O	0.52	0.48
Phosphomannomutase 2	0.52	0.57
Contactin-1	0.51	0.12
ADP/ATP translocase 1	0.51	0.08
HIV Tat-specific factor 1	0.51	0.10
Aldehyde dehydrogenase X, mitochondrial	0.51	0.04
Quinone oxidoreductase	0.51	0.05
Catenin alpha-1	0.50	0.00
Testin	0.50	0.11
Translocon-associated protein subunit alpha	0.49	0.54
Alcohol dehydrogenase [NADP(+)]	0.49	0.03
Pyridoxine-5-phosphate oxidase	0.49	0.08
Superoxide dismutase [Mn], mitochondrial	0.49	0.06
Sepiapterin reductase	0.49	0.01
Tubulin alpha-4A chain	0.49	0.06
Branched-chain-amino-acid aminotransferase, mitochondrial	0.48	0.39
Myc box-dependent-interacting protein 1	0.48	0.10
Cathepsin D;Cathepsin D light chain;Cathepsin D heavy chain	0.48	0.12
Ribonuclease UK114	0.48	0.23
Cadherin-1;E-Cad/CTF1;E-Cad/CTF2;E-Cad/CTF3	0.48	0.03
Calmin	0.48	0.18
Alpha-adducin	0.47	0.01
Thymosin beta-4;Hematopoietic system regulatory peptide	0.47	0.32
OCIA domain-containing protein 2	0.47	0.10
Cytochrome c oxidase subunit NDUFA4	0.47	0.59
NEDD8	0.46	0.37
MAGUK p55 subfamily member 6	0.45	0.06
Fibronectin;Anastellin;Ugl-Y1;Ugl-Y2;Ugl-Y3	0.44	0.04
cGMP-inhibited 3,5-cyclic phosphodiesterase A	0.44	0.14
15-hydroxyprostaglandin dehydrogenase [NAD(+)]	0.44	0.14
5-oxoprolinase	0.44	0.18
Core histone macro-H2A.2	0.44	0.08
CD59 glycoprotein	0.42	0.02
NADH dehydrogenase [ubiquinone] iron-sulfur protein 4, mitochondrial	0.42	0.28
Myotrophin	0.42	0.63
Sodium/potassium-transporting ATPase subunit gamma	0.42	0.08
PDZ and LIM domain protein 1	0.42	0.06
3-ketoacyl-CoA thiolase, mitochondrial	0.41	0.00
Na(+)/H(+) exchange regulatory cofactor NHE-RF1	0.41	0.03

Centromere protein V	0.41	0.25
Cytosolic Fe-S cluster assembly factor NUBP1	0.41	0.10
APOBEC1 complementation factor	0.40	0.17
CDGSH iron-sulfur domain-containing protein 2	0.40	0.44
DNA repair protein RAD50	0.40	0.10
Unconventional myosin-XVB	0.39	0.01
Ras-related protein Rab-27B	0.39	0.30
Signal transducer and activator of transcription 3	0.39	0.07
Alpha-soluble NSF attachment protein	0.38	0.33
Aldehyde dehydrogenase family 3 member B1;Aldehyde dehydrogenase family 3 member B2	0.37	0.15
CD44 antigen	0.37	0.07
Erlin-2	0.37	0.24
Syntaxin-4	0.37	0.06
Glutathione peroxidase 2	0.36	0.01
Peroxisomal 2,4-dienoyl-CoA reductase	0.36	0.05
Tyrosine-protein phosphatase non-receptor type 12	0.36	0.34
Proline-, glutamic acid- and leucine-rich protein 1	0.35	0.34
Transaldolase	0.35	0.00
Kinesin light chain 4	0.35	0.06
Ceramide synthase 2	0.34	0.14
Gamma-glutamyltranspeptidase 1;Gamma-glutamyltranspeptidase 1 heavy chain;Gamma-glutamyltranspeptidase 1 light chain;Putative gamma-glutamyltranspeptidase 3;Putative gamma-glutamyltranspeptidase 3 heavy chain;Putative gamma-glutamyltranspeptidase 3 light chain;Inactive gamma-glutamyltranspeptidase 2	0.34	0.01
Canalicular multispecific organic anion transporter 2	0.34	0.01
Ras-related protein Rab-34	0.33	0.11
Guanine nucleotide-binding protein G(q) subunit alpha	0.32	0.24
Signal recognition particle 9 kDa protein	0.31	0.28
MOB kinase activator 1A;MOB kinase activator 1B	0.31	0.10
Annexin A3	0.31	0.04
Protein FAM98B	0.30	0.00
Aspartyl aminopeptidase	0.30	0.05
Signal transducing adapter molecule 2	0.30	0.34
Transmembrane protein 205	0.29	0.23
Pirin	0.29	0.34
Up-regulated during skeletal muscle growth protein 5	0.29	0.17
Villin-1	0.28	0.05
Peptidyl-prolyl cis-trans isomerase FKBP2	0.27	0.34
60S ribosomal protein L29	0.27	0.52
Canalicular multispecific organic anion transporter 1	0.27	0.08
Erythrocyte band 7 integral membrane protein	0.26	0.22
Galectin-3-binding protein	0.25	0.06

Protein phosphatase 1A	0.23	0.01
Dynein light chain 2, cytoplasmic	0.20	0.08
Prenylcysteine oxidase 1	0.20	0.09
Alcohol dehydrogenase 1C;Alcohol dehydrogenase 1A	0.18	0.15
Cleavage and polyadenylation specificity factor subunit 7	0.17	0.00
Histone H1.3	0.16	0.38
Focal adhesion kinase 1	0.09	0.08
Versican core protein	0.08	0.14